

Supervisors:

Prof. Dr. ir. Roeland Samson, Dpt. of Bioscience Engineering, University of Antwerp, Belgium

Prof. Dr. Karolien De Wael, Dpt. of Chemistry, University of Antwerp, Belgium

Doctoral Jury:

Prof. Dr. Philippe De Smedt, Dpt. of Environment, University of Ghent, Belgium

Dr. Simo Spassov, Geophysical Center at Dourbes, Royal Meteorological Institute of Belgium

Prof. Dr. ir. Sarah Lebeer, Dpt. of Bioscience Engineering, University of Antwerp, Belgium

Prof. Dr. ir. Siegfried Denys, Dpt. of Bioscience Engineering, University of Antwerp, Belgium

Prof. Dr. ir. Roeland Samson, Dpt. of Bioscience Engineering, University of Antwerp, Belgium

Prof. Dr. Karolien De Wael, Dpt. of Chemistry, University of Antwerp, Belgium

Dean:

Prof. Dr. Nick Schryvers, Dpt. of Physics, University of Antwerp, Belgium

Rector

Prof. Dr. Herman Van Goethem, Faculty of Law, Belgium



Faculty of Science

Department of Bioscience Engineering

Magnetic and analytical fingerprinting of particulate matter for urban (bio)monitoring

Thesis submitted in the fulfillment of the requirements for the degree of
Doctor (PhD) in Bioscience Engineering

Ir. Ana CASTANHEIRO

Antwerp, 2020

Dutch translation of the title:

Magnetische en analytische vingerafdrukken van fijn stof voor stedelijke (bio)monitoring

Citation:

Castanheiro A., 2020. Magnetic and analytical fingerprinting of particulate matter for urban (bio)monitoring. PhD thesis, Department of Bioscience Engineering, Faculty of Science, University of Antwerp, Antwerp, Belgium.

Illustrations and cover by Ana Castanheiro

ISBN 978-90-5728-645-2

Deposit number D/2019/12.293/31

The author and the supervisors give authorization to consult and copy parts of this work for personal use only. Every other use is subject to the copyright laws. Permission to reproduce any material contained in this work should be obtained from the author.

Acknowledgments

This research and subsequent thesis was only possible thanks to the support, collaboration and generosity of several parties. I would like to start by thanking the FWO (Research Foundation Flanders) for my doctoral fellowship grant and to acknowledge both Roeland Samson and Karolien De Wael for opening the door to their research groups in 2014 when I was a MSc thesis student coming from abroad.

Roeland, thank you for all your enthusiasm, support and guidance throughout the years, for all your reviews and for keep asking more and more questions. I will keep very nice memories of all these years at the EUREC-Air research group, in part because of your endless curiosity and kind personality. Thank you also for the great week we had in Dubna and Moscow during the BIOMAP8 conference and the 2018 World Football Championship!

Karolien, thank you for all your support, guidance, motivation and strategic planning. I have always found our meetings and discussions very useful and energizing for carrying on my research. And thank you for making me feel at home whenever I was at AXES!

A big word of appreciation to my jury members (Sarah, Siegfried, Simo and Philippe) for their constructive reviews. And thank you to everyone with whom I collaborated along the different experiments and projects. A special thanks to Walter and Gert for introducing me to SEM/EDX analysis and for all their help along the way, and Tine (EMAT) for coating hundreds of samples for me. To all PMF collaborators (Sarah, Serena, Ronny, Steven, Silvia, Simo, VMM, ...), thank you for your partnership along this exciting and challenging project!

To all my colleagues at EUREC-Air, former and current ones, a huge thank you! To Karen, Jelle, Leen, Jolien, Kyra, Samira, Athari, Liesbeth, Anskje, Babette, Géraldine, ... I couldn't have asked for a better welcome from all of you, thank you for making me feel right at home. The relaxed environment and friendship without compromising our

work goals and challenges... I think this is the magical formula! A special thanks to Karen and Jelle for our “magnetic” brainstormings, to Karen and Jolien for their help with writing the *samenvatting*, and to Jelle for our joint PMF project. Another special thanks to Jolien and Kyra, you were the best office colleagues ever!

I would like to thank the entire Bioscience Engineering department for all the nice moments: birthday cakes, game evenings, Christmas lunches, and so much more. To all, thank you for your words and gestures of encouragement in the last stages of my PhD journey.

To my family and family in law, thank you for all the cherished moments together and the more to come. To all my friends, from my early-school-times to Técnico-battle-days and living-an-expat-life, thank you for being part of my life and for sticking around despite the distance. Friends are the family we choose that decided to stay.

Mom and dad, thank you for your determination at all times and for your unconditional love and support. You have always encouraged me to fly high and away, and I did it. The view from up here is amazing, as it is every time I safely return to your nest. Thank you too little brother, for the opportunity and pleasure I get in being your favorite big sister. You have filled in my childhood days with so much light and fun while also allowing me to experience the same things through a different perspective.

Hugo, my love, best friend and recently dear husband! Thank you for following me to a whole new country and for building with me our own home, away from home. Thank you for bringing calmness into my inside world and for standing by me. You are my rock.

To this day, I still remember how amazed I was by learning that the Earth was round, but specially how intrigued I felt by the fact that this meant absolutely nothing to my grandparents. Half of my grandparents do not know how to read or how to write their own name. None of them ever flew in the sky or sailed in the ocean. As an eager to learn and curious kid, I often tried to revert this by sharing with them all the fascinating

things I was discovering around us in the world; my attempts were mostly unsuccessful I must confess. My grandparents were/are simple people, yet good-hearted, and they are also the reason why I'm here in the first place. This thesis, and my doctorate in philosophy, is dedicated with all my love to them, Ana Lúcia, Ana and Laura, Joaquim and Vicente. I am aware they will never read it, yet certain of their unlimited proud on me.

Each time I tried to explain to my dad what I've been doing for a living in the past five years, his reaction was invariably the same, after a rather long silence. - Hmm, okay. But what are you going to produce in the end? - Well, dad, this is it! Enjoy!

Obrigada!

Ana

Antwerpen, 2020

Despite legislative and regulatory efforts to reduce the emission of atmospheric pollutants, air pollution remains of worldwide concern, with nine out of ten people currently breathing air exceeding the guideline values set by the World Health Organization (WHO). Among air pollutants, particulate matter (PM) poses the greatest risk to human public health due to their small inhalable size and association with hazardous components such as metals. In our increasingly populated and urbanized planet, emission sources of PM are varied and abundant. The complex nature of PM strongly depends on the emission source and is, moreover, subjected to atmospheric and meteorological transformation processes, being particularly challenging to monitor atmospheric PM within dynamic, multi-source urban environments.

In the pursuit of air quality assessment tools able to monitor atmospheric PM at high resolution in both time and space, environmental magnetism has been a hot research topic since the 1980s. More recently, the use of plant leaves as biomagnetic monitors of atmospheric PM has been suggested as a widely applicable, reliable and low-cost methodology. The exposure of plant leaves to atmospheric conditions leads to the invariable accumulation of magnetic particles, which are ubiquitously present in PM but allow to distinguish between low and high pollution levels. Throughout this PhD research, the applicability of biomagnetic monitoring as a fingerprinting and source apportionment tool for atmospheric PM was investigated across different environments, through a combination of techniques.

First, ca. 40,000 leaf-deposited particles from ivy leaves (*Hedera sp.*) collected at different sites were characterized for their particle morphology and elemental characterization using dedicated particle-analysis. The particle size distribution of analyzed PM₂₋₁₀ was biased towards the small-sized PM, with ca. 32% of the total particles being smaller than 2.5 μm (PM_{2.5}). The particles' size was influenced by the sites, with median diameters following the order roadside = industry (2.92 μm) < forest

(2.99 μm) < rural (3.02 μm) < train (3.06 μm), and also the particles' morphology was site-dependent. Leaf-deposited particles from roadside location were overall the smallest in size and the most circular in geometry. While forest and rural elemental profiles were mainly associated with natural PM (Si, Ca, S, K, Al, Mg, Na, Cl), the industry-related particles revealed the highest anthropogenic metal input, particularly in Zn, Cu, Pb and As. The PM₂₋₁₀ profiles for roadside and train were rather comparable and dominated by Si, Fe, Ca and Al, with the first site moderately enriched (compared to the forest background) in Fe, Cu, Zn, As and Ba, and the second moderately enriched in Fe, Zn and As. The discrimination between roadside and train was only possible by evaluating their fine (2 – 2.5 μm) and coarse (2.5 – 10 μm) PM characteristics. The fine particles from the roadside were 72% more enriched in Fe than its coarse fraction, whereas this size-dependent enrichment was negligible for the train, which indicated a larger contribution of combustion-derived particles (small, rather circular, Fe-enriched) at the roadside compared to the train. A Random Forest (RF) model based on the particles' morphological and compositional information was able to correctly predict the site of about half of the analyzed leaf-deposited particles in the best case scenarios. The rather modest classification accuracy of the RF model (36% - 51%) implies the influence of common, regional PM, at the same time that demands for additional fingerprinting techniques that may aid in discriminating PM sources more accurately. Magnetic analysis, namely, saturation isothermal remanent magnetization (SIRM), of those ivy leaves was evaluated against the metal content from the leaf-deposited particles. Roadside, train and industry sites exhibited larger magnetic and metal enrichment compared to the background sites. Leaf-deposited PM for roadside and train samples had similar metal profiles, including in terms of Fe content, but magnetically they exhibited different SIRM values (train > roadside). The observed magnetic distinction between leaves close to road- and railway-traffic illustrated the magnetic source apportionment prospective to identify different sites and contributing sources. Furthermore, leaf SIRM showed to be significantly correlated with a range of leaf-deposited trace metals (Fe, Cu, Zn, Cd, Pb, and Mn), confirming

SIRM-based magnetic assessment as an overall indicator of metal pollution on leaf-deposited PM, which is inevitably linked with atmospheric PM.

The concept of combining magnetic- and particle-based techniques for depicting different habitat conditions was extended to a large-scale European campaign. Leaf-deposited PM (PM_{0.3-10}) from plane tree leaves (*Platanus x acerifolia*) close to heavy-trafficked streets and within urban parks, in the urban areas of 20 European cities, were examined at the end of the in-leaf period. Common regional background PM composition and concentration were observed across all investigated cities, while certain local conditions, such as the influence of e.g. salt aerosol sources or a dry continental climate, were clearly recognized from the combined elemental and magnetic results. The percentage of Fe-based particles, with ferromagnetic properties (SIRM), emerged as a clear marker of traffic-related pollution in most of the sites, allowing the distinction between streets vs. parks. The validation of this combined methodology by monitoring leaf-deposited PM across different countries and climate types, demonstrated the fingerprinting potential of this approach.

Atmospheric dust deposition on plant leaves enables the collection of site-specific PM. Still, the underlying dynamics of leaf particle accumulation should be considered for the development of leaf biomagnetic monitoring of atmospheric PM. A leaf-level comprehensive analysis of atmospheric dust accumulation was carried out throughout a period of three months, considering two plant species (ivy, *Hedera sp.*, and strawberry, *Fragaria sp.*) with distinct leaf macro- and micro-morphology. Plant species were exposed at the same moderate road traffic site, and leaves collected every three weeks were analyzed for their magnetic signature, morphology and elemental content. Dust accumulation was observed both visually (SEM microscopy) and magnetically, while metal enrichment was limited and more variable over time. The magnetic enrichment (in small-grained, single/pseudo-single domain magnetite-like particles) was not species-specific, reflecting a common contributing source. Variations in terms of pollution contributions, meteorological phenomena, species-specific traits, particle deposition (and encapsulation) vs. micronutrients depletion, are

discussed in light of the conducted monitoring campaign. Although not completely elucidative in the performed study, the multifactorial leaf dust accumulation process can better be understood through a combination of techniques (e.g. elements/magnetic/SEM).

The development of magnetic-based air quality monitoring strategies for source identification and attribution demands for a deep understanding of the physicochemical and magnetic characteristics of source-specific PM. For this, a PM source fingerprinting campaign (PMF project), was set up to comprehensively characterize urban PM sources of interest. This project comprised, among others, simultaneous atmospheric PM sampling (as performed by conventional air quality stations) and leaf monitoring (using ivy leaves) for an uninterrupted period of seven and a half weeks at five different monitoring sites, representative of road, railway and shipping traffic, industry and background conditions. Daily atmospheric PM₁₀ filters were analyzed gravimetrically, chemically and magnetically. Atmospheric PM₁₀ concentrations decreased in the order shipping > road > industry > train. The main governing elements were Na, Fe, Ca, K, and Mg, with the industry site presenting the highest concentrations and the most diversified metal profile. The composition profiles for road and train sites were once again similar, in agreement with the previously observed for ivy leaves exposed at sites with road and railway traffic as prevalent polluting sources. The shipping site could be considered as in between those two source types (road and railway traffic, and industry). The magnetic site-fingerprinting was less straightforward than the chemical-based characterization, with all samples being dominated by low-coercivity minerals with grain sizes ca. between 0.1 and 5 µm. To include all information from PM₁₀ filters (PM and elemental concentrations, magnetic properties) improved the predictive power of the RF model compared to considering only the PM concentrations (as regularly monitored by air quality stations), with the site classification accuracy increasing from 25% to 76% up to 92% to 100%. The measured magnetic properties and ratios were accountable for 16% of the decision tree splits in the RF model, whilst the elemental concentrations

remained the main classification predictors. Gravimetric PM concentrations contributed only 1% to the site classification, suggesting that conventional gravimetric-based PM monitoring has little power to identify sampling locations mainly exposed to distinct PM sources. This discrimination can better be achieved by collecting elemental and magnetic information, from which magnetic analyses are more time- and cost-effective than chemical determination.

The leaf monitoring results were overall in accordance with the filter results, both chemically and magnetically. Furthermore, a strong linear association ($R^2 = 0.74$) was found between the mean leaf SIRM values and the cumulative PM₁₀ filter loads. This demonstrated that active leaf monitoring of atmospheric pollution at source-specific PM sites is useful to obtain time-integrated measures of local atmospheric PM, as measured by conventional PM samplers, with the advantage that a large spatial scale can be achieved using plants. The health-relevance of source-specific PM was explored by exposing human monocyte-macrophage cells to air samples collected at the PMF sites, and measuring their pro-inflammatory and oxidative stress potential. Although based on a rather reduced number of air samples, the results suggested the train (low PM concentrations, high SIRM) and shipping (high PM concentrations, low SIRM) sites to have the highest health-risk potential.

Overall, this PhD research demonstrated the application potential of biomagnetic monitoring for fingerprinting atmospheric PM sources in urban settings. A straightforward application of biomagnetic techniques to clearly recognize which PM source(s) are of most relevance at a certain mixed-source site is not possible yet. Still, our findings revealed that magnetic monitoring methodologies are of greater use for fingerprinting and source apportionment of PM than the conventional gravimetric-based monitoring approach. The study and establishment of source-specific magnetic and physicochemical signatures, and their health-risk potential, contribute to the library of knowledge on PM fingerprints, which is essential to develop reliable, up-to-date, tools for the monitoring of urban PM.

Ondanks maatregelen en wetten om de uitstoot van luchtverontreiniging te verminderen, blijft luchtvervuiling een wereldwijd probleem. Negen op tien mensen ademen momenteel lucht in die de richtwaarden van de Wereldgezondheidsorganisatie (WGO) overschrijden. Onder luchtverontreinigende stoffen vormt fijn stof (PM) het grootste risico voor de menselijke gezondheid vanwege hun kleine inhaleerbare grootte en hun associatie met gevaarlijke componenten zoals metalen. In een wereld met een constant groeiende bevolking en verstedelijking, zijn de emissiebronnen van fijn stof gevarieerd en overvloedig. De complexe aard van fijn stof is sterk afhankelijk van de emissiebron en is bovendien onderworpen aan atmosferische en meteorologische transformatieprocessen. Dit maakt monitoring van fijn stof erg uitdagend in dynamische stedelijke omgevingen waar meerdere emissiebronnen voorkomen.

In de zoektocht naar manieren om atmosferisch fijn stof te meten met hoge temporele en ruimtelijke resolutie, is omgevingsmagnetisme sinds 1980 een belangrijk onderzoeksonderwerp. Meer recent is het gebruik van bladeren van planten als biomagnetische monitors van atmosferisch fijn stof gesuggereerd als een breed toepasbare, betrouwbare en goedkope methode. De blootstelling aan atmosferisch fijn stof veroorzaakt een accumulatie van magnetische deeltjes op bladeren en andere vastgestelde oppervlakken. Deze magnetische deeltjes laten toe een onderscheid te maken tussen lage en hoge vervuilingniveaus. Tijdens dit doctoraatsonderzoek werd de toepasbaarheid van biomagnetische monitoring als een instrument voor bronkarakterisatie (zogenaamd *fingerprinting*) en brontoewijzing voor atmosferisch fijn stof onderzocht in verschillende bronlocaties, door een combinatie van technieken.

Eerst werden ca. 40.000 deeltjes, afgezet op het oppervlak van klimopbladeren (*Hedera sp.*) en verzameld op verschillende bronlocaties, gekarakteriseerd voor hun morfologie en elementaire eigenschappen met behulp van doorgedreven

deeltjesanalyse. De distributie van de deeltjesgrootte van de geanalyseerde PM₂₋₁₀ had een afwijking in de richting van de kleinere PM-deeltjes, waarbij ca. 32% van de totale deeltjes kleiner was dan 2,5 µm (PM_{2,5}). De deeltjesgrootte en de morfologie (hoogte-breedteverhouding en vorm) werden beïnvloed door de bronlocaties. Zo volgde de mediaan van de deeltjesdiameter deze gradiënt: straatkant = industrie (2,92 µm) < bos (2,99 µm) < landelijk (3,02 µm) < trein (3,06 µm). Aan de straatkant waren de op de bladeren afgezette deeltjes over het algemeen het kleinst in grootte en het meest cirkelvormig in geometrie. In bossen en op het platteland werden de elementaire profielen van de deeltjes voornamelijk geassocieerd met natuurlijk fijn stof (Si, Ca, S, K, Al, Mg, Na, Cl), terwijl in de industriezone de deeltjes de hoogste input van antropogene metalen vertoonden, met name Zn, Cu, Pb en As. De PM₂₋₁₀ profielen voor straatkant en trein waren redelijk vergelijkbaar en werden gedomineerd door Si, Fe, Ca en Al. Aan de straatkant waren de deeltjes matig verrijkt (vergeleken met de bosachtergrond) in Fe, Cu, Zn, As en Ba, en aan de treinsporen matig verrijkt in Fe, Zn en As. De discriminatie tussen straatkant en trein was enkel mogelijk door hun fijne (2 - 2,5 µm) en grove (2,5 - 10 µm) fijnstofkenmerken te evalueren. De fijne deeltjes langs de straatkant waren 72% meer verrijkt in Fe dan de grove fractie, terwijl deze grootteafhankelijke verrijking te verwaarlozen was voor de trein. Dit wijst op een grotere bijdrage aan deeltjes afgeleid van verbranding (klein, nogal cirkelvormig, verrijkte Fe) langs de straatkant vergeleken met langs de trein. Een *Random Forest* (RF)-model op basis van de morfologische en samenstellingsinformatie van de deeltjes was in staat in het beste geval de bronlocatie correct te voorspellen voor ongeveer de helft van de geanalyseerde op de bladeren geaccumuleerde deeltjes. De tamelijk bescheiden classificatienauwkeurigheid van het RF-model (36% - 51%) impliceert de invloed van gemeenschappelijke, regionale fijn stof, en vereist tegelijkertijd aanvullende “vingerafdruktechnieken” die kunnen helpen bij het nauwkeuriger onderscheiden van de fijnstofbronnen. Magnetische analyse, namelijk gesatureerde isotherme remanente magnetisatie (*saturation isothermal remanent magnetization*, SIRM) op de klimopbladeren werd vergeleken met het metaalgehalte van de op de bladeren afgezette deeltjes. De bronlocaties straatkant, trein en industrie vertoonden grotere

magnetische en metaalverrijking dan de achtergrondplaatsen. Het op de bladeren afgezette fijn stof langs de straat en de trein hadden vergelijkbare metaalprofielen, ook wat betreft Fe-gehalte, maar magnetisch vertoonden ze verschillende SIRM-waarden (trein > straatkant). Het waargenomen magnetische onderscheid tussen bladeren in de buurt van weg- en spoorwegverkeer illustreert de magnetische brontoewijzing die zou kunnen worden gebruikt om verschillende locaties en bijdragende bronnen te identificeren. Verder bleek SIRM gemeten op bladeren significant gecorreleerd te zijn met een reeks van door het blad afgezette sporenmatalen (Fe, Cu, Zn, Cd, Pb en Mn). Dit bevestigt dat een op SIRM gebaseerde magnetische beoordeling gebruikt kan worden als algemene indicator van metaalvervuiling voor fijn stof afgezet op bladeren, welke onvermijdelijk verbonden is met atmosferisch fijn stof.

De combinatie van magnetische technieken en deeltjesanalyse om de verschillende habitat condities te beschrijven, werd uitgebreid naar een grootschalige Europese campagne. In 20 Europese steden werd het fijn stof ($PM_{0.3-10}$), afgezet op plataanbladeren (*Platanus x acerifolia*) langs straten met druk verkeer en in stadsparken, onderzocht aan het einde van het groeiseizoen. In elke onderzochte stad werden gelijkaardige regionale achtergrondconcentraties en -samenstellingen van fijn stof waargenomen, terwijl bepaalde lokale condities, zoals de invloed van zoute aerosolbronnen of van een droog continentaal klimaat, duidelijk te herkennen waren uit de resultaten van de gecombineerde analyse van magnetisme en elementaire samenstelling. Het percentage Fe-gebaseerde deeltjes, met ferromagnetische eigenschappen (SIRM), kwam daarentegen naar voren als een duidelijke indicator van verkeersgerelateerde vervuiling in de meeste locaties. Hierdoor werd het mogelijk een onderscheid te maken tussen straten en stadsparken. De validatie van deze gecombineerde methode door monitoring van het op bladeren afgezette fijn stof in verschillende landen en klimaattypen toonde het potentieel van deze vingerafdruktechniek aan.

De afzetting van atmosferisch stof op plantenbladeren maakt het verzamelen van locatiespecifiek fijn stof mogelijk. Toch moet voor de ontwikkeling van biomagnetische bladmonitoring van atmosferisch fijn stof, rekening gehouden worden met de onderliggende dynamiek van de accumulatie van deeltjes op bladeren. Een uitgebreide analyse op bladniveau van de accumulatie van atmosferisch stof werd gedurende een periode van drie maanden uitgevoerd, waarbij twee plantensoorten (klimop, *Hedera sp.*, en aardbei, *Fragaria sp.*) met verschillende bladmorphologie in beschouwing werden genomen. De plantensoorten werden blootgesteld op dezelfde locatie met gematigd verkeer. De bladeren werden om de drie weken verzameld en geanalyseerd op hun magnetische signatuur, morfologie en elementaire inhoud. Stofaccumulatie werd zowel visueel (SEM-microscopie) als magnetisch waargenomen, terwijl metaalverrijking beperkt was en variabel in de tijd. De magnetische verrijking (in kleinkorrelige magnetietachtige deeltjes met enkelvoudige/pseudo-enkelvoudige Weiss-gebieden) was niet soortspecifiek en weerspiegelde een gemeenschappelijke bron. Variaties op vlak van vervuilingbijdragen, meteorologische fenomenen, soortspecifieke eigenschappen, deeltjesafzetting (en inkapseling) versus uitputting van micronutriënten worden besproken in het licht van de uitgevoerde monitoringcampagne. Hoewel niet volledig verklaard in het uitgevoerde onderzoek, kan het multifactoriële stofaccumulatie op bladeren beter worden begrepen door een combinatie van technieken (bijvoorbeeld elementair/magnetisch/SEM).

De ontwikkeling van op magnetisme gebaseerde luchtkwaliteitsmonitoring voor bronidentificatie en -toewijzing vereist een diepe kennis van de fysicochemische en magnetische eigenschappen van fijn stof. Hiervoor werd een grote meetcampagne opgezet, het zogenaamde PMF-project (*PM source Fingerprint*), om de vingerafdruktechniek te ontwikkelen door relevante stedelijke fijnstofbronnen volledig te karakteriseren. Dit project omvatte onder andere een gelijktijdige atmosferische fijnstofbemonstering (zoals uitgevoerd door conventionele luchtkwaliteit monitoringstations) en bladmonitoring (op klimopbladeren) gedurende een ononderbroken periode van zeven en een halve week op vijf verschillende monitoringslocaties, representatief voor weg-, spoorweg- en scheepvaartverkeer,

industrie en achtergrondomstandigheden. Dagelijkse atmosferische PM₁₀-filters werden gravimetrisch, chemisch en magnetisch geanalyseerd. Atmosferische PM₁₀-concentraties namen af volgens de gradiënt: scheepvaart > straatkant > industrie > trein. De belangrijkste bepalende elementen waren Na, Fe, Ca, K en Mg, waarbij de industrielocatie de hoogste concentraties en het meest gediversifieerde metaalprofiel vertoonde. De compositieprofielen voor straatkant- en treinlocaties waren nog maar eens vergelijkbaar, in overeenstemming met de voorgaande observaties van klimopbladeren blootgesteld op locaties met weg- en treinverkeer. De scheepvaartlocatie kan intermediair worden beschouwd tussen deze twee brontypen (weg- en spoorwegverkeer en industrie). De magnetische vingerafdrukken per locatie waren minder uitgesproken dan de chemisch gebaseerde karakterisering, waarbij alle monsters werden gedomineerd door mineralen met lage coërciviteit met korrelgroottes tussen 0,1 en 5 µm. Door alle informatie uit PM₁₀-filters (fijn stof en elementaire concentraties, magnetische eigenschappen) op te nemen, verbeterde het voorspellende vermogen van het RF-model in vergelijking met een model met alleen de fijnstofconcentraties (zoals standaard opgemeten door meetstations voor luchtkwaliteit), waarbij de nauwkeurigheid van de locatieclassificatie is toegenomen van 25% tot 76% en van 92% tot 100%. De gemeten magnetische eigenschappen en verhoudingen waren verantwoordelijk voor 16% van de beslissingsboomsplitsingen in het RF-model, terwijl de elementaire concentraties de belangrijkste classificatievoorspellers bleven. Gravimetrische fijnstofconcentraties droegen slechts 1% bij aan de locatieclassificatie, wat suggereert dat conventionele gravimetrische fijnstofmonitoring weinig vermogen heeft om bemonsteringslocaties te identificeren die aan specifieke fijnstofbronnen zijn blootgesteld. Deze discriminatie kan beter worden bereikt door het verzamelen van elementaire en magnetische informatie, waarbij magnetische analyses tijd- en kosteneffectiever zijn dan chemische bepalingen.

De bladmonitoringsresultaten waren in het algemeen in overeenstemming met de filterresultaten, zowel chemisch als magnetisch. Verder werd een sterke lineaire associatie ($R^2 = 0,74$) gevonden tussen de gemiddelde SIRM-bladwaarden en de

cumulatieve PM₁₀-filterladingen. Dit toonde aan dat actieve bladmonitoring van luchtverontreiniging op bronspecifieke fijnstoflocaties nuttig is om tijd geïntegreerde metingen van lokale atmosferisch fijn stof te verkrijgen, zoals gemeten met conventionele fijn stof meettoestellen, met het voordeel dat een groot ruimtelijk bereik mogelijk is met planten. De gezondheidsrelevantie van bronspecifiek fijn stof werd onderzocht door menselijke monocyt-macrophage cellen bloot te stellen aan luchtmonsters die werden verzameld op de PMF-locaties en het meten van hun pro-inflammatoire en oxidatieve stresspotentieel. Hoewel gebaseerd op een nogal beperkt aantal luchtmonsters, suggereerden de resultaten dat de trein (lage fijnstofconcentraties, hoge SIRM) en scheepvaart (hoge fijnstofconcentraties, lage SIRM) locaties het grootste potentieel voor gezondheidsrisico's hebben.

In het algemeen heeft dit doctoraatsonderzoek het toepassingspotentieel aangetoond van biomagnetische monitoring voor de karakterisatie van fijnstofbronnen (zogenaamd *fingerprinting*) in stedelijke omgevingen. Een eenvoudige toepassing van biomagnetische technieken om duidelijk te herkennen welke van de meerdere fijnstofbronnen op een bepaalde site het meest relevant zijn, is nog niet mogelijk. Toch hebben onze bevindingen aangetoond dat magnetische monitoring van groter nut zijn voor bronkarakterisatie en brontoewijzing van fijn stof dan de conventionele, gravimetrisch gebaseerde monitoringsbenadering. De studie en vaststelling van bronspecifieke magnetische en fysico-chemische signaturen en hun potentiële gezondheidsrisico's dragen bij aan de kennis over *fingerprinting* van fijn stof, wat essentieel is voor het ontwikkelen van betrouwbare, up-to-date instrumenten voor de monitoring van stedelijk fijn stof.

Summary	i
Samenvatting	vii
Contents	xiii
List of abbreviations and symbols	xv
Chapter 1	17
Introduction and scope	
Chapter 2	35
Morphological and elemental characterization of leaf-deposited PM in different source types: a microscopic investigation	
Chapter 3	75
Magnetic- and particle-based techniques for source apportionment of leaf-deposited PM	
Chapter 3.1	77
Magnetic- and particle-based techniques to investigate metal deposition on urban green	
Chapter 3.2	95
How does the amount and composition of PM deposited on <i>Platanus acerifolia</i> leaves change across different cities in Europe?	
Chapter 4	119
Leaf particle accumulation	
Chapter 5	161
Fingerprinting atmospheric PM sources towards urban monitoring and source apportionment	
Chapter 5.1	163
Setup and overview of a fingerprinting campaign of major urban PM sources	
Chapter 5.2	217
Health-relevance of source-specific PM: pro-inflammatory response across major PM sources	

Chapter 5.3	235
PM fingerprinting towards a magnetic-based source apportionment tool using leaves	
Chapter 6	257
General conclusions and future perspectives	
Appendices	271
Publications	281
Academic curriculum vitae	283
References	287

List of abbreviations and symbols

Abbreviations

AB	Abaxial leaf surface side
AC	Alternating electromagnetic field current
AD	Adaxial leaf surface side
ARM	Anhysteretic remanent magnetization
BC	Black carbon (equivalent to EC or soot)
BSE	Backscattered electron images
BVOCs	Biogenic volatile organic compounds
CA	Classification accuracy
CCSEM	Computer controlled SEM
cDNA	Complementary DNA
DC	Direct electromagnetic field current
DOY	Day of the year
EC	Elemental carbon (equivalent to BC)
ECD	Equivalent circular diameter
ED-XRF	Energy-dispersive X-ray fluorescence
EEA	European Environment Agency
EPA	United States Environmental Protection Agency
EU	European Union
HR-ICP-MS	High-resolution inductively coupled plasma mass spectrometry
IARC	International Agency for Research on Cancer
IF	Inter-comparison factor
IQR	Interquartile range, as Q3 minus Q1
IRM	Isothermal remanent magnetization
MAD	Mean absolute deviation
MD	Multi-domain
MR	Misclassification rate
mRNA	Messenger RNA
OC	Organic carbon
PAHs	Polycyclic aromatic hydrocarbons
PC	Principal component from PCA
PCA	Principal Component Analysis
PLI	Tomlinson pollution load index
PM	Particulate matter
PSD	Pseudo-single domain

Q1	First quartile
Q3	Third quartile
RF	Random Forest
RMSE	Root mean square error
SD	Single-domain
SEI	Secondary electron images
SEM	Scanning electron microscopy
SEM/EDX	SEM coupled with energy-dispersive X-ray spectroscopy
SIRM	Saturation isothermal remanent magnetization
SLA	Specific leaf area
SP	Superparamagnetic
TM	Trace metal
UFPs	Ultrafine particles, same as PM _{0.1}
VMM	Flemish Environment Agency
WHO	World Health Organization

Symbols

ARM _χ	ARM susceptibility
d ₅₀	Sampler efficiency > 50% at a particle diameter larger than
d _{eq}	Diameter of the equivalent sphere
H	Magnetic field (A m ⁻¹)
H _c	Coercivity
H _{CR}	Coercivity of remanence
M	Induced magnetization (T)
M _{RS}	Saturation remanent magnetization, equivalent to SIRM
M _S	Saturation magnetization
PM _x	PM with aerodynamic diameter below x μm (e.g. PM ₁₀ , PM _{0.1})
PM _{y-z}	PM with aerodynamic diameter between y and z μm (e.g. PM ₂₋₁₀)
Z	Atomic number
χ	Mass-specific magnetic susceptibility (m ³ kg ⁻¹)
χ _{LF}	Mass-specific low-field magnetic susceptibility (m ³ kg ⁻¹)
k	Volume magnetic susceptibility (dimensionless)

Chapter 1

Introduction and scope

“Begin at the beginning - the King said, very gravely - and go on till you come to the end: then stop”

-- Lewis Carroll

CHAPTER 1

1.1 The atmospheric world

Life begins with the very first taste of air, one might say. For humans, this coincides with the first cry as well. At our arrival into the atmospheric world, the role of respiratory gas exchange, until then ensured by the mother's placenta, is taken over by the lungs, which continue to develop until the two years of age (Donald et al., 1958; Smith et al., 2010). For the average human adult, an impressive alveolar surface area of 130 m² allows for a total lung volume of 4.3 L (Weibel, 2009). We exchange about ½ liter of air during each ventilation cycle at rest, inhaling every day more than 8,000 L of air (Arroyo and Schweickert, 2015). Breathing is essential to our survival; yet it can put our health and well-being at stake.

1.2 Air pollution

As a consequence of global industrialization and urbanization, air pollution is responsible for 4.2 million deaths each year (WHO, 2019). The contamination of the atmosphere with health-threatening pollutants is a worldwide phenomenon, with nine out of ten people breathing air exceeding the World Health Organization (WHO) air quality guidelines (WHO, 2018). Among those air pollutants, particulate matter (PM) poses the greatest risk to human public health (WHO, 2015). Due to their small size, airborne PM can penetrate into deep sensitive regions of the cardio-respiratory system, promoting a series of adverse health effects such as asthma (Anderson et al., 2012; Kampa and Castanas, 2008; Scapellato and Lotti, 2007; ; Terzano et al., 2010) and leading to premature mortality (Pascal et al., 2014). Both short- and long-term exposure to atmospheric PM have been associated with cardiovascular and respiratory diseases, and lung cancer mortality (Dockery and Pope, 1994; Pope et al., 2002).

1.3 Particulate matter

1.3.1 Sources and composition

The supply of clean uncontaminated air is compromised by natural and anthropogenic emissions of particulate matter. Natural PM includes e.g. sea salt, windblown dust,

pollen and volcanic ash, while anthropogenic PM originates from (motorized) vehicles, heating systems, agriculture and industrial processes (Almeida et al., 2006; Querol et al., 2004; Tian et al., 2016) (Figure 1.1). Anthropogenic PM can be emitted directly from a source (primary PM) or formed indirectly within the atmosphere (secondary PM), and can undergo further physical and chemical changes through e.g. coagulation and condensation phenomena during transport (Maher, 2011; Wilson et al., 2002). Primary PM originates primarily from combustion (e.g., vehicle engines) and high-temperature processes (e.g., smelting and welding operations), as well as from mechanical disruption processes (e.g., abrasion in rail tracks) and man- or wind-induced particle suspension events (e.g., street dust resuspension) (Guevara, 2016). Secondary PM is mainly formed by gas-to-particle conversion and condensation of gaseous compounds on pre-existing particles. Given such multiplicity of sources and transformation processes, PM consists of a complex mixture of fine solid and liquid particles suspended in the air, with both organic and inorganic fractions.

Main constituents of PM include elemental (EC) and organic carbon (OC), ammonia (NH_4^+), nitrates (NO_3^-), sulfates (SO_4^{2-}), sea salt, mineral dust, and a diversity of trace elements associated with certain emission sources (Pacyna and Pacyna, 2001; Putaud et al., 2004; Querol et al., 2001; Vercauteren et al., 2011; Viana et al., 2008). EC is often also denominated as black carbon (BC) or soot. While carbon emissions are mostly due to combustion processes (e.g. vehicle fuel combustion, biomass burning), $\text{NH}_4^+/\text{NO}_3^-/\text{SO}_4^{2-}$ are typical secondary aerosol components derived from agriculture (NH_4^+), vehicle exhausts (NO_3^-) or industry (SO_4^{2-}) (Buekers et al., 2014; Viana et al., 2008). Sea spray comprises ions of Cl, Na, Mg, with elements Al, Si, K, Ca, Ti, Mn, Fe, being characteristic for fugitive soil dust contributions (Almeida et al., 2006; Vercauteren et al., 2011). Trace elements can be related to fuel combustion (e.g., Pb, V and Ni), non-exhaust traffic emissions such as from tire abrasion (Cu, Zn, Cd), brake pads (Cu) or vehicle corrosion (Fe, Cu, Zn, Cd, Cr) and incinerator or industrial emissions (Cu, Zn, Cd) (Pacyna and Pacyna, 2001; Zhang et al., 2012). Within the organic fraction of PM, polycyclic aromatic hydrocarbons (PAHs) such as benzo[a]pyrene, are associated with incomplete combustion and biomass burning (Colman and Lerner, 2016).

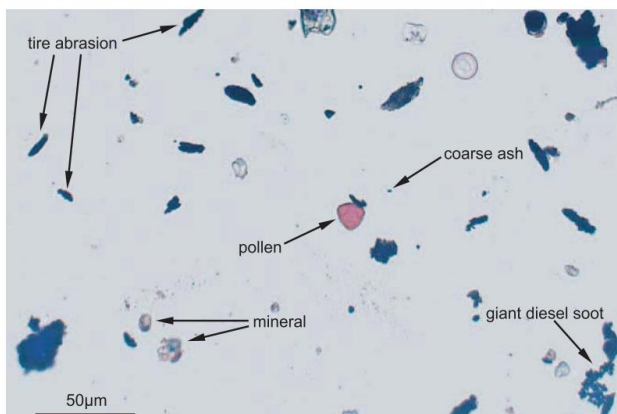


Figure 1.1 – Airborne particles collected over one week period using a passive sampler at a roadside location in Mainz, Germany. The image was obtained by Grobty et al. (2010) using a transmitted-light microscope.

1.3.2 Size and health effects

With a wide range in composition, PM is often classified according to the particle aerodynamic equivalent diameter, defined as the diameter of a theoretical sphere with unit density ($1,000 \text{ kg m}^{-3}$) that has the same aerodynamic properties as the particle in question. The size diameter of particles influences their transport, removal, collection, and respiratory tract deposition (Wilson et al., 2002) and, moreover, it can denote emission sources. PM_{10} , $\text{PM}_{2.5}$ and $\text{PM}_{0.1}$, refer to particles with an aerodynamic diameter smaller than $10 \text{ }\mu\text{m}$ (coarse PM), $2.5 \text{ }\mu\text{m}$ (fine PM) and $0.1 \text{ }\mu\text{m}$ (ultrafine PM), respectively. Coarse PM is usually associated with natural ocean spray, suspension of dust, mechanical processes such as mining and agricultural activity, while fine PM is mainly derived from combustion and high-temperature processes (Table 1.1). In Belgium, energy production and supply, transportation and industry were the largest sector contributors to $\text{PM}_{2.5}$ emissions in 2012 (Figure 1.2) (EEA, 2014).

Generally speaking, smaller particles travel longer in time and distance compared to larger particles (Table 1.1), including inside the respiratory tract. If not filtered out by the nasal and upper airways, coarse PM tends to settle in the upper throat and trachea; fine and ultrafine PM fractions can reach the alveoli and translocate into the bloodstream, as well as be transferred to the central nervous system (Guevara, 2016;

Kim et al., 2015). PM toxicity largely depends on the chemical composition as well. Particle number, size distribution (Vu et al., 2015), traffic- or combustion-related PM (Künzli et al., 2000; Laden et al., 2000), associated metals, organic compounds or biological species (Harrison and Yin, 2000; Schwarze et al., 2006) are among the components of health-relevance. Oxidative stress and inflammation are the main mechanistic precursors of PM-induced health effects (Breyse et al., 2013; Moretti et al., 2019; Schwarze et al., 2006). Evaluation of the oxidative stress and pro-inflammatory response (e.g. on human lung cells) after exposure to air can aid determining the health-risk potential of local conditions or PM sources (Moretti, 2018).

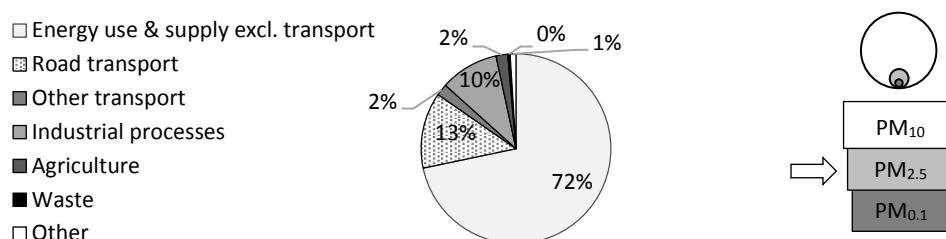


Figure 1.2 – Contribution of activity sectors to PM_{2.5} emissions in 2012 in Belgium (adapted from EEA, 2014), with a schematic representation of PM₁₀, PM_{2.5} and PM_{0.1} relative size.

Table 1.1 – Sources, composition, lifetime and travel distance of PM according to particle size for coarse and fine PM fractions. Based on Guevara (2016) and Kim et al. (2015).

	Coarse (PM ₁₀)	Fine (PM _{2.5})
Aerodynamic diameter	< 10 µm	< 2.5 µm
Sources	Resuspension of soil, street, road, industrial dust; grinding, mining, abrasion of surfaces; construction; coal and oil combustion; ocean spray	Combustion of gasoline, coal and oil; high temperature processes; smelters and steel mills; transformation products of NO _x and SO ₂ ; organics including biogenic organics
Composition	Soil and dust; coal and oil fly ash; metal oxides of Si, Al, Mg, Ti, Fe; CaCO ₃ , NaCl; pollen, mold spores and plant parts	NH ₄ ⁺ /NO ₃ ⁻ /SO ₄ ²⁻ ; EC; organic compounds such as PAHs; metals Pb, Cd, V, Ni, Cu, Zn; particle-bound water
Lifetime	Minutes to hours	Days to weeks
Travel distance	1 to 10 km	100 to 1,000 km

1.3.3 Monitoring challenges

According to the latest European report, emissions of primary PM₁₀ and PM_{2.5} have decreased by, respectively, 27% and 29% between 2000 and 2017, mainly due to the introduction or improvement of reduction measures across the energy, road transport and industry sectors (EEA, 2019a). Despite legislative and regulatory efforts to reduce PM levels, such as the inclusion of PM guidelines in the Gothenburg Protocol in 2012 (UNECE, 2012), atmospheric PM remains a serious global issue with concentrations too often exceeding the air quality reference values (Table 1.2). Between 2015 and 2017, 13% to 19% of the urban population in Europe were exposed to PM₁₀ concentrations, and 6% to 8% to PM_{2.5} concentrations, above the EU limit values; 42% to 52% and 74% to 81% of the population were exposed to, respectively, PM₁₀ and PM_{2.5} levels exceeding the more strict WHO guideline values set to protect human health (EEA, 2019a, 2019b). Still, no concentration thresholds have been identified below which no adverse health effects would be anticipated when exposed to PM (WHO, 2006).

Table 1.2 – Limit (EU) and guideline (WHO) values for PM₁₀ and PM_{2.5} daily- and annual-averaged concentrations. “n. a.” means “not applicable”.

	EU	WHO
Daily PM ₁₀	50 µg m ⁻³	50 µg m ⁻³
Annual PM ₁₀	40 µg m ⁻³	20 µg m ⁻³
Daily PM _{2.5}	n. a.	25 µg m ⁻³
Annual PM _{2.5}	25 µg m ⁻³	10 µg m ⁻³

To define and evaluate atmospheric PM levels by averaged-concentration values seems rather simplistic taking into account the complexity and multitude of physical and chemical properties of PM, particularly in urban contexts. In addition to that, urban atmospheric PM levels vary both spatially and temporally (Hofman et al., 2016; Jerrett et al., 2005; Wilson et al., 2005). The spatial variation, mainly linked to distance to contributing pollutant sources, differences in traffic intensity, and urban topology, can be observed within short distances or between neighboring streets, for instance. Temporal variations reflect day-to-day (meteorological and urban background

fluctuations), within-day (traffic dynamics) and microscale variability (single short-lived events) (Van den Bossche et al., 2015). Air quality assessments are, therefore, inherently challenging because high monitoring resolution needs, ideally, to be achieved in both space and time.

Current telemetric monitoring networks comprise accurate physicochemical monitoring instrumentation to trace atmospheric concentrations of PM, among others, at high temporal resolution. In conventional air quality monitoring stations, PM concentrations are typically determined gravimetrically from air-pumped filters. However, high investment and maintenance costs spatially limit the coverage of this type of monitoring. Moreover, it is generally recognized that morphological and chemical aerosol properties are more relevant to human health, and to reveal contributing emission sources, than the total PM mass or concentration (Kampa and Castanas, 2008; Pope and Dockery, 2006). Yet so far the latter is the only parameter routinely monitored. The morphological and chemical properties of PM are usually determined through time-consuming laboratory analyses, such as single-particle chemical or microscopic analysis, bulk analysis of trace elements or isotope ratios (Grobéty et al., 2010). The mentioned analyses can be used to gather detailed ad hoc information, however, carrying these out systematically at large temporal and/or spatial scales is unattainable.

1.4 Mitigation and biomonitoring strategies

Urban vegetation (e.g. vertical green and roof gardens, roadside shrubs) has been regularly documented to intervene positively in the problem of atmospheric pollution by promoting the capture and deposition of PM on its surface (Escobedo et al., 2011; Janhäll, 2015; Litschke and Kuttler, 2008; Weber et al., 2014). However, studies assessing the filtration performance of (existing or planned) vegetation in abating air pollutants concentration and/or quantity have not delivered undisputable outcomes until now. Modelling studies carried out for multiple locations have proposed air quality ameliorations of ca. 1% due to the removal of air pollutants (namely, O₃, NO₂, SO₂, CO, PM₁₀) by urban trees and shrubs (Escobedo and Nowak, 2009, Santiago, Chile;

CHAPTER 1

Nowak et al., 2006, nationwide United States; Selmi et al., 2016, Strasbourg, France). The urban forest of Beijing was estimated to remove 27.5 g air pollutants yr⁻¹ per m² canopy cover, from which 61% was PM₁₀ (Yang et al., 2005). Atmospheric transport model simulations in two UK conurbations suggested that planting trees in every available green space would reduce PM₁₀ concentrations from 7% (Glasgow) to 26% (West Midlands) (McDonald et al., 2007), while the roadside installation of a birch tree line in Lancaster, England, showed a > 50% reduction in the indoor PM levels of adjacent houses (Maher et al., 2013). An experimental study in a street canyon in Antwerp, Belgium, revealed an accumulation of 74 mg PM₁₀ per leaf m² by London plane trees (Hofman et al., 2014a). These authors estimated this leaf accumulation to reduce local atmospheric PM₁₀ concentrations from traffic in the street canyon between 6% to 10%. This filtration potential would decrease to 0.6 - 2.0% by taking the urban background into account, as only 10 - 20% of urban PM₁₀ concentrations in Antwerp was attributed to local traffic emissions (Hofman et al., 2014a). This proportion is, in reality, commonly observed across Europe: road transport emissions accounted for 10% and 11% of total PM₁₀ and PM_{2.5} inventory emissions in 2017 (EEA, 2019; Keuken et al., 2013). Contrastingly, the mitigation of atmospheric pollutants by near-road urban forests in the northern Finnish climate revealed to be almost negligible or insignificant (Setälä et al., 2013; Viippola et al., 2018), with exception of coarse PM, for which levels in tree-covered areas were ca. 23% lower than in open areas (Yli-Pelkonen et al., 2017). Although promoting particle deposition, vegetation can also lead to an increase in air particulate levels through direct emissions (e.g. pollen, biogenic volatile organic compounds) or by reducing the air flow, thus preventing the dilution and dispersion of pollutants (Amorim et al., 2013; Gromke and Ruck, 2009; Grote et al., 2016; Jeanjean et al., 2017; Vrancx et al., 2015).

Despite the complex interactions between vegetation (e.g. leaf porosity) and airborne PM, green elements such as plant leaves are valuable biological sensors for time-integrated monitoring of habitat and air quality (e.g., Grote et al., 2016; Hofman et al., 2017; Kardel et al., 2012; Mo et al., 2015; Sawidis et al. 2011). The micro-morphological attributes of plant leaves, with sticky epicuticular waxes, irregular structure and

topography, also often containing trichomes, promote the deposition and accumulation of atmospheric particulates on their surface (Figure 1.3) (Beckett et al., 2000; Grote et al., 2016; Liu et al., 2012a; Weerakkody et al., 2018) by gravitational sedimentation, impaction, interception and diffusion (Litschke and Kuttler, 2008).

Leaf monitoring offers a more rapid and cost efficient strategy than e.g. the collection of air-pumped filters, thus, enabling for studies with high spatial monitoring resolution. This is mostly important to investigate site-specific conditions within typically heterogeneous urban settings, as particle size and composition are known to vary considerably from source to source (Amato et al., 2009, 2011; Vercauteren et al., 2011). Previous studies have investigated PM leaf accumulation through microscopy (e.g. Wang et al., 2015a), gravimetrically (Dzierżanowski et al., 2011; Hofman et al., 2014a; Przybysz et al., 2014; Sgrigna et al., 2015; Sæbø et al., 2012), chemically (De Nicola et al., 2008), and even magnetically (Hofman et al., 2013, 2014b; Kardel et al., 2012b; Lehndorff et al., 2006). Biological sensors other than plant leaves have been used to magnetically monitor their surrounding environment or exposure conditions (i.e., biomagnetic monitoring), including lichens, mosses, tree bark, insects, crustaceans, and mammal and human tissues (Hofman et al., 2017; Muxworthy, 2015; Sant’Ovaia et al., 2015; Vuković et al., 2015; Wuyts et al., 2018).

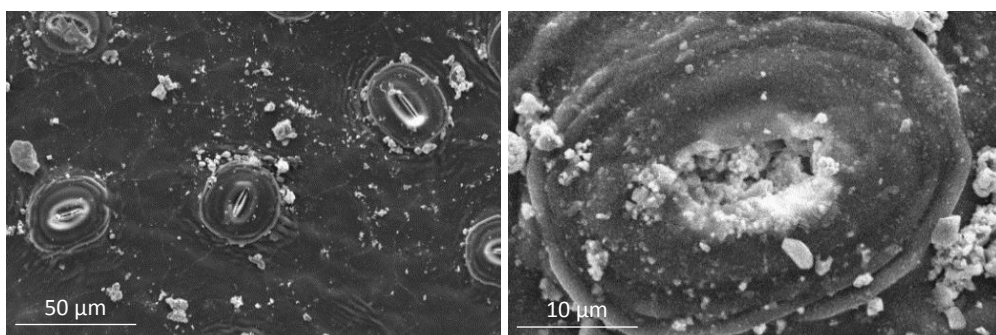


Figure 1.3 – PM deposition on the surface of ivy leaves, explored with scanning electron microscopy. Different particle shapes and sizes are observed, including particles in the PM_{0.1} range, able to enter the leaf stomata (a close-up is shown at the right side).

1.5 Biomagnetic monitoring[†]

Current and future air quality monitoring strategies face the dual need for greater spatial coverage and information on health-related pollutant species, at feasible cost. Biomagnetic monitoring, evaluating magnetic properties of biological material such as leaves, may potentially serve both purposes, acting as a widely applicable, low-cost method for assessing health-relevant pollutant species. Biomagnetic monitoring is a growing application in the field of environmental magnetism, i.e., the use of magnetic measurements to study environmental systems, driven by the fact that atmospheric pollution, in particular urban PM, invariably contains levels of magnetic minerals (e.g. iron oxides like magnetite, Fe_3O_4 , and hematite, $\alpha\text{-Fe}_2\text{O}_3$) that are easily measurable magnetically (Hunt et al., 1984; Matzka and Maher, 1999; Thompson and Oldfield, 1986). Elemental iron constitutes between 6% to 18% of urban atmospheric PM, of which magnetic iron oxides and hydroxides comprise 10% to 70% (Dedik et al., 1992; Weber et al., 2000). Sources of magnetic minerals include both natural, crustal PM sources, such as from volcanic eruptions and wind erosion of soil and dust, and anthropogenic sources, including industrial and vehicular combustion, heating and abrasion processes (Thompson and Oldfield, 1986). During industrial, domestic or vehicle combustion, carbon and organic material are released by oxidation while iron, occurring as an impurity in fossil fuels, forms non-volatile, small glassy spherules due to melting (Hofman et al., 2013). Depending on the fuel type and temperature of combustion, the resultant fine-grained magnetic spherules contain variable amounts and grain sizes of magnetite and/or hematite (Matzka and Maher, 1999). Traffic-related PM acts as a prevalent source of magnetic particles not only due to the exhaust, combustion emissions, but also due to metallic wear and abrasion (of vehicle components and road pavement, railway traffic) and re-suspension of street and road dust (McIntosh et al., 2001; Rai, 2013). Different types of industry (e.g. cement productions, smelters, steelworks) also emit distinctive magnetic PM, likely due to differences in source material, combustion temperature and/or redox conditions (Hansard et al., 2012; Wang et al., 2015b). As a consequence, magnetic particle size is also wide-ranging, varying from 0.1 - 1 μm (Mitchell and Maher, 2009), over 0.3 - 3 μm

(Matzka and Maher, 1999) to 5 - 8 μm (Sant'Ovaia et al., 2012). Small and spherical particles are associated with exhaust emissions, while abrasion releases and re-suspended dust tend to be coarser and more angular (McIntosh et al., 2007). More recently, magnetite combustion-related, airborne nanospheres < 200 nm were detected in the human brain, hypothesized to have entered directly via the olfactory bulb (Maher et al., 2016).

Biomagnetic monitoring techniques are most sensitive to ferro(i)magnetic, remanence-bearing particulates (Evans and Heller, 2003). Ferromagnetic materials (*sensu lato*) have a tight atom packing within their crystal structure, enabling quantum-mechanical exchange coupling between atomic permanent magnetic moments. This causes localized ordering of the magnetic moments even in the absence of an applied external field, providing ferromagnetic minerals the ability to retain remanent magnetization (contrary to paramagnetic materials). Depending on the sign and magnitude of the exchange interaction after application of a magnetic field, ferromagnetic minerals (*sensu lato*) can display: (1) ferromagnetic (*sensu stricto*) behavior due to positive exchange, (2) ferrimagnetic behavior due to unequal negative exchange, or (3) antiferromagnetic behavior due to equal negative exchange, in absence of a magnetic field (Figure 1.4). Hematite ($\alpha\text{-Fe}_2\text{O}_3$) is a known antiferromagnetic (or weakly ferromagnetic) mineral and widespread in rocks and soil, while magnetite (Fe_3O_4), a ferrimagnetic mineral, displays the strongest magnetism of any transition metal oxide (Evans and Heller, 2003; Teja and Kohl, 2009). Other strong ferrimagnets include iron oxide maghemite ($\gamma\text{-Fe}_2\text{O}_3$), while weaker, almost antiferromagnetic, behavior is exhibited by iron oxyhydroxides (goethite, $\alpha\text{-FeO(OH)}$) and iron sulfides (pyrrhotite, Fe_7S_8 ; greigite, Fe_3S_4). Anthropogenic PM contains different ferromagnetic phases, with Fe partly substituted by other cations like Ni, Co, Cr, Al, Mg (Hoffmann et al., 1999), resulting in a so-called magnetite-, maghemite-, hematite-like behavior when magnetically analyzed.

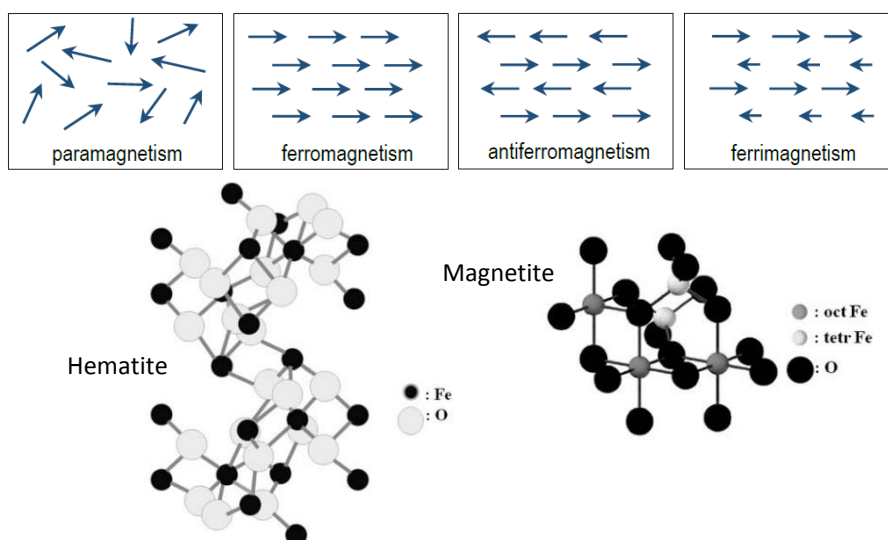


Figure 1.4– Magnetic moments alignment for paramagnetic, ferromagnetic, antiferromagnetic and ferromagnetic materials, after removal of an applied magnetic field. The crystal structures of hematite (antiferromagnetic) and magnetite (ferrimagnetic) (from Teja and Kohl, 2009) are shown.

Different types of ferromagnetic minerals can be distinguished using a set of diagnostic magnetic measurements, based on the determination of magnetic properties such as magnetic susceptibility (χ) and saturation isothermal remanent magnetization (SIRM) (Figure 1.5). These magnetic parameters are often used for environmental magnetic assessments (Flanders, 1994; Verosub and Roberts, 1995) on e.g. soils (Declercq et al., 2019; Lecoanet et al., 2001; Lu and Bai, 2006; Maher, 1986), marine sediments (Booth et al., 2005; Zhang et al., 2007), street dust (Magiera et al., 2011; Yang et al., 2010; Zhang et al., 2012), air-pumped filters (Muxworthy et al., 2001, 2003; Revuelta et al., 2014; Sagnotti et al., 2006), and a variety of biological matrices like leaves (Hofman et al., 2017; Sagnotti et al., 2009). Higher magnetic concentration values, in χ and SIRM, are typically measured with increasing proximity to PM sources, and with increasing source strength (e.g., traffic volume, industrial emissions) (Magiera et al., 2011; Mitchell and Maher, 2009; Moreno et al., 2003; Yang et al., 2010). An overview of different reported biological sensors, with ranges of χ and SIRM measured values, can be found in Hofman et al. (2017).

Magnetic hysteresis (Figure 1.5) is the magnetic response (magnetization, M) of a material to sweeping magnetic fields (H), and can be interpreted as a magnetic mineralogical signature. The height of the hysteresis loop is a function of the concentration and type of magnetic minerals, while the width of the loop is controlled by the material magnetic coercivity, influenced by both mineralogy and grain size (Dunlop and Özdemir, 1997). The shape of the hysteresis loop can be reduced to a few well-defined magnetic properties, including the saturation magnetization (M_S), the saturation remanent magnetization (M_{RS} ; also termed SIRM), the coercivity (H_C) and the coercivity of remanence (H_{CR}). By submitting a sample to a large saturating magnetic field (H), it achieves saturation (M_S), with SIRM being the (isothermal) magnetization remaining (M_{RS}) after removal of the saturating field (at $H = 0$). A sample's coercivity and coercivity of remanence (H_C and H_{CR}) are defined as the negative, opposite fields required to reduce, respectively, its magnetization and remanent magnetization (M_S and M_{RS}) back to zero (Evans and Heller, 2003). While M_S is a measure of magnetic concentration, the SIRM parameter depends on the magnetic mineralogy and grain size besides being a concentration-indicator; both H_C and H_{CR} are independent of concentration and controlled by grain size and mineralogy. Generally speaking, a sample's coercivity reflects how easily it is to magnetically reach (as well as revert) saturation: low-coercivity or "soft" minerals can get saturated at relatively low magnetic fields, high-coercivity or "hard" minerals magnetize only at high fields. Likewise, low-coercivity minerals also require smaller negative fields than high-coercivity minerals to revert the achieved saturation. Magnetite is considered a "soft" mineral, while hematite is a "hard" mineral. The (mass-specific) magnetic susceptibility χ , is derived from the volume magnetic susceptibility (k), which is the slope of the hysteresis curve (i.e., the gradient of the M acquired in response to the applied H) and illustrates how easily the sample material can get magnetized (Thompson and Oldfield, 1986).

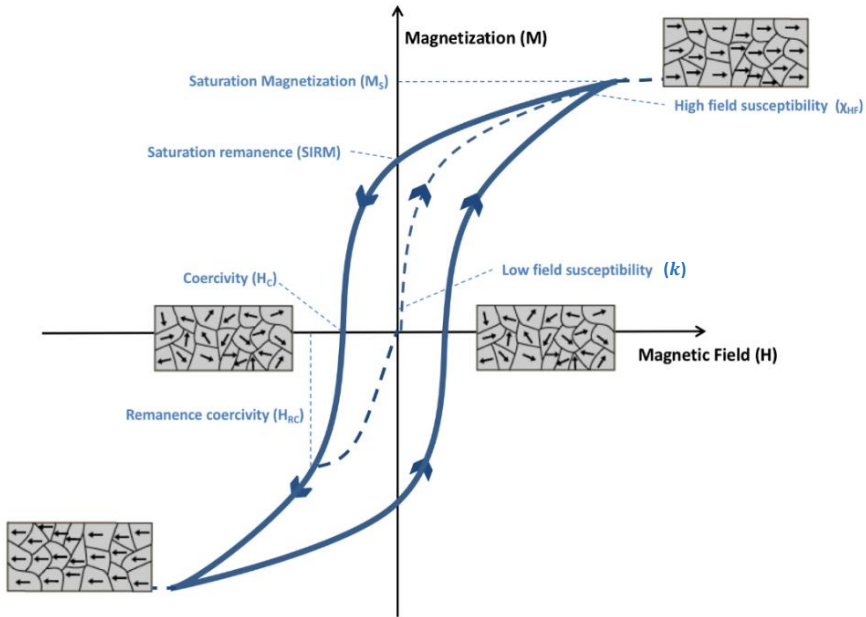


Figure 1.5 - Full magnetic hysteresis (M-H) loop of a ferromagnetic-paramagnetic mineral mixture and most frequently measured magnetic properties in magnetic studies. The magnetic moments ordering is schematically shown for the various stages within the hysteresis loop. The low- and high-field susceptibility are given by the slope of the M-H curve at low- and high-field magnetic fields, respectively. The dotted lines represent the initial magnetization (upper right quadrant) and the sample's magnetic remanence at remanence coercivity (lower left quadrant; drops to zero). Image from Hofman et al. (2017).

As mentioned, the magnetic hysteresis loop and derived properties (Figure 1.5) can provide mineralogical and compositional information, as well as information on grain size, which controls the number of magnetic domains (i.e., regions with uniform magnetization direction) into which the mineral crystal can be subdivided (Evans and Heller, 2003). But rather than defining the size of particles per se, domain structure is a defining characteristic of the magnetic particles. The optimal magnetic-domain size is mineral dependent; a 40 nm magnetite particle is analog to a 10 μm hematite particle, as they are both single-domain (Dunlop, 1981). The magnetization inside a particle is uniform for small particles, and the grain is single-domain (SD; ~ 30 - 80 nm for magnetite) (Figure 1.6). Above a certain size (~ 80 nm) it becomes energetically favorable to have more than one domain and the particle is considered multi-domain (MD) (Muxworthy and Williams, 2009). Small MD particles between ~100 nm to

~1000 nm (for magnetite) display characteristics similar to SD particles, and so, they are commonly referred to as pseudo-SD (PSD). Very small SD particles (< 30 nm) are not stable due to thermal energy and are said to be superparamagnetic (SP). These SP particles are not able to carry any room temperature remanence, but contribute significantly to the magnetic susceptibility (Dunlop 1973, 1986; Thompson and Oldfield, 1986).

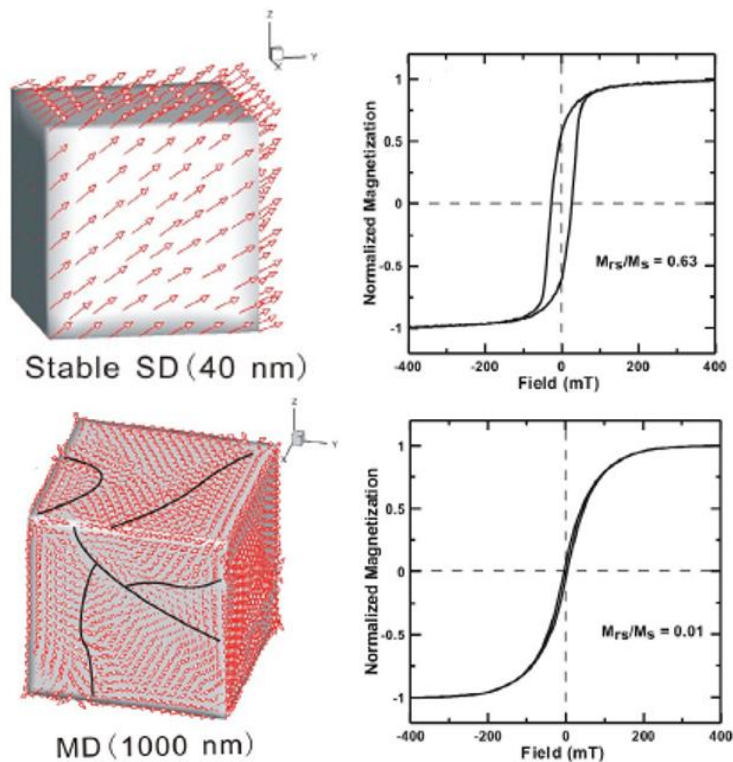


Figure 1.6 – Hysteresis loops and associated theoretical magnetic domain states, single-domain (SD - top) and multi-domain (MD - bottom), for a uniaxial magnetite cube (adapted from Liu et al., 2012b).

Biomagnetic monitoring of PM offers the opportunity to identify and quantify the sources and deposition of these particles at high spatiotemporal frameworks. Apart from some generalized, well-sounded associations (e.g. link with traffic emissions), the determination of atmospheric PM, and other health-relevant compounds, by magnetic parameters has not been developed up till now to the point where it can be implemented universally as a monitoring and regulatory strategy. Challenges remain

CHAPTER 1

mainly due to the spatiotemporal variation and source-specific physicochemical composition of atmospheric PM, and to the fact that magnetic particles only make up part of those PM emissions. At the moment, the biomagnetic approach to study environments with comparable source contributions is quite straightforward and feasible (Hofman et al., 2017); yet, its potential for the identification and discrimination of various PM sources in the multi-source urban environment is limited.

[†]Partially based on: Hofman, J., Maher, B.A., Muxworthy, A.R., Wuyts, K., Castanheiro, A., Samson, R., 2017. Biomagnetic monitoring of atmospheric pollution: a review of magnetic signatures from biological sensors. *Environmental Science & Technology* 51, 6648–6664.

1.6 Thesis objectives and outline

The overall objective of this PhD research was to investigate and to develop a biomagnetic monitoring approach for fingerprinting atmospheric particulate matter in urban settings. In the context of this research, fingerprinting referred to the investigation of signature features (or fingerprints) of PM that are characteristic of certain environments and/or can be associated with specific source types of urban pollution. A range of analytical techniques was employed in addition to the magnetic characterization in an attempt to obtain comprehensive source-specific PM fingerprints. Such knowledge is required to further advance biomagnetic strategies as an effective tool for PM fingerprinting and monitoring within multi-source urban environments. The following specific objectives were engaged for this:

1. Characterization of major urban source types of PM pollution:
 - a. by means of magnetic, chemical and microscopic techniques, to obtain source-specific magnetic, chemical and morphological PM fingerprints;
 - b. in terms of pro-inflammatory response and oxidative stress potential, to explore the associated health-risk potential.
2. Investigation of potential associations between source-specific magnetic, chemical and morphological PM fingerprints.

3. Evaluation of leaf biomagnetic monitoring as a strategy to infer atmospheric PM levels and characteristics of major PM contributing sources.

The present chapter (*Chapter 1*) describes the context, problem statement and objectives of this PhD research, and provides a short introduction on atmospheric PM and biomagnetic monitoring. In *Chapter 2*, leaf-deposited PM from environments mainly exposed to different pollution sources (named sources or source types, in the framework of this research) are investigated microscopically for their morphological characteristics and elemental composition. *Chapter 3* comprises two subchapters in which dedicated particle-analysis is combined with leaf magnetic investigation to discriminate between different source types (*Chapter 3.1*) and between urban streets and parks across 20 European cities (*Chapter 3.2*). To gain more insight on the accumulation of PM on plant leaves, a multi-approach leaf monitoring campaign is discussed in *Chapter 4*. The information gathered on the analytical techniques used and their potential for source characterization are applied in a large PM fingerprinting (PMF) project in *Chapter 5*. The PMF project comprises the monitoring and fingerprinting of five different source locations (road, railway and shipping traffic, industry and a background site) based on air-pumped samples (*Chapter 5.1*) and exposed plant leaves (*Chapter 5.3*), to obtain source-specific signatures and evaluate the applicability of leaf magnetic monitoring of PM. Among other aspects, the health-risk potential of the studied source types is also explored in terms of pro-inflammatory response (*Chapter 5.2*). The main results and general conclusions of this PhD research and perspectives for future research are given in *Chapter 6*. An overview of the research challenges and topics throughout this PhD thesis is presented in Figure 1.7.

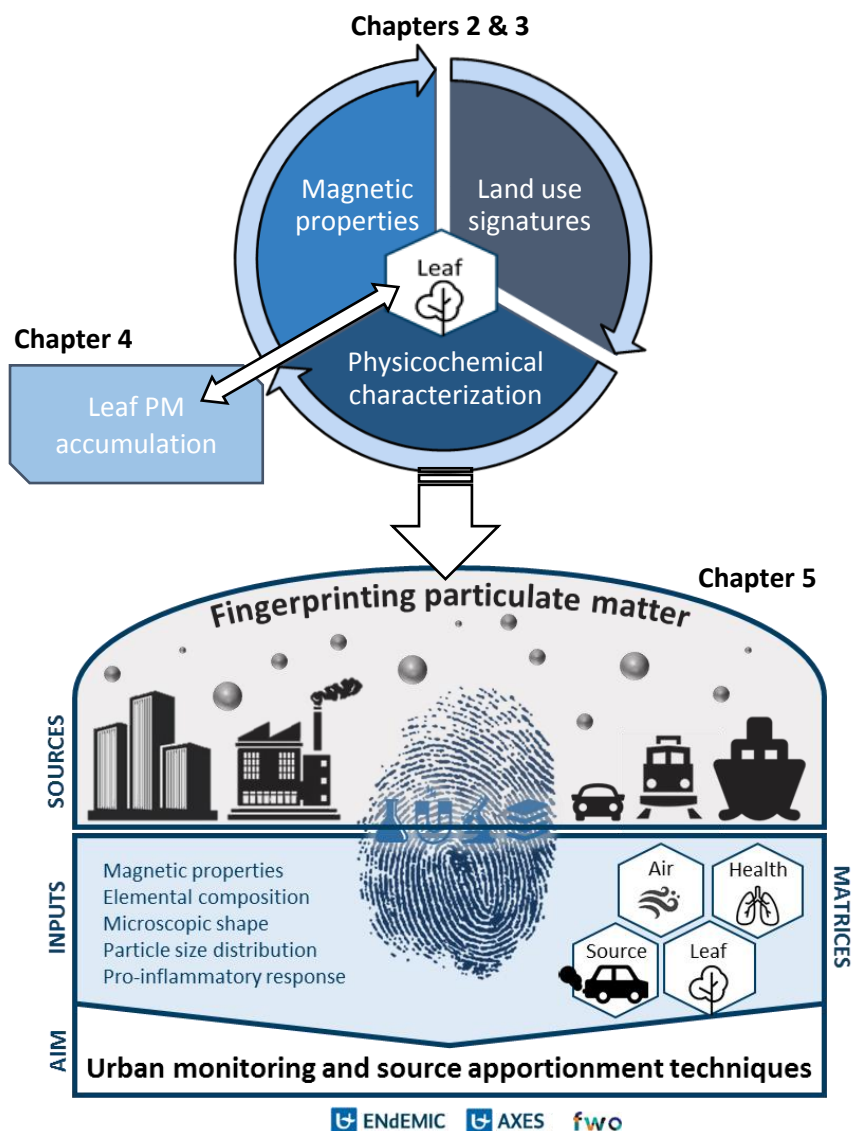


Figure 1.7 – Schematic overview of the research challenges and overall objective of this PhD research, with indication of the chapters in which they are discussed.

Chapter 2

Morphological and elemental characterization
of leaf-deposited PM from different source
types: a microscopic investigation

“What is essential is invisible to the eyes”

-- Antoine de Saint-Exupéry

Based on: Castanheiro, A., Wuyts, K. Hofman, J., De Wael, K., Samson, R., 2020. Morphological and elemental characterization of leaf-deposited particulate matter from different source types: a microscopic investigation (under preparation).

Abstract

Within this chapter, the morphological and elemental characteristics of PM deposited on leaves from five different environments (forest, rural, roadside, train, industry) were thoroughly investigated using SEM/EDX (scanning electron microscopy coupled with energy-dispersive X-ray spectroscopy). These characteristics were then explored in an attempt to identify morphologies and/or elements typical of the various source types for source apportionment purposes. To our knowledge, this study is the first to analyze such a large number of leaf-deposited particles (almost 40,000) from sites mainly exposed to different PM sources, yet within the same region. While regional PM influences are present, results demonstrated the potential of SEM/EDX as a method to fingerprint source-specific leaf-deposited PM. Taking into account the particle size diameter and certain composition indicators allowed to pinpoint, for instance, traffic and industrial sources within the tested sites.

2.1 Introduction

To use plant leaves as a monitoring tool for PM demands for a comprehensive understanding on the features and mechanisms underlying leaf PM deposition. Particle-based techniques, such as scanning electron microscopy coupled with energy-dispersive X-ray spectroscopy (SEM/EDX), applied at leaf level, allow for a close-up insight on the typical predominant characteristics of PM. Although the application of SEM/EDX to investigate particles deposited onto leaves is not original (e.g., Baldacchini et al., 2019; Ottel   et al., 2010; Sgrigna et al., 2016), it is often limited in terms of particles or source types considered. The experiment of Ottel   et al. (2010) was rather dedicated to counting particles deposited onto common ivy, only describing the composition of three leaf-deposited particles. After washing *Quercus ilex* leaves, the subsequent filters were analyzed by Sgrigna et al. (2016) for a total of 100 particles per

sample, overall up to 3,129 particles from two sampling locations and at two heights. Baldacchini et al. (2019) considered a total of 200 leaf-deposited particles per *Quercus ilex* tree (50 per leaf sample) at seven locations within the same Italian urban forest. Yet, research on how many particles are necessary to properly represent the overall leaf-deposited particles, is not available until now.

To our knowledge, the application of SEM/EDX to characterize leaf-deposited PM emitted and/or present at distinct urban contexts is still scarce, with the exception of the (SEM/EDX and SIRM-based) comparison of leaf-deposited particles at park and street sites by Baldacchini et al. (2017) (Chapter 3.2 of this thesis). The latter study, across 20 European cities from 18 countries, included sampling sites from distinct climates and background levels of pollution, which complicated further source apportionment besides the distinction between park and street conditions. The identification and characterization of specific PM sources might thus be better achieved by focusing on distinctive urban environments in a single city or region. Therefore, the present study reports on the morphological features and elemental composition of ca. 40,000 leaf-deposited particles on ivy (*Hedera sp.*) leaves collected from five source sites (forest, rural, roadside, train, industry) in the region of Antwerp, Belgium. The main objectives were to investigate how morphological and elemental characteristics of leaf-deposited PM differed across different source types, and to assess the potential of leaf microscopic (SEM/EDX) monitoring for source apportionment of PM. The morphological and elemental characterization of leaf-deposited PM, herein reported, considered the deposition of particles on both leaf sides (abaxial and adaxial). Whether the particles analyzed in this study were representative of the overall leaf-deposited particles, was also explored.

2.2 Materials and methods

2.2.1 Study area and leaf sampling

The province of Antwerp is the most populated region in Belgium, with ca. 1,845M inhabitants and a density of 644 inhabitants per km² (Flanders, 2018). The city of

Antwerp contains the second largest harbor in Europe and, consequently, has a prominent industrial area, being also characterized by high traffic intensity roads and highways. In order to investigate leaf-deposited PM under the influence of distinct environments and anthropogenic pressures, leaf samples were collected from five sites considered to be mainly exposed to different source types of pollution, namely, forest, rural, roadside, train and industry (Figure 2.1). The leaf samples collected in this study were also considered in Chapter 3.1 for their magnetic enrichment and metal deposition. The Forest and Rural sampling sites were located at Merksplas, ca. 37 km from Antwerp's city center to avoid the influence of road and railway traffic and industrial emissions. These sites were located 300 m apart in the same residential/rural area. While the Forest site (51°21'22.44"N, 4°52'53.95"E) was located in a forested area, at 30 m distance from a low-traffic road, the Rural site (51°21'13.21"N, 4°53'2.79"E) was located only 1 m away from a low-traffic road, considered the main local PM contributing source. The mentioned roads mostly serve the inhabitants of the small residential/rural neighborhood, resulting in low traffic intensities. The Roadside location (51°11'33.90"N, 4°25'19.80"E), on the other hand, was close to traffic lights and only 7 m away from a busy road intersection, resulting in high traffic densities and a lot of stop-and-go traffic. The presence of tram lines, at 30 m distance, is considered to be of minor influence compared to the high road traffic intensity on site. The Train site (51° 9'35.47"N, 4°30'6.60"E) was in rural Boechout, only 5 m distant from a railway track and with negligible road traffic contribution. Finally, the Industry site (51° 9'52.41"N, 4°20'14.00"E) was situated in Hoboken, within a non-ferrous metal industrial complex, 4 m distant from a road with low/medium traffic intensity that is mostly used by the factory workers and for cargo loading/unloading. The main contributing source on site is related with the industrial processing and recycling of precious and other (non-ferrous) metals (e.g., Ag, Au, Pt, Se, Bi, Pb, Cu, Ni), with reported exceeding emissions of As, Cd and Pb (VMM, 2017).

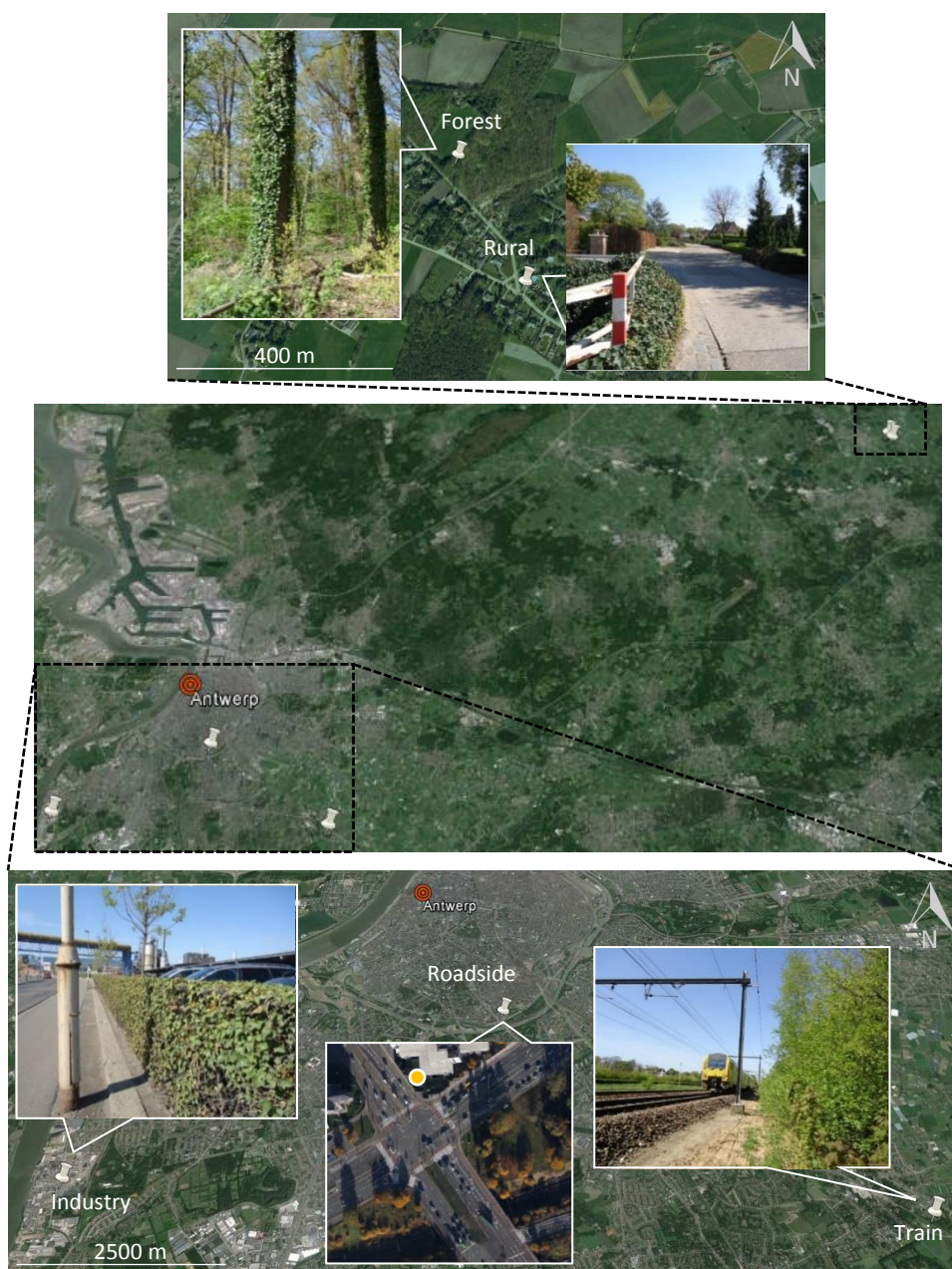


Figure 2.1 – Overview map and illustration of the five monitoring sites (forest, rural, roadside, train, industry) in the region of Antwerp, Belgium (Googole Earth).

Leaves of common ivy (*Hedera sp.*) plants were sampled in spring 2014 (on March 27 and April 16), with a total of eight fully-developed undamaged leaves per test site. Ivy was selected as test species as it is widely spread in both natural and urban settings, and as it was present within all the sampling locations. The collected ivy leaves were

picked from the outer canopy of existing plants at 1.30 - 1.70 m above ground, in order to minimize the contribution of soil dust resuspension and to simulate human inhalation height. Although fully-developed leaves were targeted for sampling, the age of the collected leaf samples was not known, as this monitoring campaign was passive (i.e., collection of existing leaves). But as this study looked into the characterization of site-specific, thus, source-dependent leaf-deposited particles, instead of quantifying their total accumulation level, we considered the uncertainty in leaf age to be of less relevance. No precipitation was recorded during leaf sampling nor on the previous three days.

2.2.2 Scanning electron microscopy coupled with energy-dispersive X-ray spectroscopy

For each collected ivy leaf, a circular sample with 1 cm in diameter (equivalent to ca. 79 mm² leaf surface area) was cut out for SEM/EDX analysis. The leaf SEM samples were retrieved from the center of the leaf lamina avoiding the main veins, by using a metallic puncher. From the total of eight leaves per sampling site, four leaves were used to obtain adaxial (upper leaf side) samples and the remaining four leaves to obtain abaxial (lower leaf side) samples. Samples were dried at room temperature for a minimum of three days, prior to be vacuum coated with carbon. For SEM/EDX analysis, a field emission gun – environmental scanning electron microscope (FEG-ESEM) equipped with an EDX detector was employed (Quanta 250, FEI, USA; at AXES and EMAT research groups, University of Antwerp, BE). The operating parameters used were: accelerating voltage of 20 kV, sample chamber pressure of 10⁻⁴ Pa, working distance of 10 mm, spot size of 3.6.

All leaf SEM samples (n = 40, 8 per sampling site: 4 adaxial and 4 abaxial) were examined for their deposited particles (Figure 2.2, inset A) in a total surface area of ca. 6 mm² per leaf. The SEM/EDX analysis was automatized and computer controlled (CCSEM) using the INCA software (Oxford Instruments, UK) for feature detection and analysis. At the beginning of each SEM session, leaf samples were briefly explored

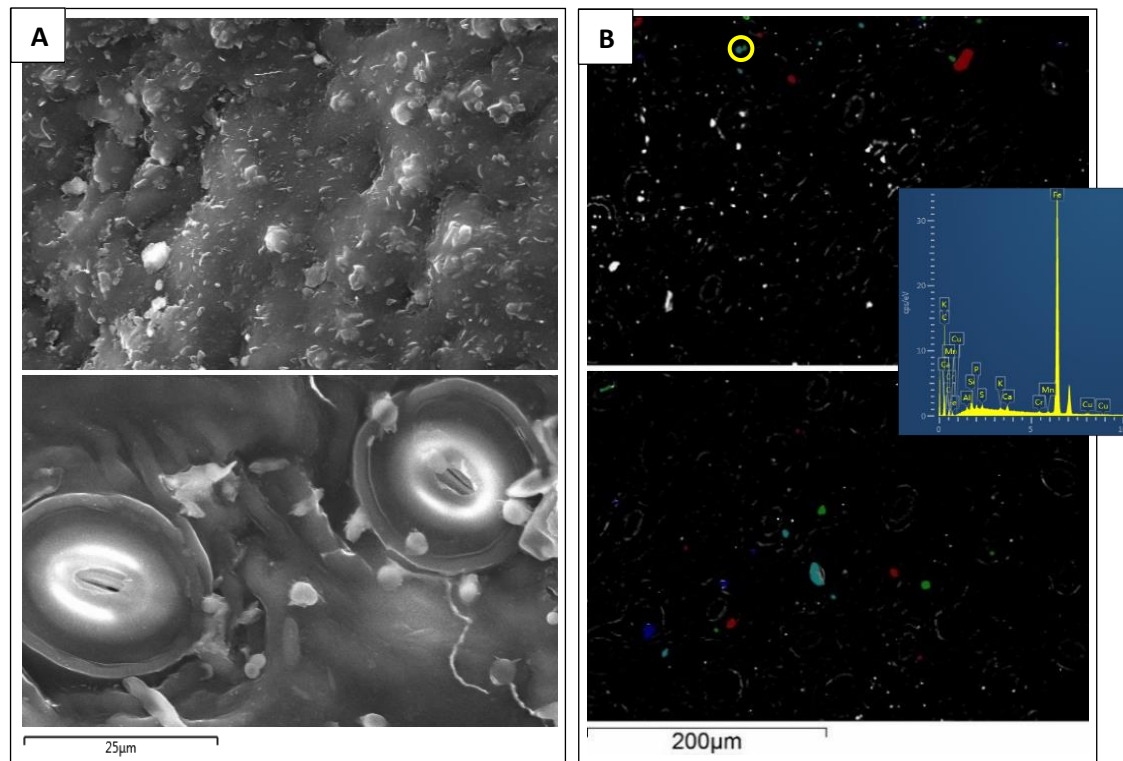
using both secondary electron images (SEI) (Figure 2.2, inset A) and backscattered electron images (BSE) (Figure 2.2, inset B). While SEI show a three-dimensional perception of the surface being analyzed (leaf surface and leaf-deposited particles), BSE provide information about its chemical composition with bright, high Z elements (deposited particles) contrasting with the leaf background surface. The detection and analysis of leaf-deposited particles by CCSEM was performed in backscattered electron configuration (Baldacchini et al., 2019). For each leaf sample, the software proposed feature detection was evaluated by comparing the secondary and backscattered electron images to ensure that all deposited particles (clearly visible in the SEI) were correctly detected at the BSE, while organic components of the leaves (e.g., trichomes) were ignored and particulate agglomerates were properly decomposed into their constituent particles. The feature thresholds of the backscattered electron detector signal (upper and lower gray level thresholds, related to the intensity of the detected signal) were adjusted, if needed, so that all features (i.e., individual deposited particles) within those thresholds were set to white and all others were set to black (Inca, 2006) (Figure 2.2, inset B). As the position and thickness of each leaf sample could affect the feature thresholds, this procedure of feature checking and adjusting of the thresholds was done for each sample, for the first segmented fields.

The central area of each leaf sample was selected and automatically segmented into 50 fields with fixed dimensions of $414 \mu\text{m} \times 285 \mu\text{m}$ each in a x - y plane. The software was set to analyze 20 particles (or features) per field, which delivered around 1,000 leaf-deposited particles for a total of 50 fields. The CCSEM scanned the particles “row-by-row”, first within the x direction before proceeding in the y direction, and this occurred consecutively until a total of 20 particles were found within each field, before moving to the next field (Figure 2.2, inset B). For the magnification used (500x), an interaction volume (i.e., the excitation volume under the sample surface as a result of the interaction with the electron beam (Marinello et al., 2008; Zhou et al., 2006)) equivalent to, at least, $1 \mu\text{m}$ in diameter was required to ensure that the deposited particles were correctly identified from the leaf surface, and were recognizable from particle agglomerates. Given that the identification of leaf-deposited particles was

computer controlled and not permanently assisted by a SEM operator, a more conservative minimum size threshold was chosen. Only particles with equivalent circular diameter (ECD; the diameter of a circle with the same area as the projected particle on the x - y plane (Xie et al., 2005), defined as the square root of $(4 \times \text{area}) / \text{perimeter}$ (Inca, 2006)) equal or larger than $2 \mu\text{m}$ were considered. The particles' ECD obtained by SEM/EDX was defined as particle size diameter in the context of this study. No maximum particle size threshold was defined in the software, but particles with an ECD larger than $50 \mu\text{m}$ were disregarded from the data analysis. From the 40 leaf samples, a total of 39,409 leaf-deposited particles were analyzed by SEM/EDX. For each particle (i), the CCSEM mode delivered a range of parameters such as the field in which the particle was found with x and y coordinates within that field, as well as their morphological features (e.g., ECD, perimeter, area, aspect ratio, shape) and composition percentage C_{xi} (% , m/m) in terms of the relative weight of each element present (x). Chemical composition (C_{xi}) was obtained for elements with atomic number (Z) between 6 (C) and 93 (Np). As the leaf samples were carbon-coated and EDX is unable to correctly measure oxygen, elements C and O were disregarded from the obtained composition. A total of 64 chemical elements were considered, with Na, Mg, Al, Si, P, S, Cl, K, Ca, Fe, Cu and Pb being the overall main identified elements in the leaf-deposited particles. The aspect ratio and shape factor estimated by SEM/EDX are useful indicators for evaluating the morphology of deposited particles. The aspect ratio was automatically calculated as the ratio of maximum to minimum Feret diameter (i.e., dimensionless, as maximum and minimum Feret diameters consist of the furthest and shortest distance between any two parallel tangents on the particle) (Inca, 2006). The shape factor, calculated as the ratio of the square of the perimeter to 4π times the area, is a measure of roundness and circularity of the particles, considering both their form and roughness (Olson, 2011; Pabst and Gregorova, 2007; equation from Inca, 2006). In the case of a spherical particle, the projection on the x - y plane is a circle, and the aspect ratio and shape are both equal to 1. For a particle with a morphology far from spherical, the aspect ratio and shape (also named circularity) are higher than the unity, with maximum values being obtained for the

least circular and most angular particles. The average field (n = 50) coverage by the selected particles (20 per field) was obtained for each leaf sample using the *y* coordinates, to estimate the leaf surface area onto which these particles were deposited (Figure 2.2, inset B). This allowed to estimate the density of leaf-deposited particles, in number of particles per cm² of leaf surface. The leaf surface area of collected leaves was determined using a LI-3100C leaf area meter (Licor Biosciences, USA).

Figure 2.2 – SEM/EDX images of leaf-deposited PM on ivy. Inset A) secondary electron images (SEI) of an adaxial (top) and an abaxial (bottom) leaf sample. Stomata are visible on the abaxial sample. Inset B) Example of two fields scanned (by SEM/EDX) on the same sample (abaxial side). Deposited particles are visible in the backscattered electron images (BSE) as bright, white spots against a dark background, as the leaf surface is of organic nature (i.e. low Z). The particles that are colored (20 per field) correspond to the particles (features) selected for SEM/EDX analysis. These particles can represent a small fraction of the particles deposited in that field (top field) or cover almost the totality of those particles in another field (bottom field). An illustrative particle-EDX spectrum is also shown.



2.2.3 Data analysis

2.2.3.1 Data processing

In order to initially handle and refine the data obtained via SEM/EDX, a customized script-code was developed in MATLAB (MathWorks, USA). Among others, the developed functions allowed for removing any incorrect particle entry (e.g., ECD > 50 μm), recalculating the composition C_{xi} after excluding O (C had been automatically excluded in the software), and calculating the weighted-volume composition percentage, $W\%_x$ (% , v/v). Two approximations were considered for the latter calculation step, namely, that particles were near-spherical in order to obtain their volume (v_i) (Equation 2.1) and that particles had constant density (Castanheiro et al., 2016; Baldacchini et al., 2017). This allowed to estimate the volume of each analyzed particle and to calculate the weighted-volume elemental composition. The weighted-volume composition in each element x ($W\%_x$) was obtained per source type (or leaf sample) by normalizing the composition percentage C_{xi} of all individual particles therein deposited (n) for their total particle volume (Equation 2.2). Errors associated with such approximations are assumed to be reduced, as a large number of particles were selected for analysis.

$$v_i = \frac{4 \pi}{3} \cdot \left(\frac{\text{ECD}_i}{2}\right)^3 \quad (2.1)$$

$$W\%_x(\%, \text{v/v}) = \frac{\sum_{i=1}^n v_i \cdot C_{xi}}{\sum_{i=1}^n v_i} \quad (2.2)$$

In order to explore the large dataset in an interactive way (Figure A.1), the scripted functions delivered the following outputs per analyzed leaf sample: descriptive statistics on particle size, size distribution plots and compositional pie charts (% , in both m/m and v/v) illustrating the mean elemental profile of all analyzed leaf-deposited particles or of particles within a specific size range (e.g. $\text{PM}_{2.5-10}$), if desired.

2.2.3.2 Particle size distribution and chemical composition

After data refinement (§2.2.3.1), statistical analyses on the morphological and compositional data obtained via SEM/EDX was performed using JMP Pro 14 (SAS Institute Inc., USA). The ranges of particle size that are reported along this study refer to the total particles (ECD 2 – 50 μm) and to the fraction PM_{2-10} (ECD 2 – 10 μm). A distinction between fine PM (ECD 2 – 2.5 μm) and coarse PM (ECD 2.5 – 10 μm) was considered whenever relevant. Due to the large predominance of small-sized particles, the particle size and other morphological data were very negatively skewed, and no algebraic transformation resulted in a normal distribution. Mann-Whitney and Kruskal-Wallis tests were performed to investigate the influence of leaf side and source type, respectively, on the morphological characterization of the leaf-deposited particles, and Spearman's correlations for assessing the association between particle features. When source or site effects were significant, the characteristics of deposited particles between the various monitoring sites were compared using the post-hoc Steel-Dwass tests.

Additionally, the weighted-volume composition per source type were used to estimate the elemental mass of leaf-deposited particles (Equation 2.3). This was done by multiplying the weighted-volume percentages of leaf-deposited particles in each element ($W\%_x$) by the estimated total particle volume and by the corresponding solid-state density, D_x (i.e., atomic mass per volume, kg m^{-3} ; values taken from www.webelements.com/periodicity/density/), following Baldacchini et al. (2019). This calculation included the particles deposited on both leaf sides, resulting in the mass of leaf-deposited particles in each element (M_x ; μg). The total mass of analyzed leaf-deposited particles (M_p) was obtained by summing the M_x of all elements.

$$M_x = W\%_x \cdot \sum_{i=1}^n v_i \cdot D_x \quad (2.3)$$

Enrichment factors usually consider measured concentrations against values found in literature of a specific crustal earth element (e.g., Al) from a certain background-

reference (Bourliva et al., 2017; Hsu et al., 2016; Ny and Lee, 2010; Vercauteren et al., 2011). However, this strategy may overlook local geochemical and lithological characteristics, as well as the influence of regional atmospheric dust (Reimann and Caritat, 2000). Alternatively, the elemental enrichment in this study was calculated using the Forest site as a reference, by comparing the mass (M_x) of leaf-deposited particles at each site against those from the Forest ($\mu\text{g source type} / \mu\text{g Forest}$). The Forest site was selected as reference because it was the most isolated monitoring site in relation to anthropogenic point sources (e.g., roads), corroborated by the natural, rather than anthropogenic, elemental composition observed at the Forest leaf-deposited PM. The estimated enrichment factors correspond to mass concentration ratios against the Forest reference site, and can also be designated contamination factors. These values were then used to calculate the Tomlinson pollution load index (PLI, Tomlinson et al., 1980) to assess how much the metal content at the studied sites exceeded the metal content in the natural, background environment. The *PLI* is defined as the n -th root of the multiplication of contamination factors (CF_{Mn}), with CF_{Mn} here being the ratio of the content of each metal M (for n considered metals) to its background value at the forest site (Equation 2.4).

$$PLI = \sqrt[n]{CF_{M1} \times CF_{M2} \times \dots \times CF_{Mn}} \quad (2.4)$$

2.2.3.3 Representativeness of analyzed particles

The obtained morphological and elemental information were cumulative-averaged to evaluate how many particles were required to obtain a representative profile of the leaf-deposited particles at a certain condition (site, leaf side). This was done for some parameters of interest such as the particle size diameter and content in e.g., Si, Fe, Pb. The cumulative-averaged data were plotted against the number of analyzed particles (in ascending order of their size diameter) in order to understand how many particles were required to achieve stable, representative values.

2.2.3.4 Source apportionment of leaf-deposited particles

Principal component analysis (PCA) was performed on the (previously scaled) compositional C_{xi} (% m/m) and morphological (ECD, aspect ratio, shape) data of leaf-deposited particles to identify groups of interrelated variables in an attempt to discriminate the investigated sites. The morphology and elemental composition of the analyzed particles, as well as the mass elemental enrichment, the *PLI* and the density of particles were examined across the different tested sites in an attempt to discriminate them. Finally, we used the Bootstrap Forest method, also known as Random Forest, to investigate the potential of SEM/EDX data for source apportioning the analyzed leaf-deposited PM. Random Forest (RF) is a powerful machine learning method for quantitative predictions and classification purposes, based on ranking input variables according to their importance for predicting the variable of interest (Breiman, 2001; Peters et al., 2007; Philibert et al., 2013). The RF predicts a response value by averaging the predicted response across many decision trees, in which each tree is constructed on a bootstrap sample (i.e., a random sample of observations, drawn with replacement) of the training data. The training dataset, used to estimate the model and set on 60% of the entire data, was validated using 20% of the data (validation dataset), while the remaining 20% was used as a test dataset, for checking the prediction after the model was constructed. This strategy of randomly splitting the dataset into training, validation and test datasets is commonly used when an independent dataset for model evaluation is lacking (Breiman, 2001; Peters et al., 2007). The morphology (size diameter, aspect ratio, shape) and composition (in major elements only) of particles (observations) were used as input variables to predict the probability of such observations belonging to the various sites (response). The observations were then classified into the source type for which its predicted probability was the highest. The application of RF method was done using the Bootstrap Forest in JMP Pro 14.

2.3 Results and discussion

2.3.1 Representativeness of analyzed particles

The particles analyzed by SEM/EDX were checked for their representativeness potential (§2.2.3.3) of the monitoring sites in question, in terms of size diameter and composition C_{xi} (%m/m) in Si (lithogenic/soil element) and Fe (soil-derived element, as well as a traffic-indicator), and in Pb for the Industry site. Stable plateaus in both Si and Fe composition were found after ca. 600 and 1,000 analyzed particles for the Forest and Rural sites, respectively (Figure 2.3). For Roadside, a stable composition in Si was observed after 200 particles, while 600 particles were necessary for Fe content to achieve a plateau. For the Train site, on the other hand, the composition seemed to be more stable just after 6,000 analyzed particles. When looking into the abaxial and adaxial leaf-deposited particles from the Industry leaves, the cumulative-averaged composition in Si, Fe and Pb reached a steadiness after 200 and 400 particles, respectively. The cumulative-averaged size diameter of particles, however, did not seem to reach stable values for any of the investigated sites, but increasing with the number of particles. Nonetheless, these values were lower in magnitude for the Roadside and Industry than for the Forest, Rural and Train sites. Although it is not consistent how many particles should be analyzed to represent the tested parameters (size diameter, Si, Fe, Pb) across the different sites, this number should be, at least, in the order of a few hundreds of particles. According to our results, for most cases the application of SEM/EDX to about 500 to 1,000 particles would already deliver information representative of the leaf-deposited particles at each condition. As atmospheric PM consists of a mix of airborne particles with both local (specific) and regional (common) influences, the number of analyzed particles should be as high as possible to increase the reliability of results. When targeting specific fractions only (e.g., within a small particle size interval, or with a content above or below certain defined values), the required number of analyzed particles could be lower than in our study.

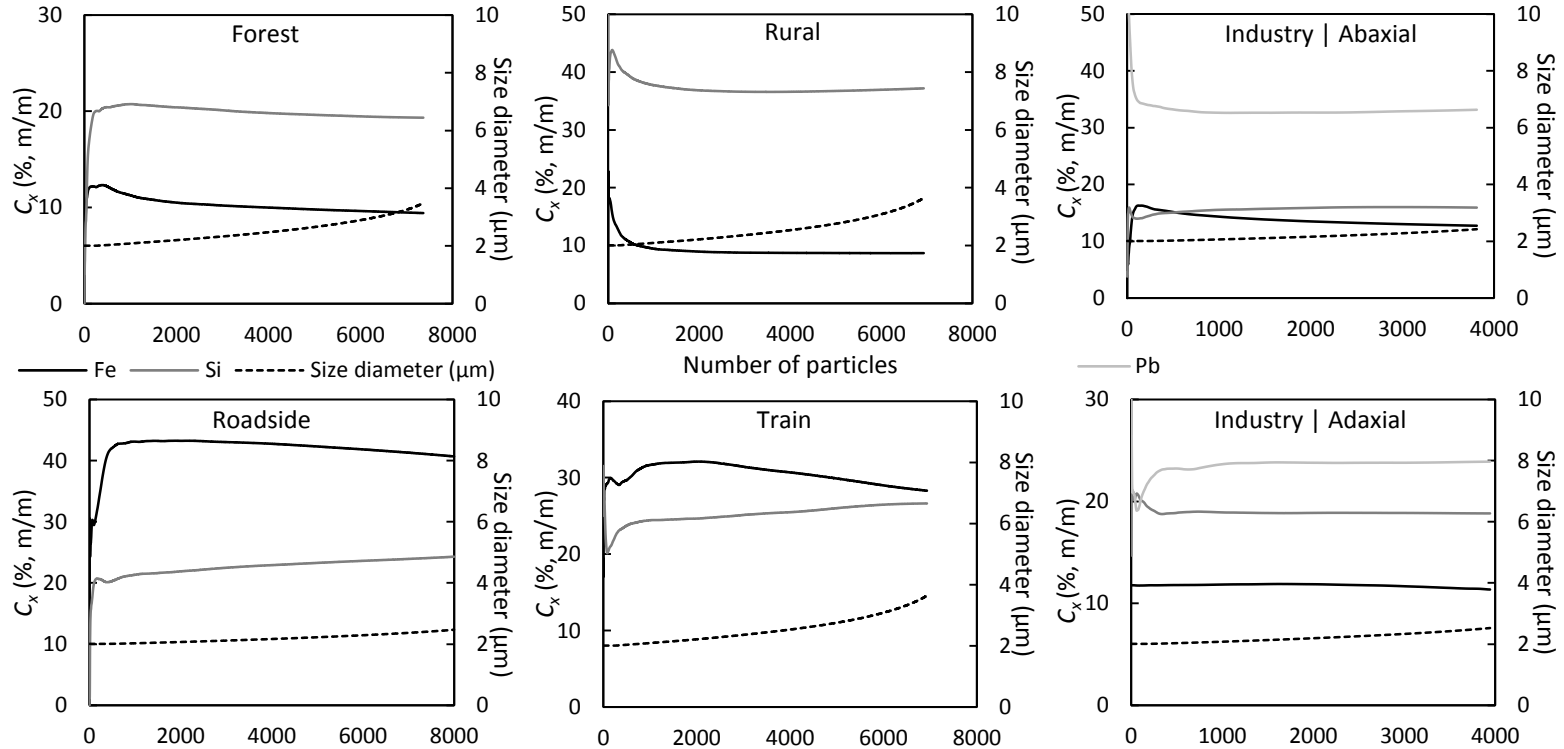


Figure 2.3 - Plots of cumulative-averaged composition C_{xi} (% , m/m) in Fe, Si and Pb, and size diameter of leaf-deposited particles (PM_{2-10}) per source type in function of the number of analyzed particles, ordered by ascending size diameter. Both adaxial and abaxial sides are included, except for the Industry site for which these data are shown separately.

2.3.2 Leaf-deposited particles per source type

2.3.2.1 Particle size and morphology

From the total of 39,409 leaf-deposited particles analyzed by SEM/EDX, 95% (37,440 particles) had a particle size diameter (ECD) $\leq 10 \mu\text{m}$ (2 - 10 μm), i.e. belonging to the range of PM₁₀. The relative contribution of very coarse particles (> 10 μm) was most evident (11%) on the abaxial surface of ivy leaves exposed at the Rural site, but still negligible in the overall analyzed particles. The mean particle size diameter for the PM₂₋₁₀ fraction was $3.52 \pm 1.58 \mu\text{m}$, with median values varying between 2.80 and 3.09 μm across the studied locations (Table 2.1).

Table 2.1 – Median values of size diameter (in μm), aspect ratio and shape (dimensionless) of leaf-deposited particles (N) per source type, considering both leaf sides (AB + AD), only the abaxial (AB) or only the adaxial (AD) leaf side. Sites not associated with the same letter (in superscript) within each line indicate significantly different median values (Steel-Dwass tests, $p < 0.05$).

AB + AD	Forest	Rural	Roadside	Train	Industry
Size Diameter	2.99 ^b	3.02 ^c	2.92 ^a	3.06 ^{bc}	2.92 ^a
Aspect Ratio	1.54 ^c	1.51 ^b	1.49 ^a	1.52 ^{bc}	1.52 ^b
Shape	1.15 ^b	1.15 ^b	1.12 ^a	1.15 ^b	1.18 ^c
<i>N</i>	7,366	6,931	7,997	7,390	7,756
AB	Forest	Rural	Roadside	Train	Industry
Size Diameter	2.95 ^b	2.99 ^{bc}	2.92 ^b	3.06 ^c	2.80 ^a
Aspect Ratio	1.59 ^c	1.52 ^b	1.47 ^a	1.58 ^c	1.49 ^a
Shape	1.18 ^d	1.15 ^c	1.10 ^a	1.20 ^e	1.13 ^b
<i>N</i>	3,938	3,182	4,017	3,527	3,812
AD	Forest	Rural	Roadside	Train	Industry
Size Diameter	3.02 ^{bc}	3.09 ^c	2.88 ^a	3.02 ^b	3.02 ^b
Aspect Ratio	1.49 ^{ab}	1.50 ^b	1.51 ^b	1.47 ^a	1.55 ^c
Shape	1.13 ^a	1.16 ^b	1.15 ^b	1.11 ^a	1.24 ^c
<i>N</i>	3,428	3,749	3,980	3,863	3,944

The particle size distribution was evidently biased towards the smaller particles (Figure 2.4). Around 50% of all leaf-deposited particles (i.e., for all tested sites and both leaf sides) had a diameter between 2 and 3 μm (Figure 2.5). Furthermore, between 28% and 35% of the particles were smaller than 2.5 μm , thus belonging to the fraction of fine PM (PM_{2.5}). Particle diameter was significantly influenced by source type (Kruskal-

Wallis, $p < 0.0001$): all monitored sites differed in particle size diameter with the exception for the comparisons Roadside-Industry, Forest-Train and Rural-Train (Steel-Dwass, $p > 0.12$) (Figure 2.6). Considering the particles deposited on both leaf sides, the median particle size followed the order RD = I ($2.92 \mu\text{m}$) < F ($2.99 \mu\text{m}$) < R ($3.02 \mu\text{m}$) < T ($3.06 \mu\text{m}$) (Table 2.1).

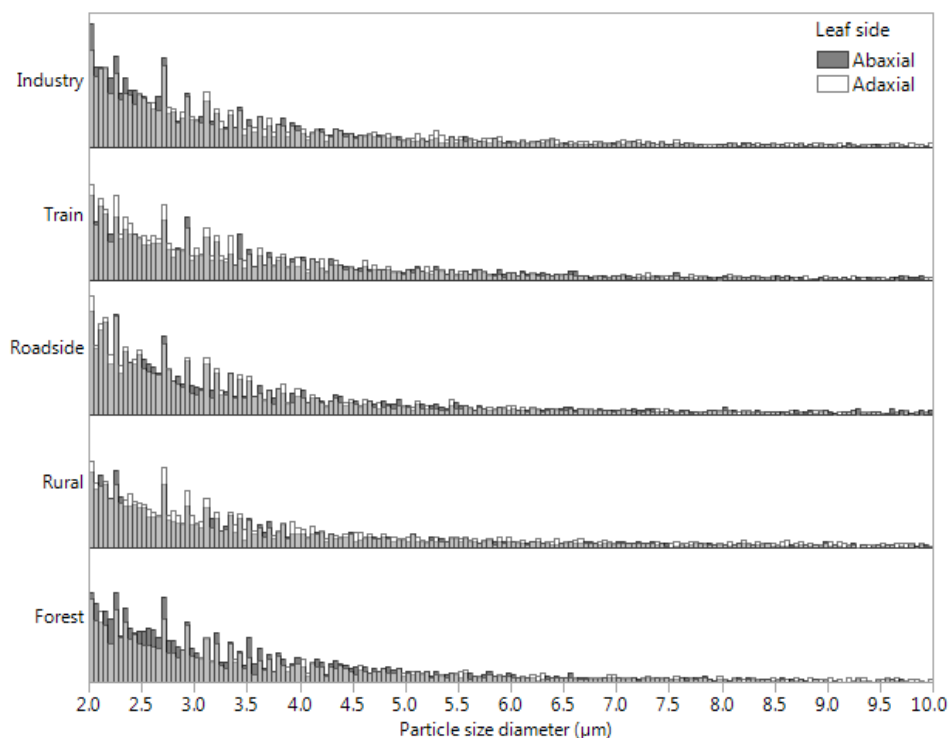


Figure 2.4 - Distribution of particle size diameter per source type and leaf side. Particles deposited on the abaxial and adaxial sides are represented by grey and white bars (both transparent), respectively.

Leaf-deposited particles are often considered spherical or with a circular shape (as in e.g. Baldacchini et al. (2017, 2019), Castanheiro et al. (2016), Sgrigna et al. (2016), and in this study) to simplify quantitative compositional calculations. However, atmospheric particles encompass a variety of shapes and geometries. The aspect ratio of the leaf-deposited particles ranged from 1.05 to 14.73. The closest the aspect ratio is to unity, the less elongated is the particle. Both symmetric and circular-like shapes are characterized by aspect ratios close to 1 (Olson, 2011). Aspect ratio estimates are

not applicable to extremely elongated particles such as fibers (aspect ratio > 5) though, but this was a minority (0.12%) in our study. Despite the variety of particle morphologies, the median aspect ratio was between 1.47 and 1.59 for all monitored sites and both leaf sides (Table 2.1). The median shape of analyzed leaf-deposited particles varied between 1.10 and 1.24 for all tested conditions (Table 2.1), with values ≈ 1 indicating circular particles (Pabst and Gregorova, 2007). The morphology of the leaf-deposited particles, in both their aspect ratio and shape, was site-dependent ($p < 0.0001$). Leaf-deposited particles from Roadside were overall the most circular and less elongated, with median aspect ratio of 1.49 and shape parameter of 1.12. The morphology of particles was significantly different in terms of aspect ratio between the Roadside and Industry, and between those and the Forest site. In terms of shape, differences were also observed between Roadside and Industry, while Forest, Rural and Train were alike. Median aspect ratio was highest for Forest (1.54), while median shape was highest for Industry (1.18).

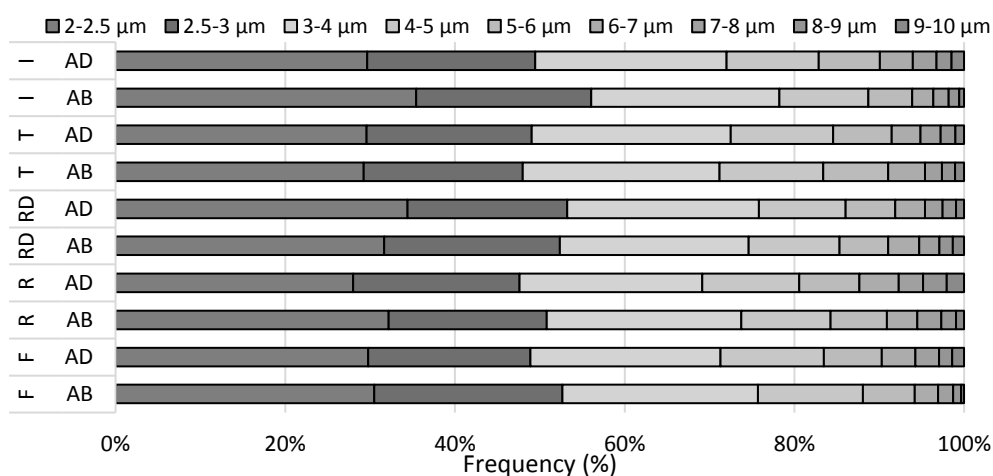


Figure 2.5 - Relative frequency of the particle size diameter (%) per source type (F - Forest, R - Rural, RD - Roadside, T - Train, I - Industry) and leaf side (AB – abaxial, AD – adaxial), in unit size bins from 2 to 10 μm , with an additional discrimination done for the particle size diameter of 2.5 μm , the upper limit of fine PM ($\text{PM}_{2.5}$).

The size diameter distribution of particles deposited on both leaf sides was comparable in terms of magnitude (Figure 2.5). Nonetheless, the median particle size differed significantly between both surfaces for three out of the five tested sites (Table 2.2).

For Forest, Rural and Industry sites, the particle size was larger ($p < 0.0004$) on the adaxial than on the abaxial side. The aspect ratio and shape of particles were also dependent on leaf side, but no consistent trend was observed across all source types. The median particle aspect ratio was significantly smaller (closer to unity, thus, indicating less elongated particles) on the adaxial side of Forest, Rural and Train leaves compared to the abaxial side, while the opposite was observed for the Roadside and Industry (Table 2.2). Similar results were obtained regarding the shape of leaf-deposited particles, with exception for the Rural site, where particles on the abaxial side had a smaller shape factor, thus, were more circular, than those on the adaxial side. Considering the particles deposited on the abaxial side of ivy, median size diameter varied between 2.80 μm (Industry) and 3.06 μm (Train), the aspect ratio between 1.47 (Roadside) and 1.59 (Forest), and the shape between 1.10 (Roadside) and 1.20 (Train). For the adaxial side, the median particle size varied between 2.88 μm (Roadside) and 3.09 μm (Rural), with the lowest and highest aspect ratio and shape for, respectively, the Train (1.47; 1.11) and Industry (1.55; 1.24) sites.

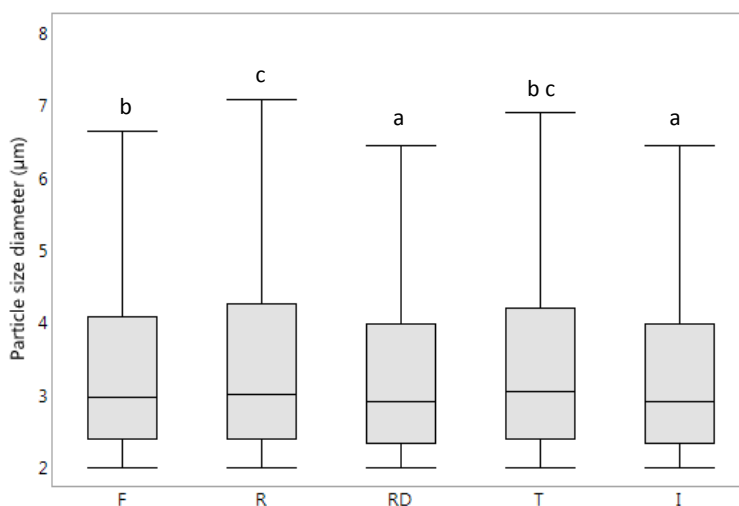


Figure 2.6 - Boxplots of particle diameter of leaf-deposited particles across the five source types (F – Forest, R – Rural, RD – Roadside, T – Train, I – Industry). Sites not associated with the same letter indicate significantly different ($p < 0.05$) particle size medians. Details regarding such differences on the adaxial and abaxial leaf sides can be found in Table 2.1. Outliers (i.e., data points below $Q1 - 1.5 \times IQR$ or above $Q3 + 1.5 \times IQR$; $Q1$ - first and $Q3$ - third, quartiles, interquartile range $IQR = Q3 - Q1$) are not shown.

Table 2.2 - Median values of size diameter (in μm), aspect ratio and shape (dimensionless) of leaf-deposited particles per source type, considering the particles deposited either on the abaxial (AB) or adaxial (AD) leaf side. For each site, significant differences (Mann-Whitney, $p < 0.01$) between abaxial and adaxial are shown with the larger value in bold.

Source type	Forest		Rural		Roadside		Train		Industry	
	AB	AD	AB	AD	AB	AD	AB	AD	AB	AD
Size Diameter	2.95	3.02	2.99	3.09	2.92	2.88	3.06	3.02	2.80	3.02
Aspect Ratio	1.59	1.49	1.52	1.50	1.47	1.51	1.58	1.47	1.49	1.55
Shape	1.18	1.13	1.15	1.16	1.10	1.15	1.20	1.11	1.13	1.24

The morphology of the particles appeared to be influenced by the particle diameter, as larger particles were also more elongated and less circular (Figure 2.7). This was transversal to all tested source types (Figure A.2), and confirmed by significant positive correlations between particle size diameter and morphology (Spearman's, $p < 0.0001$), with correlation coefficients (ρ) of 0.15 to 0.24 between the diameter and aspect ratio, and of 0.45 to 0.56 between the diameter and shape of the particles. Both aspect ratio and shape parameters fluctuated in the same direction, with ρ of 0.65 to 0.73.

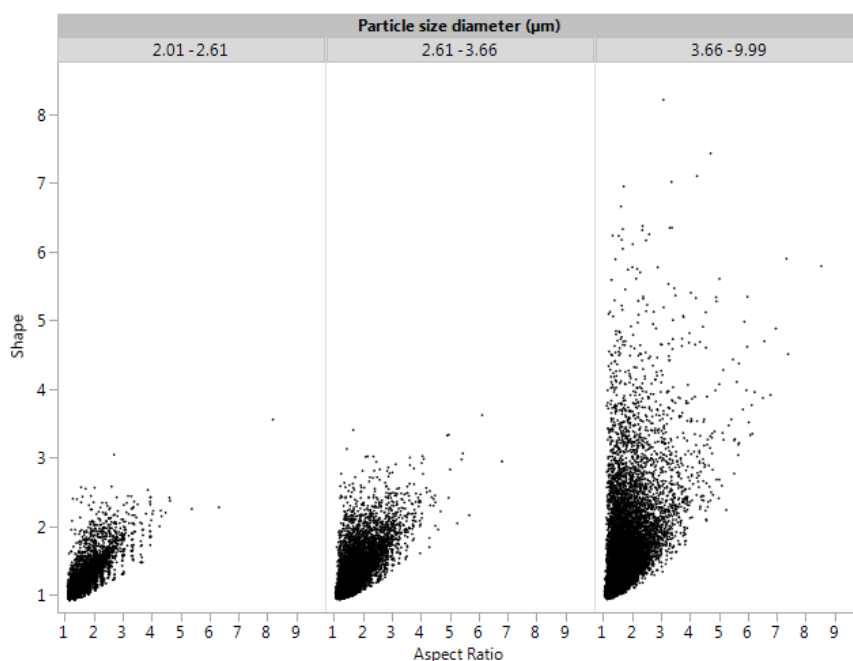


Figure 2.7 – Scatterplot of the aspect ratio (x axis) and shape (y axis) of all analyzed leaf-deposited PM_{2-10} , according to their size diameter subdivided in three equal intervals.

2.3.2.2 Particle elemental composition

The elements most contributing to the overall composition of leaf-deposited particles were, by descending order, Si, Fe, Ca, S, K, Al, Pb, Cl, Na, Mg, P and Cu, which were also the most frequently identified elements (Table 2.3). PM typically include, amongst others, fugitive crustal matter (Si, Ca, K, Al, Na, Mg, Fe, Ti, Mn), sea salt (Na, Cl, Mg) and traffic-derived compounds (e.g., Fe, Cr, Mn, Cu, Pb) (Amato et al., 2009; Vercauteren et al., 2011). Yet, the relative contribution of elements tend to vary per site. The influence of the source type on the composition profiles ($W\%$) of the analyzed particles was investigated in terms of major and trace elements (Figure 2.8), as they can point towards main polluting sources. The leaf-deposited particles from the Forest were mainly composed of Si, Ca, S, K, Fe, Al, Na and Cl. The major elements on the Rural site were Si, Ca, Al, Fe, Mg, K and for which Si contributed the most (ca. 45%) amongst all tested sites. Both Roadside and Train leaf-deposited particles had a comparable composition with Si and Fe as predominant elements, followed by Ca and Al. The highest Fe content, of ca. 24%, was observed for these two source types. The composition profile from Industry was remarkably different from the other sites, with 30% of the particles composed of Pb and 5% of Cu. These elements were negligible across the other sites though. Trace elements such as As, Te, Zn, Sn, Sb also reached their highest concentrations for the Industry site, while they were minimal for the other sites.

Although the relative elemental composition (% m/m) varied per site (Table 2.4), the study sites were also under the influence of similar regional PM as they are located in the same region. Therefore, certain elements that are recognized as PM source indicators (e.g., Vercauteren et al., 2011) were highly correlated in the leaf-deposited particles ($p < 0.01$) independently of the source type, such as Na and Cl ($p = 0.29 - 0.82$, $I < R < RD < T < F$) and Si and Al ($p = 0.36 - 0.75$, $R < RD < I < T < F$) (Table A.1), associated with sea salt and crustal matter, respectively.

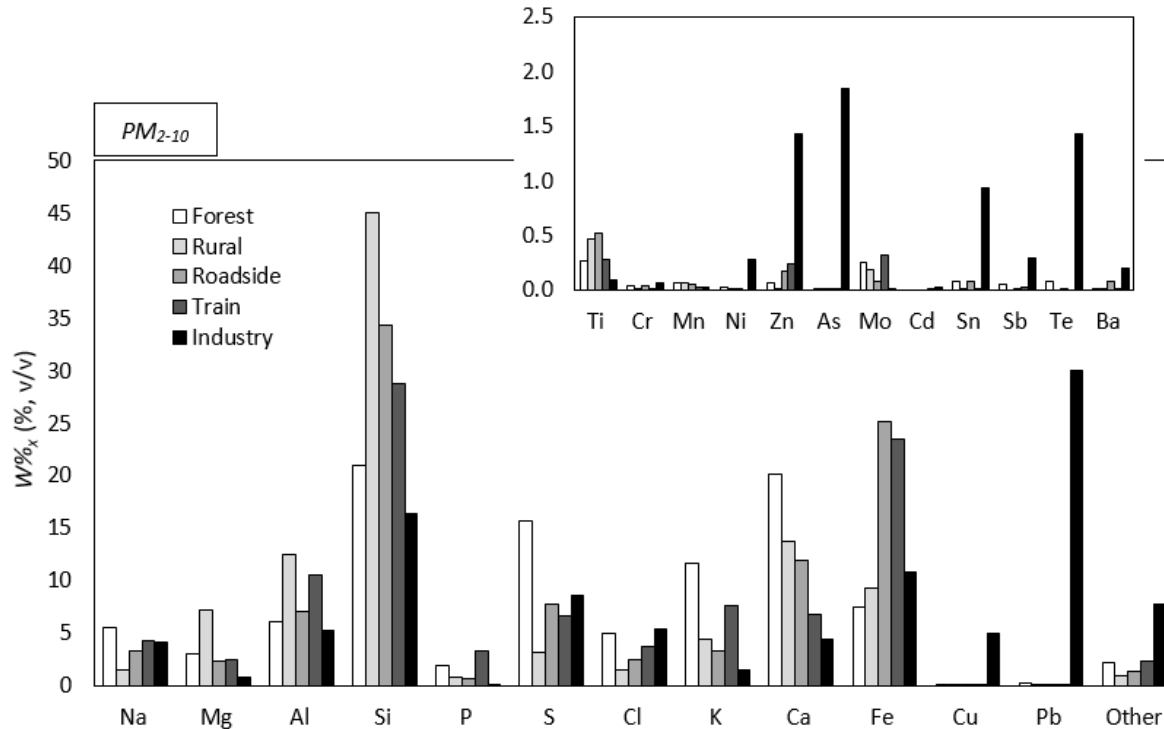


Figure 2.8 – Weighted-volume percentages (% v/v) of the major elements and trace elements (inset) quantified on the leaf-deposited particles (PM_{2-10}) by SEM/EDX. Major elements are responsible for > 92% of the overall composition, while trace elements include elements contributing to > 0.5% or metals commonly investigated in environmental studies. The class “Other” includes all remaining elements that are not considered major elements, i.e. including the trace elements shown in the inset. The composition profiles are presented per source type and include the particles deposited on both leaf sides. Discrimination between abaxial and adaxial leaf sides can be found in Figure A.3.

Table 2.3 – Frequency (#Freq, in number of times) of elements (Elem) detected and quantified in the total of 37,440 leaf-deposited particles. The elements most contributing to the overall composition (responsible for > 92%) are shaded in grey.

Elem	#Freq	Elem	#Freq	Elem	#Freq	Elem	#Freq	Elem	#Freq
Si	29,125	Ti	1,445	Zr	61	Tm	10	Pu	3
K	26,529	Zn	854	Ag	61	Ar	8	Ne	2
Ca	22,896	Te	665	F	54	Bi	8	Pd	2
Fe	22,588	Mo	660	Kr	32	Sr	7	B	1
Al	21,675	N	582	Ta	25	V	5	Y	1
S	21,177	Sn	280	Ce	23	Tl	5	Nb	1
Mg	12,774	Mn	262	Tc	20	Co	4	Rh	1
Cl	12,032	Cr	210	In	20	Sc	3	Eu	1
Na	9,988	Br	201	Np	19	I	3	Ac	1
P	5,937	Ni	167	Cd	18	La	3	Yb	0
Pb	4,372	Sb	165	Ir	18	Nd	3	Po	0
As	2,452	Ba	156	Rn	13	Pt	3		
Cu	2,275	Se	100	W	12	Pa	3		

Table 2.4 – Mean elemental composition (% m/m; major elements) of leaf-deposited particles across the five source types, considering particles deposited on both leaf sides (AB + AD). Sites not associated with the same letter within each line indicate significantly different median values (Steel-Dwass tests, $p < 0.05$).

AB + AD	Forest	Rural	Roadside	Train	Industry
Na	4.4 ^c	1.6 ^a	3.6 ^c	4.5 ^b	3.4 ^b
Mg	2.9 ^c	6.5 ^d	2.1 ^b	2.4 ^c	0.8 ^a
Al	5.8 ^a	12.0 ^e	6.2 ^c	9.8 ^d	6.2 ^b
Si	19.0 ^a	39.4 ^e	27.5 ^d	26.4 ^c	17.0 ^b
P	2.2 ^d	1.1 ^c	0.5 ^b	3.8 ^e	0.1 ^a
S	15.9 ^e	4.5 ^a	7.5 ^c	6.9 ^b	8.5 ^d
Cl	3.6 ^b	1.4 ^a	2.6 ^b	3.5 ^b	4.4 ^c
K	16.2 ^e	5.7 ^c	2.9 ^b	9.6 ^d	1.8 ^a
Ca	18.9 ^e	13.6 ^d	9.8 ^c	6.9 ^b	3.7 ^a
Fe	8.3 ^a	12.6 ^b	35.3 ^d	23.4 ^c	11.6 ^b
Cu	0.1 ^a	0.1 ^a	0.2 ^b	0.0 ^a	5.8 ^c
Pb	0.0 ^{ab}	0.0 ^a	0.1 ^b	0.1 ^{ab}	29.4 ^c

The composition of atmospheric particles is not independent of their morphology and size, and vice-versa (e.g., Marcazzan et al., 2001). Instead, the aforementioned particle characteristics greatly depend on the emission sources, posing also different risks to human health. In this context, the elemental profiles revealed two key findings when discriminating between the fine (2 – 2.5 μm) and coarse (2.5 – 10 μm) deposited PM fractions (Figure 2.9). First, coarse PM was more enriched in Si compared to fine PM

(especially for Rural and Roadside sites, with values 26% and 42% higher for the coarse PM compared to the fine PM). Second, fine particles from the Roadside were 72% more enriched in Fe than its coarse fraction. Nonetheless, the relative concentrations of all other elements were comparable between fine and coarse size ranges, and the site ordering was not altered (e.g., for Ca the order Forest > Rural > Roadside > Train > Industry was similar for as well the fine, coarse and total PM fractions). As larger particles contribute more to the estimated weighted-volume percentages ($W\%_x$), the overall composition profile (PM_{2-10}) (Figure 2.8) is very similar to the profile of coarse PM (Figure 2.9). However, the inclusion of smaller-sized particles (which are also the most health-concerning; Schwarze et al., 2006) may reveal useful relationships for the process of source apportionment. For instance, Fe is simultaneously a crustal matter constituent and an important indicator for road traffic and industrial activities (Vercauteren et al., 2011). Coarse leaf-deposited particles from Roadside and Train were equally enriched in Fe (also with the highest contribution across the five sites). This enrichment greatly increased for the fine particles of Roadside, whereas it remained constant for the fine particles of Train. The larger contribution of smaller Fe-based particles in Roadside compared to Train reveals the influence of combustion processes, which are certainly present on the first location (high intensity car traffic) but variable on the second one, as both electrical- and diesel-powered trains may be passing at the Train site. As shown in this case, considering both composition and size of particles can aid in disclosing site our source type influences.

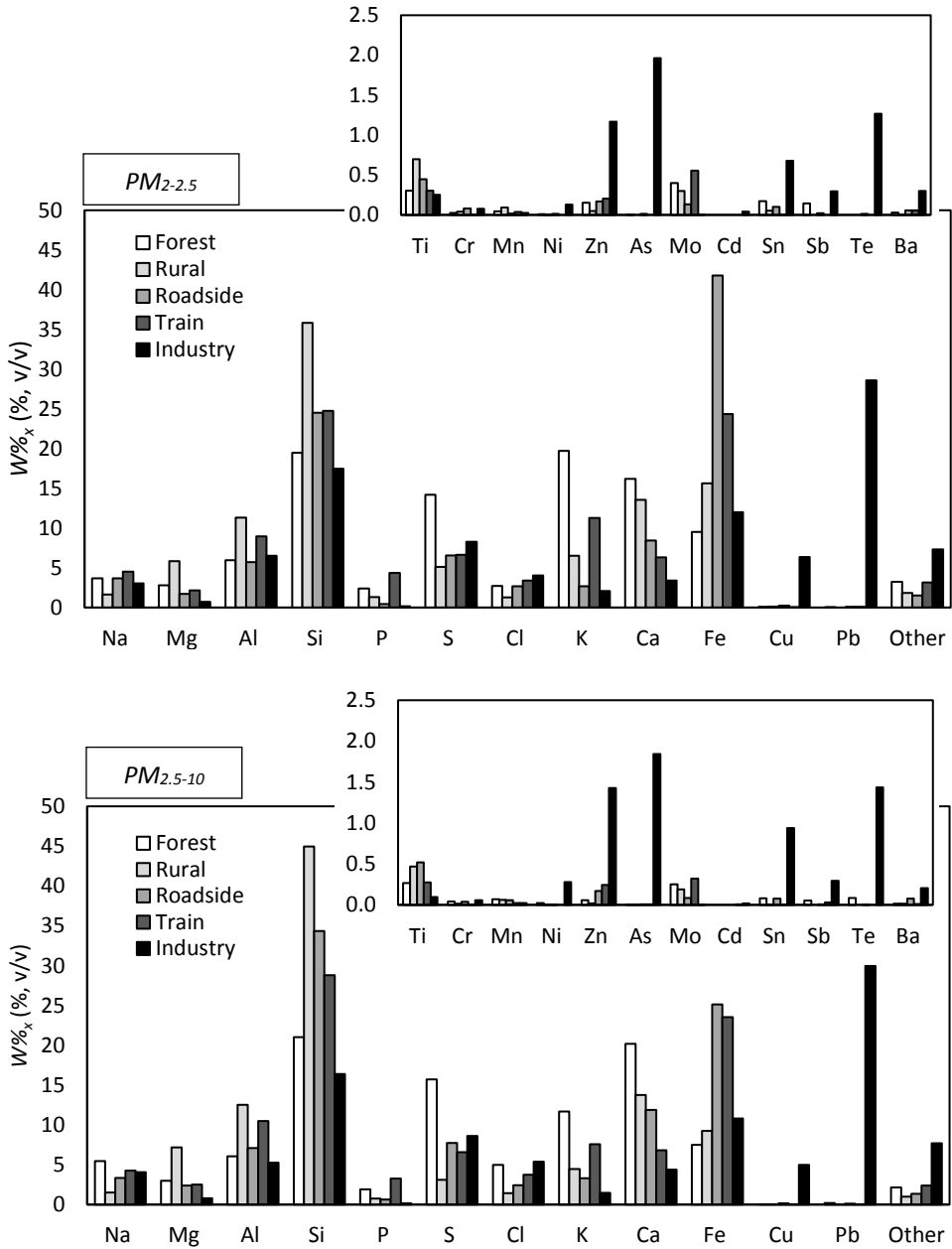


Figure 2.9 – Weighted-volume percentages (% v/v) of the major elements and trace elements (inset) quantified on the leaf-deposited fine PM (top) and coarse PM (bottom), of size 2-2.5 μm and 2.5-10 μm , respectively. Major elements are responsible for > 92% of the overall composition, while trace elements include elements contributing to > 0.5% or metals commonly investigated in environmental studies. The class “Other” includes all remaining elements that are not considered major elements, i.e. including the trace elements shown in the inset. The composition profiles are presented per source type and include the particles deposited on both leaf sides.

The Forest site was the least enriched in anthropogenic elements (Figure 2.8), given the reduced traffic and industrial emissions nearby. The elemental enrichment at the traffic and industry sites compared to the Forest site, thus used as a reference, may help assessing the importance of anthropogenic contributions across the remaining sites. Roadside particles were moderately enriched in Fe, Cu, Zn, As and Ba, while Train particles were moderately enriched in Fe, Zn and As (Table 2.5). For Roadside, the enrichment level in As and Ba was considered significant within, respectively, the fine and coarse PM fraction. Leaf-deposited particles from Industry were enriched in trace elements Sb, Sn, Ni, Ba and Te, very highly enriched in Zn and extremely enriched in Cu, Pb and As. The highest elemental enrichment ($4,734 \mu\text{g} / \mu\text{g Forest}$) was observed for Pb content in the fine fraction of Industry particles. Also remarkable was the significant Pb-enrichment of the fine particles at both Roadside ($13.4 \mu\text{g} / \mu\text{g Forest}$) and Train ($12.1 \mu\text{g} / \mu\text{g Forest}$) sites, while the enrichment was negligible within the correspondent coarse fractions. The Tomlinson *PLI* including metals Fe, Cu, Pb (major elements), Ti, Cr, Mn, Ni, Zn, As, Mo, Cd, Sn, Sb, Te and Ba (trace elements), confirmed the Industry site as the highest polluted in terms of anthropogenic metal input (Table 2.5). According to Qiao et al. (2013), degrees of pollution based on the Tomlinson *PLI* are defined as: $0 < PLI \leq 1$ unpolluted, $1 < PLI \leq 2$ moderately polluted, $3 < PLI \leq 4$ very highly polluted. Leaf-deposited particles from the Industry site even surpassed the highest defined *PLI* category, with a *PLI* of 6.8 and 7.5 for the fine and coarse PM fractions, respectively. The Rural and Train sites were considered unpolluted, while the Roadside was considered polluted, particularly for the small particles. The Roadside *PLI* was 1.2 for the particles between 2.5 and $10 \mu\text{m}$, and 1.7 for the particles between 2 and $2.5 \mu\text{m}$.

Table 2.5 – Elemental enrichment (in mass; $\mu\text{g}/\mu\text{g}$) in major and trace elements of leaf-deposited particles per source type (R – Rural, RD – Roadside, T – Train, I – Industry) and size range (PM_{2-10} ; $\text{PM}_{2-2.5}$, fine PM; $\text{PM}_{2.5-10}$, coarse PM), compared to Forest (reference site). Only enrichments > 0.05 are shown, with substantial enrichments (≥ 2) in bold. The Tomlinson PLI including the elements in grey is also shown.

Elem	PM_{2-10}				$\text{PM}_{2-2.5}$				$\text{PM}_{2.5-10}$			
	R	RD	T	I	R	RD	T	I	R	RD	T	I
Na	0.3	0.7	0.8	0.8	0.4	1.2	1.2	0.9	0.3	0.7	0.8	0.8
Mg	2.8	0.9	0.9	0.3	1.9	0.7	0.7	0.3	2.8	0.9	0.9	0.3
Al	2.4	1.3	1.9	0.9	1.8	1.1	1.5	1.2	2.4	1.3	1.9	0.9
Si	2.5	1.8	1.5	0.8	1.7	1.5	1.2	1.0	2.5	1.8	1.5	0.8
P	0.4	0.4	1.9	0.1	0.5	0.2	1.8	0.1	0.4	0.4	1.9	0.1
S	0.2	0.6	0.5	0.6	0.3	0.5	0.5	0.7	0.2	0.6	0.5	0.6
Cl	0.3	0.5	0.8	1.1	0.4	1.2	1.2	1.7	0.3	0.5	0.8	1.1
K	0.4	0.3	0.7	0.1	0.3	0.2	0.6	0.1	0.5	0.3	0.7	0.1
Ca	0.8	0.7	0.4	0.2	0.8	0.6	0.4	0.2	0.8	0.7	0.4	0.2
Fe	1.4	3.8	3.4	1.5	1.5	5.2	2.5	1.4	1.4	3.7	3.5	1.5
Cu	0.6	3.4	0.4	95.6	1.1	2.8	0.3	75.7	0.5	3.5	0.4	97.3
Pb	-	0.8	0.2	157.7	-	13.4	12.1	4733.8	-	0.7	0.1	150.5
Ti	2.0	2.2	1.1	0.4	2.1	1.7	1.0	0.9	2.0	2.2	1.1	0.4
Cr	0.4	1.0	-	1.5	1.6	4.0	0.2	3.5	0.4	0.9	-	1.4
Mn	1.0	0.9	0.4	0.3	1.9	0.4	0.8	0.6	1.0	1.0	0.4	0.3
Ni	-	0.2	-	13.5	0.2	1.5	-	14.6	-	0.2	-	13.4
Zn	0.3	3.3	4.5	26.1	0.3	1.3	1.3	8.5	0.3	3.5	5.0	28.5
As	0.4	2.6	2.2	649.8	-	8.4	-	1092.0	0.4	2.4	2.3	635.5
Mo	0.9	0.4	1.4	-	0.7	0.4	1.3	-	0.9	0.4	1.4	-
Cd	-	-	-	-	-	-	-	-	-	-	-	-
Sn	0.1	1.1	-	12.4	0.3	0.7	-	4.4	-	1.1	-	13.3
Sb	-	0.1	0.6	5.9	-	0.2	-	2.3	-	0.1	0.7	6.5
Te	-	-	-	18.2	-	-	-	-	-	-	-	17.4
Ba	1.1	6.1	0.7	15.4	0.1	2.5	2.1	12.3	1.2	6.4	0.6	15.7
PLI	0.29	0.85	0.47	6.73	0.60	1.71	0.86	7.48	0.41	1.19	0.44	6.75

The abaxial vs. adaxial elemental profiles of PM₂₋₁₀ showed comparable trends for the Rural site, whereas the leaf side seemed more relevant for the other source types (Table 2.6). Particles deposited on the adaxial side were overall more enriched in Fe compared to the abaxial side, whereas the contrary was observed for S, K and Ca (Figure A.3). The highest leaf side differences were observed in the mentioned elements for the Forest. For Roadside and Train, the weighted-volume composition in Fe was, respectively, 51% and 62% higher for the particles deposited on the adaxial side than on the abaxial side. This leaf-side influence occurred for both fine and coarse fractions (Figure 2.10) at these two source types. A distinction between the lower-Fe abaxial contributions due to fugitive soil dust and the higher-Fe traffic contributions (more combustion-related at Roadside compared to Train) on the adaxial side is suggested by our results. This possibility, however, was not reflected on the particles' size. Large particles indicate crustal matter origin (Almeida et al., 2006), but the particle size diameter was not significantly different between the two leaf sides only for Roadside and Train (§2.3.2.1). The abaxial Fe content at these two sites was still higher than at the other sites, confirming the input of anthropogenic Fe emissions.

Table 2.6 - Mean elemental composition (% m/m; major elements) of leaf-deposited particles per source type, considering the abaxial (AB) and the adaxial (AD) leaf sides.

Source type Leaf side	Forest		Rural		Roadside		Train		Industry	
	AB	AD	AB	AD	AB	AD	AB	AD	AB	AD
Na	0.3	9.0	0.6	2.4	2.6	4.7	0.7	8.0	1.6	5.1
Mg	2.3	3.5	5.4	7.5	2.0	2.1	1.7	3.0	0.6	0.9
Al	3.8	8.1	10.2	13.4	6.4	5.9	10.0	9.5	7.3	5.2
Si	14.1	24.7	36.2	42.1	29.0	26.1	26.3	26.4	15.1	18.7
P	2.5	1.9	1.7	0.6	0.7	0.3	5.6	2.3	0.1	0.1
S	23.5	7.2	7.8	1.8	12.4	2.5	11.3	2.9	8.1	8.8
Cl	0.2	7.4	0.5	2.3	0.9	4.3	0.2	6.6	3.0	5.7
K	21.1	10.6	8.0	3.7	4.3	1.6	13.7	5.8	1.9	1.7
Ca	25.0	12.0	15.8	11.7	12.6	7.1	8.6	5.3	3.7	3.7
Fe	4.5	12.8	11.7	13.4	26.9	43.8	17.8	28.5	11.5	11.8
Cu	0.0	0.1	0.1	0.0	0.1	0.4	0.0	0.0	3.9	7.6
Pb	0.0	0.1	0.0	0.0	0.1	0.1	0.1	0.0	34.8	24.3

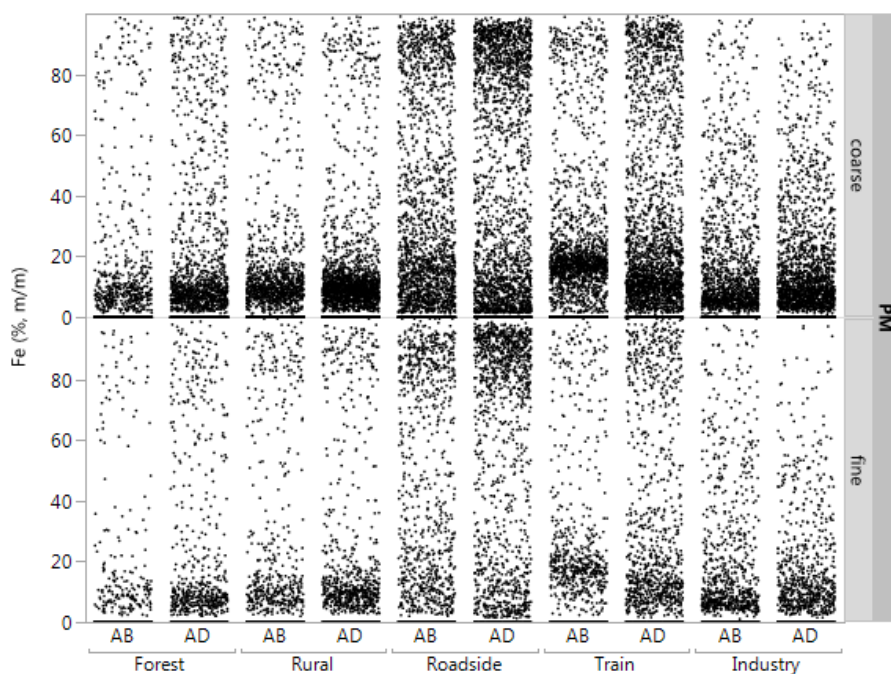


Figure 2.10 – Scatterplot of the Fe composition (% m/m) quantified on the leaf-deposited particles per source type and leaf side (AB – abaxial, AD – adaxial), for both the fine and coarse PM fractions.

2.3.2.3 Particle mass and number

The total mass of leaf-deposited particles (of all analyzed particles; M_p) in the PM₂₋₁₀ fraction was highest for Industry (181.5 μg), followed by the Roadside (111.2 μg), Train (102.8 μg), Rural (85.1 μg) and Forest (64.7 μg) (Figure 2.11). The contribution of finer particles, with diameter between 2 and 2.5 μm , to the total mass varied between 4.2% and 6.3% depending on the source type, with Roadside having the highest contribution of fine PM. The calculated mass does not refer to the total number of deposited particles on the collected ivy leaves, but to a fraction of it, as only about 1,000 particles with diameter of 2 μm to 10 μm , were analyzed per leaf sample. Given the large number of particles (ca. 7,000 per site), these estimates still provide an idea about the PM mass load across the test sites. As the number of analyzed particles was comparable across the investigated sites, and with a distribution similarly biased towards the smallest-sized particles, the calculated masses might rather be an indication of composition. The Industry site with the highest presence of metallic,

higher Z elements (§2.3.2.2), which often have high solid state density values (e.g., Pb = 11,340 kg m⁻³), had also the highest calculated mass of leaf-deposited particles.

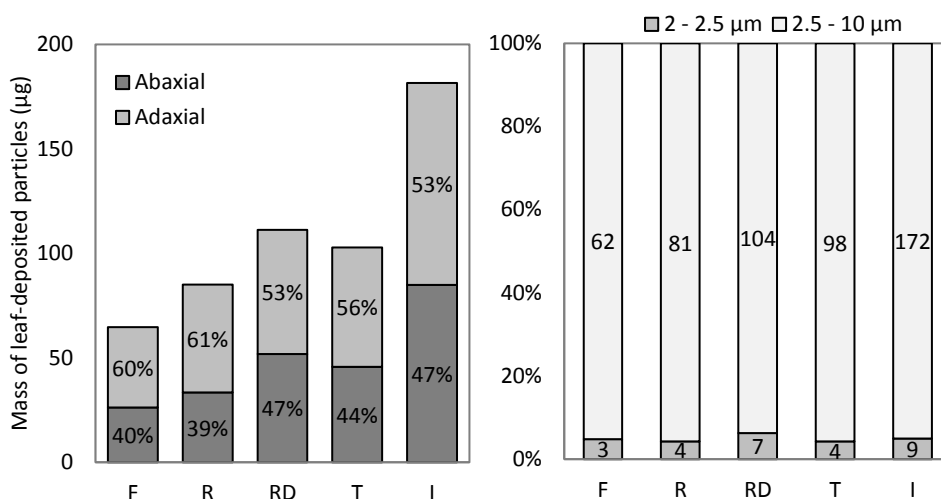


Figure 2.11 – Mass (µg) of analyzed leaf-deposited particles per source type (F – Forest, R – Rural, RD – Roadside, T – Train, I – Industry), with indication of abaxial and adaxial deposition (left panel), and size fractions PM_{2-2.5} and PM_{2.5-10} (right panel) contributions. Left panel: bars represent the total mass of leaf-deposited particles; right panel: stacked bars illustrate the contribution (in %) of fine and coarse PM (of both abaxial and adaxial deposition) to the overall mass, with mass values (in µg) shown inside the bars.

The density of leaf-deposited PM₂₋₁₀ particles per source type was, on average, 32, 54, 34, 54 and 154 x10³ particles cm⁻², for Forest, Rural, Roadside, Train and Industry, respectively. The estimated particle densities are somewhat lower than the ca. 100 to 200 x10³ particles cm⁻² (PM_{2.5-10}) observed by Baldacchini et al. (2019) on 8-months old *Quercus ilex* leaves, while they are rather comparable with the values measured on 5-months old *Platanus x acerifolia* across 20 European locations (Baldacchini et al., 2017; see Chapter 3.2). In the latter, particle densities mainly varied between 5 and 212 x10³ PM_{2.5-10} particles cm⁻², while the density of particles with a size diameter between 0.3 and 0.6 µm was up to 4 x10⁶ particles cm⁻². The particle density of leaf-deposited particles depends on several factors, such as sampling site, exposure period and plant species, as species with different leaf macro- and micro-morphological characteristics can capture PM differently (see Chapter 4). Taking into account the total leaf surface area, the number of deposited particles ranged on average between 1.2 x10⁶ (F) and

3.7×10^6 (I) particles per leaf side of ivy. Main differences in particle density across leaf samples ($n = 8$) were observed for Rural, Train and Industry (Figure 2.12). The minimum and maximum estimated number of deposited particles was 0.7 and 10.5×10^6 , respectively for Forest and Industry, and both on the abaxial leaf side.

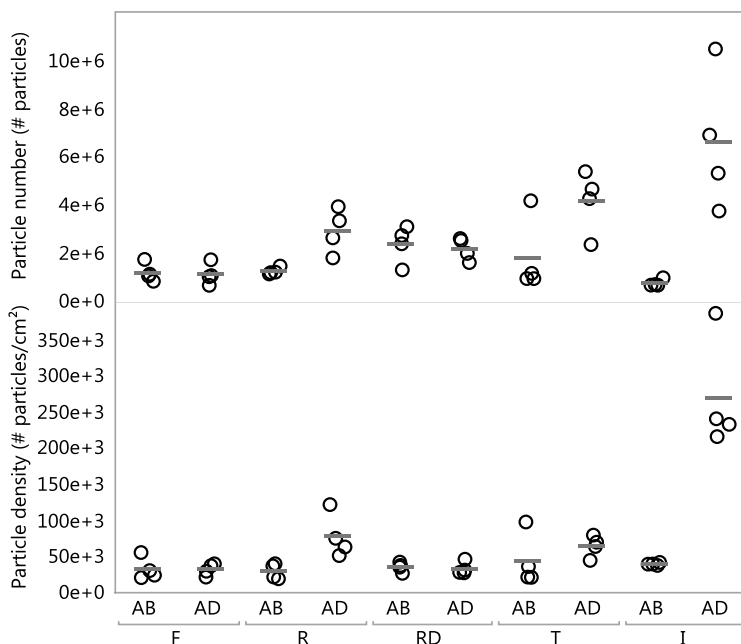


Figure 2.12 – Particle number (# particles; top panel) and density (# particles per leaf cm^2 ; bottom panel) of leaf-deposited particles per source type (F – Forest, R – Rural, RD – Roadside, T – Train, I – Industry) and leaf side (AB – abaxial, AD – adaxial). Each data circle represents a leaf sample, with the means indicated by the horizontal dashes.

Ivy leaves present similar micro-morphology on both leaf sides (epicuticular wax structure defined as platelets and a comparable trichome density) with exception of the stomatal density, as stomata are only present on the abaxial side (§Chapter 4). These stomatal openings on the lower leaf epidermis are often associated with enhanced accumulation of atmospheric particles (Sawidis et al., 2011). Several studies have shown that larger accumulation of PM occurs on the adaxial side of leaves compared to the abaxial side (Baldacchini et al., 2017; Ottel e et al., 2010; Shi et al., 2017; Wang et al., 2015a). Despite of the few leaf replicates (only four samples from each leaf side, per study site), the results of this study appear to support those findings.

The particle density was significantly higher ($p = 0.03$) on the adaxial leaf side than on the abaxial side for two out of the five test sites (Rural and Industry).

2.3.2.4 Source apportionment of leaf-deposited particles

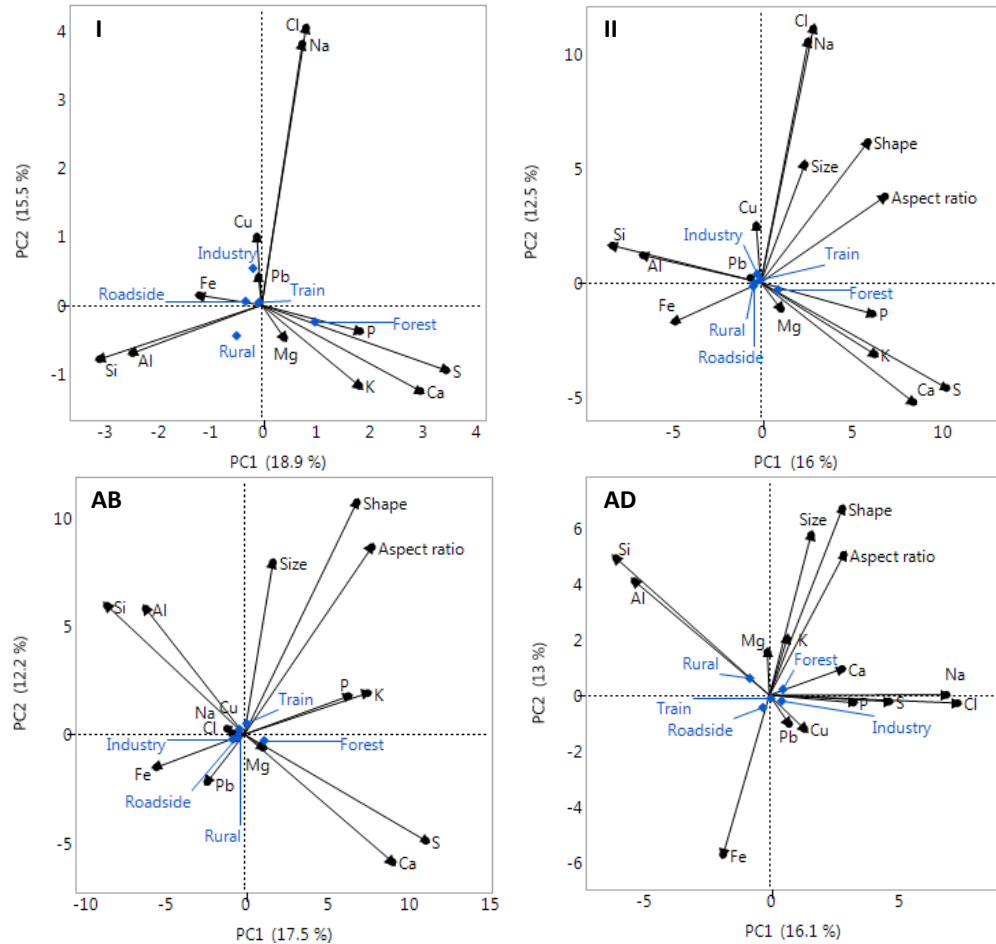
Principal component analysis (PCA) on the most representative elements (Na, Mg, Al, Si, P, S, Cl, K, Ca, Fe, Cu, Pb; %, m/m) and morphological parameters highlighted some correlated elements across the investigated sites, such as Na-Cl and Al-Si (Figure 2.13). The main discriminant components (PC1 and PC2) explained 34.4% of the total variance within the elemental composition of the 37,440 leaf-deposited particles (Figure 2.13, I). PC1 discriminated between particles based on the interrelated K, Ca, Mg, P, and S composition and, in trade off with the first, the interrelated Si and Al composition and the Fe composition. PC2 reflected the variation due to the interrelated Na and Cl composition and, to a lesser extent, the interrelated Cu and Pb composition. When including particle size diameter, aspect ratio and shape, PC1 and PC2 explained only 28.5% of the variance (Figure 2.13, II). Yet, the major elements were still grouped in the same way. The aspect ratio and shape of leaf-deposited particles varied in the same direction, as corroborated by positive correlations between those parameters (§2.3.2.1). Furthermore, this direction was contrary to the element Fe, suggesting Fe-enriched particles to be more connected than the other elements to less elongated and more circular particles. The size diameter of particles on its turn showed to be positively related with Na and Cl. The PCA biplots on the particles' morphology and composition did not reveal overall evident discrimination between the various source types. Yet, the Rural site was depicted to be more linked with elements Si and Al, the Roadside with Fe, and the Industry with Pb and Cu.

When performing the PCA separately on the particles deposited either on the abaxial or on the adaxial side, approximately the same interrelated variables are identified (Figure 2.13, AB, AD) with a few exceptions to mention. For instance, the abaxial leaf-deposited particles did not show the positive relationship between Na and Cl, and the size of particles anymore (Figure 2.13, AB). The composition in Na and Cl of the adaxial particles was rather associated with P, S and Ca, than with the particle size (Figure 2.13,

AD). Still regarding the adaxial particles, Fe-enriched particles were strongly oppositely related with the size, shape and aspect ratio, corroborating the hypothesis that Fe-rich particles were particularly smaller and more circular compared to particles rather enriched in the other major elements. Traffic-derived combustion emissions generate small Fe-rich spherules, whilst coarse, non-spherical particles are also emitted from abrasion/corrosion of e.g. vehicle tires and brake pads (Matzka and Maher, 1999). When making the distinction between coarse ($PM_{2.5-10}$) and fine ($PM_{2-2.5}$) particles (not shown), the key observation from the PCA was that coarse Fe-particles were more interrelated with Si and Al in comparison with the fine Fe-particles, suggesting the coarse Fe-derived particles to be more associated with crustal matter dust than the fine fraction.

MORPHOLOGICAL & ELEMENTAL CHARACTERIZATION OF LEAF-DEPOSITED PM PER SOURCE TYPE

Figure 2.13 - Biplots of the first two components (PC1 and PC2) of a PCA considering as input variables I) the major elements (Na, Mg, Al, Si, P, S, Cl, K, Ca, Fe, Cu, Pb; %, m/m) of leaf-deposited particles, and II) the morphological parameters (size diameter, aspect ratio and shape) in addition to the major elements. The biplots of PCA II applied separately to the abaxial (AB) and adaxial (AD) leaf-deposited particles are shown. The source types depicted from the PCA scores of the particles are shown in blue. Given the large number of particles, the PCA scores are not shown to improve readability.



According to the Bootstrap Forest, averaged over a total of 28 decision trees in the forest (the prediction model did not improve by including more trees), the input variables (size diameter, aspect ratio, shape, Na, Mg, AL, S, P, Si, Cl, K, Ca, Fe, Cu, Pb) yielded a satisfactory prediction of the source type, with a generalized R^2 of 0.83 (maximum is 1 for perfect models) and a misclassification rate of 0.28 for the training dataset (and ca. 0.33 for the validation and test datasets). The root mean square error (RMSE) and mean absolute deviation were still considerable, 0.55 and 0.49, respectively. The smaller the latter values are, the better fits they indicate. From the 15 predictor variables, the composition was rather more accountable for splits in the decision trees than the morphological parameters, with the main split contributors being K, Pb, Fe, Ca, S and Si (Table 2.7). This indicates that the content in these elements aid the most in correctly classifying the tested source types. On contrary, the diameter, aspect ratio and shape of particles, together with their content in Na and Cl, had the least discriminatory power. The first is likely due to the fact that particles' size and morphology were comparably diversified across the five tested sites, while the second reflects the regional influence, rather than site-specific influence, of sea salt. The source apportionment of leaf-deposited PM based on the RF method was most efficient for Industry and Forest, as these were highly associated with Pb and K, respectively (Table 2.8).

Table 2.7 – Variable contributions to the RF prediction model, ordered from highest to lowest contributor. Highest contributors are responsible for highest number of splits within the generated decision trees (total of 28), denoted also by the highest G^2 (likelihood-ratio chi-square) values and correspondent high portion of G^2 to the predictor.

Predictor	Nr of splits	G^2	Portion
K	1076	4729	0.228
Pb	152	3252	0.157
Fe	888	2117	0.102
Ca	919	1768	0.085
S	964	1526	0.073
Si	820	1521	0.073
Al	809	1273	0.061
P	346	1100	0.053
Mg	612	785	0.038
Cu	106	758	0.036
Cl	490	663	0.032
Na	483	532	0.026
Size diameter	695	282	0.014
Shape	649	273	0.013
Aspect ratio	577	192	0.009

Table 2.8 – Confusion matrix of predicted to actual observations, for the training dataset. The classification accuracy (CA, ratio of correctly classified observations to the total of observations) per source type is also included.

Actual	Predicted					CA
	Forest	Rural	Roadside	Train	Industry	
Forest	3480	325	210	464	20	47%
Rural	436	2480	704	425	45	36%
Roadside	348	474	3409	360	131	43%
Train	666	417	461	2833	65	38%
Industry	55	142	442	86	3983	51%

2.4 Conclusions

The morphological and elemental characteristics of PM_{2-10} deposited on ivy leaves from five different source types were thoroughly investigated using SEM/EDX. From the total of 37,440 analyzed leaf-deposited particles, the mean particle size diameter was $3.52 \pm 1.58 \mu\text{m}$, with median values ranging between 2.80 and 3.09 μm across the five studied locations. The size distribution was evidently biased towards the small-sized PM, as ca. 32% of the particles were smaller than 2.5 μm ($PM_{2.5}$). Considering the particles deposited on both leaf sides (abaxial and adaxial), the median particle size

followed the order Roadside = Industry ($2.92 \mu\text{m}$) < Forest ($2.99 \mu\text{m}$) < Rural ($3.02 \mu\text{m}$) < Train ($3.06 \mu\text{m}$). For three out of the five sites (namely, Forest, Rural and Industry), the size diameter of deposited particles was larger on the adaxial leaf side than on the abaxial. Both the particles' size and morphology (aspect ratio and shape) were influenced by source type, with Roadside particles being overall the smallest in size and the most circular in geometry. An impressive number of atmospheric leaf-deposited particles was estimated in this study (and comparable with other studies), ranging on average between 1.2×10^6 (Forest) and 3.7×10^6 (Industry) particles per leaf side of ivy.

The composition of leaf-deposited particles was overall governed by Si, Fe, Ca, S, K, Al, Pb, Cl, Na, Mg, P and Cu. While Forest and Rural elemental profiles were mainly associated with natural PM (Si, Ca, S, K, Al, Mg, Na, Cl), the Industry particles revealed the highest anthropogenic metal input, particularly in Zn, Cu, Pb and As. The PM_{2-10} profiles for Roadside and Train were rather comparable and dominated by Si, Fe, Ca and Al, with the first site moderately enriched in Fe, Cu, Zn, As and Ba, and the second moderately enriched in Fe, Zn and As. The discrimination between Roadside and Train was only possible by evaluating their fine ($2 - 2.5 \mu\text{m}$) and coarse ($2.5 - 10 \mu\text{m}$) PM characteristics. The fine particles from the Roadside were 72% more enriched in Fe than its coarse fraction, whereas this size-dependent enrichment was negligible for the Train, suggesting thus a larger contribution of combustion-derived particles (small, rather circular, Fe-enriched) at the Roadside compared to the Train. According to the Tomlinson *PLI*, Roadside (combustion-related) and Industry (metal pollution) were found to be moderately and very highly polluted sites, respectively.

Using the particles' morphological and compositional information as input variables yielded a rather good RF prediction model (generalized $R^2 = 0.83$, misclassification rate 0.28), with K, Pb and Fe as main predictors. The source apportionment of leaf-deposited PM based on the RF model was most efficient for predicting Industry (51%) and Forest (47%) particles. Yet, the rather modest classification accuracy of the RF model (36% - 51%), implies the influence of common, regional PM, at the same time

that demands for additional fingerprinting techniques that may aid in apportioning PM sources more accurately. Nevertheless, our results demonstrate that leaf particle-based analysis allows to fingerprint and pinpoint different source types, particularly when considering both the composition and morphology of leaf-deposited PM.

Chapter 3

Magnetic- and particle-based techniques for source apportionment of leaf-deposited PM

“Logic will get you from A to B. Imagination will take you everywhere”

-- Albert Einstein

Chapter 3.1

Magnetic- and particle-based techniques to investigate metal deposition on urban green

Based on: Castanheiro, A., Samson, R., De Wael, K., 2016. Magnetic- and particle-based techniques to investigate metal deposition on urban green. *Science of the Total Environment*, 571, 594–602.

Abstract

This chapter reports on the utility of combining magnetic- and particle-based techniques to investigate PM leaf deposition as a bio-indicator of atmospheric metal pollution. While particle analysis through SEM/EDX is very comprehensive for characterizing leaf-deposited and atmospheric PM, magnetic techniques, which are comparatively more expeditious and straightforward, can be used as a reliable, discriminatory tool for leaf metal deposition. In this study, the trace metal content of leaf-deposited particles, estimated by SEM/EDX as described in the previous Chapter 2, and the leaf magnetic content (SIRM) were investigated in order to examine the relationship between the leaf magnetic behavior and their particulate-deposited trace metals across different source sites (forest, rural, roadside, train, industry). The influence of the different sites was detected both magnetically and in terms of metal content, with road- and railway-traffic contributions clearly different from the background sites. Although with similar trace metal content, including in terms of Fe, those two traffic types could only be differentiated magnetically, revealing the intrinsic differences in their emission sources which is, thus, illustrative for the magnetic source apportionment prospective.

3.1.1 Introduction

Trace metals of anthropogenic origin are of particular interest within airborne PM given its non-degradability in the environment (Qian et al., 2014). In a Flemish study on the chemical composition of PM₁₀, Cr, Mn, Fe, Cu, Zn, and Pb were identified as traffic-related species (Vercauteren et al., 2011). Several trace metals are emitted through the abrasion of tires (Cu, Zn, Cd) and brake pads (Cu), corrosion (Fe, Cu, Zn, Cd, Cr), lubricating oils (Cu, Zn, Cd) or fuel additives (Zn, Cd, Pb) (Tomašević and Aničić,

2010, and references therein). Pb is strongly associated with historic leaded-fuels usage, while Cu, Cd, and Zn can be identified as industrial or incinerator emissions, in addition to traffic (Zhang et al., 2012). Still, only a small number of air monitoring stations routinely measures metal concentrations (EEA, 2013). As well as polluting the air, metal particulates can get deposited (through wet or dry processes) on terrestrial and water surfaces, building up in soils or sediments, and ultimately leading to bioaccumulation in food chains (EEA, 2013). Consequently, the transfer of metals to the biosphere (Kocić et al., 2014) as constituents of PM is one of the most complex issues within the air pollution problem.

While the accessibility to investigate the impact of PM on soil can be highly hampered in urban environments due to coverage by roads, pavements and buildings, vegetation is usually widespread in cities, providing natural surfaces for deposition and immobilization of small atmospheric particles (Freer-Smith et al., 2005; Kardel et al., 2012a; Litschke and Kutler, 2008; Mitchell et al., 2010; Weber et al., 2014) by leaf deposition or in-wax encapsulation (Kardel et al., 2011; Terzaghi et al., 2013). Several studies have used vegetation samples (such as plant leaves) as magnetic bio-indicators of air pollution (e.g. Hofman et al., 2013; Kardel et al., 2011; Matzka and Maher, 1999; Mitchell et al., 2010; Moreno et al., 2003; Norouzi et al., 2016; Sagnotti et al., 2009; Vuković et al., 2015; Yin et al., 2013), to rapidly identify e.g. PM pollution gradients and hotspots. Particle analysis in terms of composition and size should not be overlooked though, as these factors closely influence the PM impact on human health, and may add relevant information to the magnetic evaluation. SEM/EDX can be used as a particle-based technique for such an investigation, as it allows the examination of plant surfaces and deposited particulates at high resolution (Pathan et al., 2008).

The enrichment of magnetic particles has been associated with trace metals such as Cr, Mn, Fe, Cu, Zn, Cd, and Pb in both urban topsoil and leaf dust (Lu et al. 2006, 2007, 2008). However, depending on the local conditions not all metals will be present or occurring in the same proportion, and this happens similarly for magnetic particles. Because the fractions of magnetic and metal particles tend to reflect the local

anthropogenic pollution, magnetic analysis as a measure of trace metal content was applied to ivy leaves sampled from different sites (forest, rural, roadside, train, industry) in Antwerp, Belgium. The overall composition and morphology of PM deposited on these leaf samples, examined with SEM/EDX, has been thoroughly described in Chapter 2. As a step forward, the present chapter reports on the magnetic and metal content of these leaves, with the following objectives: to discriminate the influence of different source types on PM leaf deposition according to its magnetic behavior and metal content; to examine the relationship between the magnetic behavior of sampled leaves and the trace metal content of leaf-deposited PM; and to illustrate the combined use of magnetic analysis with a particle analysis technique for a more integrated study of urban leaf-deposited PM.

3.1.2 Materials and methods

3.1.2.1 Study area and leaf sampling

Ivy leaves were collected from five different sites in Antwerp region, as described in detail in Chapter 2 (§2.2.1), in an attempt to assess the influence of different source types (namely, Forest, Rural, Roadside, Train and Industry) onto the magnetic and metal content of leaf-deposited PM. Combustion processes whether domestic, industrial or vehicle, produce small Fe-bearing spherules, as Fe occurs as an impurity in fossil fuels (Hofman et al., 2013). In addition to combustion exhaust emissions, the frictional sliding and brake wear in railway (and subway) traffic releases high metallic, inhalable particles (Moreno et al., 2014; Nangung et al., 2017). Depending on the industrial activity present, the variety of metals released to the atmosphere should differ from road- and railway-traffic. The targeted industry in this study mainly handles precious and non-ferrous metals, with reported exceeding emissions of As, Cd and Pb (VMM, 2017).

3.1.2.2 Scanning electron microscopy coupled with energy-dispersive X-ray spectroscopy

In the context of this study, the trace metal content (TM) in elements Cr, Mn, Fe, Cu, Zn, Cd, and Pb, was estimated per source type. The composition of leaf-deposited PM in these metals was estimated considering the particles deposited on both leaf sides (abaxial, AB; adaxial, AD), in order to compare it with the leaf magnetic content, which was measured on the entire leaves. For each source type and element x , the total weighted-volume composition $W\%_{Tx}$ (% , v/v) was calculated arithmetically from the mean composition \bar{C}_x of abaxial ($n = 4$ samples) and adaxial ($n = 4$ samples) leaf-deposited particles and their total particle volume v following Equation 3.1.1. The trace metal content was then obtained by summing the composition in elements Cr, Mn, Fe, Cu, Zn, Cd and Pb (Equation 3.1.2).

$$W\%_{Tx}(\%, v/v) = \frac{(\bar{C}_{xAB} \times v_{AB}) + (\bar{C}_{xAD} \times v_{AD})}{v_{AB} + v_{AD}} \quad (3.1.1)$$

$$TM(\%, v/v) = \sum W\%_T[Cr, Mn, Fe, Cu, Zn, Cd, Pb] \quad (3.1.2)$$

3.1.2.3 SIRM determination

After the collection of leaf samples for SEM/EDX analysis, the remaining leaves were submitted to a SIRM-based magnetic analysis while still fresh. Leaf SIRM was measured in an attempt to discriminate between the various source types, as SIRM preferentially points towards the influence of combustion and metallic wear processes (Lehndorff et al., 2006; McIntosh et al., 2007), and its determination is rather straightforward. Each leaf was tightly packed with cling film and pressed into a 10 cm³ plastic container. Following the protocol of Hofman et al. (2014b), the sample containers were magnetized with a pulsed field of 1T using a Molspin pulse magnetizer (Molspin Ltd., UK). After magnetization, their remanent magnetic intensity (SIRM equivalent, in mA m⁻¹) was measured using a calibrated Molspin Minispin magnetometer (Molspin Ltd., UK). Each leaf was measured twice to reduce measurement errors, and the mean of the two values was considered. The magnetometer was calibrated using a

magnetically-stable rock specimen after each eight samples. The SIRM signal of empty containers was used as blank signal, therefore subtracted from the measured values. Subsequent to the magnetic analysis, leaves were removed from the sample containers and the cling film and their leaf surface area was determined using a LI-3100C (Licor Biosciences, USA) leaf area meter. The magnetic intensity values, expressed in mA m^{-1} , were normalized for the sampling container volume (10 cm^3) and for the leaf surface area (in cm^2) to obtain SIRM values normalized for leaf area, expressed in A.

3.1.2.4 Data analysis

Because of the replicates at each sampling site ($n = 8$), site effects on leaf SIRM could be distinguished from statistical outliers. Two statistical outliers within leaf SIRM results ($n = 40$) were detected using SPSS 23.0 (IBM Corp, USA) and replaced by the mean leaf SIRM of the considered study site. The mean SIRM value per source type was obtained by averaging the SIRM of the correspondent eight leaf samples, and the standard error (SE) was calculated to account for the uncertainty around the mean estimate. While the leaf magnetic measurements considered total leaves, the microscope allowed to analyze particles deposited either on the adaxial or abaxial side. To evaluate the behavior of the leaves' metal and magnetic content per source type, the total weighted-volume metal composition $W\%_{Tx}$ (% v/v) including both abaxial and adaxial particles was investigated in comparison with the mean leaf SIRM. Spearman's correlations (using JMP Pro 14) were also used to evaluate potential associations between leaf SIRM and the metal content of deposited particles, by comparing for the various leaf samples ($n = 40$) the leaf SIRM against the composition ($W\%_x$) in the metals of interest.

3.1.3 Results and discussion

3.1.3.1 Leaf SIRM

The area-normalized leaf SIRM results obtained from the collected ivy leaves ranged from 19.9 to 444.0 μA , which is in agreement with former SIRM values reported by

Hofman et al. (2014c) who observed SIRM values between 33.5 and 639.7 μA for ivy leaves collected at 1.5 m height in the same study area (city of Antwerp). Matzka and Maher (1999) observed values between 5.1 to 67.4 μA from birch (*Betula pendula*) trees in the city of Norwich, England, at a sampling height of 1.5 to 2 m. In the Flemish city of Ghent, Hofman et al. (2013) had found SIRM values between 3.5 and 64.1 μA from London plane (*Platanus x acerifolia*) tree leaves sampled at 5, 8 and 12 m height. Still in Ghent, Kardel et al. (2011) reported e.g. mean leaf SIRM values of 86 μA for *Carpinus betulus*, 99 μA for hairy *Tilia sp.*, and 46 μA for non-hairy *Tilia sp.*, for leaf samples collected at 2 - 4 m height in high polluted sites (urban and industrial areas with high traffic and industrial activity), while the low polluted sites showed mean leaf SIRM values of 15 μA for *Carpinus betulus*, 34 μA for hairy *Tilia sp.*, and 11 μA for non-hairy *Tilia sp.* These findings suggested that PM collection on leaf surfaces is species-dependent, which was also corroborated by the studies of Jordanova et al. (2010), Sæbø et al. (2012) and Speak et al. (2012). Due to differences in plant species, but also in study area, sampling height, and sampling time, it is not possible to compare directly our obtained leaf SIRM results against the values from the mentioned studies. Nonetheless, the obtained values appear to be in the same order of magnitude as former published SIRM values.

In this study, and in Hofman et al. (2014c), SIRM of ivy leaves showed to be relatively higher than published SIRM values of e.g. plane and birch leaves, possibly due to the fact that as an evergreen species, ivy leaves might have been longer exposed than deciduous leaves. When magnetically comparing leaves of evergreen oak (*Quercus ilex*) with plane tree leaves (*Platanus sp.*) collected in Rome, Moreno et al. (2003) observed that the evergreen species presented higher magnetic intensities than the deciduous species. While deciduous species only accumulate pollutants on their leaves during the vegetation season, evergreen species accumulate particles throughout the entire lifespan of their leaves.

3.1.3.2 Influence of different source types on PM leaf deposition

o Leaf SIRM

The highest SIRM values were observed at the study sites defined as Train (mean SIRM of $399.0 \mu\text{A} \pm 8.0 \mu\text{A}$) and Industry ($323.1 \mu\text{A} \pm 7.5 \mu\text{A}$). The mean SIRM measured near the Roadside was $204.6 \mu\text{A} \pm 12.9 \mu\text{A}$, while the lowest values were obtained at the Rural ($65.4 \mu\text{A} \pm 5.3 \mu\text{A}$) and Forest ($24.0 \mu\text{A} \pm 1.0 \mu\text{A}$) (Figure 3.1). As SIRM strongly correlates with atmospheric PM_{10} mass (Hofman et al., 2014b; Matzka and Maher, 1999; Mitchell and Maher, 2009; Muxworthy et al., 2003), the results suggest that the highest PM levels were exhibited in the Train and Industry source types, while Forest can be considered a non-polluted site in terms of PM. Several studies (Hansard et al., 2011; Matzka and Maher, 1999; Mitchell and Maher, 2009) have reported a high correlation between leaf or dust magnetic properties such as magnetic remanence, and atmospheric PM concentrations, indicating a coherent co-existence of magnetic and other urban dust particles. McIntosh et al. (2007) compared leaf SIRM values of London plane trees collected in Madrid with the registered atmospheric concentrations of NO_x and PM_{10} , and observed that the magnetic signal was specific to traffic-related emissions, not to the total particle mass. This link between SIRM and traffic-related PM was also confirmed by the works of e.g. Kardel et al. (2012), Sant'Ovaia et al. (2012), and Maher et al. (2008). In addition to traffic, industrial activities (Goddu et al., 2004; Hansard et al., 2011; Zhang et al., 2012) and railway lines (Kardel et al., 2012; Lorenzo et al., 2006; Moreno et al., 2003) have been recognized as important sources of magnetic particles. Our results suggest that leaf SIRM of ivy leaves can be used as a bio-indicator of anthropogenic PM, being able to distinguish between sites with different urban habitat quality. If one major pollution source such as road- or rail-traffic or industry, dominates the PM emissions, the SIRM signal can be interpreted as proportional to the amount of PM emitted by that particular source. On the other hand, the presence of multiple pollution sources can result in different relative contributions of the various sources to the magnetic signal, and might disturb the source-specific relationships observed between PM and SIRM. Leaf SIRM values

should thus be understood as indicators of anthropogenic PM emissions, instead of e.g. total PM mass.

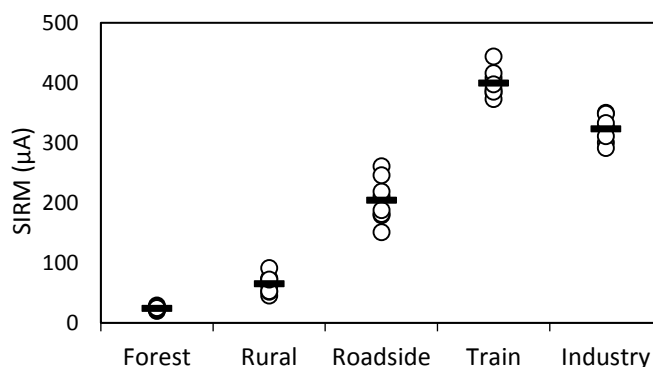


Figure 3.1 – Area-normalized SIRM for the studied source types. Each leaf SIRM is represented by a circle, while the mean SIRM per site ($n = 8$) is indicated by a dash.

Although only five different sites were considered, our results suggest that leaf-deposited PM, and its composition, is not homogeneously distributed over the city region of Antwerp, but mainly depends on local emission conditions: the highest SIRM values were found near railways, industries and intense traffic roads, in agreement with what was verified in other European cities such as Braga (Sant’Ovaia et al., 2012), Cologne (Urbat et al., 2004) and Rome (Moreno et al., 2003). Magnetic techniques including SIRM are mainly sensitive to ferro(i)magnetic particulates and, thus, preferentially characterize the fraction of atmospheric PM that derives from combustion processes or metallic wear and abrasion (Lehndorff et al., 2006; McIntosh et al., 2007). During combustion Fe forms a non-volatile residue, often comprising glassy spherules due to melting (Hofman et al., 2013). The produced spherules contain variable amounts and grain sizes of strongly magnetic (as magnetite, Fe_3O_4) and/or weakly magnetic (as hematite, Fe_2O_3) Fe-particles, depending on the fuel type and temperature of combustion (Matzka and Maher, 1999). In addition to combustion-related particles, non-spherical Fe-rich particles can be generated via metallic wear/abrasion (e.g. tire and brake wear, abrasion of vehicle parts and road pavement) (Matzka and Maher, 1999; McIntosh et al., 2007). Similar processes have also a great importance when considering rail traffic. The high magnetic signal coming from the

Train site is probably due to particles released from the mechanical wear and friction at the rail-wheel-brake interfaces, as Lorenzo et al. (2006) estimated a contribution of 67% of Fe-based particles to the PM₁₀ emissions of a very busy railway line studied in Zurich. When studying the exposure to particle emissions in the subway of New York, Chillrud et al. (2004) observed that the sampling packs carried by teenagers when using the subway had, besides higher concentrations of Mn and Cr, significantly higher concentrations of Fe than domestic indoor and ambient samples.

Because the Forest site was assumed to be representative for a non-polluted environment, a corresponding low SIRM value (mean of 24.0 μ A) was expected. Although the Rural site was only located 300 m away, mean SIRM was almost three times higher (mean of 65.4 μ A) than the value observed for the forested area. This difference, which should be explained by the low-intensity traffic road present in the Rural site, highlights again the strong contribution of vehicle traffic sources to the SIRM signal. Furthermore, the presence of trees at the Forest site likely contributed to protect that area from the pollution derived at the nearby (300 m distant) traffic road (shielding effect). The high-trafficked Roadside showed the highest deviation in terms of magnetic signal from all sampling sites, which may be related to the specific local conditions, as leaves were collected near traffic lights. While an intense brake wear and stop-and-go traffic can be expected at such site, it may also vary according to fluctuations in traffic volume and behavior.

Moreno et al. (2003) found no correlation between magnetic tree leaf properties and the hourly or daily PM₁₀ values as recorded by classical air monitoring stations. Instead of delivering an instantaneous reading of PM pollution, magnetic biomonitoring of leaves provides a time-integrated assessment of local PM exposure. This time integrating nature was also shown by Hofman et al. (2014b) who observed that leaf SIRM was related to the cumulative daily average atmospheric PM_{2.5} and PM₁₀ concentrations, while no relation was found for daily or weekly concentrations. This time-integrating character is appropriate for e.g. the study of health effects due to prolonged PM exposure.

o Trace metal content

From the almost 40,000 analyzed leaf-deposited particles, 37,440 particles had a size diameter between 2 and 10 μm (2 μm was the operating minimum threshold), and 25,811 particles belonged to the size range between 2.5 and 10 μm ($\text{PM}_{2.5-10}$). The mean metal content within the leaf-deposited $\text{PM}_{2.5-10}$, as well as for $\text{PM}_{2-2.5}$ and PM_{2-10} , was estimated per source type (Table 3.1). For all studied sites, the metals Cr, Mn and Cd, appeared to be very low (< 0.1%). The metals Cu, Zn, and in particular Pb, registered slightly higher values, particularly for Industry. In this latter site ca. 30% of the total volume of leaf-deposited particles was composed of Pb, independently of particles consisting of small-sized ($\text{PM}_{2-2.5}$) or coarse-sized ($\text{PM}_{2.5-10}$). This high Pb content suggests high atmospheric Pb concentrations at breathing height, as the leaves were collected between 1.3 and 1.7 m. Pb is a harmful neurotoxin and although its use in leaded-fuels has been internationally banned, Pb contamination is still observed in certain urban areas (Maher et al., 2008). The resuspension of soil material formerly enriched in Pb can thus act as a possible source of particulate Pb. However, the values observed for the studied Industry site are expected to be due to current industrial emissions rather than to historic pollution, as indicators of dust resuspension (e.g. Al, Ca, Si, Fe) (Jancsek-Turóczy et al., 2013) were among the lowest detected within the five source types (§Chapter 2). Studies on the topic have confirmed that, in the absence of heavy industry, the main source of magnetic particles on leaves is derived by traffic pollution (Hanesch et al., 2003; Maher et al., 2008; Moreno et al., 2003). While around industrial sites a close relation between the distribution of magnetic particles and the distribution of metals is verified (Hanesch et al., 2003; Hansard et al., 2011; Zhang et al., 2012), which was corroborated by our magnetic and particle analyses (Figure 3.2).

The trace metal profiles did not greatly depend on the size diameter of particles, with exception of the Fe profile for Roadside (Table 3.1). As it has been previously described (§2.3.2.2), small-sized leaf-deposited particles were more enriched in Fe compared to coarse-sized particles, likely due to the contribution of road-traffic combustion. This

effect was also visible, although minor, in the Rural site, from which the collected leaves were extremely close to a (low-traffic) road. On the other hand, this was quite irrelevant for the other investigated sites, due to negligible car traffic (Forest and Train) and predominance of other PM polluting sources (Industry). The total trace metal content in the elements of interest followed the order Forest \approx Rural < Train < Roadside < Industry.

Table 3.1 - Mean total weighted-volume metal content (% v/v) (calculated from both abaxial and adaxial leaf samples) per source type and for size ranges PM_{2.5-10}, PM_{2-2.5} and PM₂₋₁₀. TM corresponds to the sum of considered trace metals (Cr, Mn, Fe, Cu, Zn, Cd, and Pb). The absence or very low content (< 0.01%) is indicated with "-". N indicates the number of analyzed leaf-deposited particles.

PM _{2.5-10}	Cr	Mn	Fe	Cu	Zn	Cd	Pb	TM	N
Forest	0.05	0.09	9.72	0.08	0.06	-	0.79	10.79	5,146
Rural	0.01	0.06	9.03	0.01	0.02	-	-	9.12	4,857
Roadside	0.03	0.06	24.72	0.17	0.17	-	0.13	25.28	5,355
Train	-	0.02	24.13	0.02	0.27	0.01	0.03	24.48	5,216
Industry	0.06	0.02	10.91	5.17	1.43	0.02	29.51	47.11	5,237
PM _{2-2.5}	Cr	Mn	Fe	Cu	Zn	Cd	Pb	TM	N
Forest	0.02	0.05	10.34	0.09	0.16	-	0.01	10.66	2,220
Rural	0.04	0.08	16.20	0.11	0.07	-	-	16.50	2,074
Roadside	0.08	0.02	40.71	0.21	0.17	-	0.09	41.27	2,642
Train	0.01	0.04	24.26	0.03	0.20	-	0.09	24.62	2,174
Industry	0.07	0.02	11.94	6.90	1.06	0.03	27.41	47.43	2,519
PM ₂₋₁₀	Cr	Mn	Fe	Cu	Zn	Cd	Pb	TM	N
Forest	0.06	0.09	9.47	0.08	0.06	-	0.75	10.50	7,366
Rural	0.02	0.06	9.23	0.02	0.02	-	-	9.35	6,931
Roadside	0.04	0.06	25.52	0.17	0.17	-	0.13	26.08	7,997
Train	-	0.02	24.13	0.02	0.27	-	0.03	24.48	7,390
Industry	0.06	0.02	10.95	5.24	1.41	0.02	29.42	47.12	7,756

o Leaf SIRM as a record of metal pollution

Because the SIRM parameter quantifies the ferro(i)magnetic PM fraction (Hofman et al., 2013; Kardel et al., 2012), the obtained leaf SIRM values were compared against the estimated particle Fe content (Figure 3.2a). While leaf SIRM increased in the following order Forest < Rural < Roadside < Industry < Train, the leaf particulate Fe content displayed a somewhat different behavior. The content in Fe ranged from 9 to 12% for the Forest, Rural and Industry sites, but for Roadside and Train site ca. 25% of

the total volume of leaf-deposited particles was composed of Fe. This was even greater, up to 41%, for the Roadside $PM_{2.5}$ fraction. Although ferro(i)magnetism is by definition associated with the element Fe, an increasing Fe content does not necessarily corresponds to an increasing magnetic signal or vice-versa, as verified by the non-linear relationship obtained between leaf SIRM and the Fe content (Figure 3.2a).

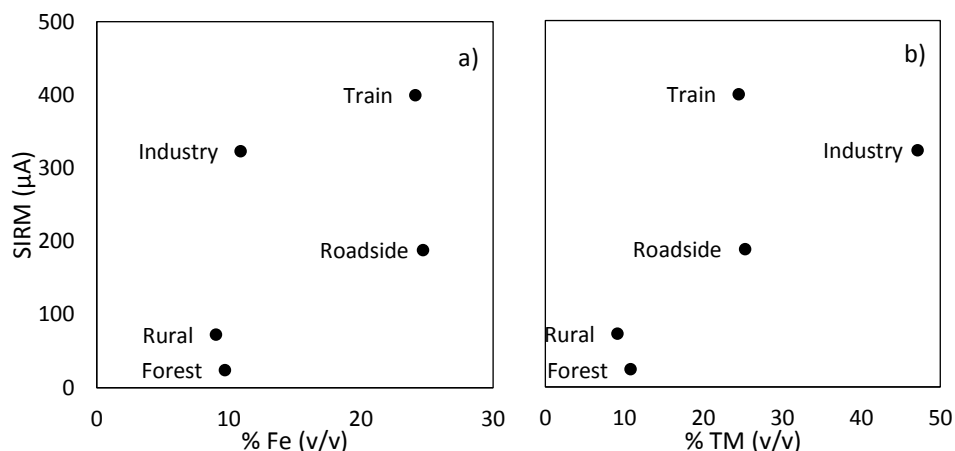


Figure 3.2 – Plot of the mean leaf SIRM against the estimated a) mean particle Fe content, and b) mean particle trace metal content (TM as the sum of Cr, Mn, Fe, Cu, Zn, Cd, and Pb, content), for $PM_{2.5-10}$ at the tested sites.

Enviromagnetic parameters reflect the presence of magnetic particles in terms of their composition, concentration and grain size (Evans and Heller, 2003), and so their interpretation might be less straightforward. While magnetic measurements are sensitive to the chemical structure (note e.g. the difference between magnetite, maghemite and hematite), the metal content obtained from the SEM/EDX is provided in terms of elemental composition, making no distinction between Fe particles with different crystal structures or oxidation states. In terms of particle size, whereas the metal content was here estimated for the range 2.5 - 10 μm , no size fractionation is done along with the leaf SIRM measurement, although it is known that smaller particles generally yield higher magnetic signals as they are more efficient at acquiring remanence (Evans and Heller, 2003). Still, the highest Fe-enrichment for the small-sized (2 – 2.5 μm) Roadside particles did not correspond to the highest leaf SIRM

values. Although additional magnetic parameters would be required to investigate further compositional or grain size effects, leaf SIRM is known to increase monotonically with the amount of magnetic material present (Evans and Heller, 2003).

The magnetic signature of urban polluted sources is mainly due to ferromagnetic minerals such as Fe-oxides, Fe-sulfides, or more rarely native Fe (Lu et al., 2011), and it is also strongly correlated with the occurrence of a variety of trace metals. Based on the recognized association between magnetic and metal particles, leaf SIRM was plotted against trace metal content composed by a wide range of metals (Cr, Mn, Cu, Zn, Cd, Pb, and Fe) (Figure 3.2b). With exception of the Train site, leaf SIRM results seemed to reflect better the content of the seven considered metals, instead of the Fe content alone. When the Train site is not considered, the relation between leaf SIRM and the leaf-deposited metal content follows an approximately linear behavior. However, given the still limited number of samples (i.e. one sampling site per source type) and source types (five), this trend should not be extrapolated to other urban locations without further study on the magnetic characterization of the main urban PM sources. Furthermore, the observed behavior is until a certain extent caused by the high Pb content observed on the leaves from the Industry site, while the other metals appeared to be of less influence.

Already in the 80s, Hunt et al. (1984) established a link between magnetic minerals and metal concentrations that holds in a variety of environmental contexts. Maher et al. (2008) observed that urban roadside tree leaves exhibit significant enhancement in their values of SIRM, Fe and Pb, when compared with leaves growing at a background site, while metals as Zn and Mn showed limited roadside enhancement. In Cologne, high contents in Pb, Fe and also Zn, identified regions affected preferentially by traffic-derived emissions in the sampled pine needles (Lehndorff and Schwark, 2010). Although the concentrations of PM and certain metals, which can be captured by vegetation, are positively correlated with magnetic parameters, the sources of the magnetic minerals and associated pollutants may be variable, such as from Fe foundries, vehicle traffic or ship emissions (Jiang et al., 2015; Xia et al., 2014).

In this study, leaf SIRM showed to be significantly correlated with Cu, Zn, Cd and Pb ($p < 0.01$), followed by the metals Mn and Fe ($p < 0.05$), while no significant correlations were observed with Cr (Table 3.2). The correlation between leaf SIRM and particulate Mn content appeared to be negative, while it was positive for the other correlated metals (Fe, Cu, Zn, Cd and Pb). Although traffic-related processes constitute the principal source of e.g. Fe, Cr, Cu and Zn, high emissions of these metals can also originate from e.g. industrial metallurgical processes. The investigated industrial site, which is associated with metal handling and processing, revealed the highest content in Zn, Cu, and Pb (Table 3.1). Given the high Pb content detected at this site, further investigations must be pursued at soil level to assess the possibility of historic industrial pollution as well. The correlation coefficient was the highest when considering the content of the seven considered metals (TM) ($\rho = 0.80$; $p < 0.01$) in comparison with the Fe content alone ($\rho = 0.38$; $p < 0.05$). Comparable correlations were obtained when considering the size fractions $PM_{2.5-10}$ and PM_{2-10} , whereas correlations between $PM_{2-2.5}$ metal content and leaf SIRM were rather weak and not significant for Mn and Fe. This suggests that leaf SIRM may be more appropriate to say something about the Fe-enrichment of coarse leaf-deposited PM than of fine PM.

Table 3.2 - Spearman's correlation coefficients (ρ) between the measured SIRM and estimated weighted-volume trace metal composition for all analyzed leaf samples ($n = 40$, no distinction between abaxial and adaxial). TM corresponds to the sum of trace metals considered (Cr, Mn, Fe, Cu, Zn, Cd, and Pb).

	Cr	Mn	Fe	Cu	Zn	Cd	Pb	TM	
SIRM	0.10	-0.40*	0.38*	0.55**	0.71**	0.52**	0.66**	0.80**	$PM_{2.5-10}$
	0.31	-0.13	0.12	0.49**	0.47**	0.53**	0.66**	0.71**	$PM_{2-2.5}$
	-0.01*	-0.41**	0.40*	0.52**	0.74**	0.57**	0.65**	0.79**	PM_{2-10}

*Correlation is significant at $p < 0.05$; **correlation is significant at $p < 0.01$.

3.1.3.3 Complementary use of leaf SIRM and SEM/EDX

Two different methodologies were employed for the investigation of leaf-deposited PM in this study: magnetic analysis via leaf SIRM and metal content estimation via SEM/EDX analysis. Leaf SIRM provides a bulk analysis of the leaf in terms of its

magnetic content, while the SEM/EDX allows a detailed, micrometer level, examination of the leaf surface and the particles deposited on it. The measurement of leaf SIRM allows a rapid and easy identification of sites with different urban activities or source types, and SEM/EDX applied to leaf-deposited PM increases the understanding on which metals and to what extent they are present across the different sites. While leaf SEM/EDX offers a close look into the composition and size of deposited particulates, which is of particular interest for PM source investigation, a high spatial city-scale resolution is impossible to reach due to time and economic constraints. Despite the differences between the two methodologies, the combined use of leaf SIRM and SEM/EDX provided complementary knowledge on urban leaf-deposited PM and metal pollution registered across different source types, with more potential for purposes of source attribution than their individual use.

An analysis solely done on the Fe content retrieved from the SEM/EDX analysis would have displayed two different groups of source types: Forest, Rural and Industry with approximately 10%, and Roadside and Train with about 25%. While the Forest and Rural sites can be associated with a similar magnetic signal, the Industry site is magnetically very distinct from those. The fact that the Fe content from the Industry is comparable to the Fe content observed within the Forest and Rural sites suggests that the targeted industry is not a major Fe emitter, and that the Fe-particles at that site may be as well derived from road traffic, or in a less proportion from crustal soil resuspension, rather than from the industrial activity at the sampling location. This finding is also in accordance with the type of industrial activity present, as the targeted industry has no reported emissions of Fe. On the other hand, the largest trace metal enrichment was observed at the Industry site, especially in Cu, Zn and Pb, which showed strong positive associations with SIRM, thus, resulting in SIRM values larger for the Industry than for the Forest and Rural sites.

Although the Roadside and Train samples exhibited leaf-deposited particles with a similar Fe content, magnetically they exhibited different SIRM values as they were exposed to different emission sources of PM, thus reflecting different local urban

conditions. The Fe-particles at the Train site should occur in a very specific way so that it leads to leaf SIRM values higher than the values measured at the Roadside location. The chemical structure of the Fe-particles at the Train site might be e.g. pure Fe or Fe-alloy, which are true ferromagnets, therefore yielding very high SIRM in comparison to the Fe content, similar at the Roadside. Because SEM/EDX only provides an estimate of the amount of elemental Fe and not its chemical structure, further research using e.g. additional magnetic parameters, is required to confirm this hypothesis. Nevertheless, the complementary information produced by leaf SIRM and SEM/EDX already facilitates source discrimination between road- and rail-traffic conditions.

3.1.4 Conclusions

Within this chapter, the metal content of leaf-deposited PM and the leaf magnetic SIRM of ivy leaves exposed at different environments were investigated to examine potential associations and behaviors that can aid in discriminating sites with different PM polluting sources. The influence of different source types was registered both by the leaf magnetic and metal analysis of leaf-deposited PM, with the Roadside, Train and Industry sites exhibiting larger magnetic and metal enrichment compared to Forest and Rural. Given the correlations observed between a range of trace metals (Fe, Cu, Zn, Cd, Pb, and Mn) and leaf SIRM, SIRM-based magnetic assessment is confirmed as an overall indicator of metal pollution on leaf-deposited PM, which is inevitably linked with atmospheric PM.

The occurrence of toxic metals in the atmosphere, which can be transferred to the other environmental spheres, is of special concern for the public health. Although only leaf-deposited particles between 2 and 10 μm were considered, leaf SIRM appeared particularly suitable to measure metal pollution in the coarse PM fraction ($\text{PM}_{2.5-10}$) compared to the fine fraction ($\text{PM}_{2-2.5}$). Despite the generally recognized higher health impact of fine PM, coarser particles contribute more in mass to the closely monitored PM_{10} concentrations, and are, still, harmful as they can be inhaled and contain toxic components such as metals. The use of magnetic parameters such as SIRM as a

discriminatory tool for this specific type of pollution is able to provide a rapid general overview before subsequent detailed monitoring, with our results corroborating the potential of leaf SIRM as a proxy for atmospheric metal PM. In addition to SIRM, other magnetic parameters such as magnetic susceptibility and anhysteretic remanent magnetization and consequent magnetic bivariate ratios and plots, are still required for further magnetic source apportionment, in terms of e.g. grain size.

In this study, ivy leaves showed to be a reliable bio-indicator for urban PM and metal pollution. Being an evergreen plant (i.e., leaves can be sampled throughout the entire year) widely available in the study area, as well as in most Europe, ivy offers a great potential for air pollution monitoring with a high spatial- and temporal-resolution. Time-integrative biomonitoring is of particular relevance as most PM-related health impacts are also due to long-term exposure.

The obtained leaf SIRM results confirmed the validity of using enviromagnetic parameters for the identification and discrimination of different urban activities and environments. The investigation of the magnetic and physicochemical differences between car and railway traffic, and industrial PM, may enable source attribution, which is key for e.g. policy implementation of targeted PM mitigation strategies. The use of SIRM alongside with SEM/EDX particle analysis allowed the distinction between the tested sites. The SEM/EDX offers an estimation of chemical composition, as well as information on particle size and shape, while magnetic measurements provide a cost-effective and efficient tool to identify pollutants. The complementary use of particle- and magnetic- based techniques is thus suggested as an integrated approach to investigate PM deposition on urban green.

Chapter 3.2

How does the amount and composition of PM deposited on *Platanus x acerifolia* leaves change across different cities in Europe?

Based on: Baldacchini, C., Castanheiro, A., Maghakyan, N., Sgrigna, G., Verhelst, J., Alonso, R., Amorim, J.H., Bellan, P., Bojović, D.Đ., Breuste, J., Bühler, O., Cântar, I.C., Cariñanos, P., Carriero, G., Churkina, G., Dinca, L., Esposito, R., Gawroński, S.W., Kern, M., Le Thiec, D., Moretti, M., Ningal, T., Rantzoudi, E.C., Sinjur, I., Stojanova, B., Aničić Urošević, M., Velikova, V., Živojinović, I., Sahakyan, L., Calfapietra, C., Samson, R., 2017. How does the amount and composition of PM deposited on *Platanus acerifolia* leaves change across different cities in Europe? *Environmental Science & Technology*. 51, 1147–1156.

Abstract

Following the potential of joined magnetic and particle analyses for depicting different environments (§Chapter 3.1), the same approach has been extended to a large-scale European campaign. In this study, leaf-deposited PM on a single tree species was sampled (using a specific, common protocol) in the urban areas of 28 European cities, over 20 countries, with the aim of testing leaf-deposited particles as indicator of atmospheric PM concentration and composition. The leaves of *Platanus x acerifolia* trees close to heavy-trafficked streets and within urban parks were examined at the end of the in-leaf period, using SEM/EDX and magnetically (SIRM). The PM quantity and size were mainly dependent on the regional background concentration of particles, while the percentage of Fe-based particles, with ferromagnetic properties, emerged as a clear marker of traffic-related pollution in most of the sites. This biomonitoring campaign revealed, thus, that *Platanus x acerifolia* is highly suitable to be used in atmospheric PM monitoring studies along different countries and climate types; and that morphological and elemental characteristics of leaf-deposited particles, combined with the leaf magnetic content, may successfully allow PM source apportionment even at more local urban scales (parks vs. streets).

3.2.1 Introduction

From the 1970s, higher plants have emerged as suitable bio-indicators in urban and industrial areas (Ristić et al., 2013). In particular, tree leaves efficiently accumulate PM mainly due to gravitational and/or inertial deposition on lamina and tips (Hofman et

al., 2014a; Tomašević et al., 2005). Different plant and tree species have shown different PM accumulation rates, and the ability of leaves to act as PM receptors depends upon height and canopy structure, leaf surface characteristics including leaf pubescence and wettability, as well as meteorological conditions (Kardel et al., 2011; Mo et al., 2015; Sawidis et al., 2011; Simon et al., 2014; Sæbø et al., 2012, 2013; Wang et al., 2013). This has further led to the conception of trees as potential PM pollution mitigation actors (Beckett et al., 1998; Escobedo et al., 2011), with the consequent development of new urban tree planting programs, prioritizing specific tree species selection, alongside choosing strategic locations for their optimal outcomes (Morani et al., 2011). Within this context, a full comprehension of the features and mechanisms of PM deposition on urban tree leaves under real conditions emerges as highly required, since it may greatly help in facing and solving the PM pollution problem in urban environments, through both PM monitoring and mitigation strategies.

Different analytical techniques have been used for leaf-deposited PM₁₀ characterization, such as atomic absorption spectrometry (AAS) (De Nicola et al., 2008; Sawidis et al., 2011), gas chromatography-mass spectrometry (GC-MS) (Castanheiro et al., 2019; De Nicola et al., 2008), inductively coupled plasma mass spectrometry (ICP-MS) (Simon et al., 2014), SEM/EDX (Baldacchini et al., 2019; Sgrigna et al., 2016; Tomašević et al., 2005; Chapter 2 of this thesis) and magnetic SIRM (Kardel et al., 2011; Hofman et al., 2014a; Moreno et al., 2003; Chapter 3.1 of this thesis). In particular, magnetic analysis of leaf material has been pointed as a rapid, easy and relatively cheap strategy for identifying pollution hot spots, especially those related with traffic and industrial activities (§Chapter 3.1) In order to separate leaf-deposited PM from the rest of the leaf material, washing procedures, and subsequent filtering of the obtained solution, have been introduced (Hofman et al., 2014a; Popek et al., 2013; Sgrigna et al., 2015, 2016; Sæbø et al., 2012, 2013). However, only SEM/EDX analyses have allowed a full characterization of individual, leaf-deposited PM₁₀ particles, both upon collection on filters (Sgrigna et al., 2016) and, most important, on 'as it is leaves' (Baldacchini et al., 2019; Davila et al., 2006; Chapter 3.1 of this thesis). Thus, the coupling of single particle techniques, such as SEM/EDX, with macroscopic leaf

material analysis, such as SIRM, is emerging as a highly promising method for obtaining a full quanti-qualitative characterization of leaf-deposited PM, as previously demonstrated in Chapters 2 and 3.1.

In July 2014, within the context of the COST Action FP1204 “Greeninurbs” (www.greeninurbs.com), a call for leaf collection in urban environments was launched among European scientists working on urban green infrastructure and urban forests, for comparing leaf-deposited PM₁₀ particles across European cities, as indicator of atmospheric PM concentration and composition. Some large-scale air quality monitoring experiments have been set up before, e.g. the “*European Network for the Assessment of Air Quality by the Use of Bioindicator Plants Cooperative*” (EuroBionet, involving 12 cities in 8 countries, by Klumpp et al., 2002) and the “*European Survey of Atmospheric Heavy Metal Deposition*” (involving 30 European countries, by Schröder et al., 2016). Moreover, the source apportionment of PM in Europe, as obtained by sampling PM through gravimetric techniques and analyzing it with a variety of analytical methodologies, has been recently reviewed within the context of the COST Action 633 (by analyzing data from 33 cities over 12 countries; Viana et al., 2008). However, the present study described and analyzed the largest dataset ever collected on leaf-deposited PM within European urban environments. The leaves of *Platanus x acerifolia* trees were used as passive air filters, and the leaf-deposited PM₁₀ particles characterized by performing SEM/EDX analysis on untreated collected leaves, also discriminating adaxial from abaxial leaf surface accumulated particles. The results obtained are discussed in comparison with leaf magnetic content, as determined by SIRM on the same samples, and with air quality data and environmental/urban metadata.

3.2.2 Materials and methods

3.2.2.1 Test species and sampling

Leaves were collected at 56 sites, in 28 cities over 20 countries (Figure 3.3). Participants were asked to collect leaf samples according to a specific protocol, together with

supporting background data (sampling information and metadata, such as geographic coordinates, city population, sampling height, distance from the nearest street and from railways, road traffic intensity, existence and distance to surrounding trees). The campaign was carried out at the end of the summer 2014 (between August 25 and September 7), with leaves being sampled after a rainless period of at least three days, to reduce the influence of the meteorological variability among the cities. The mean daily PM₁₀ concentrations obtained by the closest air quality monitoring stations were calculated for the in-leaf period, considered to be from May 1, 2014, to the sampling date. A single species was sampled to minimize possible differences in particle deposition due to differences in leaf surface characteristics. *Platanus x acerifolia* was selected as test species, due to the poor effect of rainfall on the accumulation of magnetizable PM on its leaves (Hofman et al., 2014a) and to its high capability in PM capturing, in general (Mo et al., 2015; Sawidis et al., 2011; Wang et al., 2013). *P. acerifolia* had previously shown significantly higher leaf PM retention amount than *Sophora japonica* and *Cedrus deodara*, likely due to its ridged leaf surface (Wang et al., 2013), while *P. occidentalis* (same genus as *P. acerifolia*) had the second highest amounts of leaf accumulated PM both in-wax and on surface, when compared with 23 other tree species (Mo et al., 2015). Only leaves of *Quercus variabilis* captured higher amounts of PM due to its great quantity of pubescence and rough surface (Mo et al., 2015). However, this species is only poorly distributed in Europe, while *Platanus x acerifolia* is very abundant in all the participating European countries, thanks to its wide hardiness range, which is from 5 to 9 (in a maximum of 12) according to USDA zone (USDA, 1999).

Leaves were sampled at two contrasting urban environments, in a park area and near a street characterized by heavy traffic – further named park and street sites, respectively. At each sampling location, five full grown and undamaged leaves were sampled from the outer canopy of the same tree. A sampling height between 3 m and 5 m was requested by the protocol, as the best compromise to avoid contamination by very local sources at the ground level, while ensuring a feasible procedure during

sampling and the absence of leaf contamination by citizens. Street site trees were sampled at the traffic-exposed side.

After collection, leaves were stored between clean paper sheets and enclosed in paper envelopes, avoiding mechanical stresses. The dried leaves were sent to the organizing laboratories for analysis. There, each leaf was manually cut over its main vein, to obtain two similar halves to be used in SEM/EDX (conducted in Italy, at the IBAF CNR unit in Naples) and SIRM (performed in Belgium, at the Laboratory of Environmental and Urban Ecology of University of Antwerp) analyses. A full characterization of the samples, using both SEM/EDX and SIRM, and a wide gathering of background metadata were obtained for 20 cities, while only SIRM was measured for the remaining eight, due to damages of the leaves during transport and missing information (Figure 3.3).

3.2.2.2 Morphological and elemental characterization

SEM/EDX analyses were performed on two different leaves, randomly chosen from the five available, for each sampling site. For each leaf, two portions of 1 cm² were cut from the leaf part above the left main vein, and separately used for the analysis of the abaxial and adaxial leaf surfaces. A Phenom ProX™ (Phenom-World™, NL) scanning electron microscope was used, equipped with X-ray analyzer and charge-reduction sample holder suited for biological samples. Leaf portions were mounted within the sample holder by using double coated carbon conductive PELCO Tabs™ (Ted Pella Inc., USA), after having fluxed them with compressed air.

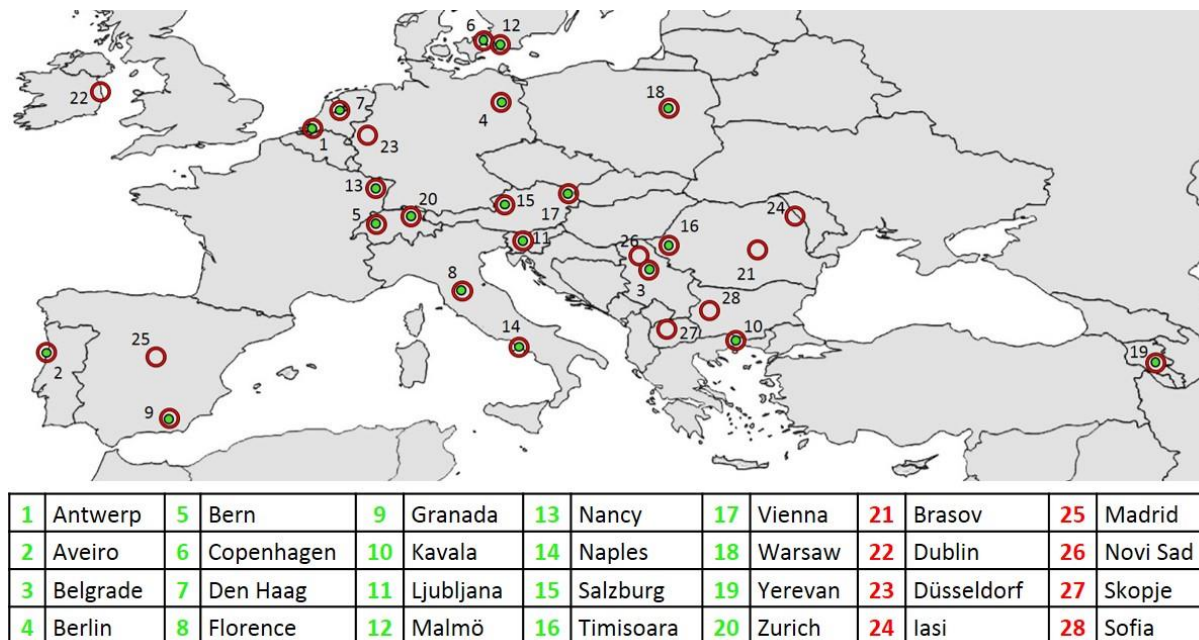


Figure 3.3 – Map of cities participating in the European sampling campaign. Samples from cities 1-20 (red-green spots; green labels in the table) have been analyzed by both SEM/EDX and SIRM. Samples from cities listed as 21-28 (red circles; red labels in the table) have been analyzed only using SIRM. The underlying map is taken from Natural Earth database.

Imaging was performed in backscattered electron configuration with an incident electron energy of 5 keV in order to limit the surface charging. The sample surface was randomly imaged by 150 μm wide scans, at a resolution of 1,024 x 1,024 pixels. For each leaf, five images were acquired at each leaf surface (Figure 3.4, a,b). On these images, PM can be easily distinguished as bright particles, with the color contrast of SEM features being proportional to the atomic number of the elemental components (*i.e.*, the brighter the particle, the heavier the components). SEM images were analyzed with Gwyddion software (Nečas and Klapetek, 2012) in order to obtain the number and dimensions of the leaf-deposited particles. In particular, the diameter of the equivalent sphere (or particle equivalent diameter, d_{eq}) was obtained for each imaged particle, with a cut-off value of 300 nm (which corresponds to the dimension of two image pixels). Particles with a d_{eq} larger than 10 μm (which accounted for less than 0.1% of the total detected particles) were excluded from the analysis. The final dataset was composed by $\text{PM}_{0.3-10}$ particles.

Elemental analysis of selected particles was performed through dedicated Phenom Pro Suite™ software. The leaf surfaces were scanned at 150 μm scan size with an incident electron energy of 15 keV for this (Figure 3.4d). Approximately 200 particles were investigated per sampling site: 50 randomly selected particles on each surface of the two leaves. The equivalent sphere diameter d_{eq} of such particles was obtained by averaging their two main Feret diameters, as measured by ImageJ software (Schneider et al., 2012). The corresponding EDX spectra (Figure 3.4e) were obtained by positioning the laser beam in the center of particles. The elements identified in the particles were C, N, O, F, Na, Mg, Al, Si, P, S, Cl, K, Ca, Ti, Cr, Mn, Fe, Ni, Cu, Zn, Mo, Sn, and Sb. The comparison of the particles' composition was based on those elements detected with a mean concentration higher than 0.1% over the whole dataset (e.g., Na, Mg, Al, Si, P, S, Cl, K, Ca, Fe), while trace metals (Ti, Cr, Mn, Ni, Cu, Zn, Mo, Sn, Sb) were grouped in a single residual variable ("Res"). C, N, O and F were excluded from the analysis due to several reasons: they can be related to biogenic factors; EDX is known to fail in the correct determination of light elements; and the high values and variability of C and O

concentrations as obtained by EDX could hinder the variability of the other elements' concentration, which are more relevant in terms of pollution. Semi-quantitative estimation of the amount of the selected elements was obtained by calculating the weighted-volume percentage $W\%_x$ (% , v/v) following Equations 2.1 and 2.2.

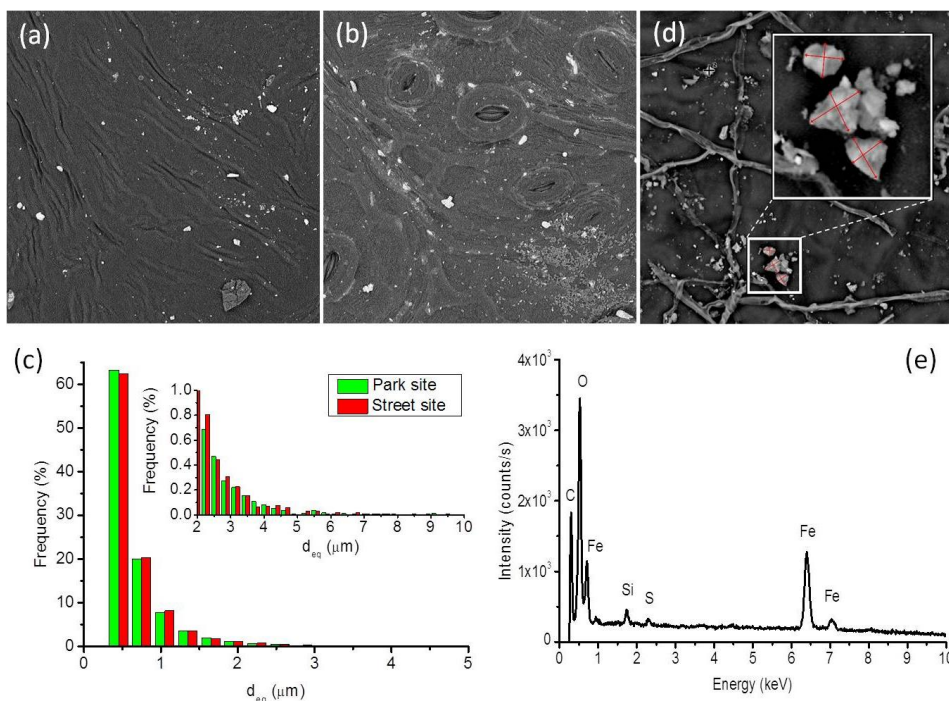


Figure 3.4 - (a,b) Representative SEM images of the adaxial (a) and abaxial (b) surfaces of a *Platanus x acerifolia* leaf (150 μm scan size, 5 keV incident electron energy). (c) Distribution as a function of the diameter of the equivalent sphere d_{eq} of $PM_{0.3-10}$ particles deposited on *P. acerifolia* leaves from park and street sites in Antwerp. (d) Particles selected for EDX investigation on the adaxial surface of a *P. acerifolia* leaf (150 μm scan size, 15 keV incident electron energy): Feret diameters are indicated by the red arrows and are better visible in the three-fold magnified inset. (e) Representative EDX spectrum of a leaf-deposited particle with a high Fe concentration.

3.2.2.3 SIRM determination

Each half leaf was digitally scanned (HP Scanjet G3110), and its surface area was measured using ImageJ software. Then, each half leaf was tightly packed in cling film and pressed into a 10 cm³ plastic container, which was magnetized with a pulsed field of 1 T using a Molspin pulse magnetizer (Molspin Ltd., UK). For each magnetized

sample, the SIRM was measured using a calibrated Molspin Minispin magnetometer (Molspin Ltd., UK). The magnetometer was calibrated using a magnetically-stable rock specimen at the beginning of every session and after every 15 measurements. Each sample was measured twice, to reduce measurement errors, and the mean of the two measured values was considered. The SIRM value of empty containers was considered as blank signal, therefore subtracted from all measured values. The SIRM values (expressed in mA m^{-1}) were normalized for the sample container volume (10 cm^3) and leaf surface area (in cm^2) (Kardel et al., 2011; §Chapter 3.1) resulting in area-normalized SIRM values, expressed in A.

3.2.2.4 Data analysis

Statistical analysis of data distributions was performed using Origin 8.1 software (OriginLab, USA). The particle surface density was analyzed by calculating, for each site, the mean value and the standard deviation, from the particle surface densities obtained from the 20 corresponding SEM images. On the other side, the mean particle equivalent diameter values (and corresponding standard deviations) were calculated, for each site, by averaging over the whole particle dataset. A mean SIRM value per site was obtained by averaging the leaf SIRM of the correspondent five samples, and the standard error (SE) was calculated in order to account for the uncertainty around the mean estimate.

Correlation, variance (ANOVA) and principal component (PCA) analyses were conducted using Statistica 7.0 (StatSoft Inc, USA). Correlation analysis was used to check the relation among experimental data and metadata (R^2 and p values are provided). ANOVA (performed by using Fisher's test, with post-hoc Wilks test for the multivariate analysis) allowed to verify the relation among experimental parameters and both the location of the sampling site and the leaf surface side (p and Wilks' λ values are provided). PCA based on correlation was applied, after suitable data variable standardization, in order to discriminate the sampling sites on the basis of the experimental variables. Sixteen new space variables (principal components, PCs) were

determined, on the basis of the least square criterion, as those maximizing the description of the sites' variability.

3.2.3 Results and discussion

3.2.3.1 Particle leaf surface density and morphology

The number of leaf-deposited particles observed in a single SEM image ($150 \times 150 \mu\text{m}^2$) ranged from 0 (Salzburg, park site) to 4,414 (Yerevan, street site) particles. The mean $\text{PM}_{0.3-10}$ surface density values, as obtained at the 40 sites, were mostly within the same order of magnitude, of 10^4 particles per mm^2 , with few exceptions. The mean particle density at the Yerevan street site was about 10^5 particles per mm^2 , likely due to the dry continental climate and arid steppe native landscape, while the Florence street site mean particle density was ca. 5×10^3 particles per mm^2 , probably because of the relatively high sampling height (12 m) (Hofman et al., 2013). The mean particle density measured at the park and street sites of the same city were not significantly different (within the standard variation range), except for Warsaw ($1.2 \pm 0.6 \times 10^4$ particles per mm^2 and $3.7 \pm 1.4 \times 10^4$ particles per mm^2 , respectively for park and street sites) (Table 3.3).

At every sampling location, the distribution of the $\text{PM}_{0.3-10}$ particles as a function of their equivalent diameter d_{eq} was monotonically decreasing (Figure 3.4c), as previously observed for the range PM_{2-10} in comparable experiments (e.g., Wilkinson et al., 2013) including the one described in Chapter 2. This is consistent with the typical distribution observed in urban areas for the aerosol particle concentration as a function of the particle size: a lognormal behavior is expected, with the main distribution peak centered at a particle diameter value of about $0.1 \mu\text{m}$ or below, and monotonically decreasing in our particle size of interest (Hussein et al., 2005; Pant and Harrison, 2013; Wu et al., 2008) Thus, the majority of the measured particles (ranging between 52.7% for Timisoara street site and 67.1% for Naples street site) was related to very fine PM (d_{eq} in the $0.3 - 0.6 \mu\text{m}$ range), while coarse particles ($d_{\text{eq}} > 2.5 \mu\text{m}$) represented less than 5% (from 0.6% for Ljubljana park site to 4.6% for Granada park site). The mean

d_{eq} of the leaf-deposited particles ranged between 0.6 μm (Aveiro, Belgrade and Ljubljana park sites; Salzburg street site) and 0.9 μm (Granada park site; Timisoara street site) and were statistically equivalent across all sites.

When the particles deposited on the adaxial and abaxial leaf surfaces were analyzed separately, clear differences emerged in terms of both mean particle density and equivalent diameter d_{eq} . At every sampled site, the adaxial leaf surfaces were characterized by higher densities of leaf-deposited particles as compared to the abaxial ones, resulting in an almost doubled mean particle leaf surface density value (3.4×10^4 particles per mm^2 vs. 1.7×10^4 particles per mm^2), throughout the sites. Moreover, the particles observed at the adaxial leaf surfaces had a larger mean d_{eq} with respect to those at the abaxial ones, with the mean values over the sampled sites being $0.75 \pm 0.07 \mu\text{m}$ and $0.67 \pm 0.04 \mu\text{m}$, respectively. These results are in line with previous observations: variations in leaf surface microstructure and wind turbulence may lead to a difference in the quantity and composition of particles accumulated at the adaxial and abaxial leaf surfaces (Mo et al., 2015; Ottel  et al., 2010).

Univariate ANOVA determined that both the mean particle density and the mean d_{eq} correlated with the leaf surface side ($p < 0.0001$ for both parameters) but not with the site location ($p = 0.18$ for the mean particle density, $p = 0.38$ for the mean d_{eq}). Multivariate ANOVA performed by using particle density and mean d_{eq} as dependent variables and leaf surface and site location as independent categorical predictor factors showed still a correlation with the leaf surface (Wilks' $\lambda = 0.67$, $p < 0.0001$) but not with the sampling site (Wilks' $\lambda = 0.97$, $p = 0.34$).

Table 3.3 - Mean particle density (particles per mm⁻²), abundances of fine (PM_{0.3-0.6}) and coarse (PM_{2.5-10}) particles (%), and mean diameter of the equivalent sphere d_{eq} (μm) of leaf-deposited PM_{0.3-10} particles deposited on *Platanus x acerifolia* trees at park and street sites of 20 cities across Europe. Standard deviations of the mean values are also shown.

City	Park site				Street site			
	Particle density (10 ⁴ part./mm ²)	Fine part. (%)	Coarse part. (%)	Mean d_{eq} (μm)	Particle density (10 ⁴ part./mm ²)	Fine part. (%)	Coarse part. (%)	Mean d_{eq} (μm)
Antwerp	3.5 ± 2.3	63.3	2.2	0.68 ± 0.54	3.4 ± 2.2	62.5	1.5	0.69 ± 0.55
Aveiro	6.1 ± 2.8	66.1	0.8	0.64 ± 0.49	4.2 ± 2.7	64.6	1.3	0.67 ± 0.53
Belgrade	0.7 ± 0.7	66.8	0.7	0.65 ± 0.63	1.8 ± 1.3	63.0	1.8	0.71 ± 0.67
Berlin	1.4 ± 1.1	56.9	2.2	0.76 ± 0.59	1.9 ± 1.3	63.6	1.7	0.70 ± 0.76
Bern	1.4 ± 1.5	62.7	1.5	0.70 ± 0.68	1.2 ± 0.8	62.5	2.5	0.74 ± 0.84
Copenhagen	0.8 ± 0.6	63.4	1.8	0.69 ± 0.51	1.9 ± 1.4	63.8	2.2	0.72 ± 0.73
Den Haag	2.1 ± 1.2	60.8	2.1	0.71 ± 0.57	3.5 ± 2.3	58.6	1.5	0.71 ± 0.53
Florence	1.6 ± 1.2	62.7	2.3	0.71 ± 0.56	0.5 ± 0.7	62.0	2.4	0.76 ± 1.02
Granada	2.9 ± 2.6	53.8	4.6	0.90 ± 1.22	1.1 ± 1.0	57.4	3.9	0.82 ± 0.89
Kavala	2.3 ± 1.0	64.7	1.7	0.69 ± 0.59	2.6 ± 1.1	61.0	1.4	0.69 ± 0.53
Ljubljana	1.9 ± 1.5	67.0	0.6	0.62 ± 0.36	2.9 ± 1.7	56.2	1.9	0.74 ± 0.61
Malmö	0.8 ± 0.7	63.2	2.1	0.72 ± 0.77	1.5 ± 1.2	66.4	1.8	0.67 ± 0.57
Nancy	3.9 ± 2.7	63.3	1.5	0.69 ± 0.59	3.7 ± 2.3	62.9	1.3	0.67 ± 0.58
Napoli	3.0 ± 1.5	63.9	1.6	0.68 ± 0.51	2.2 ± 2.0	67.1	0.9	0.64 ± 0.41
Salzburg	0.8 ± 0.6	59.6	2.3	0.74 ± 0.66	0.9 ± 0.6	66.0	1.2	0.65 ± 0.48
Timisoara	1.6 ± 1.4	61.5	3.2	0.76 ± 0.72	5.3 ± 4.2	52.7	4.0	0.86 ± 0.89
Vienna	3.1 ± 1.3	60.5	1.5	0.70 ± 0.68	3.0 ± 2.0	56.9	2.4	0.76 ± 0.62
Warsaw	1.2 ± 0.6	58.7	3.7	0.81 ± 0.94	3.7 ± 1.4	54.6	2.3	0.77 ± 0.69
Yerevan	4.4 ± 3.4	54.4	3.4	0.81 ± 0.76	11.1 ± 5.2	53.6	3.9	0.85 ± 0.97
Zurich	1.6 ± 2.0	59.0	2.4	0.77 ± 0.83	1.3 ± 1.0	61.5	2.3	0.73 ± 0.72

The almost homogeneous mean values obtained for both the particle density and the equivalent diameter of leaf-deposited particles at the 40 sampling sites were consistent with the mean daily atmospheric PM₁₀ concentration values measured by the closest air quality monitoring stations in the in-leaf period. Indeed, all the provided atmospheric PM₁₀ concentrations were in the $20 \pm 10 \mu\text{g m}^{-3}$ range, corroborating previous observations in different European cities (Barmpadimos et al., 2012). However, by comparing the mean PM_{0.3-10} leaf-deposited particle density with the corresponding mean daily atmospheric PM₁₀ concentration, no significant correlation was obtained (Figure 3.5a). A significant, positive correlation ($R^2 = 0.3$, $p < 0.05$) was observed, instead, if only the coarse particle fraction (PM_{2.5-10}) was taken into account (Figure 3.5b). This indicates that PM₁₀ concentration data, as obtained by air quality monitoring stations, is strongly biased towards coarse particles (as larger particles contribute more than smaller particles; Tittarelli et al., 2008), while our approach is a powerful tool for the detection of fine PM, which represents the majority (and the most harmful part; Pope et al., 2002) of leaf-deposited particles. The PM_{0.3-1} fraction in our data accounted for about 80% to 90% of the total PM_{0.3-10} fraction. Local pollution variations could also be hidden by monitoring urban air quality through few, disperse stations, which provide very low spatial resolution data. Conversely, the use of urban vegetation as monitoring tool could enable the study of local PM in a more comprehensive way, without the need of on-site apparatus, contributing particularly for the simplification of future research.

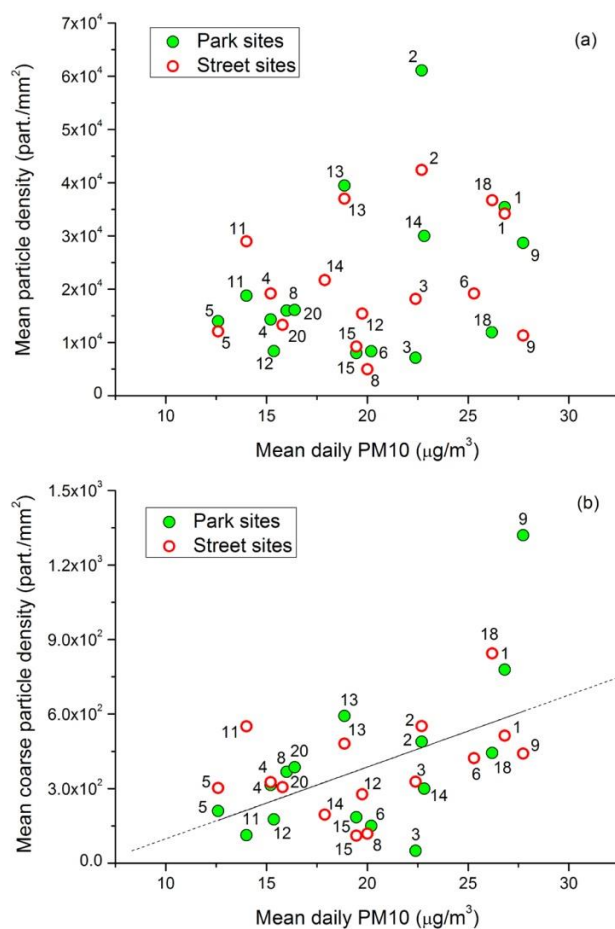


Figure 3.5 - Relationship between the PM_{0.3-10} (a) and the PM_{2.5-10} (b) mean particle leaf surface density and the corresponding mean daily atmospheric PM₁₀ concentration, as measured by the air quality monitoring station closest to the sampled tree. No correlation was obtained when the total of the PM_{0.3-10} particles is taken into account (a), while a linear correlation is obtained between PM_{2.5-10} density and PM₁₀ concentration data (black line in panel b; $R^2 = 0.3$, $p < 0.05$). The corresponding city numbers can be found in the map of cities participating in the European sampling campaign (Figure 3.3).

3.2.3.2 Particle composition and leaf magnetic response

The sum of the weighted-volume percentage $W\%$ of the elements selected for the elemental analysis represented between 12.3% (Den Haag park site) and 31.3% (Warsaw street site) of the particles' total volume. For five cities (Belgrade, Bern, Granada, Nancy, Naples), the percentages obtained at the park and street sites differed less than 1%. For Antwerp, the park site had a summed $W\%$ (18.4%) higher

than that observed at the street site (17.1%), while for all the other cities higher summed $W\%$ values were found for the street compared to the park sites. As a result, mean summed $W\%$ values of 20.4% and 23.6% were obtained by averaging all park and street sites, respectively. This difference is mainly due to the more than double mean $W\%$ of Fe at the street (3.4%) compared to the park (1.4%) sites (Table 3.4). Although Fe is an indicator of crustal soil resuspension, as well as e.g. Al, Ca, and Si, combustion processes derived from vehicle traffic are a known source of small Fe-bearing spherules. In addition to combustion sources, Fe enriched particles can be generated also via metallic wear/abrasion, such as from tire and brake wear, and road pavement abrasion (Matzka and Maher, 1999).

From the total of 28 participating cities, the individual leaf SIRM values measured on *Platanus x acerifolia* leaves ranged from 7.2 μA (Copenhagen) to 202.1 μA (Düsseldorf) in park sites, and from 9.2 μA (Kavala) to 1192.2 μA (Warsaw) in street sites. For the 20 cities that were analyzed by both SEM/EDX and SIRM (Figure 3.3), the park leaves showed a mean SIRM value of 30.2 ± 2.4 (SE) μA , while a mean SIRM value of 152.8 ± 21.7 (SE) μA was obtained for the street leaves.

The park sites showed lower leaf SIRM values than those observed for the corresponding street sites, with exception of the city of Granada, whose park site SIRM value was almost double than that at the street site (61.1 ± 6.9 μA and 25.3 ± 6.8 μA , respectively). This could be due to the fact that Granada park site tree was very close to a high traffic density street (10 m), as well as to a railway track (ca. 480 m). However, it is worth noting that also the weighted-volume percentage in Fe was doubled between Granada park and street site (2.6% and 1.3%, respectively) and that Granada leaves were characterized, at both park and street sites, by the highest coarse particle densities (4.6% and 3.9%, respectively), resulting in the highest mean particle d_{eq} (about 0.9 μm at both sites) observed throughout this large-scale campaign. Thus, both the street and the park sampling sites seem to be affected by analogous PM_{10} levels, and the most probable reason is that, only in this city, leaves have been sampled after 60 days without rain.

Table 3.4 - Elemental weighted-volume percentage W% (% v/v) of PM_{0.3-10} particles deposited on *Platanus x acerifolia* tree leaves collected in 20 cities across Europe, at both a park (P) and a street (S) site. "Res" is the sum of all metallic elements with an average W% < 0.1%; "Sum" is the sum of all the W% listed in the table for the corresponding site.

City	Site	Na	Mg	Al	Si	P	S	Cl	K	Ca	Fe	Res	Sum
Antwerp	P	0.2	1.8	3.1	6.8	0.2	0.2	0.1	0.6	1.5	3.7	0.1	18.4
	S	0.1	0.6	2.0	7.4	0.1	0.2	0.1	0.6	4.2	1.8	0.1	17.1
Aveiro	P	1.3	1.0	2.0	3.8	0.2	2.0	2.2	0.8	6.8	1.2	0.1	21.4
	S	2.1	0.8	6.0	10.3	0.1	0.8	1.1	1.8	3.4	0.9	0.0	27.3
Belgrade	P	0.4	1.3	2.7	5.8	0.3	1.4	0.2	0.8	5.7	0.6	0.0	19.2
	S	0.2	1.7	3.2	8.0	0.2	0.3	0.0	0.7	2.3	2.3	0.0	19.0
Berlin	P	0.2	1.2	3.3	9.1	0.1	0.9	0.1	0.9	4.2	3.2	0.1	23.3
	S	1.3	0.7	2.3	10.6	0.3	0.4	0.3	0.5	2.3	7.9	0.1	27.0
Bern	P	0.6	1.2	2.9	10.3	0.2	0.3	0.0	0.8	5.5	1.0	0.1	22.9
	S	0.3	0.7	1.9	5.7	0.3	0.5	1.9	2.4	6.9	3.0	0.2	23.7
Copenhag.	P	0.8	1.0	2.7	6.1	0.0	0.3	0.1	1.1	3.0	0.6	0.1	15.7
	S	1.5	0.7	2.3	7.2	0.0	0.8	0.5	0.9	4.2	7.1	0.2	25.4
Den Haag	P	0.2	1.2	1.2	3.6	0.5	0.9	0.5	0.9	2.8	0.7	0.0	12.3
	S	0.5	1.1	4.8	9.3	0.2	0.5	0.2	1.5	2.7	3.6	0.1	24.5
Florence	P	1.1	1.3	3.7	7.2	0.2	0.4	0.5	1.1	4.1	1.5	0.1	21.3
	S	1.0	1.4	1.9	7.2	0.1	0.7	0.5	1.0	7.4	1.3	0.1	22.7
Granada	P	0.8	3.4	3.8	7.0	0.1	0.4	0.0	0.7	6.4	2.6	0.2	25.5
	S	2.3	2.8	3.5	5.5	0.3	0.5	1.0	1.0	6.2	1.3	0.3	24.6
Kavala	P	0.1	1.3	3.2	5.9	0.3	0.4	0.5	1.4	4.3	1.0	0.0	18.6
	S	1.0	1.9	3.9	8.6	0.1	0.2	0.0	0.9	3.6	1.9	0.0	22.0
Ljubljana	P	0.4	0.8	1.5	7.9	0.3	0.3	0.3	0.5	4.8	0.5	0.0	17.4
	S	0.2	1.1	3.8	6.5	0.3	0.3	0.7	1.1	2.4	2.9	0.1	19.3
Malmö	P	1.9	1.6	3.5	7.9	0.5	0.7	0.3	0.5	2.9	1.4	0.3	21.6
	S	3.6	1.2	0.5	4.0	0.0	1.4	2.6	1.3	3.5	4.6	0.1	22.7
Nancy	P	0.3	1.6	3.2	9.1	0.2	0.4	0.2	0.6	2.6	0.8	0.1	19.0
	S	0.4	1.0	3.5	8.2	0.3	0.4	0.4	1.4	3.2	1.0	0.1	20.0
Naples	P	0.7	0.6	3.4	7.8	0.2	1.1	0.5	0.8	4.5	1.0	0.1	20.7
	S	0.6	0.6	2.8	7.6	0.4	1.4	0.5	1.2	4.1	1.0	0.0	20.2
Salzburg	P	1.1	1.5	3.3	8.6	0.2	0.8	0.1	0.8	3.6	0.8	0.0	21.0
	S	4.6	0.8	2.2	5.5	0.2	0.2	1.6	1.0	3.9	4.2	0.1	24.2
Timisoara	P	1.1	2.2	3.8	9.5	0.1	0.2	0.3	1.1	2.2	1.5	0.1	22.0
	S	0.9	1.5	3.9	11.0	0.3	0.5	0.3	1.0	3.9	2.9	0.4	26.6
Vienna	P	0.3	2.0	4.5	8.8	0.3	0.5	0.1	1.0	3.4	1.3	0.0	22.1
	S	0.3	1.2	2.9	10.8	0.1	0.4	0.2	0.5	3.0	4.6	0.1	24.2
Warsaw	P	0.1	3.6	2.6	7.4	0.3	0.5	0.0	0.7	4.0	1.5	0.0	20.8
	S	0.4	0.7	2.4	9.0	0.2	0.4	0.4	0.8	3.9	11.1	2.1	31.3
Yerevan	P	0.5	2.3	3.1	8.4	0.2	1.7	0.2	0.7	4.7	1.3	0.1	23.3
	S	1.8	2.0	4.3	10.4	0.0	0.4	0.3	0.7	4.6	1.1	0.1	25.7
Zurich	P	0.9	1.9	3.3	10.2	0.2	0.2	0.0	0.8	2.4	2.4	0.0	22.4
	S	0.2	1.6	4.2	8.8	0.2	0.3	0.0	1.1	5.1	2.9	0.1	24.4
Mean W%	P	0.6	1.6	3.0	7.6	0.2	0.7	0.3	0.8	4.0	1.4	0.1	20.4
	S	1.2	1.2	3.1	8.1	0.2	0.5	0.6	1.1	4.0	3.4	0.2	23.6
	Total	0.9	1.4	3.1	7.8	0.2	0.6	0.5	0.9	4.0	2.4	0.1	22.0

Almost 90% of the analyzed leaves presented SIRM < 300 μA , while the city of Warsaw showed SIRM values that are more than threefold higher, at the street site. The same site presented also the highest Fe (11.1%) and trace metals (“Res” of 2.1%) content from all analyzed cities. Moreover, the Warsaw street site had a significantly higher particle density with respect to the corresponding park site. Because the particle surface density and composition, and the leaf SIRM value of the Warsaw park site were comparable to those of the other cities’ park sites, it is plausible to assume that, at the Warsaw street site, the PM level was mainly due to local emission sources, in this case road traffic. In fact, the highest traffic intensity (ca. 41,200 vehicles h^{-1}) was registered at the street site of Warsaw, from all studied sites. Moreover, air quality in Warsaw is known to be greatly affected by traffic, due to both the city conformation (Reizer and Juda-Rezler, 2016) and the massive use of old diesel cars that characterizes the transition economies of Eastern Europe (Kronenberg and Bergier, 2012).

When comparing SIRM data with the leaf-deposited particles’ Fe content as analyzed by SEM/EDX, most of the street sites revealed both leaf SIRM and Fe content values higher than those observed at the park sites, suggesting a rather clear distinction between the two urban conditions (Figure 3.6). Street sites showed large ranges of both leaf SIRM and Fe content, with mean values from about 20 μA to almost 1000 μA , and from less than 1% to almost 11%, respectively. A good correlation was also obtained between Fe content and SIRM values over the entire street sites’ dataset ($R^2 = 0.4$, $p < 0.05$). On the other hand, the park sites showed low SIRM (< 40 μA) and Fe content (< 2%) values, with few exceptions: parks in Ljubljana and Yerevan showed a high SIRM value but a low percentage in Fe, Zurich and Berlin had a Fe content > 2% but a low SIRM value, while Antwerp and Granada revealed both Fe content > 2% and SIRM > 40 μA . As a consequence, no correlation was found between the Fe content and leaf SIRM on the park sites.

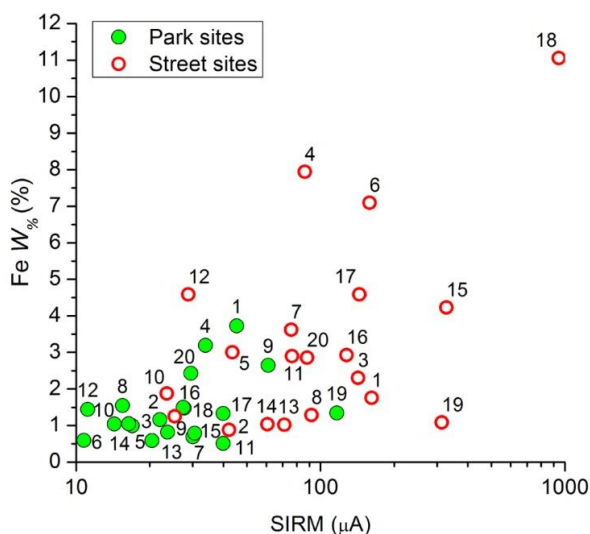


Figure 3.6 - Relationship between the Fe weighted-volume percentage of $PM_{0.3-10}$ particles deposited on *Platanus x acerifolia* leaves sampled over 20 different cities across Europe, both at a street and a park site, and the logarithm of the mean SIRM value as measured from the same leaves. For corresponding city numbers, refer to Figure 3.3.

Although the magnetic signature of urban polluted sources is mainly due to ferro(i)magnetic minerals (such as Fe-oxides, Fe-sulfides, or more rarely native Fe), magnetic parameters such as SIRM reflect the presence of magnetic particles in terms of their composition, concentration and grain size (Evans and Heller, 2003) While SEM/EDX provides the elemental composition of leaf-deposited PM, leaf SIRM values account for the particle chemical structure (crystal lattice and magnetic moments) as well. Therefore, different PM sources may induce different leaf SIRM values at comparable Fe content, or vice versa (Figure 3.6). Those sites revealing similar leaf SIRM and Fe content, such as Ljubljana (sample code 11) and Zurich (20) street sites, or Den Haag (7) and Salzburg (15) park sites, are likely exposed to similar urban PM sources. However, the street sites of e.g. Salzburg and Yerevan (19), which revealed similar leaf SIRM values but different Fe content, or of e.g. Aveiro (2) and Yerevan, with similar Fe content but different leaf SIRM, suggest the presence of different PM sources within the compared cities. Nonetheless, significant correlations are usually observed between leaf SIRM and Fe content close to high traffic density streets (Davila et al., 2006; §Chapter 3.1) as corroborated also by our magnetic and particle analyses

(Figure 3.6), suggesting similar sources across the different street sites. On the contrary, when the city background aerosol becomes more important, i.e. at park sites, the differences among the urban PM composition emerge.

3.2.3.3 Site discrimination

A PCA was performed by considering as input variables the particles' surface density and morphological characteristics (namely, percentage of $PM_{0.3-0.6}$ and of $PM_{2.5-10}$ particles, and the mean particle equivalent diameter d_{eq}), the weighted-volume percentage of the main elements represented in the leaf-deposited particles (Na, Mg, Al, Si, P, S, Cl, K, Ca, Fe; trace metals grouped in "Res"), and the logarithm of leaf SIRM. The PCA generated 16 principal components (PCs). The most discriminant component (PC1), which accounted for 27.0% of the total variance, mainly differentiates the sites with a high percentage of fine particles (positive PC1 values) from those showing a relatively high concentration of coarse particles (negative PC1) (Figure 3.7a). The PC2, explaining 16.3% of the total variance, separates the sampling sites on the basis of the composition of the leaf-deposited particles: negative PC2 values indicate high percentage of Na, Ca, Cl, Fe, trace metals ("Res") and SIRM value, while positive PC2 values characterize sites with relatively high percentage of Si, Al and Mg.

The projection of the 40 analyzed cases in the PC1-PC2 plane (Figure 3.7b) shows that the majority of the park sites are clustered in the plot region with positive PC2 values, showing high concentrations of the elements belonging to the crustal aerosol component (Amato et al., 2009; Viana et al., 2008). This suggests resuspension as the major PM source contributor within park sites, while traffic pollution, usually located relatively distant from parks, seems to be of less importance. Also some street sites (such as Belgrade, Den Haag, Ljubljana, Kavala, Nancy, Naples, and Zurich) fell in the positive PC2 region, showing low levels of source specific pollution. However, most of the street sites are spread in the negative PC2 region (Figure 3.7b), mainly divided in three groups.

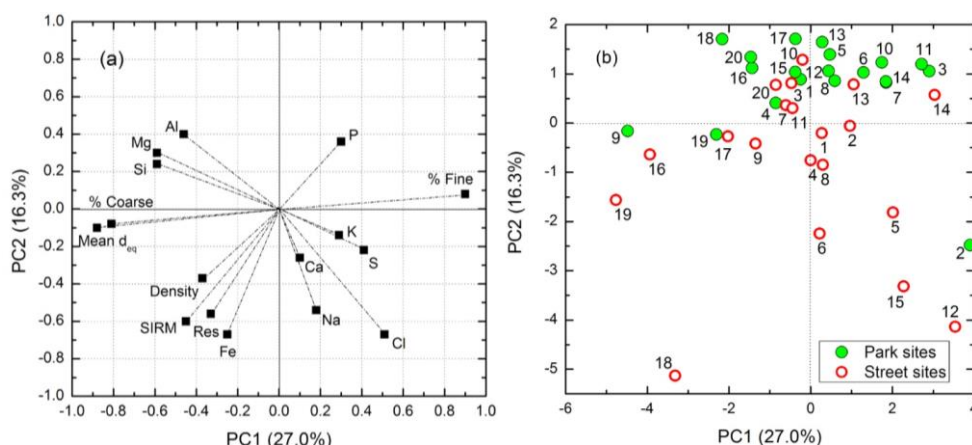


Figure 3.7 - Outputs of the PCA performed by considering as input variables the particle leaf surface density (“Density”) and morphological characteristics (percentage of fine $PM_{0.3-0.6}$ particles as “% Fine”, and of coarse $PM_{2.5-10}$ as “% Coarse”; and mean particle equivalent diameter, “Mean d_{eq} ”), the weighted-volume percentage of the main elements composing the leaf-deposited particles (Na, Mg, Al, Si, P, S, Cl, K, Ca, Fe and trace metals (“Res”), and the logarithm of leaf SIRM value. (a) Projection in the PC1-PC2 plane of the input variables contributions; (b) Projection in the PC1-PC2 plane of the coordinates of the analysed cases. For corresponding city numbers, refer to Figure 3.3.

One group (negative PC1 values) shows a high content of Fe and trace metals (Ti, Cr, Mn, Ni, Cu, Zn, Mo, Sn, Sb) and high leaf SIRM values, and it is characterized by coarser particles and higher particle densities (Granada and Yerevan park and street sites, Timisoara, Warsaw and Vienna street sites). This reveals the presence of PM mostly generated by mechanical actions such as material abrasion and/or dust resuspension, which are largely associated with anthropogenic activities and, in particular, with traffic (Pant and Harrison, 2013). In addition to Granada park site (discussed previously), also Yerevan park site belongs to this group, likely due to the extremely dry continental climate, joined with the high background urban pollution levels (Tepanosyan et al., 2016) and with the many streets with moderate and high traffic loads surrounding the sampled park.

The group at positive PC1 values is characterized by high percentages of fine particles and with high concentrations of Na and Cl (Salzburg and Malmö street sites), Ca (Bern and Florence street sites), or of these three elements together with S (Aveiro park and street sites), and low metal content, suggesting that natural sources should be relevant

at these sites. High concentrations of Na and Cl together are likely due to the presence of salt sources, which could be the marine aerosol (such as for Malmö), salt mines (Salzburg), or salines (Aveiro) (Viana et al., 2008). The high Ca and S concentrations observed at Aveiro sites are likely to originate from salines as well (Rodrigues et al., 2011). Resuspension may induce high concentration of salt particles at street sites (Amato et al., 2010) and the similarity between the park and street sites of Aveiro could be due to the proximity of the park site to the closest street (37 m). Geomorphology of the area could also partially explain the high Ca concentrations at the Bern and Florence street sites, and also the erosion of calcareous buildings present in these cities could be invoked (Cuccia et al., 2011).

Finally, Berlin and Copenhagen street sites fall in between the previous two groups, being mostly characterized by the presence of fine particles with high levels of both Na and Fe levels, possibly linked to anthropogenic sources that involve high-temperature processes (Sgrigna et al., 2016).

3.2.4 Conclusions

This chapter demonstrated that the combination of morphological characteristics and elemental composition of leaf-deposited particles, which can be used as indicators for atmospheric PM concentration and composition, and leaf SIRM, which can be interpreted as pointer of anthropogenic PM pollution, allowed to characterize at least some major PM sources for most of the explored cities across Europe. Common regional background PM composition and concentration were observed across the 20 investigated cities, while certain local conditions, such as the influence of e.g. salt aerosol sources (Malmö, Salzburg, Aveiro) or a dry continental climate and arid steppe landscape (Yerevan), were clearly recognized.

The main PM sources identified in this study are in line with those previously obtained by sampling PM with gravimetric-based techniques and analyzing it with a wide range of analytical methodologies (Viana et al., 2008). Thus, although leaf monitoring is, as a methodology, not as uniform as gravimetric ones, the use of tree leaves as natural

passive air filters was demonstrated in this study to be a good approach for comparing PM deposition in cities along a wide geographical distribution, without the need for expensive, similar and calibrated equipment in the different cities. However, a strict, common leaf sampling protocol is required, to prevent variability due to e.g. sampling procedure and meteorological differences among sites. Another advantage of PM monitoring using leaves is that this methodology is not biased to either finer or coarser PM fractions, in contrast with the conventional gravimetric methods, which tend to be largely influenced by the larger, heavier particles. In particular, the proposed methodology of combining magnetic- and particle-based techniques is highly suitable to investigate the presence in the atmosphere of inorganic, non-soluble, metallic particles, whose leaf-deposition rate is strongly depending on the leaf surface characteristics (the sampling of a single tree or plant species is thus required), while it is only slightly affected by the meteorological conditions, such as precipitation. Hence, such methodology allows to distinguish between different source types/polluted environments within a city, as a clear distinction between street and park sites was generally registered. In this regard, similar studies are pertinent to urban planners and other stakeholders, since they can reveal how local urban conditions vary within the same city, or neighborhood, and may drive the implementation of urban parks and other green infrastructures (such as green walls) at critically polluted urban sites, positively contributing to human health in cities.

Chapter 4

Leaf particle accumulation

"A forest is green for a reason."

-- Anthony T. Hincks

Based on: Castanheiro, A., Hofman, J., Nuyts, G., Joosen, S., Spassov, S., Blust, R., Lenaerts, S., De Wael, K., Samson, R., 2020. Leaf accumulation of atmospheric dust: biomagnetic, morphological and elemental evaluation using SEM, ED-XRF and HR-ICP-MS. *Atmospheric Environment* 221, 117082.

Abstract

That atmospheric dust deposition on plants enables the collection of site-specific PM, is an established fact by now. However, for developing PM monitoring strategies, the intricate underlying dynamics of leaf particle accumulation should also be taken into account. The present study aimed for a leaf-level holistic analysis of dust accumulation on plant leaves. Plant species (ivy and strawberry) with distinct leaf macro- and micro-morphology were exposed during three months at a moderate road traffic site, and leaves collected every three weeks were analyzed for their magnetic signature, morphology and elemental content, by a combination of techniques (magnetic, ED-XRF, HR-ICP-MS, SEM). Dust accumulation was observed both visually (SEM) and magnetically, while metal enrichment was limited (only evident for Cr) and more variable over time. Ivy accumulated more dust than strawberry leaves and was less susceptible to wash-off, even though strawberry leaves contain trichomes and a rugged micromorphology, leaf traits considered important for capturing PM. The magnetic enrichment (in small-grained, single/pseudo-single domain magnetite-like particles) was not species-specific, indicating a common contributing source. Variations in pollution contributions, meteorological phenomena, leaf traits, particle deposition (and encapsulation) vs. micronutrients depletion, are discussed in light of the conducted monitoring campaign.

4.1 Introduction

Besides trapping PM (mitigation action) or impacting local pollutant's dispersal and dilution (aerodynamic action), urban greening (such as plant leaves) allows for a close study of PM chemical and physical characteristics under the influence of e.g.

spatial/temporal variations and local/regional emissions (monitoring action), as it has been demonstrated in Chapters 2 and 3. Atmospheric dust deposition on leaves is mainly influenced by plant species (evergreen or deciduous, wax composition), specific leaf structure (leaf size, shape, roughness, trichomes), meteorological conditions (air humidity, rainfall, wind speed) and source-specific particle features (e.g. particle size distribution) (Chen et al., 2017; Dzierżanowski et al., 2011; Janhäll, 2015; Litschke and Kuttler, 2008; Mo et al., 2015). As leaf accumulation of dust enables the collection of site-specific PM, a further understand of the underlying accumulation dynamics is important to develop the monitoring of atmospheric PM with leaves.

In the context of this thesis, leaves and leaf-deposited PM have been examined so far through SEM/EDX and magnetic SIRM, but a diversity of other analytical approaches are possible, and may provide useful information to develop source apportionment techniques. A range of analytical methods is nowadays available for characterizing e.g. filter-collected PM, such as energy-dispersive X-ray fluorescence (ED-XRF) and high-resolution inductively coupled plasma mass spectrometry (HR-ICP-MS). These two methods differ in terms of sample preparation and detection limits (Galvão et al., 2018, and references therein). ED-XRF allows for a non-destructive, cost-effective and straightforward determination of chemical elements on leaf specimens. This is even possible in relatively small concentrations since the main vegetal constituents (C, N, H, O) are considered transparent to X-rays (Marguí et al., 2009). On the other hand, ICP-MS requires samples in a liquid state to be pumped into a sample introduction system, after which they are subjected to a series of physicochemical transformations before reaching the plasma state at high temperatures (Przybysz et al., 2014). Such complex and onerous analytical routine results in the destruction or alteration of the samples, despite offering a higher detection capability compared to ED-XRF. The coupled use of ED-XRF and HR-ICP-MS for multi-element analysis has been reported before for aerosol samples collected on e.g. Teflon and quartz fiber filters (Okuda et al., 2013; Yatkin et al., 2011). Yet, to our knowledge, the present study is the first where both techniques are applied on leaves to evaluate the accumulated dust composition. Such

evaluation can be supplemented by magnetic analysis, which has proven to be a reliable and efficient tool to capture pollution gradients and sources (Hofman et al., 2017; Maher et al., 2008; Matzka and Maher, 1999; §Chapter 3).

Several studies have examined seasonal or temporal variation in PM leaf accumulation by means of gravimetric, magnetic and microscopic analyses (e.g., Dzierżanowski et al., 2011; Hofman et al., 2014a; Lehndorff et al., 2006; Przybysz et al., 2014; Sgrigna et al., 2015; Sæbø et al., 2012; Wang et al., 2015); however, they mostly focused in comparing the end to the start of the growing season. In some cases, chemical-based techniques were also applied but to a rather small selection of samples (e.g. ICP-MS on three replicates per plants species, as in Przybysz et al., 2014) or on homogenized leaf material (e.g. ICP-MS or ED-XRF on leaf pulverized powders, as in De Nicola et al., 2008, and Kardel et al., 2018). In the present study, we aimed for a leaf-level comprehensive analysis of atmospheric dust accumulation over time. Leaves from two plant species (ivy, *Hedera sp.*, and strawberry, *Fragaria sp.*) with distinct leaf macro- and micro-morphology, exposed to similar conditions, were investigated throughout a period of three months. The magnetic signature, morphology and elemental content of the leaf accumulated dust was investigated by the combination of biomagnetic analysis, ED-XRF, ICP-MS and scanning electron microscopy (SEM). The objectives of this study were: to investigate the temporal leaf accumulation and composition of atmospheric dust throughout a period of three months; to relate the observed accumulation to different leaf characteristics or traits; and to evaluate how the various analytical techniques perform on delivering insight into the process of leaf dust accumulation.

4.2 Materials and methods

4.2.1 Leaf collection and sample preparation

Three ivy (*Hedera sp.*) and three strawberry (*Fragaria sp.*) plants were obtained from a nursery (Garden Center Claes, BE) on May 12, 2017. After collection of blank (non-exposed) leaves (0w), the six plants were planted together in all-purpose potting soil,

inside a robust plastic box (polypropylene; 43 x 36 x 26 cm, length x width x height). The box was perforated at the bottom to allow for water drainage and subsequently placed next to an air quality monitoring station (42R817) of the Flemish Environment Agency (VMM). This monitoring station (Groenenborgerlaan; 42R817; 51°10'38.17" N, 4°25'4.64" E), at ca. 100 m distance from the Campus Groenenborger of the University of Antwerp, Belgium, is located in a residential area with moderate car traffic, with the nearest traffic road at 10 m from the test plants. The land use class of the monitoring station is defined as suburban, with car traffic being the main locally contributing pollution source. Both air quality and meteorological conditions were obtained for the monitored period (§4.2.5). Since the biomonitoring campaign was carried out in summer period, plants were watered (avoiding any physical contact with the leaves) once a week to prevent soil drought stress.

Leaf collection was conducted every three weeks during a period of three months; consecutively on June 2 (3w), June 23 (6w), July 14 (9w) and August 4 (12w), 2017. Leaves were sampled at ca. 35 - 60 cm height from the ground, at a distance of at least 10 - 15 cm from the soil in the box, in order to avoid direct soil contamination and to standardize any potential influence from resuspension of the potted soil or of the soil at the test site. Twelve leaves of each species (i.e. four leaves per plant) were collected per sampling point and subsequently divided in two groups: leaves 1 to 6 were punched with a metallic puncher (48 mm in diameter) to obtain suitable, homogenous leaf sizes for elemental analysis by ED-XRF and HR-ICP-MS; leaves 7 to 12 were used for magnetic and SEM analyses. Leaves 7 and 12 were cut in half and punched (10 mm in diameter) twice to collect adaxial and abaxial leaf samples for SEM. While leaves 1 - 6 had a constant surface area of ca. 18 cm² after being punched, the leaf surface area of leaves 7 - 12 was determined using a leaf area meter LI-3100C (Licor Biosciences, USA). Prior to the analyses, leaf samples 1 - 6 were kept in the fridge (4°C), while leaves 7 - 12 were dried at 35°C for at least three days in a drying cabinet (Memmert, DE).

4.2.2 Leaf surface elemental composition: ED-XRF and HR-ICP-MS

Leaf samples 1 - 6 were analyzed for their elemental composition via ED-XRF and HR-ICP-MS, respectively at the AXES and SPHERE research groups, University of Antwerp. First, leaf samples were analyzed by ED-XRF, on both their adaxial and abaxial surface sides, for the range of elements Na – Bi. For both plant species (ivy and strawberry), element concentrations of non-exposed, blank leaves (0w) were subtracted from the concentrations of the exposed leaves. Whenever elements were highly abundant and variable (with high relative standard deviation) in the blank leaves, high quantification limits were observed and it was not possible to accurately determine their concentrations. Concentrations found for elements Mg, Al, Mn and Zn were below the detection or quantification limits (although their determination was impracticable; data not shown). Samples were measured using a PANalytical Epsilon5 (UK) which has a 600 W Gd anode tube and is equipped with several secondary targets. The following parameters were used for the analyses of (i) Mg-Sn: tube voltage of 25 kV, current of 24 mA, live time of 500 s and a Ti secondary target; (ii) Ti-Ba: 75 kV, 8 mA, 1000 s and Ge secondary target; and (iii) Se-Bi: 100 kV, 6 mA, 1000 s and Mo secondary target, in the samples. The same parameters were used for the analyses of the blank leaves, but with three times the live time. Spectra were fitted using bAxil (BrightSpec, BE), after which net peak intensities were obtained and compared to all blank measurements. Quantification was performed by using sensitivity coefficients which were determined by measuring thin reference films and using a thin-film approximation allowing the concentrations (ng cm^{-2}) to be determined. This approximation is only fully correct for exogenous elements deposited on the leaf surface, whereas for all other elements the information depth needs to be considered. As an indication, we have calculated theoretical information depths using leaf composition from literature (e.g. Hobbie et al., 2006) and an average leaf density of 0.25 g cm^{-3} (Poorter et al., 2009). The calculated information depths were 60-850 μm (Na-Sc); 0.6-1 mm (Ru-Sn); 2-8 mm (Ti-Ga), 2-5 mm (Sb-Er); 1-4 cm (Ge-Nb) and 7-18 mm (Tm-Bi). Although these are estimates, it is clear that for elements with $Z > 21$ (Sc), the full leaf thickness (or a

substantial part of it) is analyzed. In such cases, variations on thickness and bulk composition of leaves will have an influence on the X-ray response; thus, only if exogenous elements are detected, the ED-XRF quantification can be correctly performed.

Subsequent to ED-XRF analysis, leaf samples were individually transferred to acid washed 50 mL glass bottles with 15 mL of ultrapure water ($0.055 \mu\text{S cm}^{-1}$; Milli-Q, Merck, USA), which were then placed on an orbital shaker (GFL 3015, DE) for 3 minutes at 180 rpm. The selected shaking time was previously tested on collected leaves of both plant species (ivy and strawberry). The conductivity of the water solutions achieved a plateau after 3 minutes of shaking, suggesting the stagnation of ions leached from the leaves, and therefore, of dust removal (Lindberg and Lovett, 1985). The resulting washing solutions were collected and acidified with concentrated HNO_3 (Trace Metal Grade, Fisher Scientific, USA) for HR-ICP-MS analysis. The concentrations of elements Na, Mg, Al, Si, K, Ca, Ti, V, Cr, Mn, Fe, Co, Ni, Cu, Zn, As, Rb, Sr, Mo, Rh, Pd, Ag, Cd, Sb, Tl, Pb and U were determined using ELEMENT 2 (Thermo Scientific, USA). From those elements, concentrations of Rh, Pd, Tl and U were all below the method quantification limit (1 ng L^{-1} , equivalent to ca. $6 \times 10^{-2} \text{ ng L}^{-1} \text{ cm}^{-2}$). The elements determined by the two techniques, namely, Si, K, Ca, Ti, Cr, Fe, Cu, Rb, Sr, Pb, were defined as “common elements”.

4.2.3 Leaf magnetic analyses

After drying, leaf samples 7 - 12 were stored at room temperature awaiting magnetic analysis. On the day of analysis, the leaf dry mass (mg) was measured using a S-234 analytical balance (Denver Instrument, USA; 0.1 mg precision), after which the samples were individually wrapped in cling film and packed in 6.7 cm^3 sample containers. Leaf samples were then analyzed for their low-field magnetic susceptibility (χ_{LF}) and their anhysteretic and isothermal remanent magnetization (ARM and IRM, respectively). The magnetic susceptibility k , which illustrates how easily the sample material can get magnetized (Thompson and Oldfield, 1986), was measured using a Bartington MS2B

system (Bartington Instruments, UK). ARM and IRM were measured using an Agico JR-6 magnetometer (Agico Ltd., CZ). The ARM is the remanent magnetization acquired by superposing a small steady direct current (DC) magnetic field with an alternating current (AC) (Evans and Heller, 2003). While the AC field amplitude establishes which particles are involved in the magnetization process depending on their coercivity, the DC field (also named bias field) intensity controls the degree to which those particles are magnetized. Different AC/DC combinations (80mT/80 μ T, 100mT/40 μ T, 100mT/100 μ T, 200mT/100 μ T and 200mT/500 μ T) were performed for ARM acquisition using a LDA5/PAM1 system (Agico Ltd., CZ). Highest ARM values were reached at 200mT/500 μ T (ARM_{200/500}), so this field combination was used in further magnetic ratios, as well for calculating the ARM susceptibility (ARM χ), i.e. the ARM normalized for the DC bias field. IRM is acquired by imposing strong DC magnetic fields; when the applied field leads the sample to saturation, this is called saturation IRM or SIRM. The application of consecutively increasing DC fields until reaching saturation and subsequent demagnetization through the use of reverse fields can be used to characterize the type and grain size of magnetic particles present (Evans and Heller, 2003). In our study, IRM backfield curves were obtained from consecutive field applications with intensities 1T, -1T, 10mT, 20mT, 40mT, 50mT, 60mT, 70mT, 80mT, 90mT, 100mT, 120mT, 150mT, 200mT, 250mT, 300mT, 500mT and 1T, using a Molspin pulse magnetizer (Molspin Ltd., UK). In order to gain insight on the magnetic grain size and the contribution of low/high coercivity magnetic minerals, additional magnetic indicators were produced from the magnetic properties measured, namely, the S-ratio ($IRM_{-300}/SIRM$), HIRM ($0.5(SIRM+IRM_{-300})$) and ARM/SIRM. More information on environmental magnetic analysis for monitoring atmospheric pollution can be found in Hofman et al. (2017).

Magnetic intensities (ARM, IRM), expressed in mA m⁻¹, were corrected for the sample container volume (6.7 cm³) and normalized for leaf surface area (in cm²), yielding values expressed in A. The mass-specific low-field magnetic susceptibility (χ_{LF}) was obtained by dividing the volume magnetic susceptibility (k , dimensionless) by the leaf

dry mass and correcting it for the sample container volume, being expressed in $\text{m}^3 \text{kg}^{-1}$. The contribution of empty sample containers with cling foil (sample blank) was assessed for all measurements and subtracted from the magnetic signal of the corresponding leaf samples.

4.2.4 Leaf morphology and particle visualization with SEM

Each leaf sample punch (of 10 mm in diameter) was fixed on an aluminum pin stub, using conductive double-sided tape (Ted Pella Inc., USA), and left to dry at room temperature for at least three days. Leaf punches were subsequently vacuum coated with carbon (ca. 20 nm thick layer; Leica EM ACE600, DE) and investigated using a FEG-ESEM Quanta 250 (FEI, USA; at AXES and EMAT groups, University of Antwerp) at high vacuum conditions (sample chamber pressure of 10^{-4} Pa), using an accelerating voltage of 20 kV, a take-off angle of 30° , a working distance of 10 mm and a 3.6 spot size. All samples (adaxial and abaxial from leaves 7 and 12 of collection at 0w, 3w, 6w, 9w and 12w) were explored for their leaf micro-characteristics and leaf-surface deposited particles, for which illustrative secondary electron images (SEI) were taken from two opposite locations (e.g. left and right) in the sample, at magnifications 200x, 500x and 2,500x.

4.2.5 Air quality and meteorological data

Atmospheric PM (PM_{10} and $\text{PM}_{2.5}$) and nitrogen dioxide (NO_2) concentrations were obtained from the Groenenborgerlaan air quality monitoring station (42R817; VMM) for the considered exposure period (Figure 4.1). While PM concentrations were measured using an optical particle counter (Fidas 200, Palas, Germany), NO_2 was determined by chemiluminescence (TS 42i, Thermo Scientific, USA). Meteorological data (Figure 4.1) was collected from the nearest monitoring station (Luchtbal, 42M802; VMM), located 9 km away from the 42R817 station. The prevailing wind direction was SW with an average wind speed of $3.1 (\pm 1.3) \text{ m s}^{-1}$. Mean daily air temperature and relative humidity were $19^\circ\text{C} (\pm 3^\circ\text{C})$ and $66\% (\pm 9\%)$, respectively. Total cumulative precipitation was 158 mm during the three months of plant exposure, distributed

between leaf sampling events with 34 mm (0w - 3w), 19 mm (3w - 6w), 57 mm (6w - 9w) and 48 mm (9w - 12w), respectively.

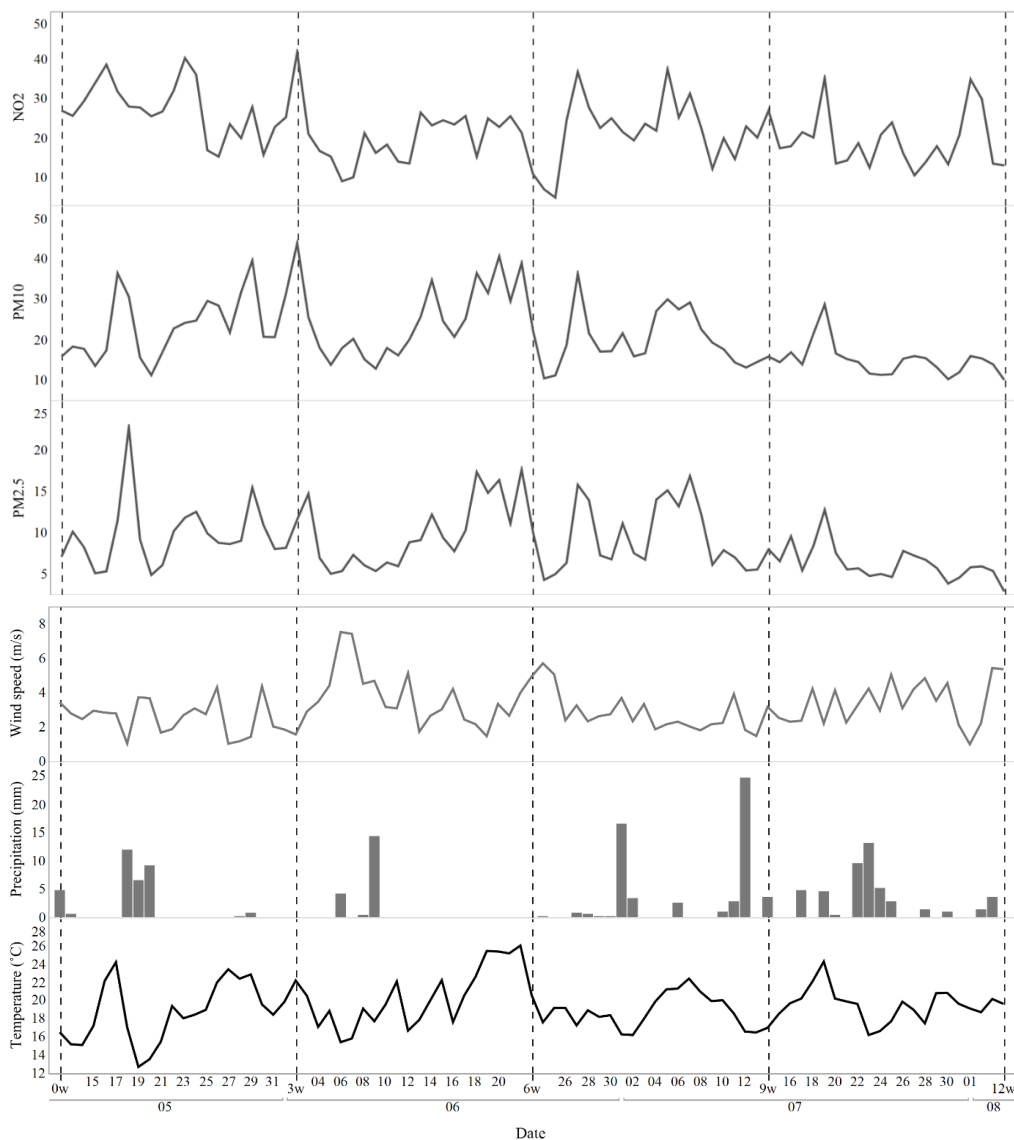


Figure 4.1 – Daily mean concentrations of atmospheric pollutants (NO_2 , PM_{10} , $\text{PM}_{2.5}$, in $\mu\text{g m}^{-3}$) (top panel) and daily meteorological conditions (temperature, precipitation and wind speed) (bottom panel) during the exposure period, as measured at monitoring stations 42R817 and 42M802, respectively. Monitoring station 42R817 is located at the test site.

4.2.1 Data analysis

Differences in leaf surface area and dry mass between ivy and strawberry plants were tested by using a one-way analysis of variance (ANOVA). Visual (histogram and Q-Q plots) and statistical (Shapiro-Wilk normality test) methods were used to assess normality of the magnetic and elemental concentrations per monitored plant species (ivy and strawberry leaves). Results were transformed logarithmically to comply with normality assumptions, however, this did not ensure that the concentrations of all elements followed a normal distribution, due to inter-leaf variability even within the same plant and same exposure conditions. Measured elemental concentrations and magnetic parameters were tested against exposure time by using linear regression fit, while differences between the two plant species were investigated using ANOVA or non-parametric testing (Mann-Whitney or Kruskal Wallis tests) whenever variables were not normally distributed even after transformation. Where applicable, Spearman Rank correlation tests were applied to evaluate associations between different variables. Principal component analysis (PCA) was performed to explore the contribution of different elements in the accumulated leaf dust. Data was processed using Microsoft Excel 2016 and statistical analyses were conducted in JMP Pro 14 (SAS Institute Inc., USA).

4.3 Results and discussion

4.3.1 Leaf macro- and micro-morphology

Both (log-transformed) leaf dry mass and surface area showed to be significantly different ($p < 0.001$) between the two studied plant species. Ivy leaves were on average broader and heavier ($35.2 \pm 7.2 \text{ cm}^2$, $356.3 \pm 93.7 \text{ mg}$; $n = 30$) than strawberry leaves ($22.2 \pm 5.4 \text{ cm}^2$, $135.3 \pm 39.5 \text{ mg}$; $n = 30$). This resulted in specific leaf area values (SLA; leaf area per unit leaf dry matter) of $10.3 (\pm 2.4) \text{ m}^2 \text{ kg}^{-1}$ for ivy and $17.2 (\pm 5.3) \text{ m}^2 \text{ kg}^{-1}$ for strawberry leaves. These leaves, collected every three weeks during a period of three months, showed an increase in their dry mass with exposure time for ivy ($p = 0.005$, $R^2 = 0.25$, $n = 30$), while changes in the leaf surface area over time were only

significant for strawberry ($p = 0.037$, $R^2 = 0.15$, $n = 30$). In terms of epicuticular wax structure, ivy leaves are characterized as platelets while strawberry leaves present wax platelets on the adaxial surface and very dense wax rodlets on the abaxial side (Barthlott et al., 1998; Kim et al., 2009). The micromorphology of strawberry leaves appeared more rugged than for ivy leaves, where an undulated topography is present (Figure 4.2, Figure 4.3). A similar micromorphology and wax structure is observed on both leaf surfaces of ivy, with a high stomatal density on the abaxial side and absence of stomata on the adaxial side. For strawberry, a comparable micromorphology but distinct wax structures are found between both leaf sides, with long trichomes and stomata present on the abaxial side only.

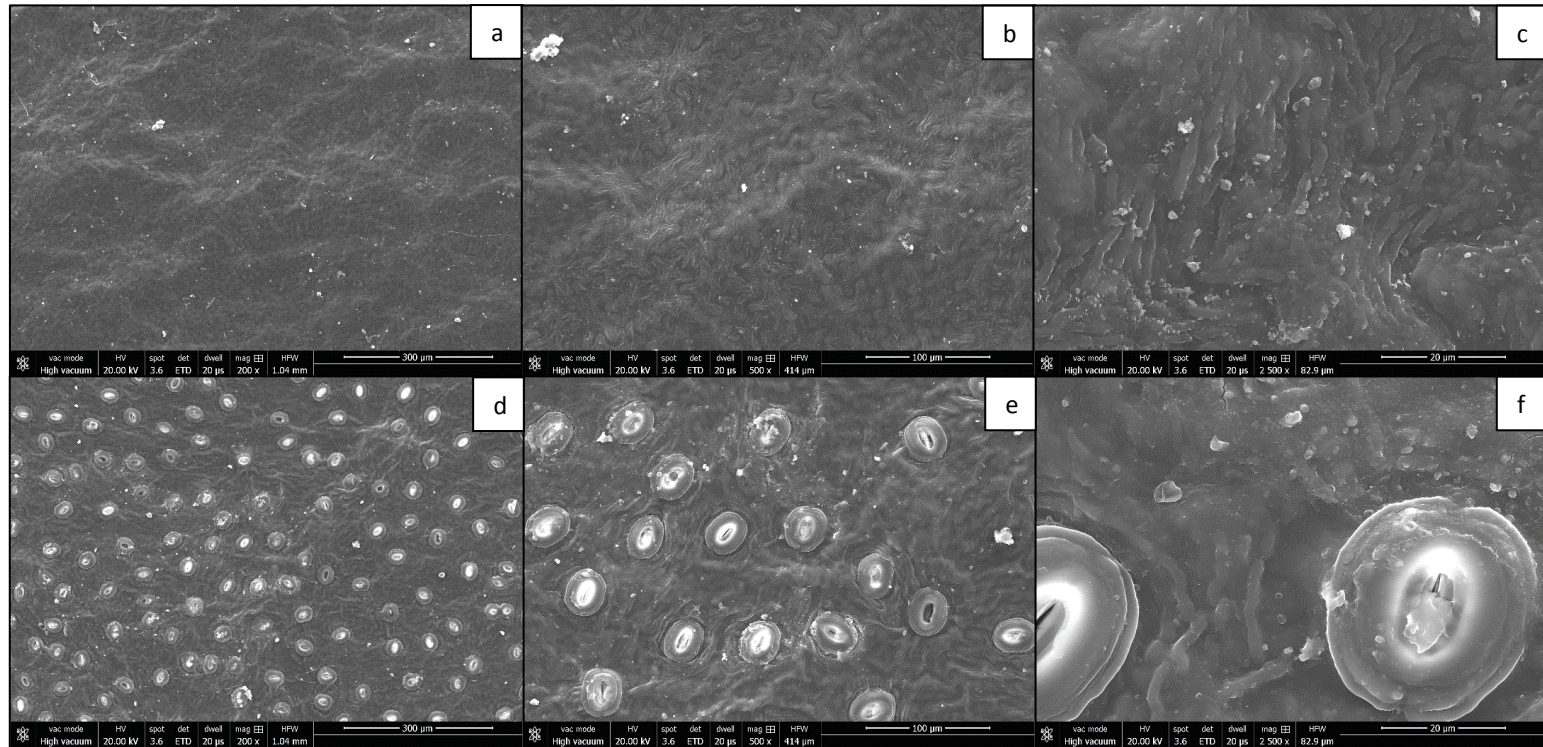


Figure 4.2 - Leaf surface SEM images from a non-exposed ivy plant leaf at magnifications 200x, 500x and 2,500x, taken at the same area of the leaf sample. Images a-c and d-f are from the adaxial and abaxial sides, respectively, ordered from lowest to highest magnification. Leaf-deposited particles are visible in all images, in which an undulated leaf micromorphology is illustrated; stomata are only visible on the abaxial surface (d-f), while trichomes are less frequent (not visible in these images); the wax platelets are characteristic for both adaxial and abaxial surfaces, but not visible at such low magnifications. The scale is mentioned at the right bottom of each SEM image.

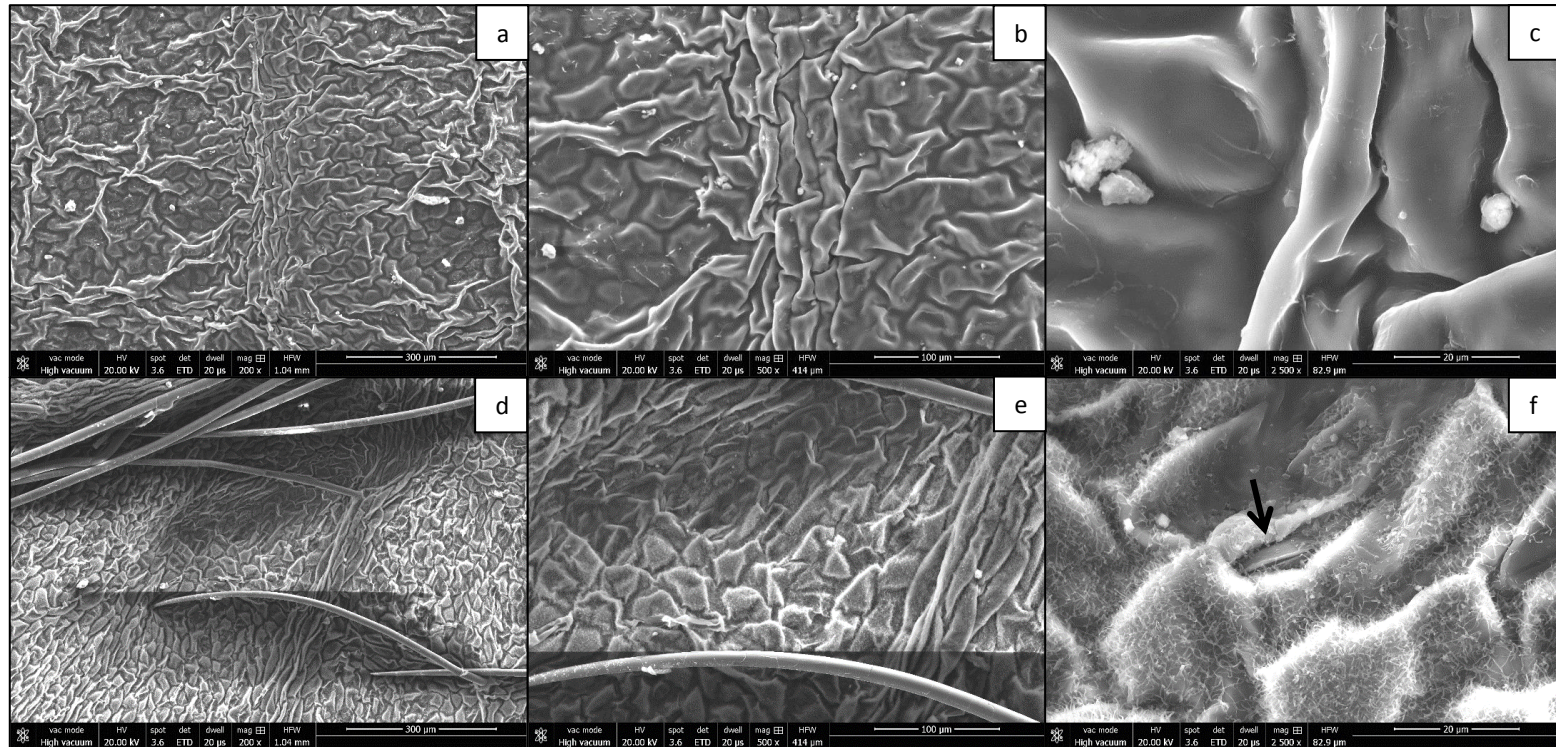


Figure 4.3 - Leaf surface SEM images from a non-exposed strawberry plant leaf at magnifications 200x, 500x and 2,500x, taken at the same area of the leaf sample. Images a-c and d-f are from the adaxial and abaxial sides, respectively, ordered from lowest to highest magnification. Leaf-deposited particles are visible in all images but in less quantity than for the ivy leaf, while the leaf micromorphology appearing more rugged on strawberry. The wax structure is defined as platelets for the adaxial surface and rodlets for the abaxial surface. The abaxial leaf side is also characterized by the presence of long trichomes (d, e). The wax rodlets on the abaxial surface almost totally cover a stomata (f; see arrow). The scale is mentioned at the right bottom of each SEM image.

4.3.2 Leaf surface elemental composition

4.3.2.1 ED-XRF

Predominant elements determined by ED-XRF included Si, Cl, Fe and Pb on both ivy and strawberry leaves. Concentration ranges for Si (a major crustal component) and Pb (traffic-related) were very comparable between ivy and strawberry leaves, with slightly higher concentrations for ivy. Fe (crustal and traffic-related) was found in more than five times higher concentrations on ivy leaves than on strawberry. On the other hand, strawberry leaves showed to be almost nine times more effective in retaining Cl (a sea salt tracer) in comparison with ivy. Elements Ti, Cr, Cu, Br, Rb and Sr were also frequently measured on ivy leaves, but rarely on strawberry leaves. While Ti, Rb and Sr are associated with crustal resuspension, metals Cr and Cu can be derived from exhaust and non-exhaust road traffic (Amato et al., 2011, 2013; Vercauteren et al., 2011). Emissions of Br have been associated with marine contribution while anthropogenic sources include vehicle emissions, pesticides and chemical manufacturing (Lammel et al., 2002). Element concentrations determined by ED-XRF ranged from 6 ng cm⁻² (e.g. Cr, Br) to more than 25,000 ng cm⁻² (Cl, K, Ca). It was found that Fe and Si accumulated more on ivy than on strawberry leaves ($p < 0.022$), while the opposite was true for elements Sr and Cl ($p < 0.006$). The concentrations throughout the entire exposure period only increased significantly for Cl and Sr on ivy leaves ($p = 0.008$, $R^2 = 0.19$, $n = 15$; $p = 0.039$, $R^2 = 0.43$, $n = 23$). Such increases were observed for both leaf sides, although losing significance for Sr when tested for each leaf side separately.

The observed variability between leaves from the same species and exposure time was larger than expected, and concentrations were frequently below detection and/or quantification limits, from blank leaves to leaves exposed for three months. ED-XRF offers many advantages for multi-element, non-destructive analysis, which can be performed directly on the sample, at relatively low cost and with rapid output. Still, drawbacks are present caused by the heterogeneity of plant material due to chemical

and physical matrix effects (Marguí et al., 2009). Particularly when samples do not meet the condition of thin-film, self-absorption effects arise that complicate the process of matrix calibration required for quantitative analysis (Bilo et al., 2017). Sample grinding or pelletization can be used to reduce such matrix effects (Marguí et al., 2005; Kardel et al., 2018), yet this was not possible in our study as the leaves analyzed via ED-XRF were subsequently used for ICP-MS determination. Still, an assessment was made of the elements present on the non-exposed leaves, as the pre-exposure conditions could have an effect on the concentrations estimated for the exposed leaves. In general, the elements Al, P, S, Cl, K, Ca, Ti, Mn, Fe, Cu, Zn, Br, Rb and Sr, were present in all blank leaves (for both ivy and strawberry, both leaf surfaces) (Figure 4.4), of which K, Ca, Mn and Fe were the most abundant elements. As mentioned (§4.2.2), for elements with $Z < 22$ (e.g. Si, Cl) the information depth is less than the leaf thickness. Differences in the adaxial and abaxial analyses can, thus, be expected for those elements in case they are deposited heterogeneously on the leaf surfaces. For all other elements, in which the information depth is larger than the leaf thickness, both surfaces, and in fact the entire leaf depth, are analyzed by ED-XRF. Testing leaf surface side as a potential influencing factor for dust accumulation, revealed significantly higher accumulations of Cl for ivy ($p = 0.029$) and strawberry ($p = 0.015$), and Si for strawberry ($p = 0.002$), at the adaxial side than at the abaxial side. The adaxial and abaxial concentrations as measured were compared against the overall leaf concentrations, i.e. obtained by averaging the adaxial and abaxial (element-specific) concentrations whenever both were available. This comparison revealed no differences regarding the analyzed ivy leaves, while for strawberry leaves, the averaged concentrations in Si differed from the abaxial values ($p = 0.047$).

The quantification on the exposed leaves of elements which were not detected on the blank leaves strongly suggests those elements to originate from the accumulation of atmospheric dust. This was the case for Ti, Cr and Pb. While the content in Ti and Cr in the blank leaves was unclear, Pb was absent on the blanks, but frequently detected on the exposed leaves. The Pb concentrations showed a similar temporal pattern for both

leaf sides of each species, and also quite consistent for both ivy and strawberry. The highest yet more variable Pb concentrations were measured after six and twelve weeks of exposure (*Figure 4.5*). The largest amount of rain (57 mm) was registered in the time interval between six and nine weeks of exposure, with 9w leaves being subject to double amounts of rain compared to the 6w leaves. The second largest precipitation period was between nine and twelve weeks (48 mm). While the precipitation between 9w and 12w was evenly distributed over the three weeks, for the period 6w – 9w a great peak of ca. 25 mm was registered only two days before the sampling of leaves 9w (*Figure 4.1*). Most probably this rain event has removed some of the leaf accumulated dust by wash-off. Chen et al. (2017) observed that PM_{2.5} removal from the leaf surface by wash-off was correlated with the amount of PM_{2.5} accumulated on the leaf before a simulated rain event, and influenced by plant species and rainfall duration.

During this biomonitoring campaign, atmospheric PM₁₀ and PM_{2.5} concentrations were, as expected, negatively influenced by precipitation ($p = 0.0009$, Spearman's $\rho = -0.35$; $p = 0.039$, $\rho = -0.22$, respectively) due to atmospheric wash-out, and by wind speed ($p < 0.0001$, $\rho = -0.42$; $p = 0.0004$, $\rho = -0.37$). Higher wind speeds result in the dispersion and dilution of pollutants (Kgabi and Mokgwetsi, 2009) in both particulate and gaseous ($p < 0.0001$, $\rho = -0.55$ for NO₂) forms. PM concentrations were positively correlated with air temperature (PM₁₀, $p < 0.0001$, $\rho = 0.48$; PM_{2.5}, $p = 0.0003$, $\rho = 0.38$) while relative humidity (being inversely related to air temperature) showed to have a negative influence, mainly on the coarse fraction of PM (PM₁₀, $p = 0.0002$, $\rho = -0.39$; PM_{2.5}, $p = 0.36$). The latter confirms previous findings that moisture aids in the deposition of atmospheric particles, thus lowering their concentration in the atmosphere, by promoting their (condensational) growth in particle size (Jayamurugan et al., 2013; Litschke and Kuttler, 2008). The influence of air temperature, on the other hand, is rather complex since it greatly depends on the climate zone and diurnal/nocturnal variations, it has an inverse impact on relative humidity, and indirectly affects the emission of pollutants due to e.g. heating needs.

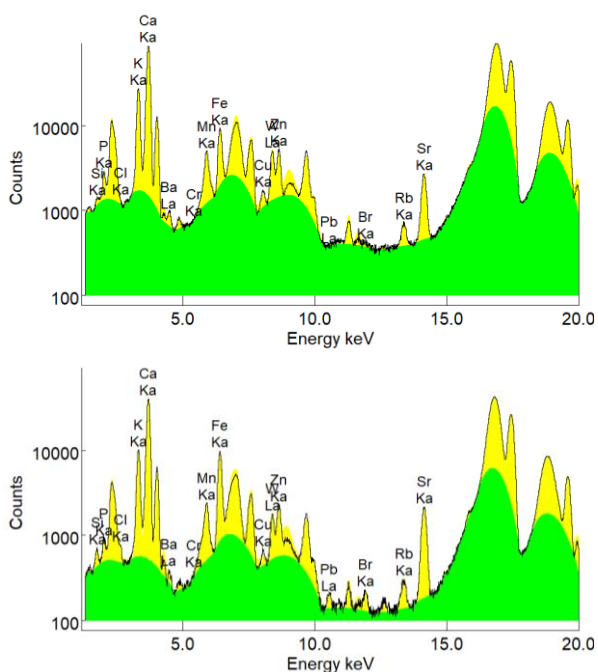


Figure 4.4 – Illustrative example of XRF spectra from a non-exposed ivy leaf (0w; top) and a three-months exposed ivy leaf (12w; bottom) obtained from Mo secondary target. Differences between the two spectra are not considerable, as elements such as K, Ca, Mn, Fe, Zn, Sr, are abundantly present in the blank leaves already.

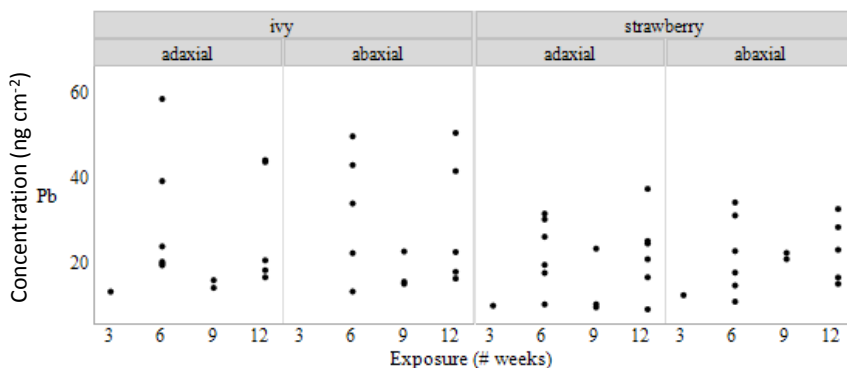


Figure 4.5 - Leaf Pb concentrations (ng cm⁻²) throughout exposure time, per plant species and leaf surface side, measured by ED-XRF.

4.3.2.2 HR-ICP-MS

Leaf concentrations measured by ICP-MS are usually performed on pulverized or powdered samples (e.g. Alfani et al., 1996; De Nicola et al., 2013). However, this

preparation procedure allows no distinction between the dust accumulated on the leaf surface (leaf-deposited particles) and the dust that becomes entrained on the leaves (leaf-encapsulated or in-wax particles). Moreover, such sample preparations are unable to exclude the intrinsic, natural leaf tissue elements. It should be noted that the elemental determination by ED-XRF on “as it is” leaves (§4.3.2.1) was also unable to completely achieve that distinction. Nevertheless, leaf-encapsulated particles can amount to or even surpass the quantity of leaf-deposited particles, depending on plant species and particle size fraction (Dzierżanowski et al., 2011; Song et al., 2015). The element concentrations were, in our study, derived from the surface washing solution of collected leaves, with values ranging from 0.01 ng cm⁻² (e.g. V, Co, Mo, Ag) up to more than 5,000 ng cm⁻² (K, Ca). Most measured elements were detected on both ivy and strawberry leaves, but concentrations were always significantly higher for ivy than for strawberry leaves for Na, Ca, Fe, Cu, Cd ($p < 0.001$), Mg, Zn ($p = 0.001$), Mn ($p = 0.005$), Sb ($p = 0.006$) and Pb ($p = 0.042$). Plant leaves subject to traffic conditions compared to traffic-poor background locations are known to get enriched in trace metals such as Cr, Fe, Cu and Pb (De Nicola et al., 2008, 2013; Maher et al., 2008), although temporal dynamics of such leaf accumulation are less studied. Log-transformed concentrations showed to decrease or increase with exposure time depending on the elements and differently for ivy and strawberry plant leaves. For ivy ($n = 25$), decreasing concentrations in Al ($R^2 = 0.17$), Ti ($R^2 = 0.31$), Zn ($R^2 = 0.31$), Rb ($R^2 = 0.19$, $n = 24$), Sr ($R^2 = 0.25$), Sb ($R^2 = 0.16$), and increasing concentrations in Mg ($R^2 = 0.35$), Cr ($R^2 = 0.35$), Mn ($R^2 = 0.37$), Co ($R^2 = 0.26$) were observed ($p < 0.05$). For strawberry ($n = 22$), decreasing concentrations in Na ($R^2 = 0.18$), Al ($R^2 = 0.54$), K ($R^2 = 0.21$), Ti ($R^2 = 0.43$), Fe ($R^2 = 0.51$, $n = 21$), Ni ($R^2 = 0.37$, $n = 20$), Cu ($R^2 = 0.31$, $n = 21$), Zn ($R^2 = 0.84$, $n = 21$), Sb ($R^2 = 0.41$, $n = 22$), and increasing concentrations in Cr ($R^2 = 0.39$, $n = 20$) were observed ($p < 0.05$).

4.3.2.3 ED-XRF vs. HR-ICP-MS

The exposed leaves were investigated using both ED-XRF and HR-ICP-MS techniques for a total of ten (common) elements (Si, K, Ca, Ti, Cr, Fe, Cu, Rb, Sr, Pb), for which

concentrations were always higher when measured by ED-XRF (Table 4.1) in comparison with the ICP-MS (Table 4.2) determination of the leaf washing solutions. However, those ten elements were detected for most analyzed leaves with ICP-MS, what was not the case for ED-XRF. For the latter, the number and frequency of detected elements was rather low, and in some cases only detected on the adaxial or on the abaxial leaf surface (e.g. Si, Ti, Cr). The contributions of each separate leaf side could not be distinguished for with ICP-MS, while with ED-XRF each leaf surface could be measured separately. Whenever both leaf sides were quantifiable for the considered elements, the average of the two leaf concentrations was calculated to obtain leaf-level ED-XRF concentration values. Otherwise, either the adaxial or abaxial concentrations were used. As mentioned before, the complex matrix of plant leaves interferes with the operational and measuring principle of ED-XRF, leading to large between-sample variability. Therefore, we consider the accumulation of elements throughout this campaign to be most accurately represented by the concentrations quantified by HR-ICP-MS on the leaf washing solutions (Figure 4.6). Elements K and Ca can originate from crustal dust (Tomašević and Aničić, 2010; Vercauteren et al., 2011), as well as from foliar exchange and leaching in the form of cations (K^+ and Ca^{2+}). K^+ is a highly mobile plant electrolyte, while Ca^{2+} is bound to structural plant tissues or enzyme complexes (Draaijers et al., 1994; Kopáček et al., 2009). As they can easily be transferred into the washing solutions, high concentrations of both K and Ca are observed (Figure 4.6, center). Disregarding those components from the composition profile (Figure 4.6, rightmost), the relative contribution of anthropogenic, traffic-related metals is comparable between ivy and strawberry species, with $Fe > Cu \approx Pb > Cr$. Yet, these relative contributions appear to be very different when compared to the obtained ED-XRF concentrations (Figure 4.6, leftmost).

Table 4.1 - Mean leaf surface concentrations (ng cm^{-2}) for common elements obtained via ED-XRF, per plant species (*I* – ivy, *S* - strawberry), leaf side (*AB* – abaxial, *AD* - adaxial) and exposure time in weeks (#W). Due to the reduced detection of elements, mean values ($n = 1$ to 6) without standard deviations are shown; “-” indicates not detected/quantified.

Plant	#W	Si	K	Ca	Ti	Cr	Fe	Cu	Rb	Sr	Pb	
<i>I</i>	<i>AB</i>	3	-	-	-	-	9.4	-	34.0	-	-	
		6	-	25986.3	-	-	8.8	4060.0	24.2	26.0	218.5	30.5
		9	-	-	-	-	-	4944.4	-	22.5	358.8	17.6
		12	-	-	-	-	-	3659.5	34.9	27.9	370.2	29.5
	<i>AD</i>	3	567.1	-	-	37.4	8.6	-	-	33.3	-	13.1
		6	1462.9	14108.0	-	88.5	11.7	3497.9	29.8	25.1	126.3	30.0
		9	929.6	-	-	30.7	-	3683.0	45.0	18.9	268.7	14.9
		12	1025.9	-	-	78.7	11.2	4787.9	27.1	22.2	272.9	28.4
<i>S</i>	<i>AB</i>	3	-	-	-	-	10.5	568.7	-	-	-	12.3
		6	-	-	-	26.8	6.3	616.7	-	-	-	21.7
		9	411.3	-	40198.1	-	-	1090.6	-	-	543.9	21.4
		12	371.1	-	-	-	-	615.9	-	-	-	23.0
	<i>AD</i>	3	-	-	-	-	-	-	-	-	-	9.8
		6	757.9	-	-	-	-	-	-	-	-	22.4
		9	1667.6	-	51342.4	-	-	-	-	-	492.8	14.3
		12	495.2	-	-	49.0	-	614.5	-	32.2	-	22.1

Table 4.2 - Mean and standard deviation (grey and white shading, respectively) of leaf surface concentrations (ng cm^{-2}) for common elements obtained via HR-ICP-MS, per plant species (*I* – ivy, *S* - strawberry) and exposure time in weeks (#W) ($n = 1$ to 6); “-” indicates not detected/quantified. Blank samples correspond to ultrapure water solutions without leaf samples.

Plant	#W	Si	K	Ca	Ti	Cr	Fe	Cu	Rb	Sr	Pb	
<i>I</i>	0	36.64	3090.62	3044.93	0.78	0.13	23.44	1.60	1.59	10.74	1.08	
		11.50	1977.39	2107.74	0.27	0.03	15.07	0.44	1.29	4.42	0.78	
	3	19.40	1856.09	1109.86	0.65	0.08	15.00	1.75	1.22	3.36	0.97	
		12.23	1183.67	993.10	0.28	0.03	6.02	0.41	0.58	1.94	0.63	
	6	53.37	1638.76	2143.87	1.28	0.09	39.67	3.08	0.71	5.14	2.49	
		29.24	1079.02	572.65	0.53	0.05	10.17	0.51	0.32	1.49	1.41	
	9	50.89	1422.65	1871.07	0.29	0.22	18.53	1.17	0.59	4.02	1.18	
		69.77	1248.29	1720.39	0.12	0.07	13.18	0.32	0.26	2.76	0.26	
	12	39.37	1260.61	1209.33	0.35	0.24	13.90	1.52	0.73	2.83	2.01	
		52.86	609.33	429.12	0.17	0.06	8.58	0.49	0.43	1.53	1.10	
	<i>S</i>	0	87.38	2827.98	374.10	0.74	0.06	14.94	1.50	1.20	3.13	1.16
			104.39	617.48	220.77	0.26	0.03	5.06	0.87	1.21	2.54	0.97
3		72.37	2257.68	685.42	0.49	0.07	7.84	0.82	1.06	3.38	0.59	
		73.48	1158.33	347.57	0.17	0.03	1.41	0.13	0.63	0.94	0.09	
6		30.14	2398.66	464.33	0.96	0.05	13.10	1.34	1.15	4.08	1.90	
		31.23	911.87	377.97	0.48	0.06	5.85	0.44	0.59	2.51	0.93	
9		71.09	2360.93	1180.23	0.22	0.12	4.76	0.42	0.78	5.10	0.51	
		95.19	1342.80	775.58	0.06	0.04	0.85	0.13	0.47	2.74	0.17	
12		11.20	951.70	254.80	0.13	0.36	4.29	0.58	0.36	1.34	0.60	
		7.77	923.40	225.01	0.08	0.10	1.85	0.08	0.28	1.12	0.41	
Blank		-	11.83	24.37	0.04	0.31	0.80	-	0.08	-	0.01	
		-	11.04	-	0.04	-	0.62	-	0.06	-	-	

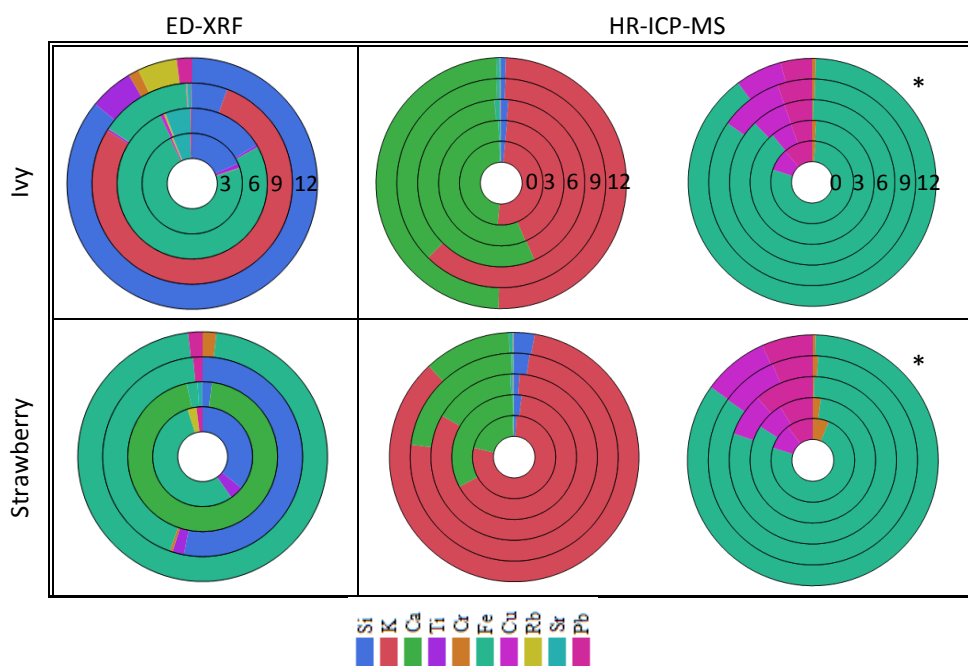


Figure 4.6 - Pie charts of average leaf surface elemental concentrations (Si, K, Ca, Ti, Cr, Fe, Cu, Rb, Sr, Pb) measured by ED-XRF and HR-ICP-MS for ivy and strawberry leaves throughout the exposure campaign (0-3-6-9-12 weeks). The pie charts in the rightmost column (indicated with *) display a selection of the traffic-related elements (Cr, Fe, Cu, Pb).

The evolution of ED-XRF leaf concentrations over exposure time was not linear nor consistent among all investigated elements (Figure 4.7). However, leaf concentrations showed a relative decrease after six weeks of exposure with values growing again on 12w leaves for Si, Ti and Pb. The concentrations measured via ICP-MS on the leaf washing solutions did not show a consistent temporal pattern either. The concentrations in Ti, Cu and Pb were the highest for the 6w leaves, with values decreasing on 9w and then increasing for 12w leaves. On the other hand, such patterns were rather diverse for the remaining elements (Si, K, Ca, Cr, Fe, Cu, Rb, Sr) and also species-dependent. When comparing the leaves obtained at the end of the exposure campaign (12w) against the non-exposed leaves (0w), elemental concentrations of K (strawberry, $p = 0.016$), Ca (ivy, $p = 0.008$), Ti (ivy and strawberry, $p = 0.032$ and $p = 0.016$) and Fe (strawberry, $p = 0.036$) decreased significantly, suggesting a reduced contribution of crustal dust matter (K, Ca, Ti, Fe) (Vercauteren et al., 2011). In contrast, a significant enrichment in Cr, often linked to traffic and corrosion sources (especially

under railway/subway influences, considered negligible at the test site though) (Gehrig et al., 2007), was displayed on both ivy and strawberry. An exploratory PCA on the surface elemental concentrations (determined by ICP-MS) throughout the exposure period (Figure 4.8) also suggests the contribution of Cr to be closely connected with the exposure time at the test site. The two most discriminant components, PC1 and PC2, accounted for 55.7% of the total variance in all sampled leaves. The element Cr and “Exposure” (negative PC1 values) are separated from the remaining elements (Figure 4.8a), and reflected in the gradient going from non-exposed to 12-weeks exposed leaves (Figure 4.8b). The PC2 allows the distinction between interrelated crustal dust and leaf-occurring elements (K, Rb, Sr; negative PC2 values) and anthropogenic dust (Fe, Cu, Pb, Cr; positive PC2 values). Comparable conclusions were obtained from analyzing the two plant species separately, with the highest concentrations in traffic-derived elements (Fe, Cu, Pb, Cr) being clearly depicted by 6w and 12w leaves.

The test site, located in a residential area and close to the university campus, is considered to be subjected to moderate car traffic. However, the intensity of car traffic may have decreased gradually during our exposure campaign, particularly from the end of June onwards with the start of the summer holidays period. This “holiday effect” is supported by the relatively lower particulate and gaseous atmospheric concentrations observed during the second half of July (Figure 4.1), and further confirmed by negative Spearman’s correlations ($p < 0.01$) between NO_2 ($\rho = -0.36$), PM_{10} ($\rho = -0.43$) and $\text{PM}_{2.5}$ ($\rho = -0.32$) concentrations with day of the year (DOY) during the campaign. Daily fluctuations of atmospheric pollutants were consistent over the entire exposure period ($p < 0.01$; $\rho = 0.90$ between PM_{10} and $\text{PM}_{2.5}$ concentrations, $\rho = 0.43$ and $\rho = 0.41$ between $\text{PM}_{2.5}$ and NO_2 , and PM_{10} and NO_2 , respectively), suggesting road traffic (NO_x and PM) as main local contributing source (McIntosh et al., 2007).

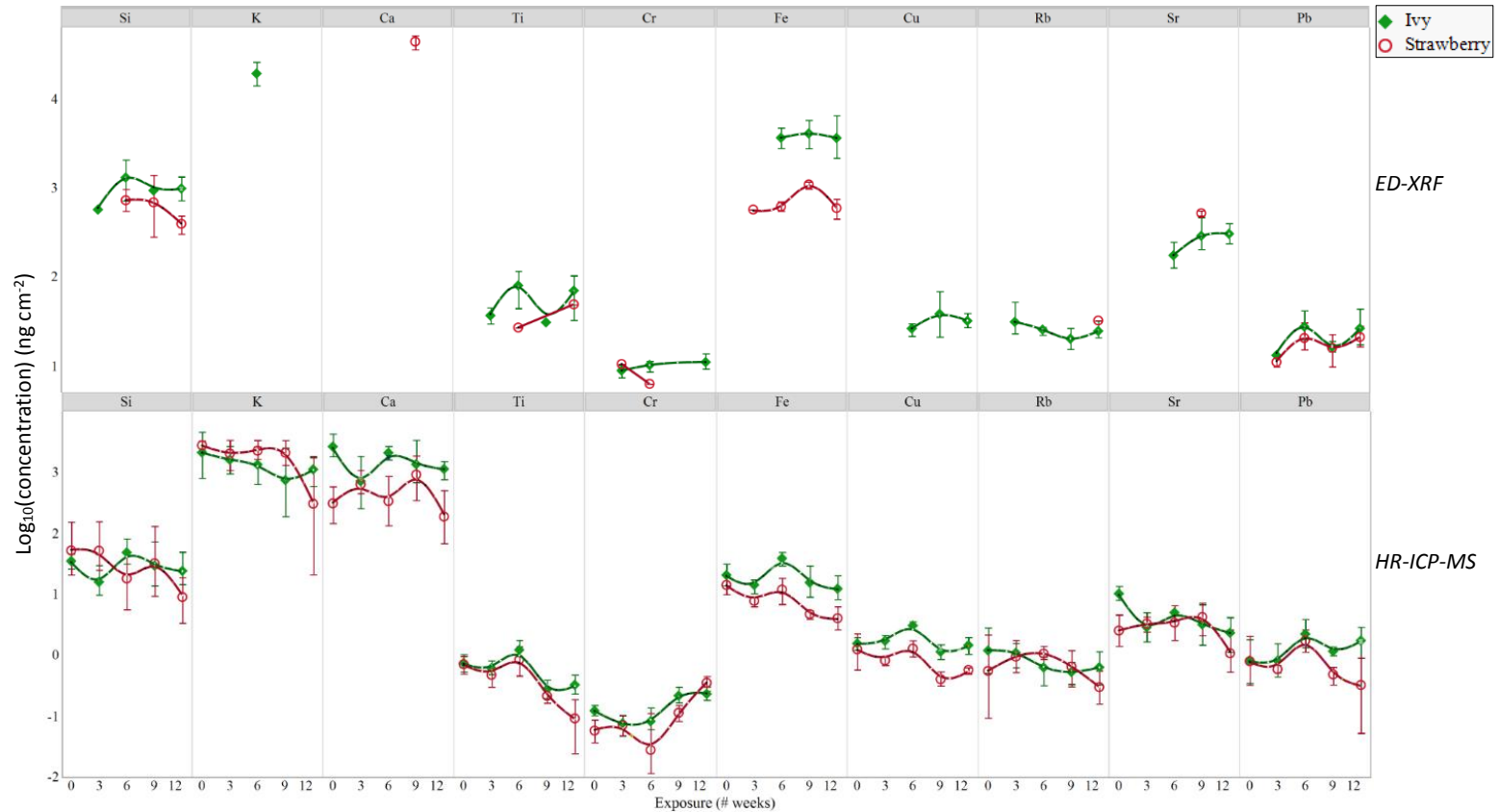


Figure 4.7 – Evolution of (log-transformed) elemental concentrations (Si, K, Ca, Ti, Cr, Fe, Cu, Rb, Sr, Pb) found for ivy (in green) and strawberry (in red) plant leaves throughout exposure time, as measured by ED-XRF (top) and HR-ICP-MS (bottom). Mean values are presented and the interval bars represent the interquartile ranges.

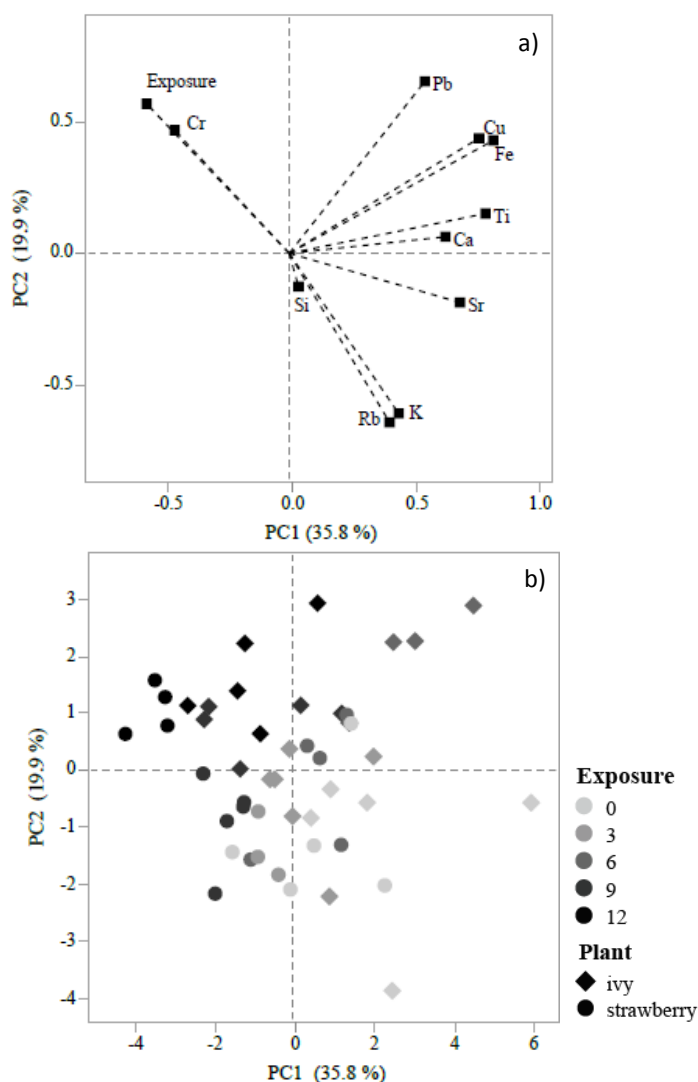


Figure 4.8 - Outputs of the PCA performed on the elemental concentrations measured by HR-ICP-MS on the leaf washing solutions, considering as input variables the 10 elements (Si, K, Ca, Ti, Cr, Fe, Cu, Rb, Sr, Pb) and the exposure time (in weeks). The projection in the PC1-PC2 plane of the a) input variables and b) analyzed samples according to plant species and exposure period, are shown, with PC1 and PC2 explaining 55.7% of the total variance.

4.3.3 Leaf magnetic analyses

Magnetic susceptibility of exposed leaves was almost negligible and often negative, with χ_{LF} values ranging from -6.5 to $4.4 \times 10^{-8} \text{ m}^3 \text{ kg}^{-1}$ for ivy, and from -12.1 to $21.4 \times 10^{-8} \text{ m}^3 \text{ kg}^{-1}$ for strawberry. Although values are comparable with results obtained in other leaf monitoring studies, e.g. from pine needles exposed for 3 - 8 months in Cologne,

Germany (Lehndorff et al., 2006) or from leaves of *Platanus spp.*, *Quercus spp.*, *Tilia spp.*, *Nerium oleander* sampled monthly during 4 - 10 months in Northern Portugal (Sant'Ovaia et al., 2012), the k values measured in our study (range from -3 to 4×10^{-6} SI) are very close to the resolution of the measuring equipment (2×10^{-6} SI). This indicates that the concentration of magnetic particles accumulated over 3-months of exposure at the selected site was not sufficient to overcome the diamagnetic nature of the plant leaves, which are mainly composed of water and organic content. A similar observation was made for lime tree leaves collected at the end of the growing season in Lancaster, England (Mitchell and Maher, 2009). Rodríguez-Germade et al. (2014) have also reported negative and low susceptibility values for leaves of *Platanus x hispanica* in the urban region of Madrid, Spain, yet with a more than thirty-fold increase (maximum of $32.2 \times 10^{-8} \text{ m}^3 \text{ kg}^{-1}$) after a total exposure of eight months. Such increasing trend over time was not evident in our data though (Table 4.3).

The application of various AC/DC combinations for leaf samples to acquire ARM (§4.2.3), showed that the largest intensity fields (AC 200mT and DC 500 μ T, ARM_{200/500}) led to the highest ARM values. ARM depends on the mineralogy and concentration of magnetic particles, as well as on their magnetic grain size, with small single-domain (SD) grains acquiring ARM more efficiently than multi-domain (MD) grains (Liu et al., 2012b). Raw (magnetic moment) ARM_{200/500} values were significantly larger for ivy than for strawberry ($p < 0.0001$), with exposed ivy (3w, 6w, 9w, 12w) and strawberry leaves (6w, 9w) exhibiting higher values compared to the non-exposed (0w) leaves ($p < 0.035$ and $p < 0.045$, respectively) (Figure 4.9). For magnetic concentration indicators, as is the case of χ_{LF} , SIRM and ARM, it is more useful to consider the values normalized for either mass or leaf surface area than the obtained magnetic moments to allow for comparisons between different samples or studies. While mass-normalization is logical for assessing e.g. the amount and concentration of dust collected actively on pumped-air PM filters that have the same size, leaf monitoring is based on the fact that leaves accumulate PM passively on their surface. For the same plant species and equal exposure to pollutants, leaves with large surfaces accumulate more. ARM_{200/500} ranged

between 0.24 μA and 1.09 μA for ivy and between 0.15 μA and 1.18 for strawberry species, being on average larger for ivy than for strawberry ($p < 0.0001$).

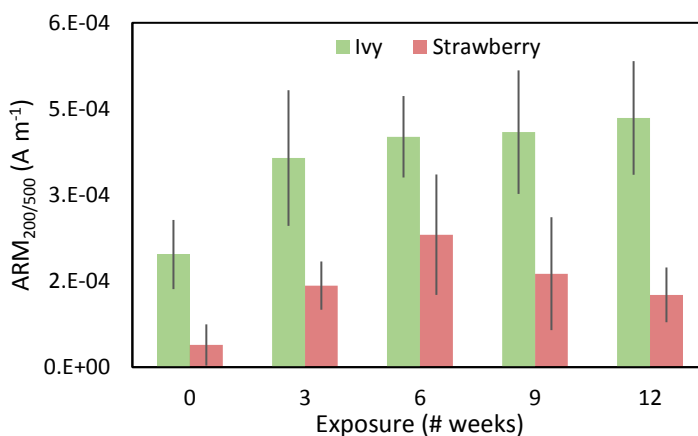


Figure 4.9 – Mean $\text{ARM}_{200/500}$ values (in A m^{-1}) of ivy (in green) and strawberry (in red) leaves collected throughout the exposure period; the error bars indicate the standard deviations from the means ($n = 6$).

For SIRM, one of the most investigated properties in the field of environmental magnetism, values ranged from 5.24 μA to 19.27 μA (Table 4.3). Ivy leaves accumulated higher concentrations of magnetic particles in comparison to strawberry ($p = 0.003$), with an average SIRM of $13.15 \mu\text{A} \pm 3.57 \mu\text{A}$ against $10.06 \mu\text{A} \pm 4.18 \mu\text{A}$, respectively. The obtained results are relatively low and comparable to values measured in parks or green areas, not reflecting the car traffic (although moderate and likely to have declined during the exposure campaign) in the nearby street road. In the province of Antwerp, passive monitoring studies using ivy from distinct environments had shown a mean SIRM of 24 μA for a forested site compared to 205 μA for a busy roadside intersection with intense traffic (§Chapter 3.1). In the same study area Smets et al. (2016) could magnetically discriminate urban areas (mean SIRM of 200 μA) from green residential areas (mean of 31 μA). Similar outcomes were reported after a wide spatial study with 110 sampling locations in the city of Antwerp, in which the SIRM of ivy leaves was found to be correlated with traffic intensity (Hofman et al., 2014c). At a European-scale, leaf SIRM of *Platanus x acerifolia* tree leaves collected at the end of their growing season revealed mean SIRM values of 30 μA and 153 μA for park and

street sites, respectively (§Chapter 3.2). The minimum values of 7 μA (park site in Copenhagen, Denmark) and 9 μA (street site in Kavala, Greece) obtained in that leaf monitoring study are in line with the values measured in this study.

The evolution of leaf SIRM throughout the exposure period was distinct for the two test species (Figure 4.10). Leaf SIRM of ivy increased significantly from three weeks onwards, as leaves from 6w, 9w and 12w had higher SIRM values than the non-exposed leaves ($p < 0.01$). For strawberry, an enrichment in magnetic grains was evident after three weeks of exposure as well, with the highest SIRM values obtained for 6w leaves ($p < 0.04$). However, this magnetic enrichment appeared to decrease after six weeks until the end of the exposure campaign. The latter results are unexpected as SIRM accumulation throughout the in-leaf season was found to be significant for 2-weekly collected Plane tree leaves in the same street of our monitored site, only affected at the end of the in-leaf season by leaf senescence (Hofman et al., 2014b). We hypothesize that the observed decrease may be due to the heavy rainfall after six weeks and that strawberry leaves are more sensitive to wash-off compared to ivy leaves. Furthermore, we noticed during leaf sampling that new leaves (both for ivy and strawberry) rapidly sprouted between the various sampling moments. This complicated the distinction between leaves exposed since the beginning of the campaign and newly emerged leaves, particularly at the end of the exposure period. This possible variation in exposure period may have influenced our results, as dust accumulation on the leaves was not so evident in terms of surface deposited elements nor magnetic enrichment, and a large variation was sometimes observed within the leaves sampled at the same moment. Leaf monitoring campaigns following this study were improved by labelling all plant leaves at the start of the exposure period. Nonetheless, meteorological conditions and the moderate road traffic, even considered to have declined at the second half of the exposure period, appear to be key factors in the leaf accumulation of dust at this test site. Such influences should not be overlooked as they are also relevant in terms of human exposure to atmospheric PM. Moreover, the test site is rather open, leading to ventilation effects, i.e. diluting the air pollutants (Janhäll, 2015).

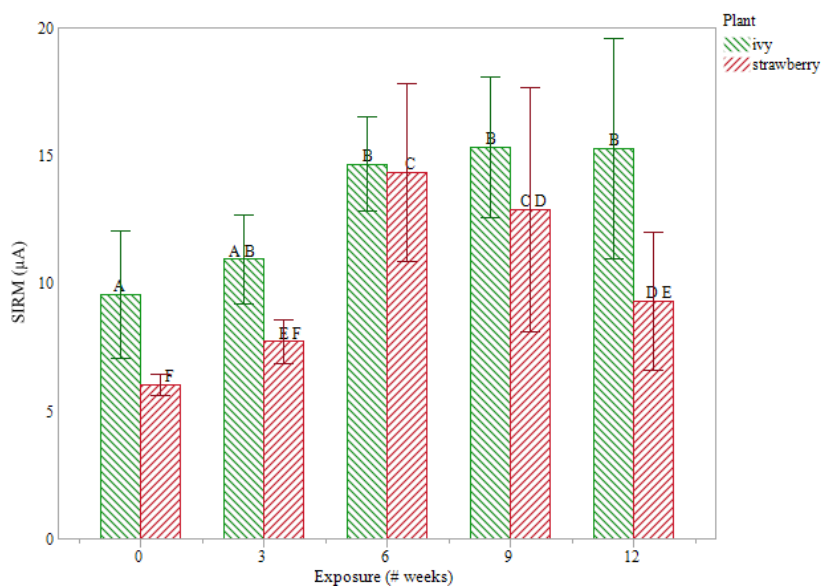


Figure 4.10 – Evolution of leaf SIRM for ivy (in green) and strawberry (in red) plant leaves throughout the exposure time in weeks. Mean values ($n = 6$) and standard deviations, as error bars, are shown. Levels not associated with the same letter indicate (log-transformed) SIRM to be significantly different at $p < 0.01$ for ivy (A, B) and at $p < 0.04$ for strawberry (C, D, E, F) leaves.

Obtained IRM₋₃₀₀ values were similar to SIRM values (Table 4.3), with subsequent S-ratio close to the unity (0.94 to 0.99 for ivy, 0.90 to 1.11 for strawberry), which indicates the remanence to be dominated by low-coercivity carriers such as magnetite-type minerals (Evans and Heller, 2003; Hansard et al., 2011; Hofman et al., 2017). Mean HIRM values varied throughout the exposure campaign between 0.09 – 0.33 μA and 0.06 – 0.40 μA for ivy and strawberry leaves, respectively. Such low HIRM values reflect that saturation is already achieved by 300 mT for most leaf samples, as corroborated by the S-ratio and obtained IRM backfield curves (Figure 4.11). The exposed leaves achieved ca. 22% and 69% of the total SIRM at 50 mT and 100 mT, respectively, with the remaining 30% to be acquired between 100 mT and 1 T. The contribution of antiferromagnetic grains (e.g. hematite) is negligible since only 3% of the total SIRM was reached above 300 mT (Evans and Heller, 2003). The S-ratio and HIRM, i.e. descriptors of the relative contribution of low- to high-coercivity components, were similar for both test species, as they were exposed to the same polluting conditions.

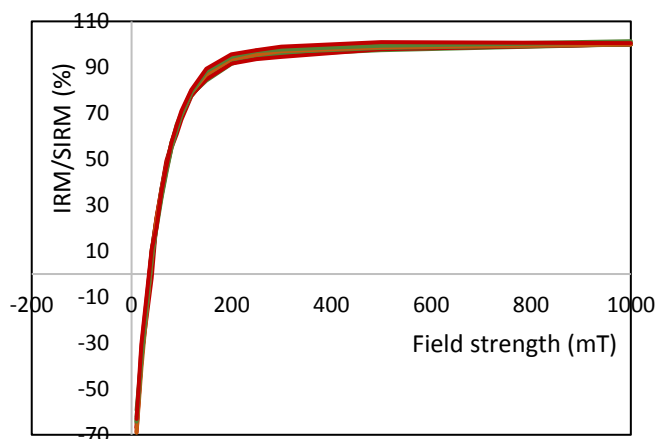


Figure 4.11 – Mean IRM backfield curves (IRM/SIRM, in %) for ivy (in green) and strawberry (in red) leaves, with each plotted line the mean of six leaves. Samples were first saturated (-1T; not shown) and the backfield acquisition IRM curves obtained by applying stepwise field strengths in the opposite direction from 10mT up to 1T (§4.2.3). The followed trend is similar for the two species and between the various time points (0w, 3w, 6w, 9w, 12w), resulting in similar backfield curves (total of 10) for all tested conditions.

ARM/SIRM can be used as a grain size indicator, with higher values representing more fine-grained (SD or PSD) particles in contrast with MD grains (Evans and Heller, 2003; Shi et al., 2014). The ratio ARM/SIRM (24.5 to 71.2×10^{-3}), or equivalent $ARM_x/SIRM$ (3.5 to 17.9 m A^{-1}), was statistically larger for ivy than for strawberry leaves ($p < 0.0001$), however, with values falling within the standard deviation ranges of each other (Figure 4.12). Taking these uncertainties into account, the ranges of ARM/SIRM values are still comparable between ivy and strawberry, while also not largely changing throughout the exposure period. This reveals no change in magnetic grain size of the deposited PM at the monitored site, as the main polluting source registered on site was invariably the same (i.e., road traffic). Furthermore, the difference in leaf macro- and micro-morphological characteristics between ivy and strawberry appears not to have a grain size selective influence on the accumulation of atmospheric dust. Our values (S-ratio and ARM/SIRM) are comparable to the observations of Shi et al. (2014) and Wang et al. (2017) for daily PM filters, and suggest high contributions of small-grained SD/PSD magnetite particles within the accumulated atmospheric dust (Evans

and Heller, 2003), which are often associated with road traffic contributions (e.g., Mitchell and Maher, 2009).

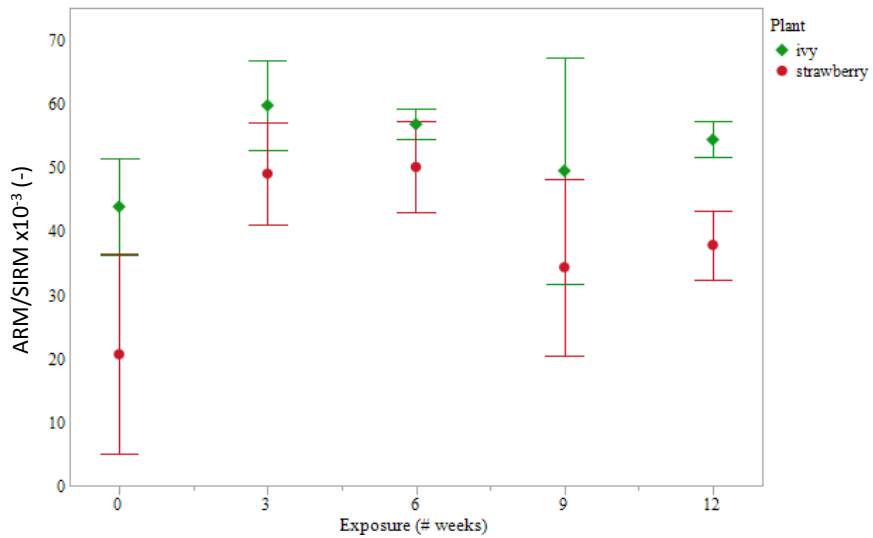


Figure 4.12 – Mean ARM/SIRM values for ivy (green) and strawberry (red) leaves collected throughout the exposure campaign. Error bars are constructed using one standard deviation from the mean.

Table 4.3 - Mean (in grey), standard deviation (Std) and range (Min – minimum, Max - maximum) ($n = 6$) of measured leaf magnetic properties and calculated ratios, per plant species (I – ivy, S - strawberry) and exposure time in weeks.

Plant	# Weeks	$\chi_{LF} \times 10^{-8}$ ($m^3 kg^{-1}$)	ARM _{200/500} (μA)	ARM _X $\times 10^{-8}$ ($m^3 kg^{-1}$)	SIRM (μA)	IRM _{L-300} (μA)	HIRM (μA)	S-ratio (-)	ARM/SIRM $\times 10^{-3}$ (-)	
I	0	0.24	0.43	1.21	9.57	9.39	0.09	0.98	43.80	Mean
		3.90	0.15	0.42	2.51	2.45	0.05	0.01	7.55	Std
		-6.48	0.24	0.64	7.43	7.29	0.03	0.97	31.97	Min
		3.81	0.69	1.91	14.47	14.16	0.16	0.99	54.08	Max
	3	0.52	0.66	1.93	10.94	10.55	0.19	0.96	59.70	Mean
		2.82	0.15	0.74	1.75	1.67	0.05	0.01	6.99	Std
		-3.56	0.46	1.20	8.80	8.51	0.14	0.96	52.67	Min
		4.37	0.88	3.15	13.94	13.37	0.28	0.97	71.22	Max
	6	0.53	0.83	1.74	14.67	14.01	0.33	0.96	56.74	Mean
		1.40	0.10	0.38	1.86	1.75	0.10	0.01	2.42	Std
		-1.89	0.74	1.30	12.48	12.12	0.18	0.94	52.86	Min
		2.06	1.00	2.41	17.22	16.46	0.45	0.97	59.04	Max
	9	-0.88	0.75	1.98	15.32	14.79	0.26	0.97	49.44	Mean
		2.30	0.26	0.50	2.74	2.13	0.14	0.01	6.16	Std
		-3.78	0.30	1.33	12.44	12.06	0.16	0.95	24.46	Min
		2.73	0.99	2.78	18.90	18.22	0.47	0.98	66.12	Max
	12	-0.69	0.82	1.80	15.26	14.90	0.18	0.98	54.31	Mean
		1.45	0.22	0.52	4.30	4.12	0.13	0.01	2.83	Std
		-2.43	0.56	1.09	9.93	9.66	0.04	0.96	49.64	Min
		1.10	1.09	2.42	19.27	18.62	0.32	0.99	56.39	Max
S	0	4.53	0.13	0.46	6.03	5.88	0.08	0.98	20.62	Mean
		4.51	0.10	0.37	0.43	0.44	0.07	0.02	15.72	Std
		0.00	0.00	0.00	5.24	5.10	-0.03	0.95	0.00	Min
		12.12	0.23	0.90	6.39	6.45	0.15	1.01	38.19	Max
	3	-0.97	0.38	1.64	7.72	7.60	0.06	0.98	48.98	Mean
		11.67	0.10	0.60	0.86	1.32	0.27	0.06	8.02	Std
		-12.06	0.26	1.13	6.71	6.31	-0.48	0.94	38.70	Min
		21.39	0.56	2.72	9.05	10.01	0.20	1.11	61.53	Max
	6	-5.25	0.74	3.00	14.34	13.54	0.40	0.95	50.04	Mean
		4.80	0.28	0.94	3.46	3.21	0.24	0.02	7.13	Std
		-11.18	0.48	1.64	10.92	10.38	0.24	0.90	43.62	Min
		0.00	1.18	4.50	18.78	17.94	0.87	0.96	62.89	Max
	9	-0.34	0.48	2.19	12.88	12.47	0.21	0.97	34.29	Mean
		5.05	0.35	0.97	4.78	4.98	0.17	0.01	8.29	Std
		-8.07	0.15	1.29	9.22	9.00	0.10	0.95	14.12	Min
		5.32	1.11	3.91	22.22	21.20	0.51	0.98	50.05	Max
	12	-1.72	0.36	1.43	9.31	9.15	0.08	0.99	37.78	Mean
		3.37	0.15	0.58	2.69	2.47	0.15	0.05	5.39	Std
		-6.97	0.20	0.77	5.84	6.28	-0.22	0.96	29.51	Min
		2.14	0.61	2.31	13.41	13.05	0.18	1.08	45.32	Max

4.3.4 Leaf-surface particle deposition

The accumulation of atmospheric dust in this monitoring study has shown to be species- (ivy accumulated more than strawberry) and element-specific (temporal trends of deposited elements varied per element), rather than influenced by the buildup of pollutants, which was not as substantial as we would expect. Nevertheless, the accumulation of particles was corroborated by SEM images (Figure 4.13, Figure 4.14), with larger amounts of deposited particles found on ivy than on strawberry leaves and with 6w leaves showing the highest quantities. The size and shape of leaf-surface deposited particles is diverse, as reported before (Ottel  et al., 2010; Sgrigna et al., 2015; Song et al., 2015). The most striking information is related with the dust accumulation over time, with particle number increasing from the non-exposed to the 6w leaves. Subsequently, the number of deposited particles decreased after nine weeks (9w) and slightly increased again at the end of the campaign (12w). This temporal pattern was also verified in the concentration of some leaf-accumulated elements (Si, Ti and Pb, with ED-XRF; Ti, Cu and Pb, with HR-ICP-MS) and by the leaf SIRM of strawberry leaves. Particle removal processes (e.g. due to rain) as hypothesized earlier, therefore, seem to be confirmed.

Leaves with rough ridges and containing trichomes accumulate more PM than smooth leaf surfaces (Mo et al., 2015; S eb  et al, 2012; Weerakkody et al., 2018). Despite strawberry leaves contain more trichomes and have a more rugged micro-topography than ivy (§4.3.1), the ivy leaves in our study had higher SIRM (Figure 4.10) and displayed a larger quantity of deposited particles compared to strawberry (Figure 4.13, Figure 4.14). In a recent study of Muhammad et al. (2019), a total of 96 plant species (mainly tree and shrub species) grown in a common garden at ca. 250 m from our test site, were studied to investigate the relation between leaf traits and particle accumulation measured by SIRM. Although the density of leaf trichomes was again confirmed as enhancing the accumulation of particles, some plant species with high trichome density but low leaf wettability showed reduced particle accumulation (i.e., low SIRM) (Muhammad et al., 2019). Both ivy and strawberry leaves are considered to

be hydrophilic (Walker et al., 2015). Yet, we hypothesize that strawberry leaves are less hydrophilic than ivy leaves (Figure 4.2, Figure 4.3), which may prevent the deposition of particles (Bakker et al., 1999; Barima et al., 2016). A wind tunnel experiment also showed that the permeability of strawberry leaves, i.e. the ability to let pass an air-flow, is significantly lower compared to the permeability of ivy leaves (Koch et al., 2019), which may difficult the accumulation of PM, whereas Baker and Hunt (1986) described difficulties in penetrating the trichome arrangements of strawberry leaves with simulated rain. To clarify the remaining questions on the particle accumulation dynamics between ivy and strawberry leaves, future leaf monitoring campaigns should include controlled scenarios on rain exposure (e.g. plants protected/unprotected from rain) and leaf age (labeling to avoid sampling of newly emergent leaves).

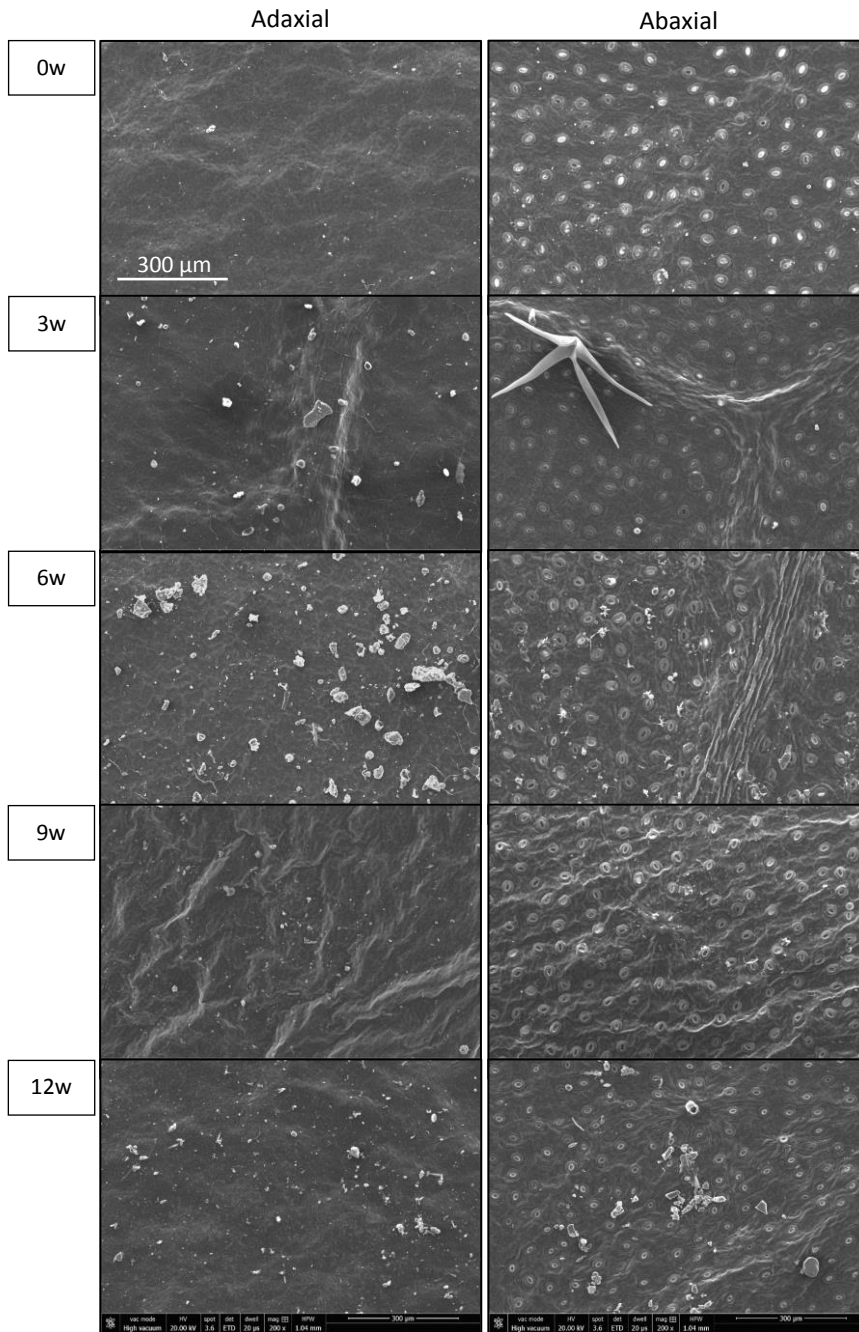


Figure 4.13 - Leaf surface SEM images from ivy leaves collected every three weeks (0w-3w-6w-9w-12w) throughout the total exposure period of three months. Both leaf sides display leaf-deposited particles. A typical leaf trichome on ivy, of the stellate type (Ackerfield and Wen, 2002), is visible on image 3w-Abaxial. Magnification used is 200x, and the scale indicated in the upper left panel is similar for all panels.

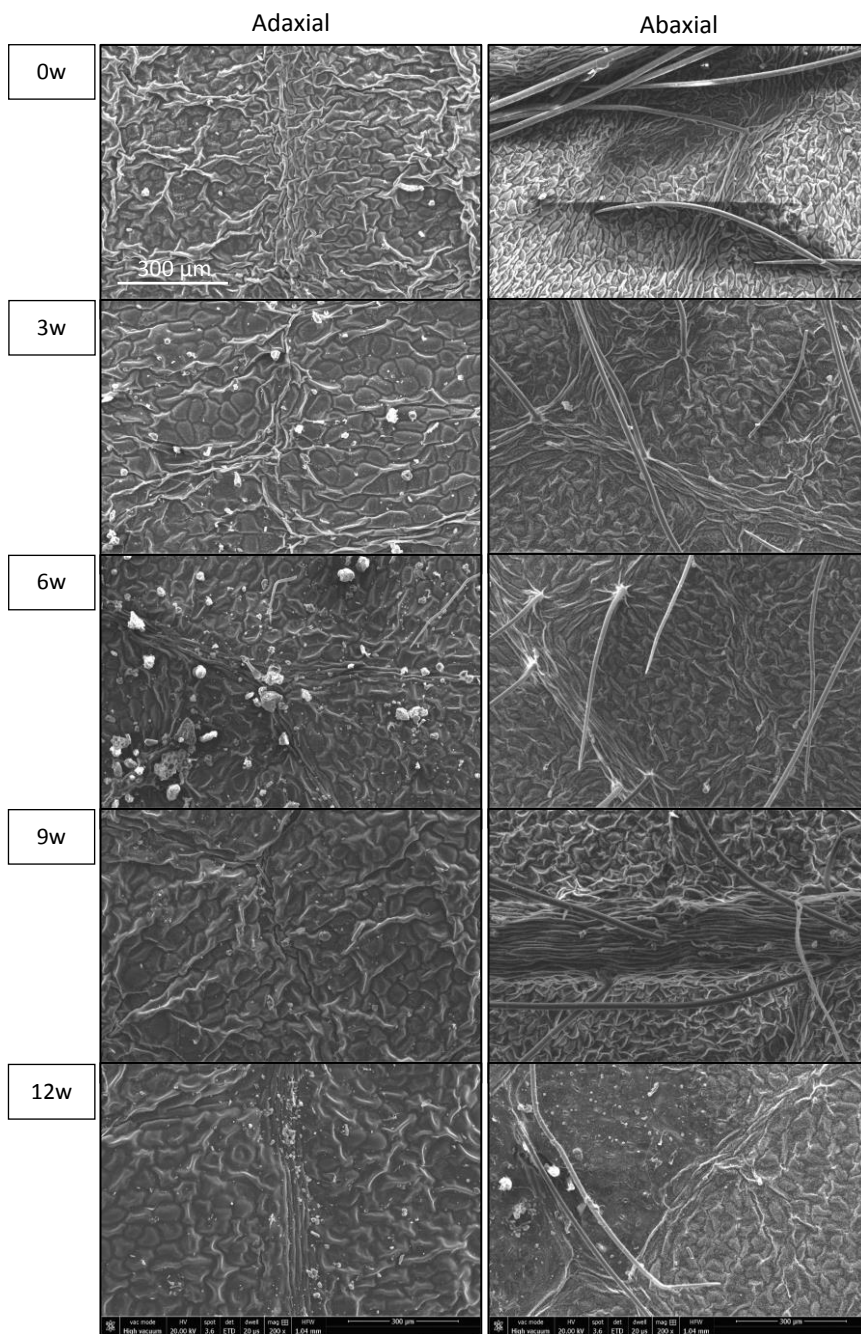


Figure 4.14 - Leaf surface SEM images from strawberry leaves collected every three weeks (0w-3w-6w-9w-12w) throughout the total exposure period of three months. Both leaf sides display leaf-deposited particles. Long trichomes are visible in all abaxial images. Magnification used is 200x, and the scale indicated in the upper left panel is similar for all panels.

4.3.5 Leaf particle accumulation - holistic analysis of a complex interaction

Due to the aforementioned reasons (low frequency of detection and large between-sample variability; §4.3.2), concentrations of the accumulated elements were better assessed by analyzing the leaf leachates with ICP-MS than directly with ED-XRF. Reproducibility of the latter could be improved by grinding the leaf material, while sensitivity could be increased by e.g. combining selective excitation (through different secondary targets) with the reduction of the background of X-ray spectra (using polarized-beam instrumentation, PED-XRF) (Marguí et al., 2009).

For the elements measured by ICP-MS, trace metals such as Cr, Mn, Fe, Cu, Zn, and Pb, are of particular interest due to their potential hazardousness and link with anthropogenic pollution. With exception of Cr, which clearly built-up on the exposed leaves, the other metals have shown some fluctuation during the experiment (Figure 4.15). Concentrations of Cu and Pb increased with exposure time until the 6w leaves (maximum values), after which they decreased slightly in a way that the overall enrichment at the end of the campaign is almost negligible. For other elements, however, the concentrations at the 0w leaves were the highest or equally high as for the 6w leaves, with values decreasing between 0w and 3w and increasing again between 3w and 6w. This is the case for Zn, Cu and Fe, which are known plant micronutrients (Gupta et al., 2008). We suspect that the enhanced concentrations in these metals at 0w are derived from the use of fertilizers or other treatments at the garden center, where the plants are kept attractive for people to purchase them. The low concentrations in Cr and Co at the 0w leaves support this argumentation, since they are not considered micronutrients. We hypothesize, thus, that between 0 and 3 weeks of exposure there is a natural depletion of Zn, Cu, and Fe due to decreasing fertilizer concentration. While traffic-related contributions start to accumulate on the leaves from the moment of exposure (Figure 4.13, Figure 4.14), they do not overcome the natural, plant-internal contributions, and there is a decrease in total concentrations. Between 3 and 6 weeks, traffic contributions prevail and the elemental concentrations of Zn, Cu and Fe increase at 6w leaves. Between 6 and 12 weeks, these

concentrations decrease again because of the rain (dust wash-off), the decrease in local atmospheric PM concentrations (particularly after 9w, leading to lower accumulation rates) and possibly the further natural depletion. In contrast to ICP-MS, the magnetic concentration indicators (ARM, SIRM) refer exclusively to traffic-related PM, in the absence of industrial activity, as is the case. Regarding strawberry leaves, ARM and SIRM were the smallest at 0w, then increased until 6w and started to decrease until 12w (Figure 4.10). The same trend is observed for ivy until 6w, but then the magnetic enrichment remained constant as there was not much further accumulation. The fact that there is no decrease (in ARM or SIRM) for ivy could be related to the different leaf macro/micro morphology with respect to strawberry, as for ivy leaves the decrease due to rain wash-off appears compensated by the accumulation of PM. Our study and previous studies on aerodynamics (Baker and Hunt, 1986; Koch et al., 2019) suggest strawberry leaves to be relatively slow accumulators of atmospheric dust. They also appear to be more susceptible to e.g. wash-off effects and/or variation in PM contributions compared to ivy leaves, as the elemental and magnetic depletion after 6w occurred much rapidly for strawberry than for ivy. In order to estimate the degree of natural depletion of micronutrients, a blank plant growing in the laboratory should be monitored along with the plants exposed to pollution. This side process may be of even more relevance for monitoring low-polluted sites. Lastly, the difference in dust accumulation between ivy and strawberry might be related with the degree and/or rate of encapsulation of deposited particles, which become thus unsusceptible to wash-off. The influence of precipitation on the exposed leaves was difficult to evaluate because the leaves exposed for longer periods (thus, expected to accumulate more dust) were also subjected to total larger rain volumes. Studies on the leaf wettability of ivy and strawberry leaves, as well as on the dynamics of leaf encapsulation of particles (in addition to the deposition) would be required to disentangle the observed species-specific accumulation patterns.

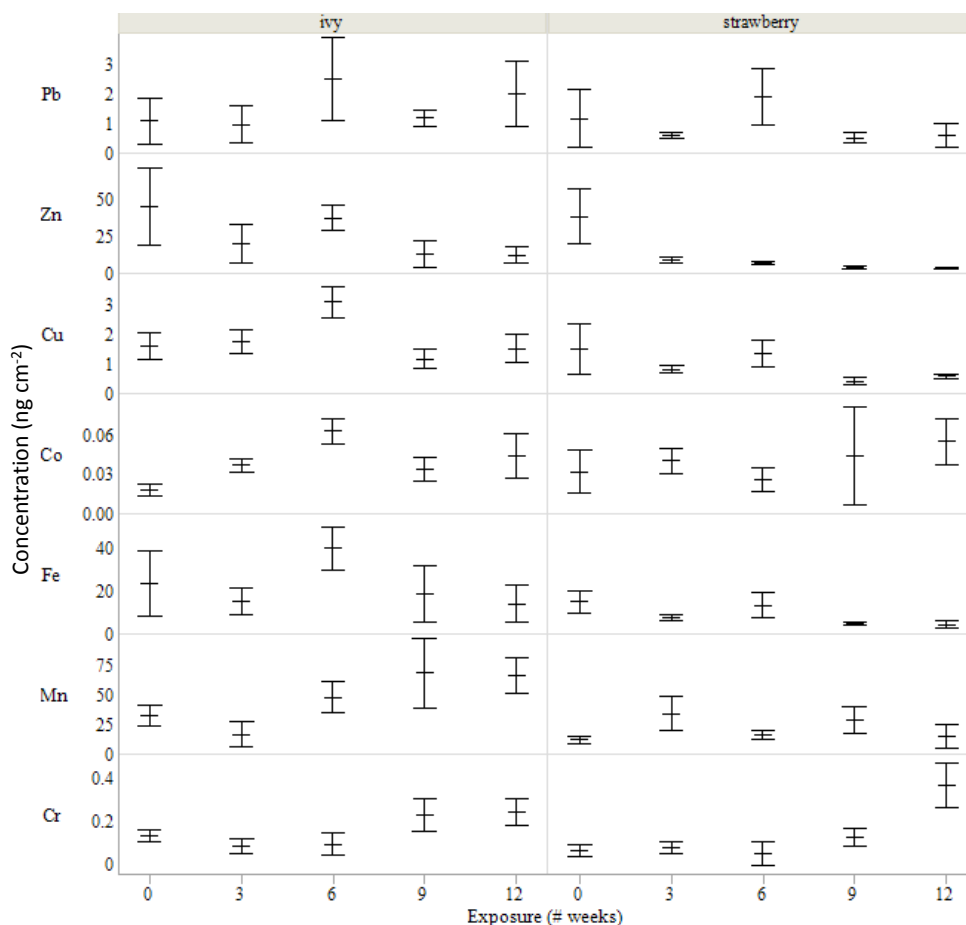


Figure 4.15 - Mean metal concentrations (Cr, Mn, Fe, Co, Cu, Zn, Pb; ng cm^{-2}) for ivy and strawberry leaves collected throughout the exposure campaign. Error bars are constructed using one standard deviation from the mean ($n = 6$).

The elemental concentrations on the exposed leaves (ICP-MS) were for some elements (Cr, Co, Mn, Fe, Zn) correlated with the cumulative atmospheric pollutants concentrations (PM_{10} , $\text{PM}_{2.5}$) at the test site. For both ivy and strawberry, Cr was positively correlated with cumulative PM_{10} and $\text{PM}_{2.5}$ ($\rho = 0.65 - 0.75$, $p < 0.0004$), whereas Zn was negatively correlated ($\rho = -0.56 - -0.94$, $p < 0.003$). When relating the cumulative PM with the measured leaf magnetic properties, the indicators $\text{ARM}_{200/500}$, SIRM and ARM_{χ} were positively correlated for ivy ($\rho = 0.36 - 0.62$, $p < 0.048$), and SIRM and ARM_{χ} for strawberry ($\rho = 0.38 - 0.51$, $p < 0.036$). The mean trace elements concentrations and magnetic indicators were compared for the five sampling events

(0w, 3w, 6w, 9w, 12w). Significant correlations ($p = 0.038$; $p = 0.9$) were found for ivy only, between $ARM_{200/500}$ and the metals Co and Pb, and between SIRM and Mn. Although these correlations have been estimated from somewhat redundant data (at a common test site, the cumulative pollutants concentrations are the same for each sampling event) and reduced sample sizes (mean values correspond to a total of five per species, one value per sampling event), they demonstrate that the trace metal and magnetic content from leaves reflect the atmospheric PM conditions. Additional research should include performing these analyses (ICP-MS and magnetic) on the same leaves, to properly investigate the relationships between leaf magnetic properties and enrichment in trace elements, in terms of dust-polluting contributions and natural depletion.

4.4 Conclusions

In the present monitoring study, ivy and strawberry plants were exposed outdoors at a moderate road traffic site for a period of three months. Leaves collected every three weeks were analyzed for their elemental and magnetic content, as well as microscopically, in order to evaluate the accumulated leaf dust. Dust accumulation was mainly observed visually (SEM) and magnetically, on both ivy and strawberry leaves, while the enrichment in metals was limited (only Cr increased over time for both species). Dust wash-off effects due to rain and lowered atmospheric PM concentrations, between 6w and 12w, were reflected in the obtained results (mainly magnetically and via SEM images). The overall dust accumulation was not as substantial as expected, possibly due to the aforementioned reasons, and to the fact that traffic-related contributions were only moderate. Yet, significant differences were observed between the two test species. Ivy accumulated more dust (elements/magnetically/SEM) than strawberry leaves, even though strawberry leaves are characterized by the presence of long trichomes and a rugged micromorphology, which are considered important leaf traits to capture atmospheric dust. In addition to accumulating less, strawberry leaves also seemed to be more susceptible to wash-off effects. The magnetic enrichment of exposed ivy and strawberry leaves was,

nonetheless, equally derived from small-grained SD/PSD magnetite particles. The results from this campaign support ivy leaves to be useful and reliable in the monitoring of atmospheric dust, having also the advantage of being a resilient, evergreen species, widely available in a variety of environments, from natural to urban settings.

Leaf surface elemental concentrations were obtained from the same leaf samples with ED-XRF and HR-ICP-MS in an attempt to check the feasibility of both techniques for analyzing leaf-accumulated atmospheric dust. Although ED-XRF requires no sample preparation and is reliable for the analysis of PM-filters, the observed blank variability was too high to get reliable quantifications, related with the fact that the leaf matrix is rather heterogeneous, chemically and in terms of thickness. The high frequency and consistency of elements detected by HR-ICP-MS in the leaf leachates supports this methodology as a useful approach to investigate the accumulation of atmospheric dust on leaf surfaces. By comparing the ICP-MS concentrations with the magnetic properties for the non-exposed leaves, there was evidence that certain elements (Cu, Fe, Zn) associated with traffic-related pollution might have been derived from the plants per se through the use of fertilizers (plant micronutrients).

Although plant leaves are valuable for monitoring the surrounding habitat quality, this biomonitoring campaign illustrated how complex and multifaceted the interaction between atmospheric dust and its accumulation on leaves can be. Variations in terms of pollution contributions, meteorological phenomena, species-specific traits, particle deposition (and encapsulation) vs. micronutrients depletion, will normally have a different outcome depending on e.g. the polluting source/level, monitoring period and species used. Although not being completely elucidative, such multifactorial leaf dust accumulation process can better be understood through a combination of techniques (elements/magnetic/SEM).

Chapter 5

Fingerprinting atmospheric PM sources towards urban monitoring and source apportionment

“If you think that the environment is less important than the economy, try holding your breath while you count your money”

-- Dr. Guy McPherson

Chapter 5.1

Setup and overview of a fingerprinting
campaign of major urban PM sources

CHAPTER 5.1

Based on: Castanheiro, A., Hofman, J., Nuyts, G., Joosen, S., Spassov, S., Moretti, S., VMM, Lebeer, S., Blust, R., Lenaerts, S., De Wael, K., Samson, R, 2020. Particulate matter fingerprinting – a comprehensive chemical and magnetic characterization of atmospheric PM sources. (under preparation)

Abstract

This chapter describes a PM source fingerprinting campaign, aimed to characterize specific urban PM sources magnetically and chemically, and relate this to atmospheric PM concentrations as measured by conventional gravimetric-based air quality monitoring. For this setup, monitoring sites were selected in an attempt to have them influenced as much as possible by a single and specific polluting source. The considered sources were road, train and shipping traffic and industry, in addition to a background site. The conducted campaign combined continuous atmospheric monitoring and point-time measurements at the five monitored sites throughout 7.5 weeks, delivering an extensive dataset in terms of elemental and magnetic properties of the sampled PM. An overview of the source-specific characteristics is provided in the present chapter, and their apportionment is discussed in terms of elemental and magnetic profiles.

5.1.1 Introduction

Urban population, i.e. more than half of the total global population, is greatly affected by air pollution (WHO, 2015, 2016), mainly in the form of PM, due to the great abundance and diversity of emission sources in urban settings. The worldwide monitoring of PM levels by gravimetric analysis is insufficient to track specific and hazardous polluting sources, as health effects are more associated with the size, surface area and composition of PM than with their total mass (Kampa and Castanas, 2008; Pope and Dockery, 2006; Valavanidis et al., 2008). Moreover, current air quality monitoring networks with limited spatial coverage, prevent a detailed study and

characterization of major sources of PM pollution, which is known to peak e.g. close to traffic highways or industrial facilities.

As it has been demonstrated throughout this PhD thesis, magnetic measurements offer great potential to discriminate between source types (§Chapter 3.1) or local variations between streets and urban parks (§Chapter 3.2). Most important outcomes of biomagnetic monitoring of atmospheric PM have been compiled in the review of Hofman et al. (2017). Still, the development of magnetic-based air quality monitoring strategies for source identification and attribution demands for a deep understanding of their physicochemical and magnetic characteristics. For this, a large PM fingerprinting (PMF) campaign aimed to comprehensively characterize PM sources of interest was set up in the region of Antwerp, Belgium. To relate with the conventional gravimetric-based methodology, daily PM-loaded filters collected during seven and a half weeks at Road, Train, Shipping, Industry and a Background, sites, were investigated gravimetrically, chemically and magnetically.

5.1.2 Materials and methods

5.1.2.1 Monitoring sites

Antwerp, in Flanders, Belgium, has been considered to be within the top fifty most polluted cities around the world (Bradshaw, 2018). Antwerp is the second most populated Belgian city, after the capital Brussels, thus, heavily urbanized. Adding to the intense road network and industrial sector in the region, the harbor of Antwerp is considered the largest integrated chemical cluster in Europe (Port of Antwerp, 2018) with cargo numbers increasing yearly. In 2018, a total of 14,595 seagoing vessels have operated in the port of Antwerp, with a total transshipment of 235 million tons (Port of Antwerp, 2018). Monitoring sites (Table 5.1, Figure 5.1) were selected in and around the region of Antwerp in order to investigate major sources of atmospheric PM in urban contexts, namely, road and railway traffic, shipping and industry. Fingerprinting of PM sources requires to have such sources as isolated from each other possible, which is not straightforward in highly urbanized areas where multiple contributing

sources are present. In addition to well isolated PM sources, the following requisites were used for selecting the monitoring sites: to be within an enclosed and safe site (while still outdoors) to prevent vandalism, to have access to electricity supply, to be downwind (NE) from the major emitting source. Both Road (R) and Train (or railway, T) monitoring sites were situated within a citizen's private property, the Shipping (S) site within a harbor cargo company and the Industry (I) within the enclosure of an official air quality monitoring station (40HB23, VMM). A Background monitoring site (B) in Retie, at ca. 42 km from the city of Antwerp, was also in the enclosure of an air quality monitoring station (26RT01, VMM). Road and Train monitoring sites (Figure 5.2) were located in more rural, residential areas where road and railway traffic were, respectively, the most polluting local sources on site. The Background site was isolated from major PM emission sources, with the nearest road, with low traffic intensity, at 280 m distance. The movement of ships and transshipments in the area of the Shipping site (Figure 5.3) required the activity of specific road vehicles as well. In addition to this road traffic influence, which is difficult to exclude in cargo shipping environments, contributions from chemical and nuclear plants in the harbor of Antwerp are also expected. A non-ferrous metal recycling plant was the main emission source present at the Industry site, which was located in a residential area with negligible road traffic.

Table 5.1 – Site description and geographic coordinates of monitoring sites.

Monitoring site	Site description	Geographic coordinates
Background (B)	Within the enclosure of air quality monitoring station 26RT01 (VMM) in Retie, at 42 km distance from Antwerp; inside a forested area from which the nearest road, of low-intensity traffic, is 280 m away.	51°13'51.07''N 5°03'11.89''O
Road (R)	At the back of a private property (Achterste Moereind, in Lille), 25 m from highway E34 (direction Antwerp-Turnhout); 26 km distance from Antwerp.	51°15'13.47''N 4°47'56.78''O
Train (T)	At the back of a private property (Rechtstraat, in Duffel), 4 m from railway tracks; 12 km distance from Antwerp; the nearest road, of low-intensity traffic, was 170 m way.	51°06'20.67''N 4°29'20.35''O
Shipping (S)	In the Deurganckdok at the harbor of Antwerp, at ca. 5 m from river Scheldt; 13 km distance from Antwerp.	51°17'56.00''N 4°16'26.42''O
Industry (I)	Within the enclosure of air quality monitoring station 40HB23 (VMM) in Curiestraat, Hoboken, at ca. 20 m from the metal industry; 6 km distance from Antwerp.	51°10'12.89''N 4°20'27.34''O



Figure 5.1 - Overview map of the five monitoring sites (B – Background, R – Road, T – Train, S – Shipping, I – Industry) in relation to the city of Antwerp, Belgium (Google Earth).

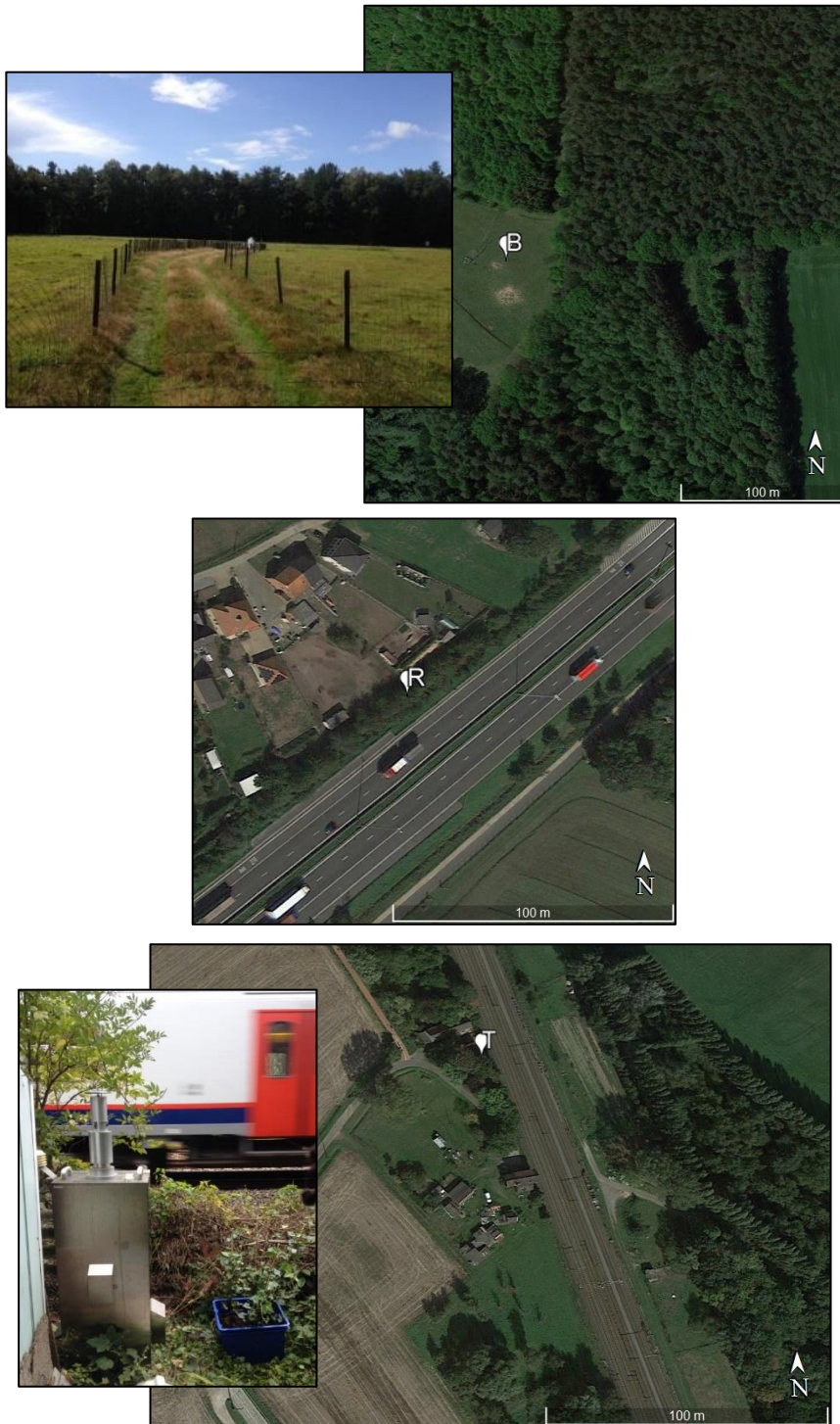


Figure 5.2 – Close-up view of monitoring sites B (Background; top), R (Road; center) and T (Train; bottom) (Google Earth; photos taken on site).

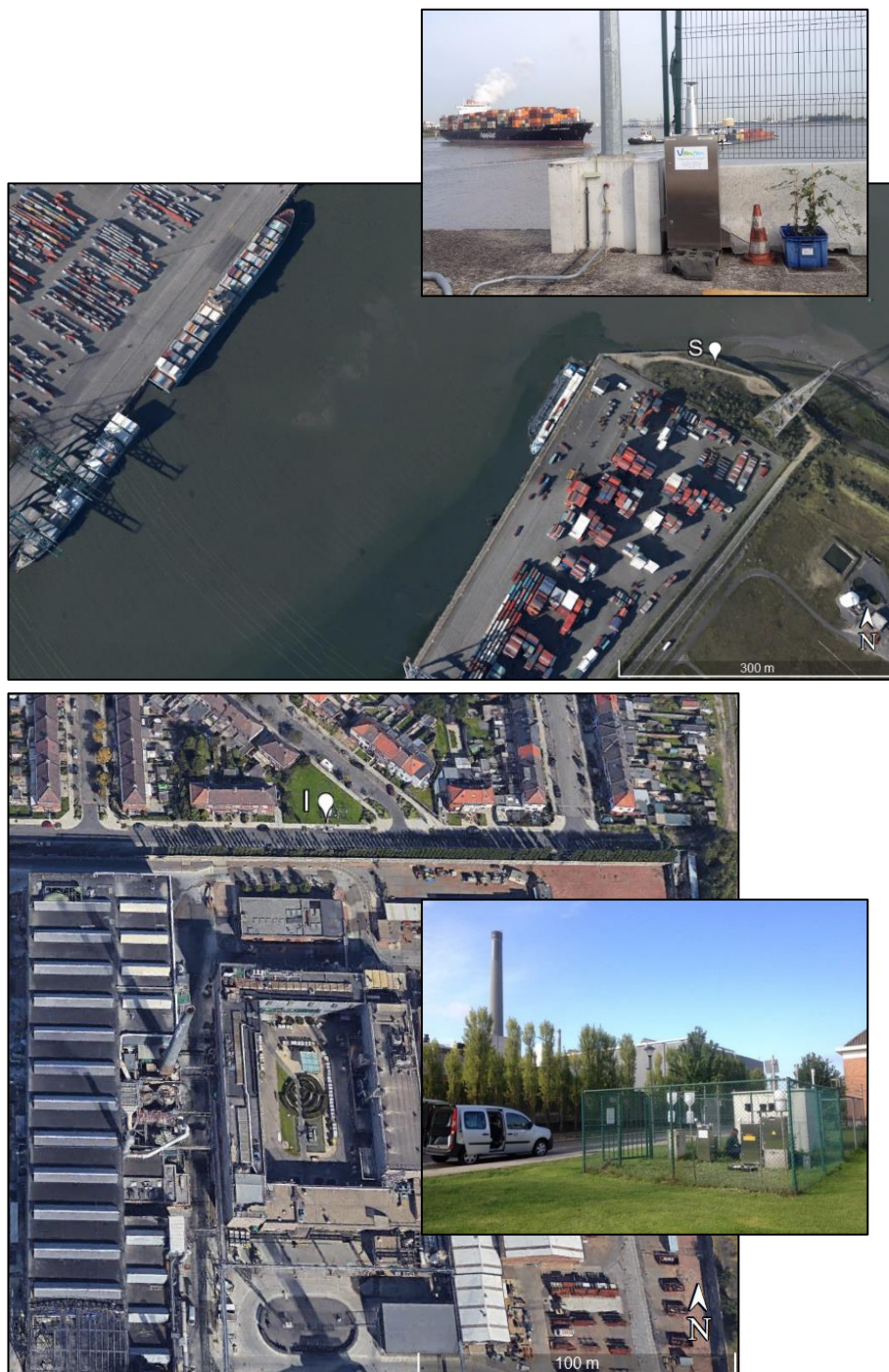


Figure 5.3 - Close-up view of monitoring sites S (Shipping; top) and I (Industry; bottom) (Google Earth; photos taken on site).

5.1.2.2 Monitoring equipment

This monitoring campaign was carried out at the five study sites (four PM sources and one background) between September 16 and November 7, 2017, in a total of 53 days (7.5 weeks). PM monitoring (Figure 5.4) included continuous gravimetric PM₁₀ sampling (active monitoring; present Chapter) and leaf biomonitoring by exposure of ivy plants (passive monitoring; §Chapter 5.3). Point measurements were done weekly using portable instruments (PM₁₀, BC, UFP) and air samples were obtained also weekly through a Coriolis impinger for quantifying the health-risk potential at each study site (§Chapter 5.2).

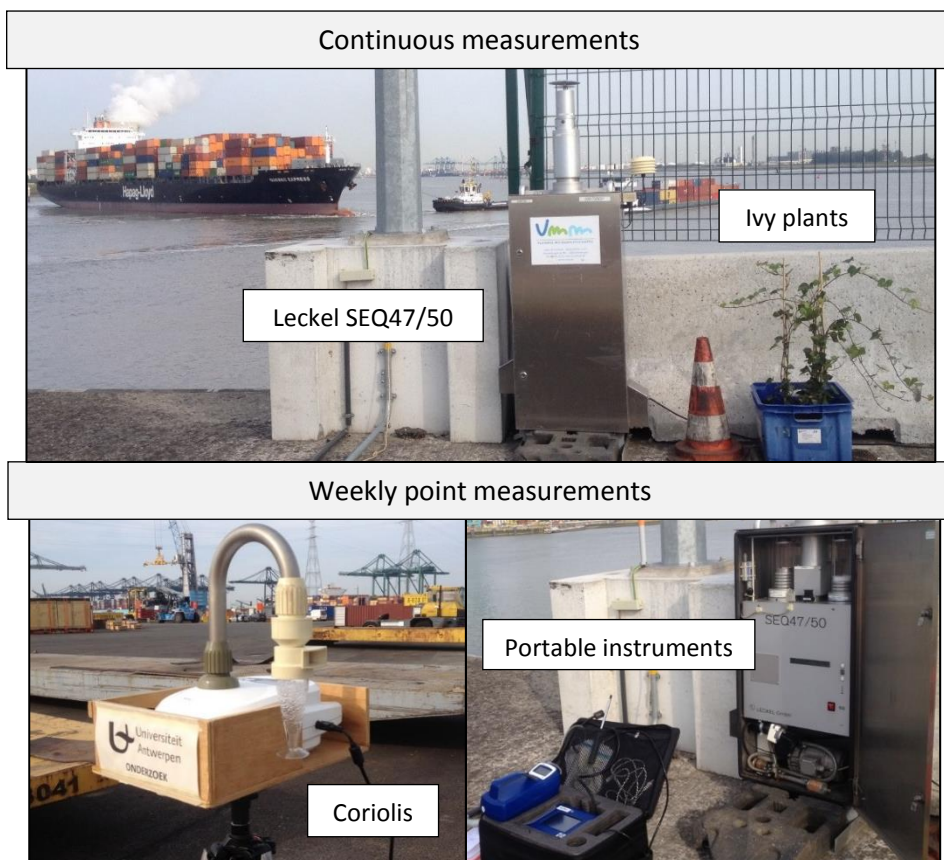


Figure 5.4 - Illustration of the continuous (top) and weekly (bottom) monitoring and sampling equipment setup at a monitoring site (Shipping is shown).

- o Gravimetric PM sampling

Cumulative 24-hour air-pumped PM₁₀ was collected on quartz membrane filters (Tissuquartz 2500 QAT-UP; 47 mm in diameter) (Pall Corporation, USA) at a flow rate of approximately 2.3 m³ h⁻¹ (55.2 m³ day⁻¹) for 7.5 weeks, using a low-volume Leckel SEQ 47/50 (Leckel, DE) gravimetric sampler at study sites R, T, S, and I. The sampling flow of the Leckels (2.3 m³ h⁻¹ ≈ 38.33 lpm) was calibrated on-site before deployment, using a BGI DeltaCal air flow calibrator (Mesalabs, USA), and checked (max 5% deviation; 36.41 - 40.25 lpm) during each of the weekly point measurements. After the 24-hour sampling, PM₁₀-loaded filters were automatically stored internally in filter cartridges, before being transported to the laboratory. The filter cartridges, changed every fortnight, contained a procedure blank filter each (four procedure blanks per monitoring site). The flow rate (m³ h⁻¹), sampling time, sampled air volume (m³), ambient and internal atmospheric temperature (°C) and pressure (mbar) were registered automatically by the SEQ 47/50 samplers, and consulted using the supplied StatusView software (Leckel, v2.45). For the Background location (B), PM-loaded filters were available from a low-volume Derenda (Comde-Derenda, DE) PM sampler operating for the Flemish Environment Agency (VMM) in similar working conditions than the Leckels. However, the impactor head of the Derenda had a smaller size cut-off collecting PM_{2.5} instead of PM₁₀. Due to the impossibility to obtain PM₁₀ samples at this location, a subsequent study was carried out in 2018 to assess the inter-comparison between PM_{2.5}-Derenda and PM₁₀-Leckel samples. This study consisted on the simultaneous operation of a Derenda (PM_{2.5}) and a Leckel (PM₁₀) PM sampler between the same period of time the following year (September 16 - November 7, 2018) (Figure 5.6). The ratio PM₁₀ to PM_{2.5} concentrations was on average 1.66 (n = 53), which fits within the range observed in other studies across Europe (Barmpadimos et al., 2012; Pandolfi et al., 2011; Querol et al., 2001; Van Dingenen et al., 2004). Although PM₁₀/PM_{2.5} ratios are influenced by meteorological conditions and source variations, which most likely have been different between the same periods in 2017

and in 2018, the inter-comparison factor was used to calculate PM₁₀ concentrations at the Background site from the 2017 Derenda samples.

A number of PM₁₀-loaded filters out of the 53 monitored days were disregarded from analysis due to e.g. electricity shortages or miscommunication with the Leckel samplers (i.e., running time < 24h). This was the case for five filters from the road site (sample codes R918, R919, R920, R104, R105), three from the train (T115, T116, T117) and one from the industry site (I117). For the Background location, only a selection of filters (Derenda PM_{2.5}) were available from the air quality station, in total 33 out of the 53 daily filters.

- Point-time measurements of PM₁₀, BC and UFP

Weekly (n = 6) at each monitoring site, 10 second-averaged atmospheric measurements of PM₁₀, BC and UFP were collected for 40 min with portable instruments. A total of 4 hours of monitoring data was obtained per pollutant per monitoring site. Atmospheric PM₁₀ concentrations were measured with a Dusttrak™ II (TSI, USA) equipped with a 10 µm particle size cut-off impactor. Concentrations of optically absorbing aerosol particles (black carbon equivalent, in ng m⁻³) were determined using a AE51 microaethalometer (Aethlabs, USA). UFP measurements were performed with a P-Trak® ultrafine particle counter (Model 8525, TSI, USA) quantifying atmospheric particles with aerodynamic diameter between 0.02 and 1 µm, by optical particle counting following condensational particle growth (using isopropyl alcohol). Any abnormal occurrences (e.g., active fires in neighboring houses, grass mowing activities) or relevant information (such as the number of passing trains at the train site) during the weekly point measurements were registered in a logbook.

5.1.2.3 Laboratory analyses

- Gravimetric PM

Following the European EN12341 standard for gravimetric PM₁₀ sampling, the quartz filters were pre-weighed after a preconditioning period of > 48 h in a climatized

weighing room at a relative humidity of 50%, using a MT5 microbalance (Mettler-Toledo Ltd., AT) with 1 μg sensitivity. A second pre-weighing was conducted after another conditioning period of > 12 hours (weight difference $\leq 40 \mu\text{g}$). The pre-weighed filters (plus a procedure blank per filter set) were loaded in filter cartridges, which were then inserted in the Leckel PM samplers. After sampling and arrival to the laboratory, the PM-loaded filters were conditioned for > 48 h and post-weighed. A second post-weighing was conducted in a 24 - 72 h time window, provided that the post-weighing difference did not exceed 60 μg . Otherwise, another conditioning period of 24 h was required before a third post-weighing. The average filter loading (post-weighing minus the pre-weighing; in μg) was divided by the sampled volume of air to obtain average daily atmospheric PM_{10} concentrations ($\mu\text{g m}^{-3}$). For the Background site, atmospheric PM_{10} concentrations were calculated from the determined atmospheric $\text{PM}_{2.5}$ concentrations as mentioned (§5.1.2.2).

Subsequently, filters were analyzed for their PM composition with ED-XRF. After, filters were cut in half, with one half filter used for HR-ICP-MS analysis, and the other half filter for magnetic analysis. A selection of PM filters were also frozen and stored for PAHs analysis, while another selection of PM filters were stored to perform hysteresis loop measurements (data not shown) at the Environmental Magnetism laboratory of the Geophysical Centre of the Royal Meteorological Institute, BE). Processing of the obtained PAHs analysis and hysteresis loop curves is part of future research.

- Elemental PM composition

Different analytical techniques exist for chemical and physical characterization of PM (Galvão et al., 2018), which is key in the process of fingerprinting PM sources. In order to quantify trace element concentrations (e.g. metals), representative analytical techniques (for comparison with regulatory EU data) with low detection limits were selected. The collected PM samples were analyzed for their elemental composition by two different techniques, using X-ray (ED-XRF; non-destructive) and atomic spectrometry (HR-ICP-MS; destructive) principles (Galvão et al., 2018).

First, the full PM-loaded filters were analyzed for 73 elements within the range Na – Bi by ED-XRF (energy-dispersive X-ray fluorescence) (§4.2.2). Due to the nature of the filters (pure quartz), elements with $Z < 15$ (Mg, Al, Si, P) could not be quantified. The following parameters were used for the analyses of Na-Sc and Ru-Sn: tube voltage of 25 kV, current of 24 mA, live time of 500 s and a Ti secondary target; Ti-Ga and Sb-Er: 75 kV, 8 mA, 1000 s and Ge secondary target; Ge-Nb, Se-Bi: 100 kV, 6 mA, 1000 s and Mo secondary target, in the samples. The same parameters were used for the analyses of the blanks, but with three times the life time. Four procedure blank filters per monitoring site (excepting for Background) were used together with four regular blank filters. All concentrations (ng cm^{-2}) that fell below the limits of detection (that varied between 0.1 and $5 \mu\text{g cm}^{-2}$ for the different elements) or quantification, were disregarded from analysis. The concentrations were recalculated for the analyzed PM-loaded spot diameter (39 mm) in the filters (47 mm) and the volume of sampled air, to obtain atmospheric element concentrations (ng m^{-3}). From the elements measured, elemental PM concentrations in 21 elements (S, Cl, K, Ca, Ti, V, Cr, Mn, Fe, Co, Ni, Cu, Zn, Se, Br, Rb, Sr, Sn, Ba, Pb, Bi) were obtained.

Second, HR-ICP-MS (high-resolution inductively coupled plasma mass spectrometry) was applied on filter half samples. For element extraction, each half filter was transferred to a polypropylene tube with 125 μL concentrated HNO_3 and heated for 60 minutes at 115°C using a heating block (HotBlock, Environmental Express, USA). Samples were analyzed by HR-ICP-MS for 27 elements (Na, Mg, Al, Si, K, Ca, Ti, V, Cr, Mn, Fe, Co, Ni, Cu, Zn, As, Rb, Sr, Mo, Rh, Pd, Ag, Cd, Sb, Tl, Pb, U). The obtained element concentrations ($\mu\text{g L}^{-1}$) corrected for the procedure blank concentrations were normalized to the applied analytical volume and dilution, and recalculated to atmospheric element concentrations (ng m^{-3}) using the volume of sampled air and doubled to obtain full-filter values (for comparison against ED-XRF results). For element concentrations falling below the detection limit ($< 0.001 - 0.5 \mu\text{g L}^{-1}$ depending on the element), all calculations were conducted using half the limit of detection, after Custer et al. (2000)). Whenever the filter element concentrations were

negative after subtraction of procedure blank concentrations, these were considered to be null.

Both ED-XRF and ICP-MS are reliable, largely accepted techniques to measure PM-bound elements on filters (including on quartz Pall's 2500 QAT-UP filters) (Okuda et al., 2013; Vercauteren et al., 2011; Yatkin et al., 2011, 2012). Yet, and although being a destructive methodology, ICP-MS allows for lower detection limits than ED-XRF. And in this study, both PM₁₀ filters and Coriolis air samples were analyzed using HR-ICP-MS. For comparative reasons, the filter elemental PM₁₀ composition herein reported is mainly supported by the ICP-MS data. The filter ED-XRF data is also presented in part to investigate the relationship between the two analytical techniques, similarly as it has been done in Chapter 4 for leaf samples.

- Magnetic PM analysis

The PM-loaded filter samples (half filters) were analyzed for a range of magnetic properties. Bulk low-frequency magnetic susceptibility (k ; SI) under 200 A m⁻¹ bias field was determined at the laboratory of Environmental Magnetism (Geophysical Centre of the Royal Meteorological Institute of Belgium) with a highly sensitive (2 x10⁻⁸ SI) KLY-4 Kappabridge (AGICO Inc., CZ), as the MS2B system (Bartington Instruments, UK) sensitivity (2 x10⁻⁶ SI) revealed to be insufficient for our filter samples. The mass-specific low-field magnetic susceptibility (χ_{LF}) was obtained by dividing the volume bulk susceptibility by the mass of collected PM on the sample (half filter) and correcting it for the sample container volume, being expressed in m³ kg⁻¹.

The PM filter samples were then transported to the magnetic lab of the Bioscience Engineering Department of the University of Antwerp, and analyzed for their anhysteretic remanent magnetization under 200 mT AC and 500 μ T bias DC field (ARM_{200/500}; A m⁻¹), saturation isothermal remanent magnetization (SIRM; A m⁻¹) and 300 mT backfield magnetization (IRM₋₃₀₀; A m⁻¹). Primarily, several ARM AC/DC fields were tested for a selection of samples (four filters per site), but the combination 200

mT/500 μ T was applied to all filters as this yielded the highest magnetic moment intensities, just like observed for the leaf samples in Chapter 4.

A LDA5/PAM1 system (AGICO Inc., CZ) was used for the acquisition of ARM_{200/500} and a Molspin pulse magnetizer (Molspin Ltd., UK) for assessing SIRM and IRM₋₃₀₀, which were all subsequently measured using an AGICO JR-6 magnetometer. From these magnetic properties, magnetic indicators S-ratio (IRM₋₃₀₀/SIRM), HIRM ($0.5 \times (\text{SIRM} + \text{IRM}_{-300})$), SIRM/ χ_{LF} , and ARM/SIRM were calculated, providing information on the relative contribution of high- (antiferromagnetic) to low-coercivity (ferromagnetic) magnetic minerals and magnetic grain size (Evans and Heller, 2003; Hofman et al., 2017). SIRM and ARM exhibit grain size dependence, while χ_{LF} is more dependent on the magnetic composition and concentration than on the size, reflecting how easy it is to magnetize a sample. In general, superparamagnetic (SP, very small) and multidomain (MD, very large) grains are easier to magnetize (thus, have higher χ_{LF}) than single (SD) and pseudo-single (PSD) particles. Hence, high SIRM/ χ_{LF} and ARM/SIRM ratios indicate high contributions of smaller-grained SD or PSD magnetite particles (Hofman et al., 2017). ARM susceptibility (ARM χ ; ARM normalized for the DC bias field) was also determined for plotting the King plot (King et al., 1982). The measured magnetic properties were normalized by the weight of collected PM (half filter) and corrected by the used sample pot volume (6.7 cm^3), resulting in units of $\text{m}^3 \text{ kg}^{-1}$ for χ_{LF} and ARM χ , and of $\text{A m}^2 \text{ kg}^{-1}$ for ARM and (S)IRM.

o Polycyclic Aromatic Hydrocarbons (PAHs)

A selection of PM-loaded filters was analyzed for PAHs at the Comprehensive Molecular Analytics (CMA) laboratory, Munich (DE). To avoid the influence of large within-week variations, filters from the same weekday (Tuesdays) were chosen, in a total of eight filters per monitoring site (only six filters were available from the Background site). A total of 59 PAHs were determined from the PM-loaded filters, including benzo[a]pyrene, fluoranthene, naphthalene and anthracene (data not shown).

5.1.2.4 Meteorological data

Meteorological data on air temperature ($^{\circ}\text{C}$), wind speed (m s^{-1}) and wind direction ($^{\circ}$), precipitation (mm) and relative air humidity (%), was available from a meteorological monitoring station in Antwerp (42M802, in Luchtbal; VMM). During this monitoring campaign (Figure 5.5), the mean daily air temperature was 13.6°C ($\pm 2.9^{\circ}\text{C}$), with a relative air humidity of 82.7% ($\pm 5.9\%$) and a total precipitation volume of 3.3 mm . The prevalent wind direction was SW, with mean daily wind speed of 3.7 (± 1.4) m s^{-1} .

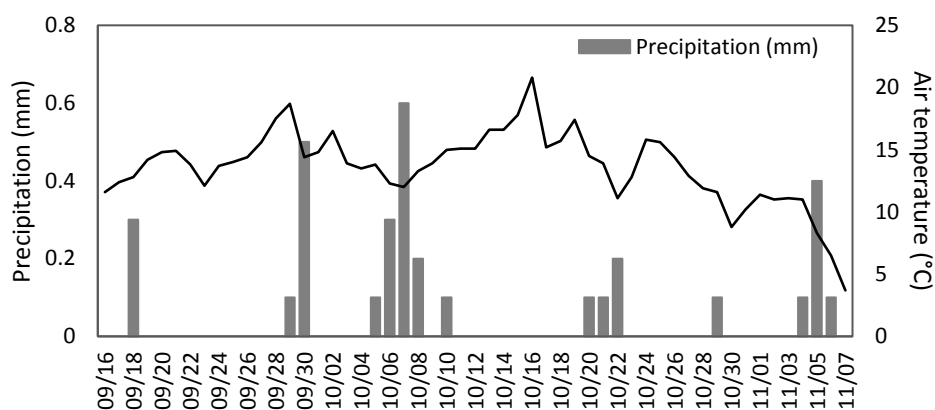


Figure 5.5 – Mean daily air temperature and precipitation registered at the meteorological monitoring station in Antwerp (42M802; VMM).

5.1.2.5 Data analysis

The distribution of the obtained data, checked visually (histogram and Q-Q plots) and with Shapiro-Wilk tests, showed that most variables were not normally distributed. While log-transformations would make the distribution of most measured variables normal, such transformation could not be applied to all considered variables (e.g. magnetic susceptibility was often negative). Therefore, non-parametric statistical tests were used for testing the influence of monitoring sites (Kruskal-Wallis) on the atmospheric PM concentrations, elements and magnetic properties, and the influence of weekday vs. weekend (Wilcoxon) on the PM concentrations. To compare the same-day results (PM, elements and magnetics) amongst the different monitoring sites, obtained simultaneously, paired-samples Wilcoxon tests were used. Linear mixed

models based on the monitoring sites or sources (fixed effect) and considering the temporal variability (as random effect; day of the year, DOY), were built for predicting PM concentrations. Pairwise Pearson correlations on log-transformed PM concentrations were also checked to assess their behavior throughout the monitored period across the different sites. The comparison of elemental concentrations measured by ED-XRF and HR-ICP-MS on the same filter samples was evaluated by paired-samples Wilcoxon tests. Further analysis on the elemental composition was always conducted using the HR-ICP-MS results, to compare the elemental concentrations thereby obtained for the filters with the concentrations determined in the Coriolis air samples (§Chapter 5.2) and for the exposed ivy leaves (§Chapter 5.3). Spearman Rank correlation tests were employed to check for associations within, and between, the elements and magnetic properties measured.

In an attempt to discriminate between the monitored sites, representing important PM sources, principal component analysis (PCA) was performed considering the atmospheric PM concentrations, elemental composition (HR-ICP-MS) and magnetic properties as input variables, and the monitored sites as supplementary variables. Random Forest (RF) was applied to the dataset considering separately the PM concentrations (RF “PM”), the elemental concentrations (RF “Elem”) and the magnetic properties (RF “Magn”), to evaluate their prediction power in classifying the monitoring sites (response) based on the observations (PM₁₀ filters). To check whether the combination of multiple monitoring approaches would improve the classification of the monitoring sites, RF was additionally applied to all possible combinations, namely, to “PM & Elem”, “PM & Magn”, “Elem & Magn” and “PM & Elem & Magn”. The response predicted by each performed RF was the averaging result from a total of 100 decision trees. From the entire dataset, 60% was randomly used as training dataset, 20% as validation dataset and the remaining 20% as test dataset (for details about RF, see §2.2.3.4). Furthermore, the agreement between the samples’ actual monitoring sites and their classification based on the RF predictions was checked using the Kappa index of agreement (0 to 1), which evaluates whether the agreements found

are reliable (Kappa = 1) or a matter of chance (Kappa = 0) (Cook, 2005; McHugh, 2012). The application of the Kappa index of agreement in this context allowed to determine whether the RF model predictions performed better than a random assignment of the sites. The RF method was applied using the Bootstrap Forest tool, and the Kappa index of agreement using the Rater Agreement tool, in JMP Pro 14 (SAS Institute Inc., USA).

The Background site, monitored through air-pumped PM_{2.5} filters, was not considered in the PCA or analyses, which was only focused on PM₁₀-loaded filter samples (Road, Train, Shipping, Industry sites). All statistical and multivariate analyses were conducted in JMP Pro 14 and graphs were designed using JMP Pro 14 and Microsoft Excel 2016.

5.1.3 Results and discussion

5.1.3.1 PM₁₀ concentrations

As mentioned, the PM-loaded filters obtained from the Background site (VMM) were PM_{2.5} filters (Derenda sampler), and a year later an inter-comparison study between PM_{2.5}-Derenda and PM₁₀-Leckel was carried out to assess the PM₁₀/PM_{2.5} ratio. According to the data available, the atmospheric PM_{2.5}-Derenda concentrations measured in the same periods of 2017 and 2018 were within the same ranges (2.8 – 23.1 µg m⁻³ and 3.1 – 21.9 µg m⁻³, for 2017 and 2018, respectively). Despite the observed, and expected fluctuations (as air quality and meteorological conditions vary daily, weekly, and of course, yearly), all Background PM_{2.5} concentrations were below 25 µg m⁻³ (Figure 5.6a), with on average 7.8 (± 4.9) µg m⁻³ (n = 33) in 2017 and 9.2 (± 4.1) µg m⁻³ (n = 53) in 2018. The PM₁₀/PM_{2.5} ratio (of 1.66) obtained from the 2018 dataset was used to estimate the atmospheric PM₁₀ concentrations for the monitoring campaign of 2017 (Figure 5.6b).

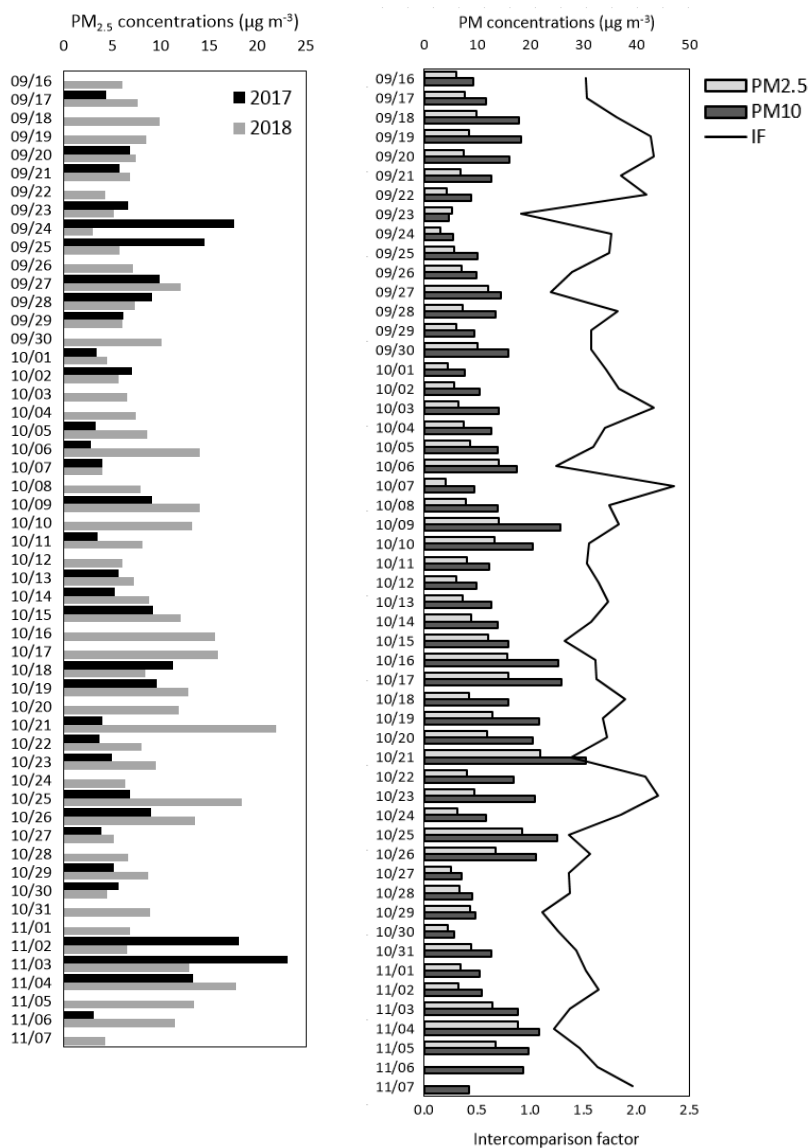


Figure 5.6 - Atmospheric daily PM concentrations measured on the PM-loaded filters at the Background site: a) comparison of PM_{2.5} between 2017 and 2018; b) comparison of PM_{2.5} and PM₁₀ for the 2018 dataset, with the subsequently calculated inter-comparison factor (IF) being the ratio PM₁₀/PM_{2.5}.

Atmospheric PM concentrations registered at the traffic (Road, Train, Shipping) and Industry sites ranged between 4.0 and 40.9 µg m⁻³ during the monitoring campaign. For the Background site, estimated PM₁₀ concentrations ranged between 4.7 and 38.3 µg m⁻³, with gravimetrically determined PM_{2.5} values between 2.8 and 23.1 µg m⁻³. The

daily PM₁₀ concentrations were on average highest at the Shipping ($20.9 \pm 8.6 \mu\text{g m}^{-3}$; $n = 53$), followed by Road ($19.2 \pm 8.3 \mu\text{g m}^{-3}$; $n = 48$), Industry ($16.6 \pm 7.6 \mu\text{g m}^{-3}$; $n = 52$) and Train ($16.5 \mu\text{g} \pm 7.7 \text{ m}^{-3}$; $n = 50$) sites, and then Background ($12.9 \pm 8.1 \mu\text{g m}^{-3}$; $n = 33$). PM concentrations were overall site-specific (Kruskal-Wallis, $p < 0.0001$). According to paired-samples Wilcoxon tests, which examined the same-day concentrations at the various sites, all sites had significantly higher concentrations compared to the Background site ($p < 0.01$), more protected from direct polluting sources, with the Shipping having significantly higher concentrations than Train and Industry (Figure 5.7).

A basic linear mixed-effects model considering time (in the format of DOY) as random effect, with site being the fixed effect, improved the significant effect of site on the PM concentrations ($p < 0.0001$). The model also revealed that approximately 83% of the variance was significantly dependent on time (DOY), indicating that although PM concentrations were site-specific, they were largely influenced by day-to-day variability. The existence of temporal variability, implicit from the relatively large ranges of measured PM concentrations throughout this 7.5 weeks' campaign, is quite established by now (Amato et al., 2016; Qadir et al., 2014). Such PM fluctuations are often transversal to geographically nearby locations, as confirmed in this study by strong positive pairwise Pearson's correlations on the (log-transformed) PM concentrations ($p < 0.0001$), with correlation coefficients between 0.64 and 0.92. This implicates that comparison of sites or sources should be done simultaneously to properly grasp on site or source-specificities, or through time-integrative approaches such as leaf monitoring, so that seasonal and temporal effects do not overrule the discrimination of local PM polluting sources.

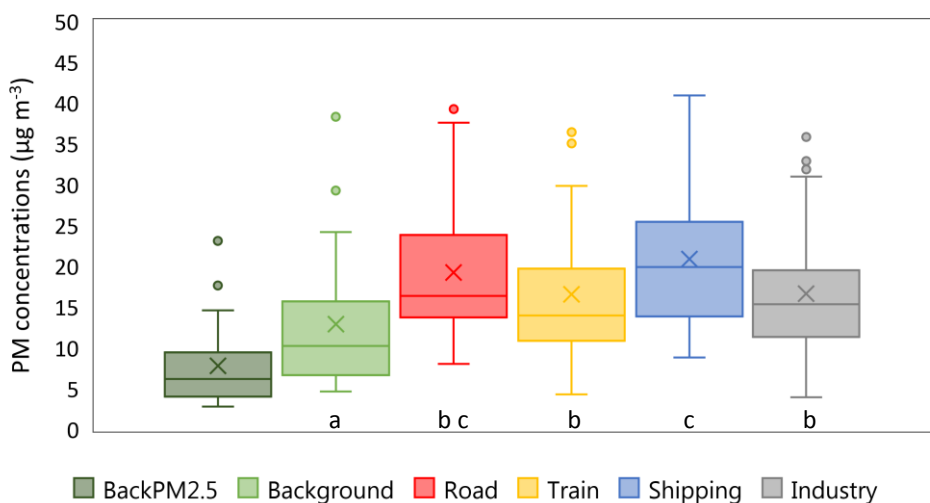


Figure 5.7 - Atmospheric daily PM₁₀ concentrations measured on the PM-loaded filters at the different monitoring sites (with BackPM_{2.5} representing the measured PM_{2.5} concentrations, from which the PM₁₀ values were obtained). The crosses indicate the mean values and circles the data outliers (i.e., above or below 1.5×IQR; Q1 - first and Q3 - third, quartiles, interquartile range IQR = Q3 – Q1). Sites not associated with the same letter are significantly different (paired-samples Wilcoxon, $p < 0.01$).

Temporal dynamics of PM₁₀ concentrations during the monitoring campaign showed to be quite comparable across the different monitoring sites (Figure 5.9a), with the highest concentrations registered during weeks 2, 5 and 7 of the campaign and major peaks at the Shipping site. In general, PM₁₀ concentrations were higher during weekdays than on the weekends, but these differences were only statistically different for the Shipping (Wilcoxon; $p = 0.029$) and Industry ($p = 0.011$) sites. The overall peak registered around the 16/10 - 18/10 might have been influenced by Sahara Desert's dust contributions and by forest fires occurring in Portugal and Spain (logbook notes), known to increase particulate and gaseous atmospheric pollutants (Garcia-Hurtado et al., 2014; Querol et al., 2001).

5.1.3.2 Elemental PM₁₀ composition

The PM₁₀ composition determined from the PM-loaded filters (by HR-ICP-MS) was mainly governed by Na, Fe, Ca, K and Mg across all monitored sites (Figure 5.8). The

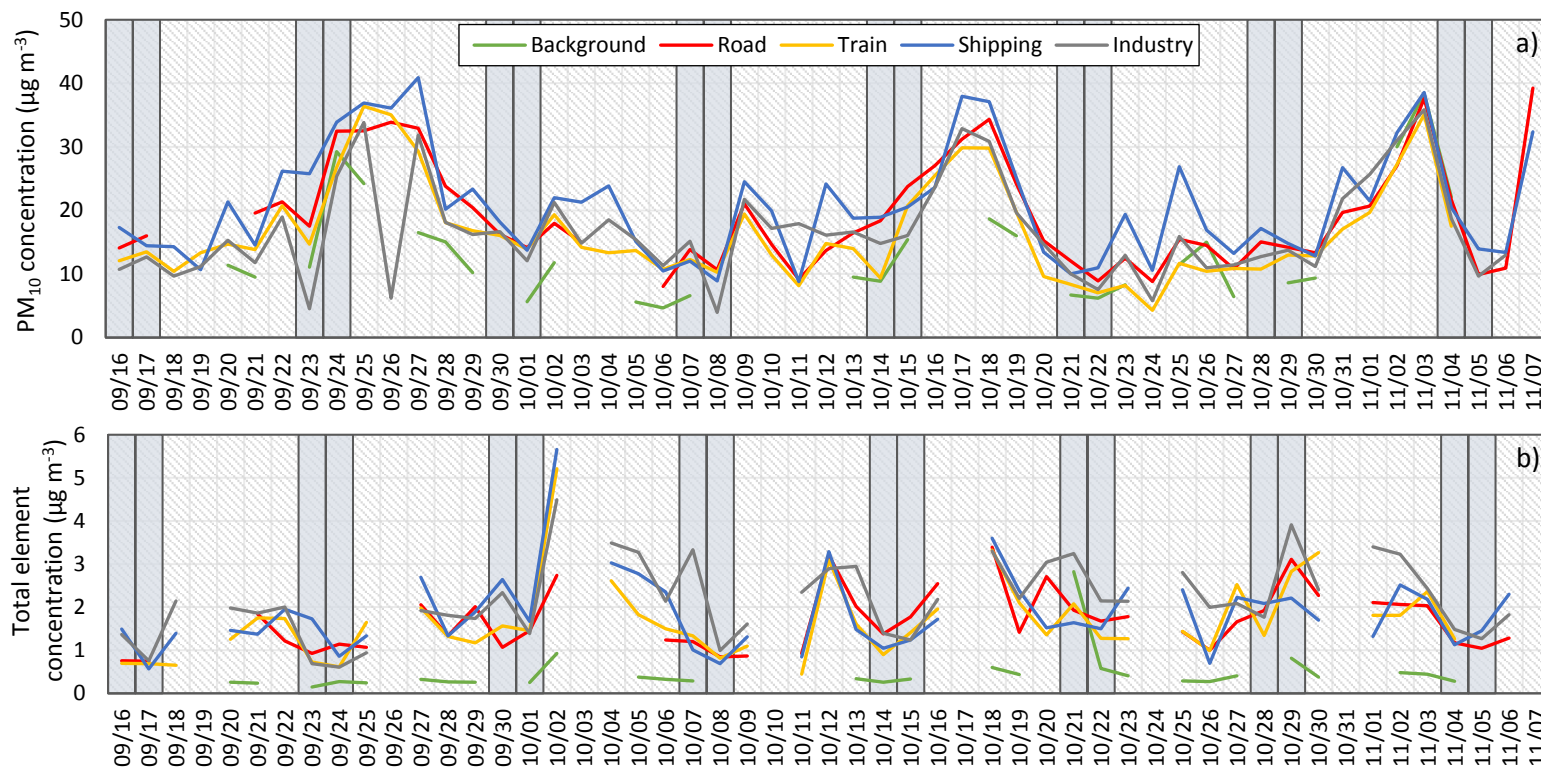


Figure 5.9 - Atmospheric daily a) PM_{10} concentrations ($\mu\text{g m}^{-3}$) (top), and b) total element concentrations (in $\mu\text{g m}^{-3}$; determined with HR-ICP-MS, total of 27 elements) (bottom), determined from the PM-loaded filters across the different monitoring sites throughout the entire monitoring campaign. For the Background site, PM_{10} concentrations were calculated using the inter-comparison factor, with elemental concentrations derived from the $PM_{2.5}$ samples. Vertical bars in grey represent the weekends.

CHAPTER 5.1

Table 5.2 – Mean (in grey) daily element concentrations followed by the range (min – max) (ng m^{-3} , determined with HR-ICP-MS), of the PM_{10} -loaded filters across the different monitoring sites ($\text{PM}_{2.5}$ for the Background). Concentrations in Rh, Pd, Tl and U ($< 0.1 \text{ ng m}^{-3}$) are not shown. Sites not associated with the same letter (in superscript) indicate significantly different concentrations throughout the monitoring campaign (paired-samples Wilcoxon, $p < 0.05$). “n” represents the number of analyzed filter samples.

	Background		Road		Train		Shipping		Industry	
Na	102.2 ^a	(3.8 – 571.3)	596.5 ^b	(39.7 – 2490.9)	670.8 ^b	(37.6 – 4330.3)	796.0 ^b	(115.3 – 4276.8)	809.5 ^b	(72.7 – 2896.2)
Mg	21.1 ^a	(2.5 – 137.9)	101.3 ^b	(19.8 – 337.3)	103.4 ^b	(14.9 – 385.6)	140.8 ^c	(31.9 – 419.0)	126.4 ^c	(20.8 – 444.0)
Al	6.0 ^a	(0.2 – 22.5)	40.6 ^b	(4.7 – 150.2)	36.8 ^b	(9.1 – 131.5)	48.6 ^b	(5.8 – 148.3)	43.7 ^b	(10.9 – 146.3)
Si	87.6 ^d	(39.3 – 127.5)	29.4 ^b	(0.0 – 153.8)	13.6 ^a	(0.0 – 86.9)	40.6 ^{bc}	(0.0 – 210.6)	49.2 ^c	(0.0 – 148.0)
K	147.6 ^a	(23.0 – 2382.2)	158.0 ^b	(55.2 – 299.3)	144.8 ^b	(55.8 – 266.9)	153.2 ^b	(43.1 – 435.0)	143.0 ^b	(56.7 – 274.3)
Ca	0.7 ^a	(0.0 – 10.6)	196.3 ^b	(0.0 – 600.4)	181.5 ^b	(0.0 – 508.1)	364.2 ^c	(30.8 – 1024.7)	280.3 ^c	(0.5 – 911.6)
Ti	0.4 ^a	(0.0 – 1.0)	2.1 ^c	(0.4 – 5.5)	1.6 ^b	(0.2 – 4.8)	2.8 ^c	(0.3 – 6.1)	2.3 ^c	(0.5 – 5.9)
V	0.3 ^a	(0.0 – 1.7)	0.6 ^b	(0.1 – 2.4)	0.6 ^b	(0.1 – 2.0)	2.5 ^c	(0.3 – 10.2)	0.6 ^b	(0.0 – 2.1)
Cr	0.2 ^a	(0.0 – 1.5)	1.3 ^c	(0.0 – 3.5)	0.9 ^c	(0.0 – 3.9)	0.7 ^b	(0.0 – 3.3)	1.3 ^c	(0.0 – 8.5)
Mn	2.3 ^a	(0.4 – 6.3)	7.3 ^b	(0.6 – 19.3)	7.5 ^b	(1.9 – 18.4)	6.9 ^b	(0.5 – 19.0)	9.0 ^b	(1.5 – 25.9)
Fe	43.4 ^a	(1.9 – 136.6)	460.7 ^d	(35.4 – 1045.4)	446.5 ^{cd}	(40.5 – 1364.2)	260.1 ^b	(26.3 – 817.6)	292.5 ^{bc}	(58.5 – 700.5)
Co	0.0 ^a	(0.0 – 0.1)	0.2 ^b	(0.0 – 2.6)	0.1 ^b	(0.0 – 0.8)	0.2 ^c	(0.0 – 1.0)	0.4 ^c	(0.0 – 2.4)
Ni	0.7 ^a	(0.1 – 3.3)	1.0 ^b	(0.2 – 3.9)	1.1 ^b	(0.3 – 3.4)	3.7 ^c	(0.2 – 14.3)	4.7 ^c	(0.6 – 31.3)
Cu	2.8 ^a	(0.0 – 17.2)	23.2 ^c	(0.4 – 126.2)	22.6 ^c	(0.9 – 70.0)	7.3 ^b	(0.0 – 31.8)	39.4 ^d	(2.9 – 133.5)
Zn	8.7 ^a	(0.0 – 45.7)	34.8 ^b	(3.5 – 112.7)	32.0 ^b	(3.8 – 118.6)	27.0 ^a	(0.0 – 252.2)	51.9 ^c	(4.8 – 154.1)
As	0.4 ^a	(0.0 – 1.2)	1.0 ^b	(0.1 – 3.6)	0.6 ^a	(0.0 – 2.4)	0.5 ^a	(0.0 – 4.7)	13.2 ^c	(0.5 – 65.6)
Rb	0.0 ^a	(0.0 – 0.2)	0.1 ^b	(0.0 – 1.0)	0.1 ^b	(0.0 – 0.9)	0.4 ^c	(0.0 – 2.6)	0.1 ^b	(0.0 – 1.4)
Sr	0.2 ^a	(0.0 – 1.0)	1.2 ^b	(0.2 – 4.3)	1.0 ^b	(0.0 – 2.2)	1.6 ^c	(0.3 – 4.6)	1.6 ^c	(0.2 – 4.7)
Mo	1.4 ^a	(0.2 – 15.5)	1.3 ^b	(0.1 – 4.5)	1.9 ^b	(0.0 – 13.4)	1.0 ^a	(0.0 – 7.6)	1.0 ^a	(0.1 – 4.5)
Ag	0.0 ^a	(0.0 – 0.0)	0.0 ^a	(0.0 – 0.0)	0.0 ^a	(0.0 – 0.0)	0.0 ^a	(0.0 – 0.0)	13.9 ^b	(0.0 – 138.7)
Cd	0.1 ^a	(0.0 – 0.4)	0.2 ^b	(0.0 – 0.6)	0.2 ^b	(0.0 – 1.9)	0.2 ^b	(0.0 – 0.9)	2.3 ^c	(0.1 – 8.6)
Sb	0.3 ^a	(0.0 – 1.8)	1.0 ^d	(0.0 – 6.1)	0.5 ^c	(0.0 – 1.8)	0.6 ^{bc}	(0.0 – 4.1)	28.8 ^e	(0.1 – 173.9)
Pb	4.6 ^a	(0.6 – 11.9)	9.1 ^b	(1.6 – 27.4)	8.2 ^b	(1.5 – 24.4)	10.2 ^b	(0.4 – 36.4)	273.5 ^c	(7.5 – 1122.0)
n	33		41		43		45		45	

The variation of PM in certain elements, such as Na, Ca and Fe, throughout the monitored period was quite consistent across all traffic and industry sites, with the Na peaks being particularly synchronized (Figure 5.10). On one hand, the Na peaks, on weeks 3 and 4 and on weekend 7 of the monitoring campaign, did not match with the peaks of PM concentrations (Figure 5.9a). On the other hand, the content in Ca and Fe was highest during weeks 2, 5 and 7, similarly to what was observed for PM concentrations. Possibly due to distinct elemental contributions throughout time as observed for these elements, the PM concentration peaks were not perceptible from the measured total element concentrations (Figure 5.9b), which varied mostly between 1 to 4 $\mu\text{g m}^{-3}$.

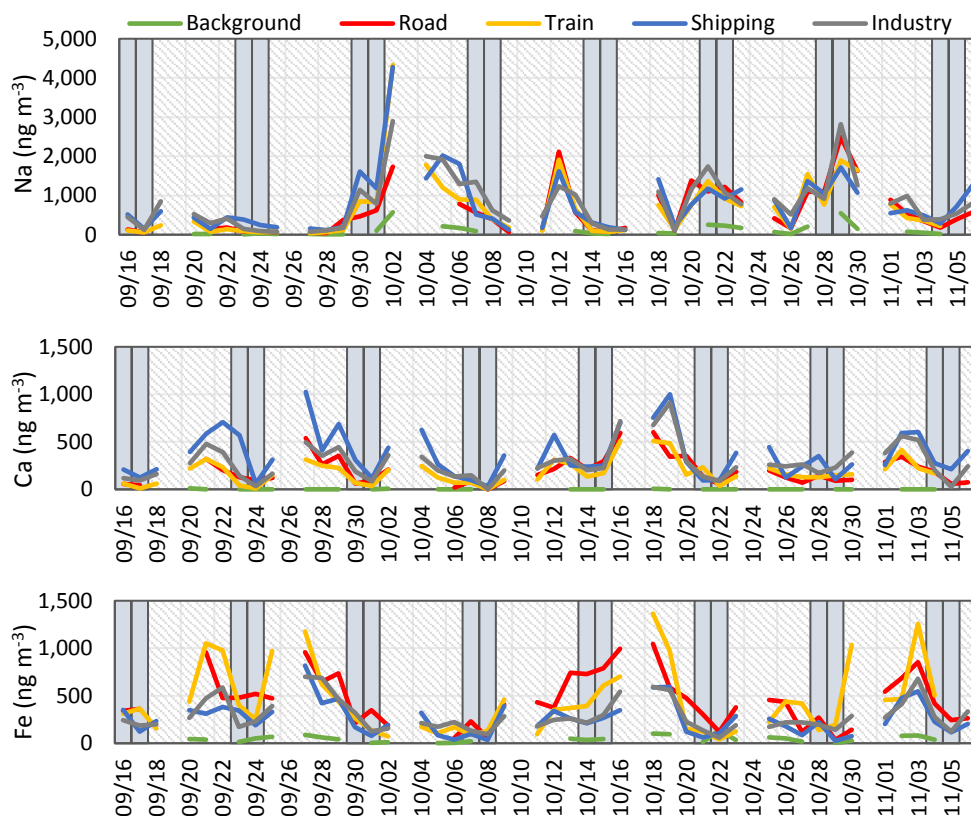


Figure 5.10 - Daily concentrations of Na, Ca and Fe (ng m^{-3}), measured on the PM_{10} -loaded filters (analyzed with HR-ICP-MS) across the different monitoring sites ($\text{PM}_{2.5}$ for Background), throughout the entire monitoring campaign. Vertical bars in grey represent the weekends.

5.1.3.3 Comparison HR-ICP-MS vs. ED-XRF

Daily-averaged atmospheric concentrations calculated from HR-ICP-MS and ED-XRF analyses reached a maximum of 4,330.3 ng m⁻³ and 2,608.5 ng m⁻³, respectively. Although different elements were considered by the two techniques (§5.1.2.3), the elemental profiles of PM-loaded filters measured by ED-XRF were somewhat comparable to those from the HR-ICP-MS determination. From the elements quantifiable by ED-XRF, the composition was ruled by the elements Fe, Cl, S, Ca and K, across all monitored sites. The Road and Train sites had the most alike composition, with the Industry site revealing again a high enrichment in metals such as Cu, Zn, Se, Br, Sn, Ba, Pb and Bi (Table 5.3). When focusing on the range of elements assessed by the two techniques (K, Ca, Ti, V, Cr, Mn, Fe, Co, Ni, Cu, Zn, Rb, Sr, Pb), similar elemental profiles and concentration ranges were obtained with both ED-XRF and HR-ICP-MS (Figure 5.11). Both methodologies yielded comparable results on the relative differences and similarities in composition across the different sites. Still, paired Wilcoxon tests (as the two methodologies were applied to the same filter samples) showed that for some elements significantly ($p < 0.05$) higher concentrations were measured by ED-XRF or ICP-MS. For all polluted sites (traffic and Industry), ED-XRF delivered higher values than HR-ICP-MS for Ti, Cr, Co and Sr, while the contrary was observed for K (exception for Shipping).

Table 5.3 – Mean (in grey) daily element concentrations followed by the range (min – max) (ng m^{-3} , determined with ED-XRF), of the PM_{10} -loaded filters across the different monitoring sites ($\text{PM}_{2.5}$ for the Background). Although the same filters were analyzed subsequently with ED-XRF and HR-ICP-MS, mean ED-XRF values were obtained from less filters as concentrations were often below quantification and/or detection limits depending on the elements (i.e., $n \text{ ED-XRF} \leq n \text{ HR-ICP-MS}$). “-” indicate elements not detected/quantified; elements in bold were also determined with HR-ICP-MS.

	Background		Road		Train		Shipping		Industry	
<i>S</i>	135.8	(24.8 - 445.4)	310.4	(95.0 - 836.8)	301.4	(91.7 - 822.9)	430.8	(148.8 - 1086.3)	359.0	(102.2 - 102.2)
<i>Cl</i>	74.9	(5.2 - 541.9)	310.8	(12.4 - 1315.3)	384.7	(16.6 - 1804.0)	505.5	(17.6 - 1873.3)	599.4	(7.9 - 2608.5)
<i>K</i>	32.4	(15.0 - 89.2)	93.2	(33.2 - 315.3)	88.5	(33.0 - 370.2)	131.3	(42.1 - 315.2)	94.2	(26.7 - 316.2)
<i>Ca</i>	25.4	(11.9 - 44.5)	222.4	(25.6 - 638.6)	220.1	(29.5 - 649.1)	396.1	(72.2 - 1066.1)	325.5	(46.9 - 886.2)
<i>Ti</i>	4.8	(4.5 - 5.0)	13.6	(4.2 - 48.7)	11.5	(4.4 - 46.3)	23.2	(5.1 - 128.7)	15.7	(6.0 - 52.3)
<i>V</i>	-	-	3.3	(2.3 - 4.0)	3.3	(2.4 - 5.0)	4.5	(2.2 - 11.4)	4.2	(3.7 - 5.4)
<i>Cr</i>	3.0	(1.8 - 5.8)	6.6	(2.0 - 15.8)	5.3	(1.9 - 15.8)	5.0	(1.9 - 18.1)	7.2	(2.1 - 26.6)
<i>Mn</i>	2.7	(1.3 - 4.9)	7.8	(2.4 - 20.0)	7.7	(1.5 - 19.2)	7.5	(1.4 - 19.0)	10.1	(1.8 - 30.7)
<i>Fe</i>	51.0	(13.1 - 113.8)	559.5	(45.9 - 1222.2)	566.6	(83.4 - 1761.8)	391.5	(66.5 - 1112.4)	414.4	(94.3 - 945.1)
<i>Co</i>	-	-	3.3	(1.1 - 16.4)	2.9	(1.0 - 7.8)	2.2	(1.0 - 6.0)	2.4	(1.1 - 4.9)
<i>Ni</i>	3.6	(1.2 - 26.7)	5.1	(4.8 - 5.3)	5.1	(4.9 - 5.3)	7.0	(4.8 - 13.8)	9.3	(4.8 - 31.6)
<i>Cu</i>	2.3	(1.1 - 6.0)	18.9	(1.2 - 48.9)	20.6	(1.9 - 61.5)	7.6	(1.3 - 28.5)	36.1	(3.0 - 123.3)
<i>Zn</i>	11.0	(3.5 - 46.3)	30.0	(5.2 - 107.4)	29.7	(5.5 - 133.9)	33.8	(5.4 - 175.0)	54.0	(6.3 - 170.8)
<i>Se</i>	-	-	-	-	-	-	-	-	14.7	(2.3 - 47.7)
<i>Br</i>	2.7	(1.7 - 4.4)	4.1	(2.2 - 9.4)	4.5	(2.3 - 10.2)	6.2	(2.3 - 12.1)	16.3	(4.2 - 43.1)
<i>Rb</i>	1.4	(1.4 - 1.6)	1.5	(1.2 - 2.6)	1.8	(1.5 - 2.1)	2.2	(1.4 - 4.2)	1.2	(1.2 - 1.2)
<i>Sr</i>	2.1	(1.7 - 2.7)	2.5	(1.6 - 4.1)	2.4	(1.6 - 4.4)	2.9	(1.6 - 4.8)	3.0	(1.6 - 5.5)
<i>Sn</i>	13.0	(10.1 - 17.1)	24.5	(12.1 - 54.1)	22.0	(11.7 - 63.0)	28.1	(11.9 - 53.1)	41.3	(16.1 - 278.8)
<i>Ba</i>	-	-	9.2	(7.4 - 13.4)	8.8	(7.5 - 10.9)	-	-	13.5	(9.7 - 17.9)
<i>Pb</i>	5.9	(2.6 - 12.5)	9.5	(2.9 - 25.1)	8.2	(3.0 - 26.0)	11.6	(2.8 - 42.3)	390.7	(7.6 - 1506.5)
<i>Bi</i>	2.8	-	-	-	-	-	-	-	26.8	(2.9 - 103.0)

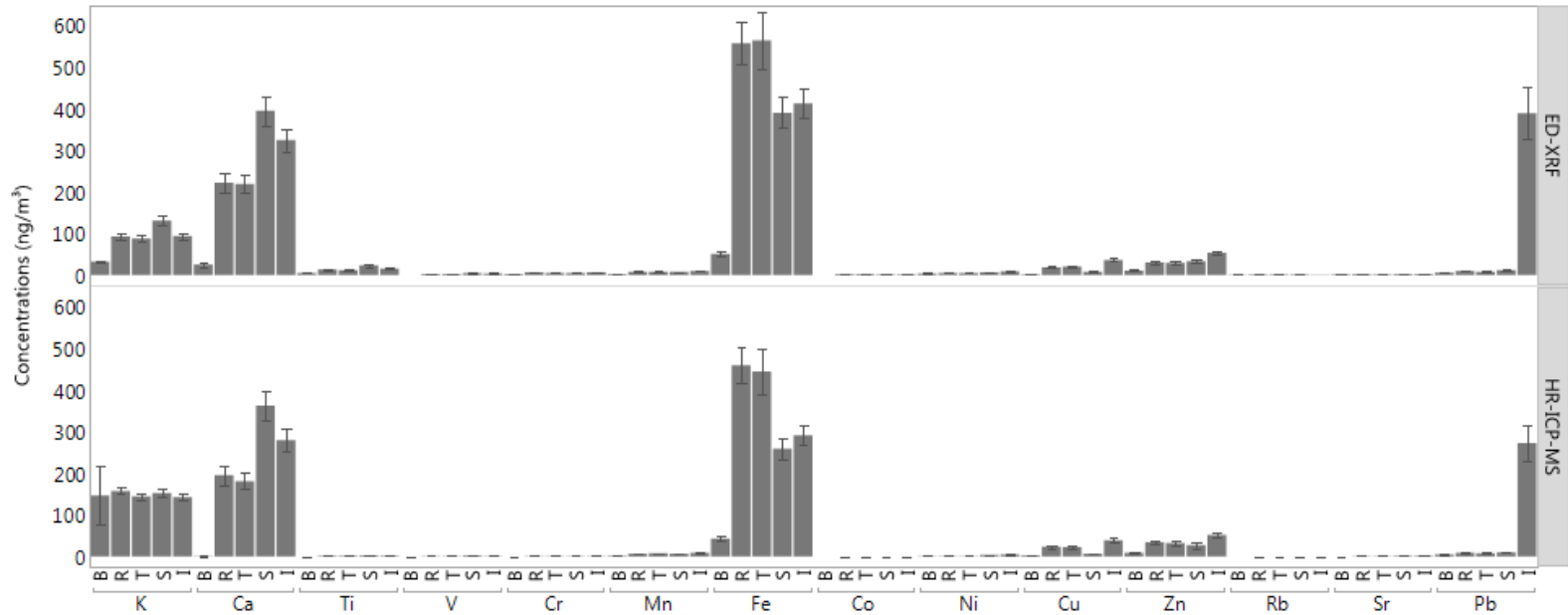


Figure 5.11 – Comparison of mean elemental concentrations (ng m⁻³) obtained from ED-XRF (top) and HR-ICP-MS (bottom) analyses on the PM₁₀-loaded filters across the monitored sites (B – Background, PM_{2.5}; R – Road, T – Train, S – Shipping, I – Industry). Error bars are constructed using one standard error from the mean.

5.1.3.4 Magnetic PM characterization

Magnetic susceptibility (χ_{LF}) of atmospheric PM₁₀-loaded filters ranged between -1,670 and 6,770 $\times 10^{-8}$ m³ kg⁻¹, with mean χ_{LF} values of -48 $\times 10^{-8}$ m³ kg⁻¹ for the Background site, 620 $\times 10^{-8}$ m³ kg⁻¹ for Shipping, 829 $\times 10^{-8}$ m³ kg⁻¹ for Industry, 880 $\times 10^{-8}$ m³ kg⁻¹ for Road and 1,188 $\times 10^{-8}$ m³ kg⁻¹ for Train (Table 5.4). Some of the extremely small negative values obtained for the Background PM_{2.5} filters (minimum of -1,670 $\times 10^{-8}$ m³ kg⁻¹) are even smaller than the susceptibility of the strongest diamagnetic material (i.e., with the smallest, most negative susceptibility), which is pyrolytic carbon (Fischbach, 1961; Pinot and Silvestri, 2019). We hypothesize this may be due to the rather low PM filter loads collected at the site (down to 78 μ g), when compared to those obtained at the other sites (average of 490 μ g). As the PM load mass is divided from the measured volume susceptibility to calculate the mass-specific susceptibility (χ_{LF}), this resulted in very large (negative) values. Another possibility may be related with the procedure blank filters used to correct for the filters' diamagnetic contribution, as quartz is a diamagnetic material. This was done by subtracting the susceptibility of the procedure blank filters from that of the sampled filters (to obtain the susceptibility of collected PM), using the average of the four procedure filters per monitoring site (§5.1.2.3). However, all PM filters from the Background site were provided by the air quality station and procedure blank filters were not available. The mentioned correction for the Background filters was done using the average of all procedure filters from the other test sites (total of 16) instead. Even with the influence of these two situations (low PM loads, different procedure filters), the strong negative χ_{LF} values obtained for the Background site seem to be unrealistically low. To improve the reliability of susceptibility measurements for low mass samples, it is advisable in future experiments to include more sample material per determination (e.g., multiple filters).

Mean ARM_{200/500} and ARM χ ranged, respectively, between 3.49 and 5.98 $\times 10^{-3}$ A m² kg⁻¹ and between 876 and 1,501 $\times 10^{-3}$ m³ kg⁻¹, increasing in the following order across the monitored sites: S < R < T < I < B. ARM depends not only on the mineralogy and concentration of magnetic particles, but also on their magnetic grain size with small

single-domain (SD) grains acquiring ARM more efficiently than multi-domain (MD) grains (Liu et al., 2012b). It is important to note that the analyzed Background filters consisted of PM_{2.5}, which means that collected magnetic particles are most likely to be smaller compared to those collected on PM₁₀ filters, thus, resulting in higher ARM values. SIRM values ranged between 178 and 2,950 x10⁻⁴ A m² kg⁻¹.

Table 5.4 – Descriptive statistics (mean in grey; standard deviation as Std Dev; median, min and max values) of magnetic properties and ratios from the daily PM₁₀-loaded filters (PM_{2.5} for the Background) across the different monitoring sites (B – Background, n = 33; R – Road, n = 41; T – Train, n = 43; S – Shipping, n = 45; I – Industry, n = 45).

	$\chi_{LF} \times 10^8$ (m ³ kg ⁻¹)	ARM _{200/500} x10 ⁻³ (A m ² kg ⁻¹)	ARM χ x10 ⁻⁸ (m ³ kg ⁻¹)	SIRM x10 ⁻⁴ (A m ² kg ⁻¹)	IRM ₋₃₀₀ x10 ⁻⁴ (A m ² kg ⁻¹)	HIRM x10 ⁻⁴ (A m ² kg ⁻¹)	S-ratio (-)	SIRM/ χ_{LF} x10 ³ (A m ⁻¹)	ARM/SIRM x10 ⁻³ (-)	
B	-48.3	6.0	1500.9	642.8	615.8	13.4	0.95	11.4	102.0	Mean
	687.3	2.9	721.5	495.5	492.9	7.3	0.02	267.7	20.0	Std Dev
	-6.0	5.3	1320.0	499.0	472.0	12.4	0.95	-6.0	102.0	Median
	-1670.0	2.4	590.0	199.0	186.0	3.6	0.91	-802.0	50.0	Min
	2190.0	16.1	4040.0	2950.0	2940.0	37.4	1.00	1260.0	170.0	Max
R	879.6	4.4	1107.3	630.0	599.1	18.9	0.94	4.0	72.0	Mean
	633.8	1.3	315.7	200.7	181.4	32.0	0.07	14.4	8.1	Std Dev
	931.0	4.2	1060.0	624.0	591.0	12.7	0.96	6.4	69.0	Median
	-453.0	1.9	468.0	202.0	172.0	-10.5	0.63	-77.5	60.0	Min
	3160.0	8.0	2010.0	1160.0	1120.0	197.0	1.00	16.9	100.0	Max
T	1188.0	5.3	1330.6	785.3	753.2	16.2	0.96	8.2	73.0	Mean
	1026.7	2.0	508.2	464.8	450.7	9.3	0.02	4.5	12.8	Std Dev
	992.0	5.0	1250.0	714.0	678.0	14.9	0.96	7.2	72.0	Median
	118.0	1.8	457.0	216.0	204.0	6.3	0.90	1.5	50.0	Min
	6770.0	12.0	3010.0	2600.0	2490.0	57.0	0.98	28.2	100.0	Max
S	619.6	3.5	876.2	460.8	435.1	12.9	0.94	15.2	78.0	Mean
	797.3	1.3	322.6	210.4	196.9	8.7	0.02	30.8	9.4	Std Dev
	541.0	3.2	800.0	425.0	406.0	10.3	0.95	9.0	76.0	Median
	-89.0	1.6	389.0	178.0	169.0	-0.1	0.90	-31.6	60.0	Min
	5360.0	8.1	2020.0	1370.0	1270.0	48.5	1.00	151.0	100.0	Max
I	829.3	5.5	1382.4	685.1	654.4	15.3	0.96	8.4	81.0	Mean
	511.3	3.0	750.7	364.0	341.2	13.7	0.02	12.6	8.2	Std Dev
	699.0	4.4	1090.0	554.0	524.0	10.9	0.96	8.2	80.0	Median
	-91.3	2.3	571.0	264.0	255.0	0.9	0.92	-61.0	60.0	Min
	2100.0	15.3	3830.0	1880.0	1730.0	75.1	1.00	41.0	100.0	Max

The mentioned magnetic properties (χ_{LF} , ARM_{200/500}, ARM χ , SIRM) were all significantly influenced by the monitoring sites (Kruskal-Wallis, p < 0.0001). For SIRM, one of the most used enviromagnetic indicators, lowest values were obtained for the Shipping (paired Wilcoxon, p < 0.025) with a median of 425 x10⁻⁴ A m² kg⁻¹ and the Background

site ($499 \times 10^{-4} \text{ A m}^2 \text{ kg}^{-1}$), followed by the Industry ($554 \times 10^{-4} \text{ A m}^2 \text{ kg}^{-1}$), Road ($624 \times 10^{-4} \text{ A m}^2 \text{ kg}^{-1}$) and Train ($714 \times 10^{-4} \text{ A m}^2 \text{ kg}^{-1}$) sites (Figure 5.12). Throughout the monitoring period, the Shipping site consistently exhibited the lowest SIRM values, while Train, Industry and Road conditions showed the highest magnetic concentrations. Nevertheless, SIRM peaks were occasionally observed amongst all five monitored sites, e.g. on 22/09, 20/10, 31/10, which mainly occurred on weekdays (Figure 5.13).

It is worth noting that the values of χ_{LF} , $\text{ARM}\chi$ and SIRM obtained in this study are within comparable ranges of values measured on e.g. PM filter samples from Barcelona, Spain (Revuelta et al., 2012) and from Nanjing (Wang et al., 2017) or Beijing (Shi et al., 2014), in China, as well as from surface-collected air suspended particles in 38 Indian cities (Gargiulo et al., 2016). The comparison between such studies, that examine atmospheric PM collected on different matrices or surfaces, is possible because reported values are usually normalized for the amount of PM mass sampled. The rather good agreement across studies carried out on distinct climates, continents and time periods, using different sampling parameters or equipment, is due to the fact that atmospheric sources of magnetic minerals are ubiquitous within urban and non-urban environments (Hofman et al., 2017). This denotes the potential for magnetic-based monitoring strategies, but also the challenge in obtaining source-specific magnetic signatures, as PM sources (and subsequent physicochemical features) are intermingled in the atmosphere.

Obtained IRM_{-300} values were similar to SIRM values (Table 5.4), with subsequent S-ratio close to the unity, with mean values between 0.94 and 0.96 for all sites. This means that on average 94% to 96% of the total SIRM was already reached at 300 mT, indicating that the atmospheric PM samples are dominated by magnetically soft (i.e., low-coercivity) particles such as magnetite (Revuelta et al., 2014).

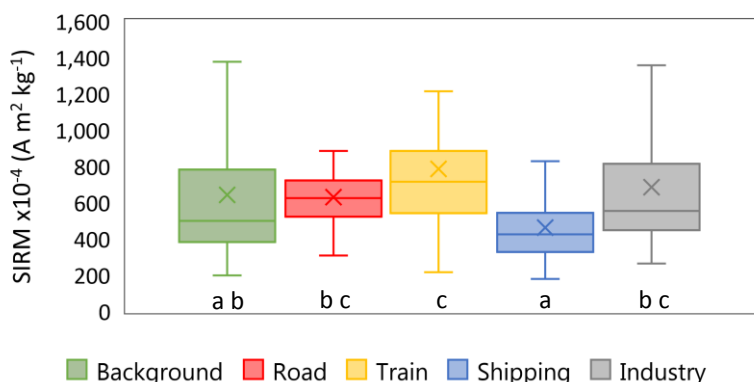


Figure 5.12 - Daily SIRM measured on the PM_{10} -loaded filters at the different monitoring sites ($PM_{2.5}$ for the Background site). The crosses indicate the mean values; data outliers (seven in total) are not shown. Sites not associated with the same letter are significantly different (paired Wilcoxon, $p < 0.025$).

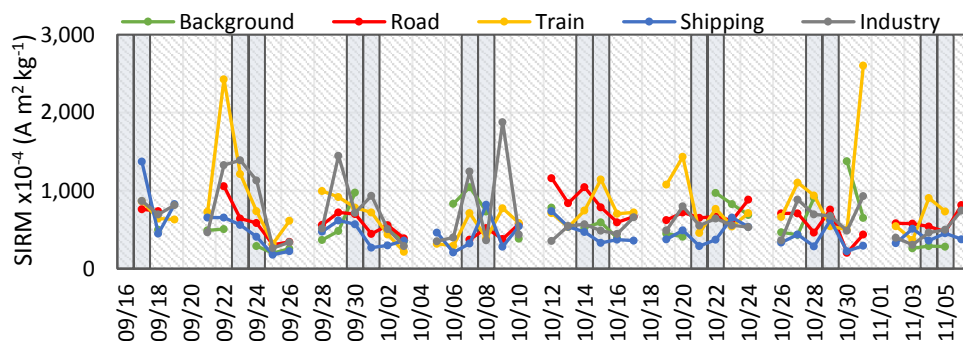


Figure 5.13 - Daily dynamics of SIRM values measured on the PM_{10} -loaded filters at the different sites ($PM_{2.5}$ for the Background site) throughout the entire monitoring campaign. Vertical grey bars represent the weekends.

For HIRM, another descriptor of the relative contribution of low-to-high coercivity components such as the S-ratio, the mean values varied between 13 and 19 $\times 10^{-4} \text{ A m}^2 \text{ kg}^{-1}$. The HIRM values were lowest for Background and Shipping, and highest at the Road site, although differences between sites were not significant ($p = 0.25$). While negative HIRM values are not possible in theory, they were observed in our study (for three filters) and confirm the high similarity, in amplitude, between SIRM and IRM_{-300} values. The little discrepancies between them that resulted in negative HIRM ($SIRM < IRM_{-300}$) is likely due to equipment measuring errors. The proportion of high-coercivity minerals (as antiferromagnetic hematite) relative to the total remanence-carrying

assemblage can be estimated by $\text{HIRM}_{\%} = 100 \times (\text{HIRM}/\text{SIRM})$ (Shu et al., 2000). This proportion ranged between 2.1% and 3% on average for all sites, confirming the dominance of low-coercivity minerals in our atmospheric PM samples.

The ratio ARM/SIRM, in contrast with the other ratios, was significantly site-dependent (Kruskal-Wallis, $p < 0.0001$), based on the ARM and SIRM parameters that varied differently across the studied sites. This ratio was highest for the Background (mean of 102×10^{-3}), followed by the Industry site and then the traffic sites, with overall mean values between 72 and 81×10^{-3} for the latter. The mean ratio $\text{SIRM}/\chi_{\text{LF}}$ was highest for Shipping ($15 \times 10^3 \text{ A m}^{-1}$) and Background ($11 \times 10^3 \text{ A m}^{-1}$), then Industry and Train ($8 \times 10^3 \text{ A m}^{-1}$ for both), and Road ($4 \times 10^3 \text{ A m}^{-1}$). While ARM and SIRM exhibit grain size dependence, particularly ARM, the susceptibility χ_{LF} is mainly considered grain size-independent (Evans and Heller, 2003; Hofman et al., 2017). The Background PM-loaded filters, which represent $\text{PM}_{2.5}$, exhibited relatively high ARM/SIRM as well as $\text{SIRM}/\chi_{\text{LF}}$, compared to the other sites (although not significantly). High ARM/SIRM and $\text{SIRM}/\chi_{\text{LF}}$ values as observed for the Background site suggests that these filters contained smaller-grained SD or PSD particles compared to the industrial and traffic sites (Hofman et al., 2017), as it would be expected when comparing $\text{PM}_{2.5}$ against PM_{10} filters. The plot of $\text{ARM}\chi$ ($389 - 4,040 \times 10^{-8} \text{ m}^3 \text{ kg}^{-1}$) against χ_{LF} ($-1,670 - 6,770 \times 10^{-8} \text{ m}^3 \text{ kg}^{-1}$), also named the King plot (King et al., 1982), revealed that the magnetic mineralogy was not size homogenous amongst all measured samples (Figure 5.14). The King plot has been originally derived from experimental data on magnetite and under the assumption of particles being equidimensional, which is not necessarily the case in atmospheric PM (§Chapter 2). Nonetheless, it is considered a good representation to qualitatively evaluate the magnetic grain size of minerals dominated by magnetite, a low-coercivity mineral (Evans and Heller, 2003). High-coercivity minerals, on the other hand, can be considered excluded from our samples, as the S-ratio was close to unity and $\text{HIRM}_{\%}$ not larger than 3% for all monitored sites. For the Background ($\text{PM}_{2.5}$), most magnetic carriers had a size smaller than $0.1 \mu\text{m}$, whilst for the other sites (PM_{10}), the magnetic grain size was broader, varying from $0.2 \mu\text{m}$ up to $5 \mu\text{m}$ mostly, with some grain sizes $< 0.1 \mu\text{m}$ and $> 20 \mu\text{m}$ as well, the latter suggesting the existence of MD

grains (King et al., 1982) (Figure 5.14). A previous study on air suspended particles across several cities in India revealed comparable magnetic grain sizes of 1 to 5 μm across residential, vehicular and industrial sampling sites (Gargiulo et al., 2016). Filter samples collected at two monitoring stations within high traffic congestion areas in Munich, Germany, and with magnetite identified as main magnetic mineral, showed a predominant grain size between 0.2 and 5 μm , with some grains being slightly larger than 10 μm (Muxworthy et al., 2001). The study of Mitchell and Maher (2009) on traffic-derived pollution in Lancaster, UK, in which magnetite and/or partially oxidized magnetite were the dominant magnetic components for both leaf (*Tilia platyphyllos*) and filter (1 μm pore size polytetrafluoroethylene) samples, revealed magnetic grain sizes between 0.1 and 1 μm .

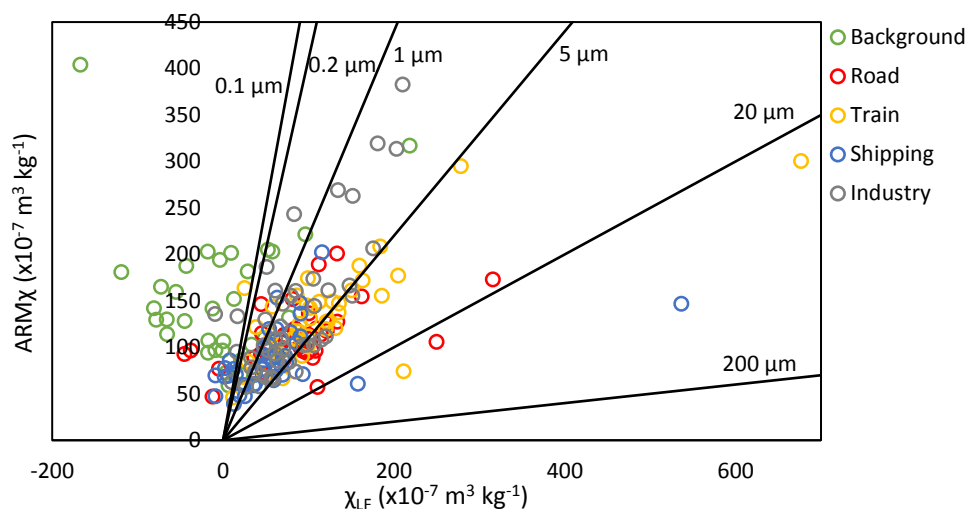


Figure 5.14 – King plot ($ARM\chi$ as a function of χ_{LF}) for PM_{10} -loaded filters at the different monitoring sites ($PM_{2.5}$ for the Background site), with grain size reference lines for equidimensional magnetite derived from Evans and Heller (2003).

The aforementioned magnetic properties have been mass-normalized (§5.1.2.3), which is a commonly used practice to standardize as it allows to compare samples from different contexts. For the case of comparing PM_{10} filters (Road, Train, Shipping, Industry) with $PM_{2.5}$ filters (Background), the normalization by PM mass might complicate things when comparing the various magnetic parameters together. For instance, high saturation remanence measured for heavily loaded filters (i.e., high

mass) might become rather equivalent to low-remanence and low-mass samples after such normalization. This normalization bias was visible when checking for correlations between the mass-normalized magnetic properties, and will be mentioned only to alert for potential thereby derived misinterpretations.

Positive significant correlations were observed between mass-normalized ARM (and $ARM\chi$) and SIRM when focusing either on the PM_{10} -filters (i.e., disregarding the Background site) or on the $PM_{2.5}$ -filters (of Background site only) (Table 5.5), but this was different for susceptibility χ_{LF} . For PM_{10} samples (industrial and traffic monitored sites), χ_{LF} was positively linked with ARM and SIRM, while negatively correlated with the ratio $SIRM/\chi_{LF}$, as might be expected since χ_{LF} is the ratio denominator. The higher the χ_{LF} values, the lower the ratio $SIRM/\chi_{LF}$, according to the correlations. For $PM_{2.5}$ samples (Background site), however, the χ_{LF} was only significantly correlated, and positively, with the ratio $SIRM/\chi_{LF}$, with higher χ_{LF} leading to higher $SIRM/\chi_{LF}$ values. This different behavior might be due to the very low, more than one order of magnitude lower (and often negative) χ_{LF} values for the Background $PM_{2.5}$ samples compared to the other sites (Table 5.4) or to their lower mass loading (Figure 5.7).

Magnetic susceptibility reflects the total concentration of Fe-bearing particles, yet largely influenced by the total concentration in ferrimagnetic minerals (Shu et al., 2000). SIRM measures the total remanence of the mineral assemblage, mostly controlled by stable SD magnetite concentrations. But unlike SIRM, χ_{LF} is also influenced by paramagnetic and diamagnetic minerals such as biologically-derived components, that have negative susceptibility (Thompson and Oldfield, 1986). Different relationships were observed between SIRM and χ_{LF} for the Background site in comparison to the other sites. Good linear relationships ($p < 0.01$) between (mass-normalized) χ_{LF} and SIRM were obtained for all traffic and Industry sites ($R^2 = 0.22 - 0.69$), with the highest linear association at the Train site ($R^2 = 0.69$). According to Zhang et al. (2012), the observed strong correlations ($R^2 = 0.87$) between χ_{LF} and SIRM values for street dust samples in the industrial city of Loudi, China, indicated that ferro(i)magnetic phases were the predominant magnetic minerals. Similar conclusions

were derived from PM_{2.5} quartz-filters in heavily industrialized Nanjing, China, which revealed linear correlations ($R^2 = 0.94$) between χ_{LF} and SIRM (Wang et al., 2017). However, χ_{LF} and SIRM values from our PM_{2.5} Background samples did not correlate linearly ($p = 0.39$, $R^2 = 0.02$), possibly due to the biogenic contribution on site.

Table 5.5 - Spearman's correlation coefficients (ρ) between the mass-normalized magnetic properties measured on the PM-loaded filters (PM₁₀ filters comprise Road, Train, Shipping and Industry sites; PM_{2.5} filters comprise the Background site). Only statistically significant coefficients are shown ($p < 0.05$; $p < 0.01$ in bold). ARM_{200/500} and ARM χ are equivalent, so only the latter is shown.

Spearman's correlation ρ	$\chi_{LF} \times 10^{-8}$ ($m^3 kg^{-1}$)	ARM $\chi \times 10^{-8}$ ($m^3 kg^{-1}$)	SIRM $\times 10^{-4}$ ($A m^2 kg^{-1}$)	IRM ₋₃₀₀ $\times 10^{-4}$ ($A m^2 kg^{-1}$)	HIRM $\times 10^{-4}$ ($A m^2 kg^{-1}$)	S-ratio (-)	SIRM/ χ_{LF} $\times 10^3$ ($A m^{-1}$)	ARM/SIRM $\times 10^{-3}$ (-)	
χ_{LF} $\times 10^{-8}$ ($m^3 kg^{-1}$)		0.64	0.70	0.70	0.36	0.25	-0.49	-0.46	PM ₁₀
ARM χ $\times 10^{-8}$ ($m^3 kg^{-1}$)			0.96	0.95	0.65			-0.28	
SIRM $\times 10^{-4}$ ($A m^2 kg^{-1}$)		0.94		0.99	0.63			-0.52	
IRM ₋₃₀₀ $\times 10^{-4}$ ($A m^2 kg^{-1}$)		0.94	1.00		0.59	0.18		-0.51	
HIRM $\times 10^{-4}$ ($A m^2 kg^{-1}$)		0.43	0.44	0.43		-0.62		-0.24	
S-ratio (-)		0.47	0.49	0.49	-0.42			-0.25	
SIRM/ χ_{LF} $\times 10^3$ ($A m^{-1}$)	0.55								
ARM/SIRM $\times 10^{-3}$ (-)		-0.41	-0.62	-0.62		-0.34			
	PM_{2.5}								

Comparatively to the other sites, the Background site, a forested area, is assumed to be more exposed to biogenic-derived compounds from the surrounding trees, such as biogenic volatile organic compounds (BVOCs), that contribute to the formation of secondary aerosols (Calfapietra et al., 2009), which can represent 20% to 80% of PM_{2.5} (Cai et al., 2017). Fungal unicellular spores and fragments can also fit within the PM_{2.5} particle size distribution (Yamamoto et al., 2012). We may hypothesize that the smaller-sized PM at this site exhibited lower χ_{LF} , corroborated by low concentrations in Fe (Table 5.2), due to biogenic-related compounds, yet with magnetic remanence

comparable to the Shipping site. But without having sampled PM_{2.5} at the other monitored sites, and PM₁₀ at the Background site, it is difficult to further elaborate on these site comparisons.

Although the abovementioned hypothetical reasoning might still be considered, given the expected biogenic component at the Background rather than at the polluted sites, this would most probably equally affect the susceptibility and SIRM values. By not considering the mass-normalization for these magnetic parameters, and looking at their raw, induced magnetization, comparable associations between χ_{LF} and SIRM were actually found for both PM₁₀ and PM_{2.5} filters, from both the polluted and Background samples (Table A.2). The correlation coefficients found between (not mass-normalized) χ_{LF} and SIRM were $\rho = 0.80$ ($p < 0.01$) and $\rho = 0.42$ ($p < 0.05$), respectively, for PM₁₀ and PM_{2.5} samples. Still, this positive relationship between χ_{LF} and SIRM for the PM_{2.5} Background samples did not result in a significant linear association ($p = 0.09$, $R^2 = 0.09$) (Figure 5.15), which were evident for the other, polluted monitored sites ($p < 0.0001$, $R^2 = 0.34 - 0.77$). For eventual comparison with other studies, the non-normalized magnetic properties as measured in this study are shown in Table A.3.

To analyze the correlations between magnetic properties did not reveal additional source-specific information on the monitored source types, but enlightened the fact that PM_{2.5} and PM₁₀ filter samples may deliver different magnetic information. The mass-normalization bias as herein discussed serves mainly to alert other researchers for the cases in which normalization may complicate the interpretation of results, such as when comparing different types of samples (PM_{2.5} vs. PM₁₀ filters). For those cases, the normalization of measured magnetic variables should be done with caution, being advisable to compare its outcomes with the results suggested by the non mass-normalized variables. Finally, the discussion of magnetic properties in scientific studies should always clearly indicate whether the variables have been mass-normalized or are considered without mass-normalization, particularly when using them in combination with other variables. To prevent this normalization bias when establishing correlations between magnetic properties and e.g. chemical composition, one could

eventually work with magnetic vs. chemical enrichment factors, as long as comparable conditions are met between the background and test sites.

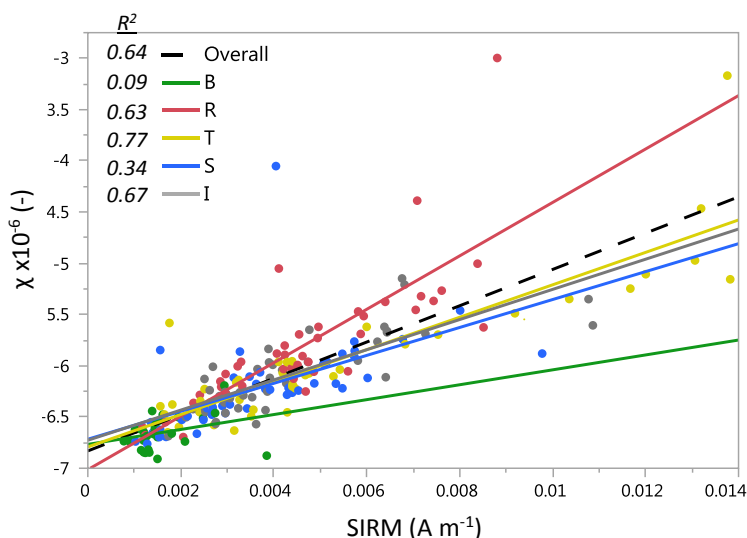


Figure 5.15 – Scatterplot of χ_{LF} and SIRM values (not normalized) of the PM-loaded filters from the different monitoring sites (B – Background, R – Road, T – Train, S – Shipping, I – Industry, Overall – all samples, with $n = 207$), with linear fit models (R^2 are indicated).

5.1.3.5 Source fingerprinting: gravimetric, elemental and magnetic PM

Atmospheric PM levels are influenced by transnational, national and regional contributions, with local polluting sources usually peaking from the urban background conditions (Keuken et al., 2013). In the present study, both gravimetric (§5.1.3.1) and elemental (§5.1.3.2) concentrations of atmospheric PM have revealed differences and similarities amongst the studied monitoring sites, representative of different source types yet submitted to a common background influence. Although atmospheric PM_{10} concentrations were highest for the Shipping site, the elemental PM_{10} concentrations at that site were often comparable or comparatively lower than for Road and Train sites, while the greatest metal contributions were observed at the Industry (Figure 5.16). Moreover, chemical analysis (such as HR-ICP-MS) is related with the mass contribution of the PM sources, while magnetic measurements are sensitive to their compositional contribution in terms of magnetic minerals. In order to associate

physicochemical source characteristics with magnetic fingerprints, multivariate data analysis was used on the gravimetric, elemental and magnetic input obtained from the PM-loaded filters.

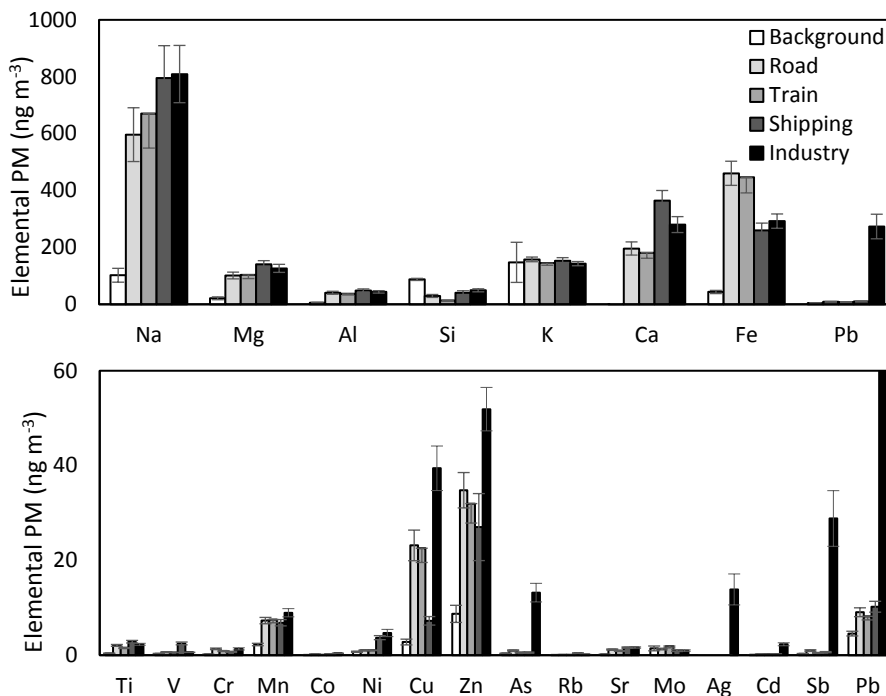


Figure 5.16 – Elemental concentrations (ng m^{-3}) determined from the PM_{10} -loaded filters (HR-ICP-MS) across the different monitoring sites ($\text{PM}_{2.5}$ for Background), for both major (top) and minor elements (bottom). Pb is shown in both graphs for comparison. Bars represent the elemental concentration means, and error bars the standard errors around the means.

Some PM_{10} elements (HR-ICP-MS) had significantly higher concentrations than others depending on the monitoring site, and this consistently over the monitored period, as previously shown in Table 5.2. The association between the measured elements and the monitoring sites has been summarized in Table 5.6, with a list of major source types typically denoted from such chemical (elemental) markers according to literature (Moreno et al., 2014; Qadir et al., 2014; Viana et al., 2009; Vercauteren et al., 2011; Watson et al., 2016). When disregarding the Background site (as these samples were $\text{PM}_{2.5}$), the Industry and Shipping had the highest elemental concentrations in a variety of components, from crustal matter contributions (e.g., Si, Ca) to fuel and coal combustion processes (Ni, V, As, Pb). Specifically for maritime

traffic, Viana et al. (2009) have found the ratio V/Ni to be a tracer for shipping emissions when values were between 2.5 and 5. In our study, highest V/Ni values were indeed observed at the Shipping site, but these values were close to the aforementioned range, between 2.3 and 2.6, only for three days; mean V/Ni values were $0.8 (\pm 0.6)$. Elements often identified as traffic-related species, namely, Ti, Cr, Fe, Cu, Zn, Mo, showed significant high concentrations (the highest for some cases) at the Road and Train sites. Mining-related (Rb, Sr, Ag, Sb) and metal processing (Co, Cr) elements were also observed amongst the monitored sites (Table 5.6).

Table 5.6 – Association between chemical elements determined from the PM₁₀-loaded filters and the monitoring sites (R – Road, T – Train, S – Shipping, I – Industry) with significantly highest concentrations, and typical major source types. The source type “road dust” comprises a variety of sources, such as re-suspended road dust, asphalt abrasion, tire and brake wear, and engine corrosion. For elements with similar concentrations across the sites, the “-” is used; whenever relevant, the sites with the second highest concentration levels are also shown in italic (elements Cu and Zn).

	Site	Major source types†
<i>Na</i>	-	Sea salt
<i>Mg</i>	S, I	Crustal material
<i>Al</i>	-	Crustal material; engine exhaust
<i>Si</i>	S, I	Crustal material
<i>K</i>	-	Crustal material
<i>Ca</i>	S, I	Crustal material
<i>Ti</i>	R, S, I	Crustal material; rail friction
<i>V</i>	S	Heavy fuel oil combustion; shipping
<i>Cr</i>	R, T, I	Metal processing; residual fuel combustion; road dust; rail friction
<i>Mn</i>	-	Metal processing; rail friction
<i>Fe</i>	R, T, I	Crustal material; road dust; engine exhaust; rail friction
<i>Co</i>	S, I	Metal processing; rail friction
<i>Ni</i>	S, I	Heavy fuel oil combustion; rail friction; shipping
<i>Cu</i>	<i>R, T, I</i>	Road dust
<i>Zn</i>	<i>R, T, I</i>	Engine exhaust; coal combustion; road dust; rail friction
<i>As</i>	I	Coal combustion
<i>Rb</i>	S	Mining
<i>Sr</i>	S, I	Mining
<i>Mo</i>	R, T	Mining; engine exhaust
<i>Ag</i>	I	Mining
<i>Cd</i>	I	Coal combustion
<i>Sb</i>	I	Mining; road dust
<i>Pb</i>	I	Smelting; fuel and coal combustion

† Major source types compiled from literature: Moreno et al. (2014), Qadir et al. (2014), Viana et al. (2009), Vercauteren et al. (2011), Watson et al. (2016).

For the polluted sites (traffic and industrial), the determined elemental concentrations were for all elements, except Ag and Mg, significantly correlated with the PM₁₀ concentrations (Spearman's, $p < 0.01$; $p < 0.05$ for Si). These correlations were mostly positive (except for Na, $\rho = -0.31$) and highest for elements Mo, Mn, Fe, Ti and Al (Spearman's, $\rho = 0.61 - 0.69$), and Zn, V, Co, Cr, Ca, K ($\rho = 0.47 - 0.59$). The PM concentrations, at all sites, were positively correlated with the magnetic indicators, namely, with χ_{LF} , ARM and SIRM, as long as non-normalized data was considered (Table 5.7). When plotting the atmospheric PM concentrations alongside with the (non-normalized) SIRM throughout the monitored period, some of the highest registered SIRM values corresponded to the highest PM concentrations, particularly at the Train site (Figure 5.17). Across this monitoring campaign, χ_{LF} , ARM and SIRM (both normalized and non-normalized for PM mass), correlated significantly with elements such as Cr, Mn, Fe, Cu, Mo (Table 5.8).

Table 5.7 - Spearman's correlation coefficients (ρ) between the magnetic properties and ratios (both mass-normalized and not mass-normalized, the latter indicated in grey) and the PM concentrations (PM₁₀ filters comprise Road, Train, Shipping and Industry sites; PM_{2.5} filters the Background site; overall comprises all sites together). Only statistically significant coefficients are shown ($p < 0.05$; $p < 0.01$ in bold). For SIRM/ χ_{LF} , normalized and not normalized (yet with same units) are included; for S-ratio and ARM/SIRM, mass-normalized and not normalized values are equivalent.

Spearman's correlation ρ	PM ₁₀	PM _{2.5}	Overall
χ_{LF} (-)	0.52		0.64
$\chi_{LF} \times 10^{-8}$ (m ³ kg ⁻¹)			0.26
ARM (A m ⁻¹)	0.58	0.61	0.68
ARM χ $\times 10^{-8}$ (m ³ kg ⁻¹)	-0.40	-0.86	-0.49
SIRM (A m ⁻¹)	0.57	0.44	0.67
SIRM $\times 10^{-4}$ (A m ² kg ⁻¹)	-0.27	-0.88	-0.25
HIRM $\times 10^{-4}$ (A m ² kg ⁻¹)	-0.18	-0.37	-0.18
S-ratio (-)		-0.46	
SIRM/ χ_{LF} (A m ⁻¹)	-0.57	-0.44	-0.67
SIRM/ $\chi_{LF} \times 10^3$ (A m ⁻¹)			
ARM/SIRM $\times 10^{-3}$ (-)	-0.30		-0.45

Table 5.8 – Spearman’s correlation coefficients (ρ) between PM and elements (ng m^{-3}) and magnetic properties (both mass-normalized and not mass-normalized (in grey) of PM_{10} -loaded filters (Road, Train, Shipping, Industry sites). Only statistically significant coefficients are shown ($p < 0.05$; $p < 0.01$ in bold). For $\text{SIRM}/\chi_{\text{LF}}$, normalized and not normalized (yet with same units) are included; for S-ratio and ARM/SIRM , mass-normalized and not normalized values are equivalent.

Spearman’s correlation ρ	χ_{LF} (-)	χ_{LF} ($\text{m}^3 \text{kg}^{-1}$)	ARM (A m^{-1})	ARM χ ($\text{m}^3 \text{kg}^{-1}$)	SIRM (A m^{-1})	SIRM ($\text{A m}^2 \text{kg}^{-1}$)	IRM ₃₀₀ ($\text{A m}^2 \text{kg}^{-1}$)	HIRM ($\text{A m}^2 \text{kg}^{-1}$)	S-ratio (-)	SIRM/ χ_{LF} (A m^{-1})	SIRM/ χ_{LF} (A m^{-1})	ARM/SIRM M (-)
Na	-0.35	-0.25	-0.45	-0.21	-0.47	-0.28	-0.30		-0.28	0.47		0.35
Mg	-0.18	-0.16	-0.28	-0.22	-0.30	-0.28	-0.30		-0.26	0.29		0.27
Al	0.62	0.35	0.69		0.65					-0.65	-0.23	-0.24
Si				-0.17		-0.22	-0.20	-0.17				0.23
K	0.39		0.44		0.46					-0.46		-0.36
Ca	0.48	0.23	0.51		0.48					-0.48	-0.19	-0.17
Ti	0.61	0.29	0.65		0.64					-0.64	-0.18	-0.32
V	0.20		0.31	-0.20	0.30					-0.30		-0.16
Cr	0.76	0.50	0.75	0.21	0.75	0.31	0.32		0.30	-0.76	-0.29	-0.48
Mn	0.74	0.47	0.83	0.23	0.81	0.30	0.30	0.27		0.80	-0.25	-0.38
Fe	0.84	0.57	0.89	0.30	0.92	0.44	0.45	0.22	0.23	-0.92	-0.24	-0.66
Co	0.31		0.46		0.42					-0.41		
Ni	0.18		0.26		0.20					-0.20		
Cu	0.55	0.38	0.55	0.24	0.55	0.31	0.32		0.38	-0.56	-0.24	-0.38
Zn		0.34	0.54		0.52	0.16			0.24	-0.52	-0.32	-0.23
As	0.29		0.38		0.33		0.16		0.20	-0.33		
Rb			0.22		0.25		0.16	0.23	-0.25	-0.23	0.21	-0.23
Sr				-0.22		-0.19	-0.20					
Mo	0.63	0.39	0.77	0.21	0.78	0.33	0.33	0.18	0.16	-0.77		-0.52
Ag									0.16			0.28
Cd	0.29		0.42		0.37					-0.37		
Sb	0.31	0.16	0.38		0.36	0.15	0.15		0.24	-0.35		
Pb	0.24		0.40		0.33					-0.32		

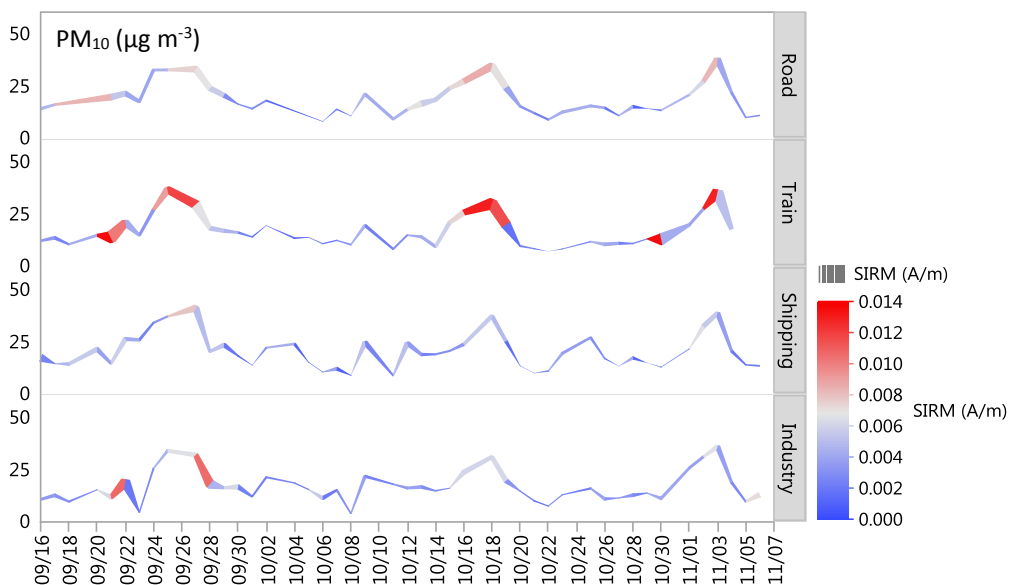


Figure 5.17 – PM concentrations and SIRM (non-normalized; in $A m^{-1}$) measured at the various monitoring sites, with SIRM values depicted in terms of thickness and color gradient (thicker and red segments represent higher values).

A PCA was carried out on all measured variables: PM₁₀ concentrations, elemental concentrations (Na, Mg, Al, Si, K, Ca, Ti, V, Cr, Mn, Fe, Co, Ni, Cu, Zn, As, Rb, Sr, Mo, Ag, Cd, Sb, Pb), and magnetic properties and ratios (non-normalized χ_{LF} , ARM, SIRM, and SIRM/ χ ; and ARM/ χ , S-ratio, HIRM and ARM/SIRM), using the monitoring sites (Road, Train, Shipping, Industry) as supplementary variables. The non-normalized magnetic variables were used as they in general showed better correlations with the analyzed metals than the mass-normalized variables, and magnetic properties are intended to be used as a proxy for the elemental PM composition rather than for its mass concentration (Table 5.8). The resulting PCA (Figure 5.18) on the refined 30 variables yielded the two main discriminant components (PC1 and PC2) accounting for 49.3% of the total variance for the 174 daily PM₁₀-loaded filters.

PC1 clearly separates between samples that are either high in the interrelated variables PM, Fe, Mo, K, Al, Ca, Cr, Ti, Mn, χ_{LF} , ARM and SIRM, or high in SIRM/ χ . This seems to only slightly differentiate between PM₁₀-loaded filters from the Train site and those from the other sites. The ratio SIRM/ χ (and ARM/SIRM, yet less) is displayed in opposite direction to the magnetic concentration-dependence properties (χ_{LF} , ARM

and SIRM) (and elements Fe and Mo), corroborating the previous negative correlations found between those two types of magnetic indicators (Table A.3). PC2 relates with Sb, Pb, As, Cd, Ni and Ag, and discriminates the Industry samples, high in concentration of these metals, from the other sites, low in these variables. The first quadrant of the PCA biplot (positive PC1 and PC2) contains most considered elements: the group of metals As, Cd, Sb, Pb, Ag and Ni, greatly associated with the Industry source (Table 5.6); a group with Sr, Co, Cu; the element Zn standing rather alone; and the interrelated Ca and Ti. The second quadrant (negative PC1 and positive PC2) includes the ratios SIRM/ χ and ARM/SIRM and elements Na and Mg, the latter associated with sea salt and crustal dust, respectively. No variables scored in the third quadrant (negative PC1 and PC2), although most samples, and from various sites, were projected there. The fourth quadrant (positive PC1 and negative PC2) includes Fe and Mo, and χ_{LF} , ARM and SIRM.

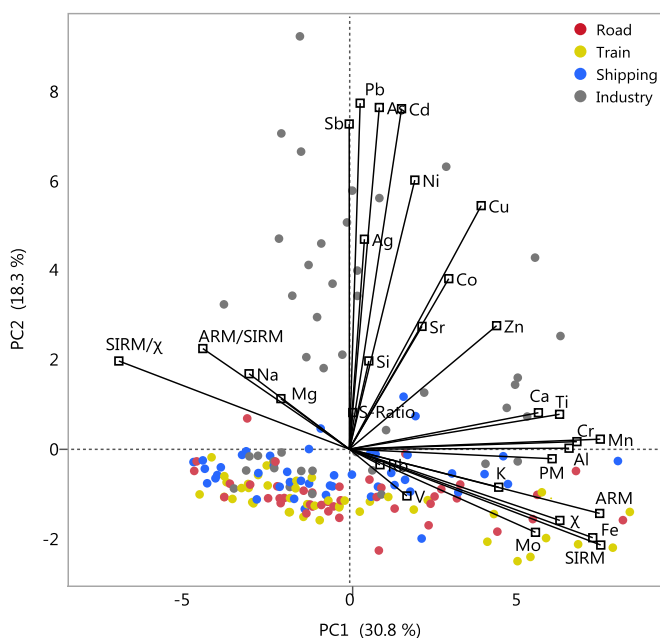


Figure 5.18 – Biplot of PCA (PC1 and PC2) on the gravimetric (PM_{10} concentrations), elemental (Na, Mg, Al, Si, K, Ca, Ti, V, Cr, Mn, Fe, Co, Ni, Cu, Zn, As, Rb, Sr, Mo, Ag, Cd, Sb, Pb) and magnetic measured variables (χ_{LF} , ARM, SIRM, SIRM/ χ , ARM/SIRM; not mass-normalized) for the monitored sites (circles) Road (red), Train (yellow), Shipping (blue), Industry (grey). The two first principal components (PC1 and PC2) account for 49.3% of the total variance.

The projection of the measured PM₁₀-filters in the PC1-PC2 plane mostly showed a separation between Industry and the other monitored sites (Figure 5.18), driven by the high metal enrichment observed at the former. The third principal component (PC3; explaining 10% of the variance) was plotted against PC1 and PC2 (Figure 5.19) in an attempt to further discriminate between the traffic sites (Road, Train and Shipping). PC3 is able to differentiate between Shipping on one hand, and Train and Road on the other hand, mainly related to Na, Mg, Rb, V and Sr. Na and Mg are sea salt indicators, thus, rather denoting the proximity to salty water at the Shipping site than the contribution of shipping sources. On the other hand, Rb and Sr, associated with mining activities, and V, often a tracer for shipping and heavy fuel oil combustion (Table 5.6), appear to point towards the Shipping site in the conducted study. Whether this V contribution was derived from shipping activities or from the chemical plants in the harbor, or both, remains unclear. Correlations between the considered variables and the three main discriminant components (PC1, PC2 and PC3; explaining 59.1% of the variance), confirmed PC1 to be most linked to anthropogenic elements (namely, Cr, Mn, Fe, Co, Cu, Zn, As, Mo, Cd, Sb, Pb) and co-emitted magnetic particles (χ_{LF} , ARM, SIRM) (Table A.4). PC2 exhibited associations with natural PM (Si, Na, Mg), but also with Ni and Ag, while the strongest connections with PC3 were observed for Na, Mg, V and Sr.

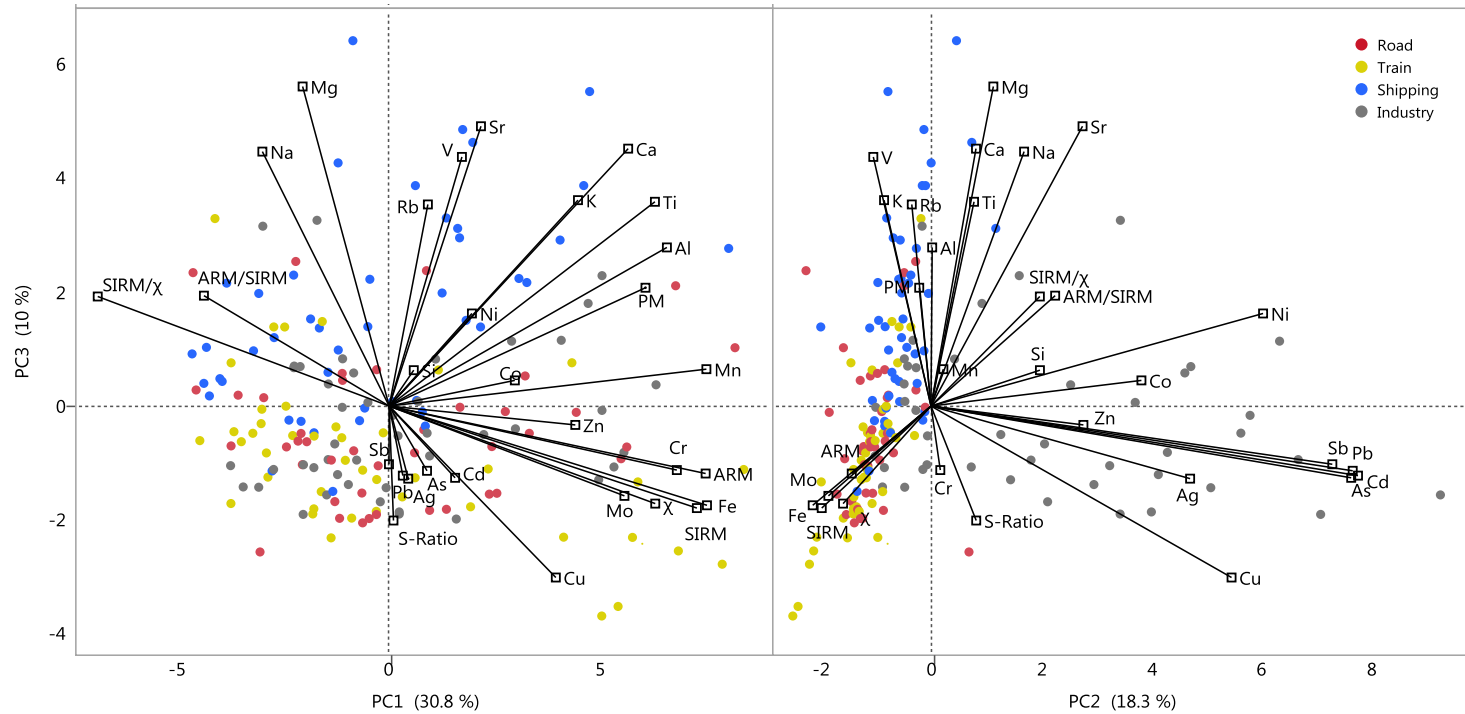


Figure 5.19 - Biplot of PCA (PC1 and PC2 plotted against PC3) on the gravimetric (PM_{10} concentrations), elemental (Na, Mg, Al, Si, K, Ca, Ti, V, Cr, Mn, Fe, Co, Ni, Cu, Zn, As, Rb, Sr, Mo, Ag, Cd, Sb, Pb) and magnetic measured variables (χ_{LF} , ARM, SIRM, SIRM/ χ , ARM/SIRM; not mass-normalized) for the monitored sites (circles) Road (red), Train (yellow), Shipping (blue), Industry (grey). The three first principal components (PC1, PC2 and PC3) account for 59.3% of the total variance.

The “PM” RF (Random Forest), considering only the atmospheric PM concentrations as input variable, yielded a generalized R^2 of 0.53 and a misclassification rate (MR) of 0.38, with RMSE and mean absolute deviation (MAD) of 0.64 and 0.62, respectively (Table 5.9). The atmospheric PM concentrations were reasonable at predicting the Train, Shipping and Industry sites (classification accuracy, CA, between 63% and 76%), but performed rather bad for correctly classifying the Road site (CA < 25%) (Table A.5). Furthermore, the agreement found between actual and predicted sites appeared to be chance related, as Kappa = 0.31 indicates a fair agreement only (McHugh, 2012). The “Elem” RF (based on the elemental concentrations) showed better predictive power than the “PM” RF, with a generalized R^2 of 0.87 and a MR of 0.04 (RMSE and MAD of 0.42 and 0.39). The CA was $\geq 90\%$ for all monitored sites, for which the predicted sites substantially agreed with the actual sites (Kappa = 0.78). From the 23 predictor variables considered in the “Elem” RF, the elements Pb, Ni, As, V, Ag, Sb and Cu, accounted for most splits (59%) in the RF decision trees, so they were the main classification contributors. Highest concentrations in these elements were observed for the Industry (Pb, As, Ag, Sb and Cu) and Shipping (Ni and V) sites (Table 5.6). These sites were also the most easily to discriminate from the PCA (Figure 5.18, Figure 5.19). The “Magn” RF (based on the χ_{LF} , ARM, HIRM, SIRM, S-ratio, SIRM/ χ , ARM/SIRM; mass-normalized, as normalization would be required in large-scale magnetic monitoring campaigns) was intermediate between the “PM” and “Elem” RFs for classifying the monitoring sites ($R^2 = 0.55$, MR = 0.32), with a CA $\geq 40\%$ for all sites and a moderate agreement (Kappa = 0.42) between the actual and predicted sites (McHugh, 2012). The variables ARM/SIRM, ARM and SIRM were, amongst the seven magnetic predictors, the most prediction contributors. A RF model using the non-normalized magnetic properties as predictor variables (not shown) had a predictive power slightly inferior ($R^2 = 0.48$, MR = 0.30) than that of the “Magn” RF, but the main prediction contributors were still ARM/SIRM, ARM and SIRM.

The inclusion of elemental concentrations (“PM & Elem”) or of magnetic properties (“PM & Magn”) in addition to the gravimetric monitoring of PM improved the site classification in comparison to using each approach separately (Table 5.9), with a CA

between 88% and 100% for “PM & Elem” and between 65% and 88% for “PM & Magn” (Table A.5). Within the predictor variables, the atmospheric concentrations of PM (gravimetric) were amongst the least contributors for building the RF decision trees. In fact, the combination of elemental and magnetic information (“Elem & Magn”), performed the best in correctly classifying the studied monitoring sites, with a R^2 of 0.89 and a MR of 0.03 (the lowest observed), a CA \geq 90% and an almost perfect agreement between actual and predicted sites (Kappa = 0.82) (McHugh, 2012). To include the gravimetric PM concentrations (“PM & Elem & Magn”) did not improve nor worsen those model predictions. Having all the aforementioned variables (i.e., entire dataset of 31 variables; “PM & Elem & Magn”) yielded a CA of the monitored sites between 92% and 100%. The magnetic properties were only accountable for 16% of the splits in the RF decision trees, whilst the elemental concentrations remained the main classification predictors, responsible for 83% of the RF splits. The PM concentrations contributed only 1% to the site classification, suggesting once more that conventional gravimetric-based PM monitoring (e.g., Leckel samplers) has little power to discriminate between sampling locations that are mainly exposed to different PM emissions. This discrimination can better be achieved by complementing the traditional air quality monitoring systems with elemental and magnetic information, from which magnetic analyses are more cost-effective than chemical determination.

Based on the results obtained during this campaign, the elemental characterization delivered the most useful information in order to identify and separate between the monitoring sites. This was partly due to the rich metal content observed at the Industry and Shipping sites (Table 5.6). As the Shipping site was located within the chemical and industrial complex that constitutes the harbor of Antwerp, metal contributions from the nearby operating industrial processes were expected. Nonetheless, the element V, a typical shipping tracer due to the low volatility residual oil (high in S, V and Ni) used as diesel in marine engines (Viana et al., 2009), was depicted from the Shipping site, suggesting the selected location as appropriate to further investigate the PM fingerprint of Shipping sources. To monitor additional locations within the harbor of

Antwerp, eventually nearby specific industrial plants, could bring further information on the maritime shipping emissions vs. the industrial contributions in the area. In a last stage of the PMF project, specific direct-sources (i.e., dust samples) including the exhaust pipe of a boat and e.g. several road traffic components (brake disks, tires, exhaust tubes, road dust), were sampled and submitted to magnetic characterization (data not analyzed nor shown), in an attempt to link such specific sources to the atmospheric PM. This type of sampling revealed to be more difficult to perform and standardize when compared to filter or leaf samples, although it may provide important insights on the magnetic source signatures.

Table 5.9 – Output of Random Forests predictions to classify the PM₁₀-loaded filters, based on the atmospheric PM₁₀ concentrations (“PM”), elemental concentrations (“Elem”), magnetic properties (“Magn”) and all possible combinations (i.e., “PM & Elem”, “PM & Magn”, “Elem & Magn”, “PM & Elem & Magn”): generalized R², misclassification rate (MR), root mean square error (RMSE) and mean absolute deviation (MAD). The Kappa index of agreement is also shown. All parameters vary between 0 and 1, with best agreements having high R² and low MR, RMSE and MAD; Kappa close to 1 indicates perfect agreement between actual and predicted sites, and close to 0 indicates random agreement.

RF	R ²	MR	RMSE	MAD	Kappa
PM	0.53	0.38	0.64	0.62	0.31
Elem	0.87	0.04	0.42	0.39	0.78
Magn	0.55	0.32	0.63	0.62	0.42
PM & Elem	0.89	0.05	0.40	0.36	0.78
PM & Magn	0.70	0.20	0.56	0.55	0.54
Elem & Magn	0.89	0.03	0.40	0.36	0.82
PM & Elem & Magn	0.88	0.03	0.40	0.37	0.81

The disentanglement of the four polluted monitored sites (Road, Train, Shipping, Industry) based on the magnetic characterization of their collected air-pumped PM₁₀ filters (Leckel samplers) revealed to be rather complicated. According to the magnetic properties and ratios measured during this monitoring campaign, magnetic mineralogy was dominated by low-coercivity SD/PSD magnetic minerals with grain sizes ca. between 0.1 and 5 µm, at all studied sites. Similar findings have been reported in other

studies investigating the magnetic properties of atmospheric PM (e.g., Gargiulo et al., 2016; Revuelta et al., 2014; Shi et al., 2014; Wang et al., 2017).

From the variety of room-temperature magnetic measurements used in this study, susceptibility (χ_{LF}) and saturation remanence (SIRM) are the most investigated ones (Hofman et al., 2017). In case the samples are not very strong magnetically, χ_{LF} is highly susceptible to be influenced by the diamagnetic or paramagnetic behavior of the sample matrix (such as quartz filters or plant material); therefore, SIRM is often considered as a more sensitive and reliable parameter, than χ_{LF} , to assess the magnetic content of atmospheric samples (Muxworthy et al., 2001, 2003), which is confirmed in this study. Sagnotti et al. (2006) obtained strong associations between χ_{LF} and atmospheric PM₁₀ concentrations measured at six automatic stations in Latium, Italy, during one year, after a sample selection by considering only the values within $\pm 20\%$ of the arithmetic mean χ_{LF} . This corresponded to discard between 45 and 67% of the sampled days, during which less typical meteorological conditions (yet not described) were observed. While meteorological and temporal (e.g. seasonal heating pollution) variations affect PM concentrations and composition, such dynamics, although highly complex to standardize, also influence the personal exposure of citizens to atmospheric PM. Correlations between SIRM and PM concentrations have been reported more often (e.g., Revuelta et al., 2014; Wang et al., 2017) than those between χ_{LF} and PM. From the samples measured in the present study, overall positive associations were found between the magnetic moment of SIRM and PM concentrations, mainly for PM₁₀ (Table 5.7). Linear associations between SIRM and PM₁₀ followed this order: Road ($R^2 = 0.52$) > Train ($R^2 = 0.36$) > Shipping ($R^2 = 0.34$) > Industry ($R^2 = 0.13$) (Figure 5.20). The comparison between measured SIRM and the Fe concentrations delivered better associations than to consider the full PM-mass concentrations, as Fe-rich particles in PM are the main remanence carriers. For this association, the order was: Train ($R^2 = 0.94$) > Road ($R^2 = 0.90$) > Industry ($R^2 = 0.72$) > Shipping ($R^2 = 0.67$). For the PM_{2.5} Background samples, no linear behavior was observed between SIRM and PM nor between SIRM and Fe content ($R^2 < 0.06$). The fact that the monitoring sites relate differently (notice the different linear regression

slopes between sites; Figure 5.20) for the links SIRM-PM and SIRM-Fe, comes as a consequence of the different elemental composition at the sites. Moreover, although SIRM can be used as a general proxy for atmospheric PM₁₀ levels, the results from the conducted campaign indicate that SIRM is greatly connected with traffic and industry sources, particularly for railway and road traffic conditions. The Fe content determined by HR-ICP-MS consists of elemental Fe only, not allowing to discriminate between potential different oxidation states across the monitoring sites. Low- and high-temperature magnetic measurements and Mössbauer spectroscopy (Muxworthy et al., 2002; Petrovský et al., 2013), for instance, could possibly elucidate the contribution of different oxidation states and refine the magnetic PM fingerprints for the tested sources. Muxworthy et al. (2002) disserted about two magnetic phases on collected urban PM samples at Munich, Germany, a metallic iron phase and maghemite (γ -Fe₂O₃). In case the two phases did not have separate origins, a “two-shell” particle model was suggested by Muxworthy et al. (2002) for magnetic PM, consisting of a metallic iron core and a thin surface iron oxide layer (in their study, maghemite). The iron oxide layer could be comprised by maghemite, hematite or magnetite, since these have been described before as surface iron oxidation products (Banerjee et al., 2000; Zhao et al., 1996). On additional road surface dust samples in two parallel streets with and without trams, Muxworthy et al. (2002) observed metallic iron to be derived from the railway tram activity. Although several studies focused on magnetic properties of atmospheric PM indicated magnetite or magnetite/hematite as dominant magnetic minerals instead of maghemite (e.g., Hansard et al., 2012; Muxworthy et al., 2003; Revuelta et al., 2014; Shi et al., 2014; Wang et al., 2017), the core and shell structure proposed by Muxworthy et al. (2002) has been suggested by the research of Sagnotti et al. (2009) and Revuelta et al. (2014). Further research on this topic could include the application of thermomagnetic curves and Mössbauer spectroscopy on the PM-loaded filters and related direct-sources (Sagnotti et al., 2009) in an attempt to understand the magnetic particle structures and mineral contributions across the studied PM sources (road, train and shipping traffic, and industry associated with the release of health-threatening metals). Abrasion at railway tracks and car disk brakes, and releases

in diesel and gasoline exhaust pipes, typically have distinguishable magnetic features (Kim et al., 2007; Moreno et al., 2014; Sagnotti et al., 2009) that get mingled together in the atmosphere. Having in mind the high oxidative stress potential of metallic iron and related iron oxides (Moretti et al., 2019; Valavanidis et al., 2005, 2008), gaining insight on the magnetic fingerprints of PM sources may allow to explore the health-relevance of air magnetic monitoring as well.

5.1.4 Conclusions

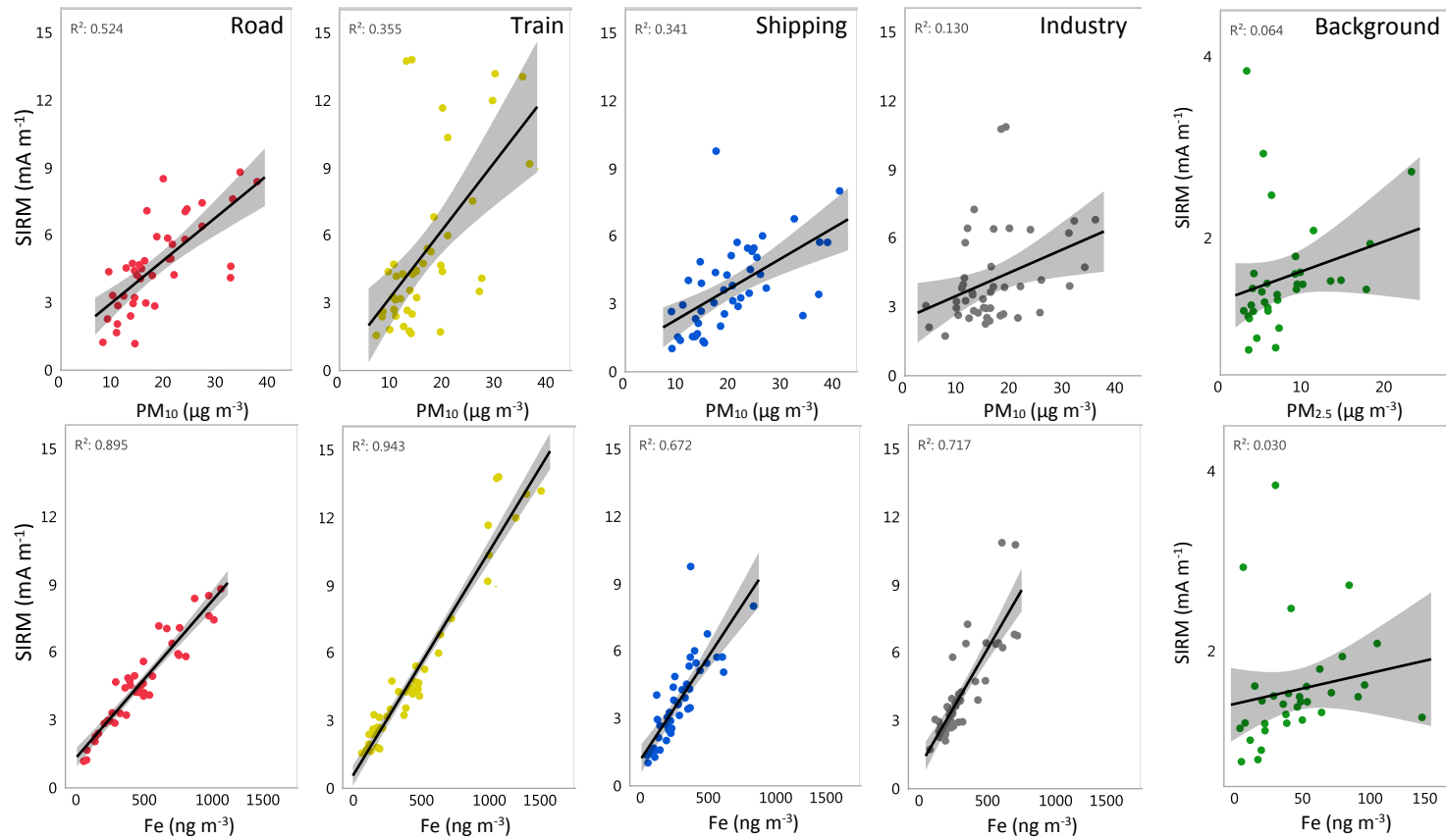
This chapter described the setup of the PMF monitoring campaign conducted simultaneously at five monitoring sites (Road, Train, Shipping, Industry, Background) during 7.5 weeks. The gravimetric, chemical and magnetic results of atmospheric PM filters have been presented and discussed in an attempt to define source-specific chemical and magnetic profiles. Daily atmospheric PM₁₀ concentrations, as measured by conventional air quality monitoring networks, were always below the European reference value (50 µg m⁻³), with mean values decreasing in the order Shipping > Road > Industry > Train. At these sites, the main governing elements were Na Fe, Ca, K, and Mg, with the Industry site presenting the highest and most diversified metal profile, comprising e.g. Pb, As, Ag, Sb, Mn. The elemental profiles of Road and Train sites were similar, while Industry was strongly associated with high metal concentrations. The Shipping elemental profile could be considered as in between those two source types. Temporal variations were significantly consistent across the sites, leading to the conclusion that site or source comparisons should be done simultaneously and over a period of time, to prevent source-specificities to be overlooked by seasonal/temporal effects.

The magnetic discrimination between the different monitoring sites, representative of specific PM sources, was not straightforward. According to our measured magnetic properties and calculated ratios, magnetic PM₁₀ was overall dominated by low-coercivity minerals of magnetite-type, with grain sizes varying between 0.2 and 5 µm. Magnetic remanence (SIRM; Train ≥ Industry ≥ Road > Shipping) showed to be highly

associated with the concentration in Fe rather than with the PM concentrations, particularly for Train and Road sites.

The combination of gravimetric, elemental and magnetic observations in a PCA yielded possible recognition of Industry and Shipping sites, whereas Road and Train were too much alike. Even though the inclusion of magnetic information did not greatly improve, or not as much as the elemental concentrations, the predictive power of built RF models for site classification, the collection of magnetic data is generally more rapid and cost-effective compared to the chemical-based analyses. Additional magnetic analyses, such as hysteresis loops and thermomagnetic curves, or others (e.g. Mössbauer spectroscopy) may provide useful, complementary, information for the source-specific magnetic signatures, which was not fully accomplished here. Further research on specific direct-sources (e.g., railway tram, car brakes and tires, car and boat exhaust pipes) should also be carried out to disentangle their magnetic and elemental fingerprints. The panoply of urban PM sources intermingled in the atmosphere complicates their discrimination. Nonetheless, multi-approach monitoring campaigns, such as this PMF project, contribute to the library of knowledge on the characteristics of important PM sources.

Figure 5.20 - Scatterplot of SIRM (mA m^{-1} ; not mass-normalized) as function of PM ($\mu\text{g m}^{-3}$) and Fe (ng m^{-3}) concentrations for the monitoring sites (PM_{10} for Road, Train, Shipping, Industry; $\text{PM}_{2.5}$ for Background). Black lines indicate the linear regressions (R^2 are shown) with 95% of confidence (in grey).



Chapter 5.2

Health-relevance of source-specific PM:
pro-inflammatory response across major PM
sources

CHAPTER 5.2

Based on: Castanheiro, A., Hofman, J., Moretti, S., Joosen, S., VMM, Lebeer, S., Blust, R., Lenaerts, S., De Wael, K., Samson, R., 2020. Health-relevance of particulate matter fingerprinting – pro-inflammatory response across atmospheric PM sources. (under preparation)

Abstract

The health-relevance of source-specific PM was investigated in the context of the PMF project, by exposing human monocyte-macrophage cells to air collected samples and measuring their pro-inflammatory and oxidative stress potential. Although this exploratory study consisted on a rather reduced number of samples, obtained during the weekly point time measurements, the results suggest the Train and Shipping sites as having the highest health-risk potential. Associations of pro-inflammatory response were also evaluated against the metal concentrations measured on the air samples, which were all collected using a Coriolis impinger.

5.2.1 Introduction

The impact of PM on human health mainly depends on the particle size and chemical composition, with adverse health effects ranging from asthma and cardiovascular diseases to lung cancer (Anderson et al., 2012; Breysse et al., 2013; Kampa and Castanas, 2008; Martinelli et al., 2013; Pope and Dockery, 2006; Scapellato and Lotti, 2007). According to the body of epidemiological and toxicological research available, PM exposure can lead to several, and eventually synergistic, mechanisms of hostile cellular effects, such as cytotoxicity through oxidative stress mechanisms, oxygen-free radical-generating activity, DNA oxidative damage, mutagenicity, and stimulation of pro-inflammatory factors (Donaldson et al., 2003; Li et al., 2003; Valavanidis et al., 2008). From those, inflammation and oxidative stress are generally recognized as the main mechanistic precursors of PM-induced health effects (Bernstein et al., 2004; Li et al., 2003; Moretti et al., 2019; Scapellato and Lotti, 2007; Schins et al., 2004; Schwarze et al., 2006). To identify which specific PM components are to blame for triggering such responses is not a simple task, in part due to the complexity of atmospheric PM (in e.g.

physicochemical properties and emission sources), especially in cities. Particle number, size distribution (Vu et al., 2015), traffic- or combustion-related PM (Cassee et al., 2013; Künzli et al., 2000; Laden et al., 2000), associated metals (Moretti et al., 2019; Schins et al., 2004), organic compounds or biological species (Harrison and Yin, 2000; Schwarze et al., 2006) are among the PM components of health-relevance. A number of source types, including motor vehicle emissions, metals industry and biomass combustion, are linked with health effects as well (Bernstein et al., 2004; EPA, 2009). The WHO International Agency for Research on Cancer (IARC) have classified diesel engine exhausts as category 1 carcinogens to humans (category 1 is defined as existing enough evidence in both humans and animals and strong mechanistic data in humans) (IARC, 2012). Notwithstanding the many PM constituents and sources linked with multiple health effects, the evidences gathered are not sufficient to differentiate nor quantify the constituents or sources more closely related to specific health outcomes (EPA, 2009; WHO, 2013).

To understand the toxicological mechanisms behind the detrimental health effects to PM exposure, or to pinpoint the PM constituents underlying them, is out of the scope of this PhD research. Still, PM-related health problems are the driving force to improve air quality monitoring policies and strategies, to which source fingerprinting may be key. Therefore, our designed PMF (PM fingerprinting) project (§Chapter 5.1) included a component of health-relevance assessment. Point time collections at the five PMF monitoring sites were done using an impinger-based sampling strategy, previously established (Moretti et al., 2018, 2019), and the obtained air samples were investigated for their pro-inflammatory potential and metal content. The aim of this research section was to evaluate the health-risk potential at each site, illustrative of specific PM sources, by quantifying the pro-inflammatory response of human macrophage-like cells after exposure to the collected air samples. To explore potential connections between the pro-inflammatory response of certain source types and their elemental/metal/magnetic profiles was another aim of this study, partially disclosed in this chapter.

5.2.2 Materials and methods

An overview of the PMF campaign and monitoring sites can be found in §Chapter 5.1. Given the specificity of the experimental part, which is not core to this PhD research and has been achieved in collaboration (Moretti, S.), not every experimental detail is fully explained, neither are the pro-inflammatory response mechanisms. Aside from that, all sampling and analyses details are provided or referenced to, and the information necessary for a correct interpretation of the obtained results, is provided.

5.2.2.1 Coriolis® air sampling

During the weekly point measurements ($n = 6$), samples were collected during 40 min at a height of ca. 1.6 m (human inhalation height) using the Coriolis® μ air sampler (Bertin Technologies, FR), in which air was drawn in a pyrogen-free, polycarbonate cone containing 15 mL of ultra-pure water. The air drawn in at a flow rate of 300 L min^{-1} (12 m^3 in 40 min) generates a vortex in the cone, and airborne particles deposit in the water by centrifugal force (Moretti et al., 2018, 2019) (Figure 5.21). The Coriolis sampler technology has been certified by the ISO 14698-1 for biological/physical efficiency, with a $d_{50} < 0.5 \mu\text{m}$ (i.e. sampler efficiency $> 50\%$ at a particle diameter $> 0.5 \mu\text{m}$). After collection, samples were transported on ice to the laboratory of Applied Microbiology and Biotechnology of the Bioscience Engineering Department of the University of Antwerp. The volume of every sample was normalized to 15 mL with ultra-pure water to compensate for evaporation losses during sampling. The samples were vortexed (10 s), aliquoted accordingly for the various assays, and stored in glass vials at $-20 \text{ }^\circ\text{C}$ (typically within 12 h after sampling) until analysis.

One glass vial of every collected sample was analyzed for metal concentrations using HR-ICP-MS, following Moretti et al. (2019). The following metals were considered: Al, Cr, Mn, Fe, Co, Ni, Cu, Zn, As, Ag, Cd, Pb. Another glass vial was used for testing the pro-inflammatory response at messenger RNA (mRNA) level of PMA-differentiated human macrophage-like cell line U937 (ATCC® CRL-1593.2™) after 3-hour exposure to the collected samples.

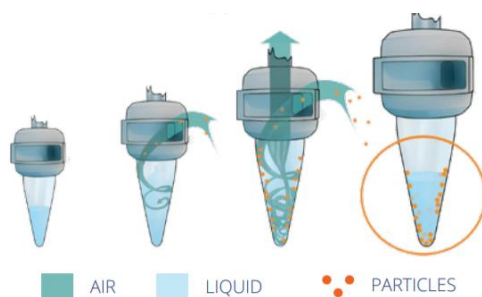


Figure 5.21 - Illustration of the operational principle of Coriolis® μ air sampler (Bertin Technologies, FR).

5.2.2.2 Monitoring of pro-inflammatory response genes at mRNA level

Macrophages and bronchial epithelial cells are the first line of defense for inhaled particles. Once detected, intracellular signaling cascades are activated. For PM, these signaling cascades often lead to the induction of a pro-inflammatory response. These may include the production of chemokines - which recruit more immune cells to the site, and pro-inflammatory cytokines - which drive further inflammation (Moretti, 2018). The human monocyte cell line U937 (kindly donated by Prof. Cos, Laboratory for Microbiology, Parasitology and Hygiene, University of Antwerp, BE) was cultured in Roswell Park Memorial Institute (RPMI) medium (Gibco, Life Technologies, USA) supplemented with 10% heat-inactivated FBS (Hyclone, GE Healthcare, UK), streptomycin ($100 \mu\text{g mL}^{-1}$) and penicillin ($100 \text{ units mL}^{-1}$; Gibco), and maintained at 37°C in a humidified incubator containing 5% CO_2 . Cells were seeded in 12-well plates at a concentration of $5 \times 10^5 \text{ cells mL}^{-1}$ in complete growth medium with phorbol 12-myristate 13-acetate (PMA, 100 ng mL^{-1} ; Sigma Aldrich, USA) to allow for differentiation to an adherent macrophage-like stage for 48 h. Thereafter, the PMA and non-adherent cells were removed by replacing the RPMI medium (without supplements) for a further incubation of 24 h. The medium was removed and cells were co-incubated for 3 h with a 10x RPMI media (Sigma Aldrich, USA) diluted out with the supplements sodium bicarbonate (2 g L^{-1}), folic acid (1 mg L^{-1}), GlutaMAX (2 mM) and sample (at a 1:1 ratio), a positive control (100 ng/well lipopolysaccharide from *E. coli* 0111:B4; Sigma Aldrich) or the negative control (unsupplemented RPMI).

After co-incubation, total RNA was isolated with the RNeasy Mini kit (Qiagen, DE) following the manufacturer's instructions and stored at -80°C . RNA integrity was verified on a 1% (v/v) bleach gel as described by Aranda et al. (2012). One μg of RNA (quantified with Qubit 3.0; Thermo Fisher, USA) was used for complementary DNA (cDNA) synthesis with the ReadyScript[®] cDNA Synthesis Mix (Sigma Aldrich). The expression of three selected pro-inflammatory cytokines (IL-8, IL-1 β and TNF α), a marker for oxidative stress (HO-1) and two reference genes ($M = 0.083$, $CV = 0.029$) were quantified by reverse transcription quantitative PCR (RT-qPCR) on a StepOne Plus Real-Time PCR System (v.2.0; Applied Biosystems, USA). *Guanine nucleotide binding protein beta polypeptide 2-like 1 (GNB2L1)* and *cytochrome c-1 (CYC1)* were selected as the best reference genes, following the GeNorm analysis in Qbase⁺ (Vandesompele et al., 2002). All primers were tested for efficiencies between 90 - 110% and their sequences can be found in Table 5.10.

Table 5.10 - Primer sequences of gene expression from U937 cells.

Gene	Forward primer (5 – 3')	Reverse primer (5 – 3')	nt
<i>IL-8</i>	TGGCAGCCTTCCTGATTCT	TTAGCACTCCTTGGCAAAACTG	61
<i>TNFα</i>	TCTTCTCGAACCCCGAGTGA	CCTCTGATGGCACCCACAG	151
<i>IL-1β</i>	TTGCTCAAGTGCTGAAGCAGC	CAAGTCATCCTCATTGCCACTG	89
<i>GNBL</i>	CACTGTCCAGGATGAGAGCCA	CATACCTTGACCAGCTTGTC	111
<i>CYC1</i>	CATGTCCCAGATAGCCAAGGA	CTTGTGCCGCTTTATGGTGTAG	145
<i>HO-1[†]</i>	GGCTCCCTCTGGGAGTCT	AGCTGCTGACCCATGACAC	115

Primer sequences following Moretti et al. (2019), except for [†], acquired from qPrimerDepot (<http://primerdepot.nci.nih.gov/>).

Every cDNA sample was used in duplicate, each 20 μL reaction consisting of Power SYBR[®] Green PCR Master Mix (Applied Biosystems), 0.3 μM of each primer, 31.25 ng of diluted cDNA, and nuclease-free water. The resulting data were analyzed using the Qbase⁺ software package (Hellemans et al., 2007), calculating relative expression levels of the cytokines and HO-1 as compared to the reference genes. Finally, expression levels of the studied health markers are expressed relative to the negative control, represented by an expression of one (Moretti, 2018).

5.2.2.3 Coriolis vs. Leckel air sampling

The Coriolis air sampling performed almost weekly ($n = 6$) throughout the monitoring campaign consisted of 40 min collection (12 m^3) each time, contrasting with the continuous 24 h sampling (ca. 55 m^3) carried out with the Leckel PM samplers (§Chapter 5.1). Point time measurements occurred during regular working hours on weekdays (on Wednesdays and Thursdays, and once on a Friday), in which the weekdays and periods (morning/afternoon) monitored were shifted between the various monitoring sites along the six point time measurements. Overall, PM_{10} concentrations ranged between 4 and $41 \mu\text{g m}^{-3}$ for Road, Train, Shipping and Industry sites, and $\text{PM}_{2.5}$ concentrations between 3 and $23 \mu\text{g m}^{-3}$ for Background (§Chapter 5.1). The Coriolis point time measurements were conducted on days that together comprised a rather good variation in terms of atmospheric PM concentrations. This way, the selected days appear to nicely represent the diversity of PM levels measured at the five monitored sites (Figure 5.22). In addition to regional and temporal PM variations, PM can change hourly and such fluctuations may strongly affect point time measurements of this nature. A logbook of such point short-time samplings is thus important to register any useful observations that might aid in the analysis of the results *a posteriori*. Nonetheless, the results presented in this Chapter include all obtained data without exclusions based on the logbook observations (not shown), which will be revisited at a later stage of the overall PMF research project.

5.2.2.4 Data analysis

Metal concentrations determined from the Coriolis air samples and the Leckel PM samplers were compared using paired-sample Wilcoxon tests. Associations between metal concentrations and the expression levels of tested health markers in the Coriolis air samples were checked using Spearman's correlations. A principal component analysis (PCA) on these metal concentrations and health markers was carried out in an attempt to discriminate the monitored sites.

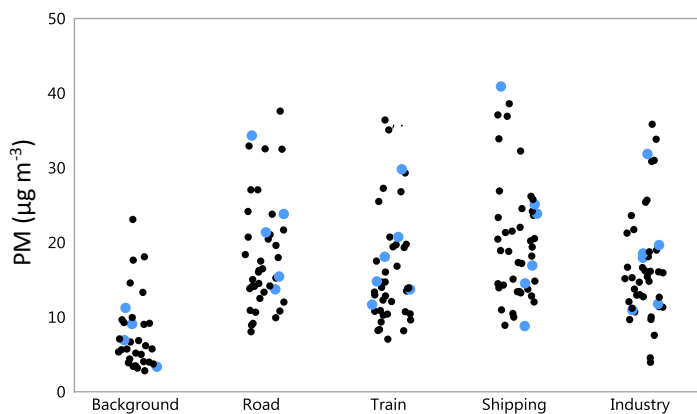


Figure 5.22 - Scatterplot of atmospheric daily PM concentrations measured at the five monitoring sites (PM_{10} for Road, Train, Shipping, Industry; $PM_{2.5}$ for Background) throughout the campaign, with indication of days (in blue) from which Coriolis samples were also obtained (point time measurements).

5.2.3 Results and discussion

5.2.3.1 Coriolis and conventional sampling of PM

In a previous study in the region of Antwerp using the same Coriolis sampling procedure, the obtained metal concentrations were comparable with those measured by the conventional air quality monitoring stations (VMM) (Moretti et al., 2019). The PM concentrations measured with the continuous Leckel samplers in this study are equivalent to the conventional measurements, as similar or comparable instruments are used in air quality stations of the VMM. The site-specific concentrations obtained for the metals of interest (Al, Cr, Mn, Fe, Co, Ni, Cu, Zn, As, Ag, Pb), and other elements, using the Leckel PM samplers are presented in Table 5.2 (§Chapter 5.1). For the days that were also sampled with the Coriolis impinger, metal concentrations obtained with the two approaches (Coriolis and Leckel) can be found in Table 5.11. Differences between the two methodologies include the fact that the Coriolis-sampling was limited in time and done within regular working hours whereas the Leckel-sampling considered the complete daily/nocturnal PM conditions, i.e. averaging higher concentrations during the day together with lower night concentrations (Van den Bossche et al., 2015). The Coriolis-sampling gives more relevance than the Leckel-

sampling to the PM conditions to what city dwellers are exposed to during the day, and it is, therefore, well suited for gaining insight into potential health effects. Moreover, the Coriolis-sampling involves the collection of PM into an aqueous solution and the Leckel-sampling consists of a dry PM collection. The Coriolis-sampling generally showed higher metal readings than the Leckel-sampling, which can be linked to the increased activity and release of PM during the day. Given the small sample size ($n \leq 6$), statistical comparisons of the two methods are rather prone to mistakes and should be interpreted with caution. Nonetheless, the concentrations determined with both methodologies were overall comparable for most considered metals (Table 5.11).

5.3.2.2 Metal concentrations across PM sources

From the Coriolis results (Table 5.11), the lowest metal concentrations were measured at the Background site, followed by the Road and Train sites. As observed for the Leckel-sampling results, the latter two sites showed again the most alike metal profiles. The Ni content was substantially higher at the Train compared to the Road site, but all other metals revealed quite comparable ranges of values. The Shipping site revealed particularly higher concentrations in Al, Cr, Mn, Fe and Zn, compared to the other monitored sites (Figure 5.23). The air samples collected at the Industry site, located near a metal recycling plant, had the highest enrichment in Co, Ni, Cu, As, Ag, Cd and Pb. The mean concentrations at this site even surpassed the European annual target limits for As and Ni (6 ng m^{-3} and 20 ng m^{-3} , respectively).

It was observed that the highest concentrations of Al, Cr, Mn, Fe, Co and Zn at the Shipping site, were always measured on Wednesdays rather than on Thursdays. We hypothesized this could be due to weekly patterns in the shipping or loading/unloading of cargo at the harbor, but the information provided by the harbor company where the monitoring site was located did not confirm this, with no major reported differences in the company operations between Wednesdays and Thursdays. In future, the Coriolis air sampling could be carried out daily for at least a week at this specific site to enlighten this observation. This weekday-influence was not evident at the other monitoring sites, suggesting it is not due to a regional or meteorological influence.

Table 5.11 – A comparison of the mean metal atmospheric concentrations (ng m^{-3} , HR-ICP-MS; in grey), followed by the range (min – max), measured on the same days by the 24-h PM_{10} -loaded filters ($\text{PM}_{2.5}$ for the Background; $n = 4 - 6$) and the 40-min Coriolis ($n = 6$) across the different monitoring sites. Values in bold are significantly higher when comparing both sampling methods (paired Wilcoxon, $p < 0.05$). Values underlined indicate exceedances to the EU annual target limits (As, 6 ng m^{-3} ; Ni, 20 ng m^{-3}).

	Background		Road		Train		Shipping		Industry	
24-h PM-loaded filters (ng m^{-3})										
Al	9.3	(1.6 – 16.7)	60.5	(35.2 – 119.0)	48.2	(15.8 – 89.9)	77.9	(12.7 – 130.3)	67.8	(37.2 – 105.6)
Cr	0.4	(0.0 – 1.0)	1.7	(0.8 – 3.4)	1.2	(0.0 – 2.9)	1.3	(0.4 – 3.3)	2.8	(0.3 – 8.5)
Mn	2.6	(0.6 – 5.4)	10.2	(6.4 – 17.5)	9.2	(2.2 – 18.4)	9.5	(3.7 – 19.0)	13.3	(5.7 – 25.9)
Fe	57.1	(1.9 – 103.4)	599.6	(374.7 – 1045.4)	608.0	(107.0 – 1364.2)	400.2	(178.2 – 817.6)	390.6	(178.1 – 700.5)
Co	0.0	(0.0 – 0.0)	0.7	(0.0 – 2.6)	0.1	(0.0 – 0.2)	0.4	(0.1 – 1.0)	0.8	(0.2 – 2.4)
Ni	0.7	(0.4 – 1.2)	1.1	(0.7 – 2.0)	1.1	(0.4 – 2.2)	4.5	(0.6 – 12.2)	10.5	(2.2 – 31.3)
Cu	1.9	(0.30 – 3.6)	27.6	(14.8 – 45.4)	27.3	(5.2 – 59.0)	13.5	(4.7 – 31.8)	55.2	(25.8 – 133.5)
Zn	8.3	(0.0 – 20.3)	31.9	(14.4 – 54.3)	36.7	(14.6 – 96.2)	33.3	(6.4 – 87.7)	69.9	(38.5 – 126.4)
As	0.2	(0.0 – 0.7)	1.1	(0.3 – 1.7)	0.6	(0.1 – 1.6)	1.1	(0.0 – 4.7)	<u>19.4</u>	(3.0 – 47.5)
Ag	0.0	(0.0 – 0.0)	0.0	(0.0 – 0.0)	0.0	(0.0 – 0.0)	0.0	(0.0 – 0.0)	12.8	(2.5 – 36.7)
Cd	0.1	(0.0 – 0.1)	0.2	(0.1 – 0.4)	0.4	(0.0 – 1.9)	0.2	(0.0 – 0.7)	3.0	(0.3 – 8.6)
Pb	3.8	(1.8 – 6.4)	9.7	(4.6 – 16.2)	8.2	(3.5 – 18.4)	11.6	(4.3 – 27.9)	316.6	(30.7 – 768.2)
40-min Coriolis air samples (ng m^{-3})										
Al	43.5	(14.3 – 74.8)	74.5	(53.6 – 105.1)	107.8	(38.6 – 158.2)	401.2	(43.8 – 856.5)	147.1	(62.9 – 229.7)
Cr	0.7	(0.5 – 0.9)	1.1	(0.7 – 1.4)	1.3	(0.5 – 2.5)	3.2	(0.7 – 5.5)	1.7	(0.8 – 2.8)
Mn	5.0	(1.9 – 8.0)	7.6	(4.7 – 10.7)	10.9	(3.6 – 20.5)	40.2	(4.4 – 76.1)	17.7	(5.3 – 26.4)
Fe	73.5	(16.4 – 133.3)	154.7	(115.5 – 214.3)	205.9	(68.1 – 355.5)	796.2	(115.5 – 1524.7)	337.3	(126.0 – 457.4)
Co	0.2	(0.0 – 0.7)	0.1	(0.1 – 0.2)	0.1	(0.0 – 0.2)	1.2	(0.1 – 3.7)	2.6	(0.4 – 10.8)
Ni	8.4	(0.0 – 25.3)	1.3	(0.0 – 3.3)	8.9	(0.0 – 26.4)	2.5	(0.0 – 9.9)	<u>20.3</u>	(0.0 – 68.5)
Cu	15.4	(4.0 – 26.6)	21.1	(10.3 – 48.2)	19.6	(9.7 – 27.8)	33.8	(12.4 – 72.1)	146.1	(41.2 – 338.2)
Zn	16.5	(4.1 – 34.6)	24.7	(15.2 – 39.7)	22.1	(8.4 – 35.8)	128.5	(23.5 – 234.3)	106.9	(44.0 – 247.6)
As	0.4	(0.1 – 0.6)	0.3	(0.1 – 0.9)	0.4	(0.2 – 0.7)	1.9	(0.3 – 5.8)	<u>46.4</u>	(4.9 – 96.0)
Ag	0.0	(0.0 – 0.1)	0.0	(0.0 – 0.1)	0.1	(0.0 – 0.4)	0.1	(0.0 – 0.2)	4.7	(0.7 – 20.1)
Cd	0.1	(0.1 – 0.2)	0.2	(0.1 – 0.4)	0.1	(0.1 – 0.2)	0.5	(0.1 – 1.2)	4.9	(1.4 – 11.1)
Pb	1.1	(0.4 – 1.5)	2.5	(1.1 – 7.2)	3.0	(1.5 – 4.6)	26.1	(3.9 – 60.1)	454.2	(88.3 – 993.2)

HEALTH-RELEVANCE ACROSS MAJOR PM SOURCES

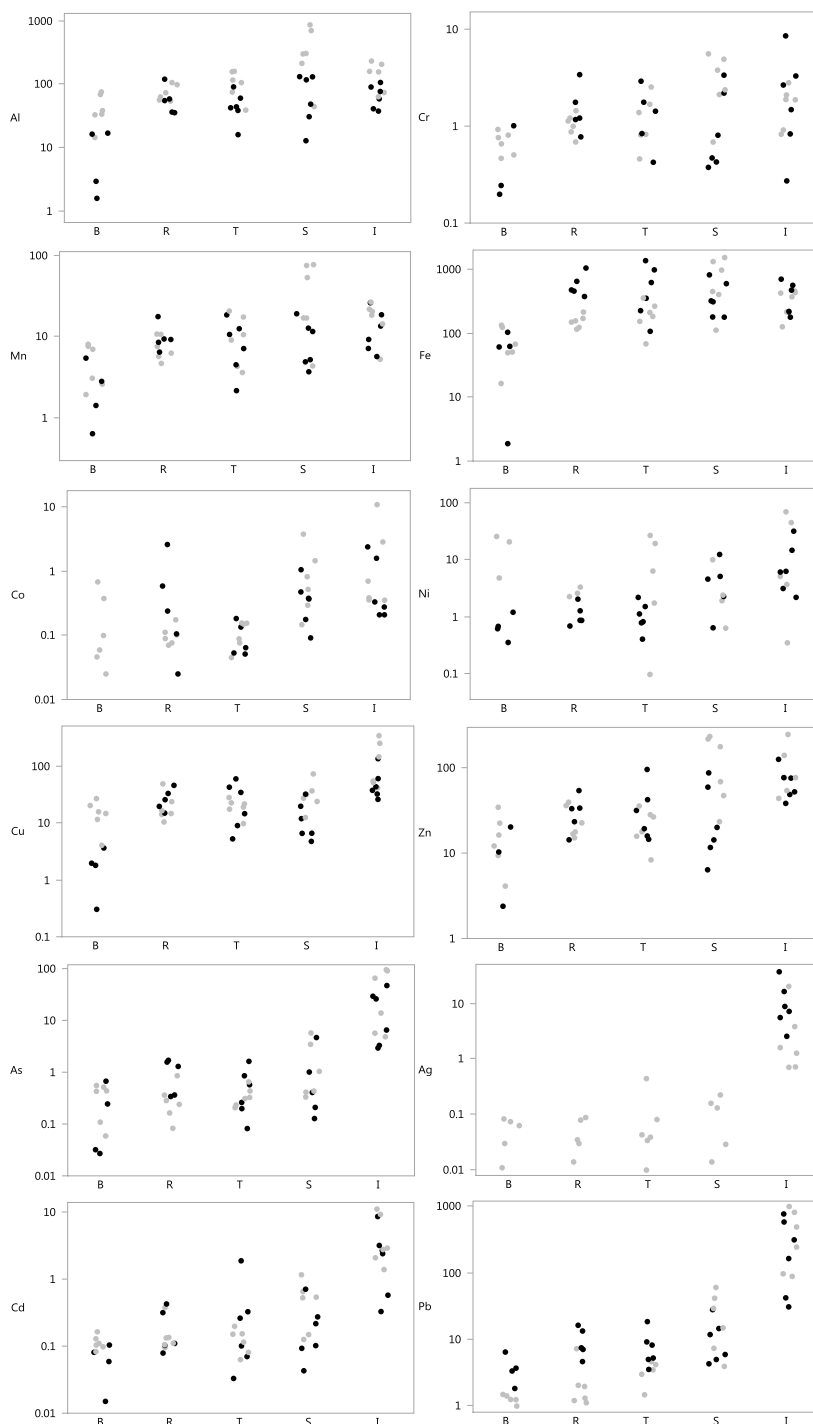


Figure 5.23 – Metal concentrations (ng m^{-3} ; HR-ICP-MS) determined on the same days by the 24-h Leckel (black dots) and the 40-min Coriolis sampling (grey dots) across the monitored sites (B - Background, R – Road, T – Train, S – Shipping, I – Industry). Leckel samples consisted of PM_{10} -loaded filters except for the Background site ($\text{PM}_{2.5}$).

5.3.2.3 Pro-inflammatory response across PM sources

Within the hierarchical oxidative stress model to PM exposure, HO-1 is identified as one of the more than 200 antioxidant and detoxification enzymes that, at a still low level of oxidative stress (tier 1), are actively transcribed to restore cellular redox homeostasis (Bernstein et al., 2004; Li et al., 2003; Moretti, 2018). If oxidative stress persists (tier 2), these enzymes can no longer prevent the effects of reactive oxygen species (ROS) and pro-inflammatory responses are induced, including cytokines (signaling molecules) IL-8, IL-1 β , and TNF α . In a last stage, at higher levels of oxidative stress (tier 3), cellular apoptosis and necrosis occur. Generally speaking, an increase in pro-inflammatory response can be caused from an overflow of oxidative stress, but pro-inflammatory response can also be independently activated (Moretti, 2018).

The expression of pro-inflammatory (IL-8, IL-1 β , and TNF α) and oxidative stress (HO-1) markers, in terms of mRNA, after exposure to the Coriolis air samples was overall highest at the Train and Shipping sites (Figure 5.24). The observed high expression of health-relevant indicators at the Train and Shipping conditions was true for markers IL-8, IL-1 β , and TNF α , associated with tier 2 of PM-induced inflammatory cascades, but not for the HO-1 (tier 1). The mRNA response at the Road site was comparable to the Background, with exception of one sampled day. The response measured at the Industry site was rather similar to the latter two sites in terms of pro-inflammatory markers, on one hand. On the other hand, it was at the Industry that the highest expression of the oxidative stress marker (HO-1) was measured, which might indicate a relative high level of PM-induced oxidative stress. The activation of pro-inflammatory responses (IL-8, IL-1 β , and TNF α) gained more expression at the Train and Shipping sites, while higher oxidative stress levels (HO-1) were observed at the Industry, therefore, suggesting a higher health-risk potential at these monitored sites compared to the Background and Road sites.

The between-days variability within the pro-inflammatory response is particularly notorious for the Train and Shipping sites, whereas minimal at the Background, Road (except of one day) and Industry (except for HO-1). The variability being inconsistent

across all sites suggests it may be due to source-specific effects rather than to regional effects.

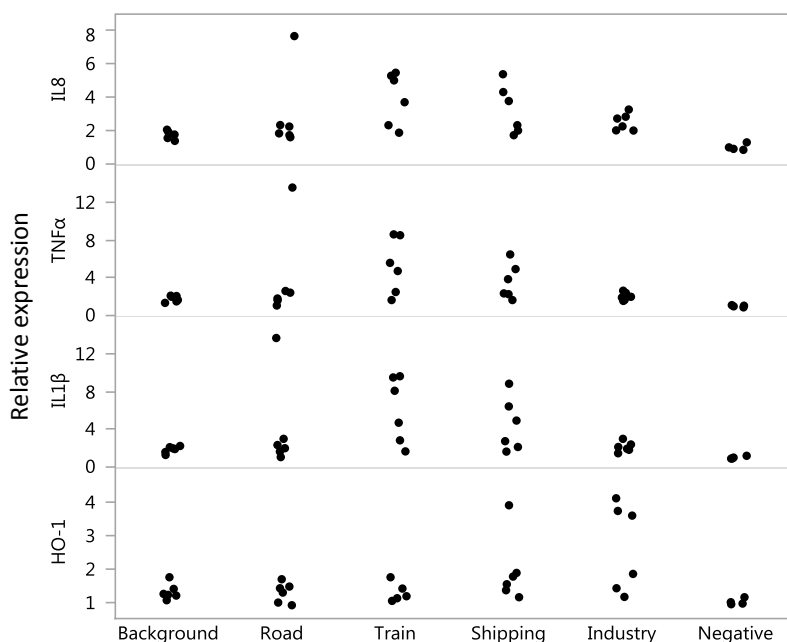


Figure 5.24 – Relative pro-inflammatory response of air samples across the five monitoring sites. Values represent mRNA levels of the pro-inflammatory markers IL-8, IL-1 β , and TNF α , and oxidative stress marker HO-1, measured in human macrophage-like U937 cells after exposure with the air samples collected with the Coriolis, in comparison to the negative control.

5.3.2.4 Associations between source composition and health response

Despite of the small sample size, correlations were tested between the metals and pro-inflammatory and oxidative stress markers across the five monitoring sites. In general, correlations were mostly found between metals and the oxidative stress marker (HO-1). This was the case for the Background and Shipping sites, with positive correlations between HO-1 and Al, Co and Pb ($\rho = 0.89$, $p = 0.02$), and between HO-1 and Al, Cr, Fe, Co, Ni, Cu, Zn ($\rho = 0.81 - 1.00$, $p < 0.05$), respectively. The high relative expression of pro-inflammatory markers at the Shipping site did not appear to be significantly linked with the measured metals on site. Still, the highest metal concentrations for Shipping were mainly measured on the same days (on Wednesdays rather than on Thursdays) that revealed the highest pro-inflammatory response (IL-8, IL-1 β , TNF α). This

association is not reflected in the statistical correlations, possibly because from the six point time measurements, three were done on a Wednesday (high values) and three on a Thursday (low values). At the Road site, Fe and Mn were, respectively, positively ($\rho = 0.89$, $p < 0.02$) and negatively ($\rho = -0.94$, $p < 0.005$) associated with marker HO-1, while the concentration in Al was significantly linked with all three pro-inflammatory markers (IL-8, $\rho = 0.83$, $p = 0.04$; IL-1 β and TNF α , $\rho = 0.94$, $p = 0.005$). At the Train site, IL-8 was correlated with metal Cu ($\rho = 0.83$, $p = 0.04$), but negatively associated with Ni (IL-8, $\rho = -1.00$, $p < 0.0001$; IL-1 β and TNF α , $\rho = -0.94$, $p = 0.005$). Lastly, at the Industry site, Mn and Co were best correlated with the IL-1 β response ($\rho = 0.94$, $p = 0.005$), Cr with IL-8 ($\rho = 0.83$, $p = 0.04$), As with TNF α ($\rho = 0.83$, $p = 0.04$), and Zn with HO-1 ($\rho = 0.89$, $p = 0.02$). The diversity of associations between the metals and immune response markers appear to indicate differences between the monitoring sites, but large sample pools are necessary to increase robustness of this study, and before achieving additional conclusions. When considering the entire dataset together, most metals were positively linked with the oxidative stress marker HO-1 (Al, Cr, Mn, Fe, Co, Cu, Zn, Ag, Pb) and the pro-inflammatory marker IL-8 (Al, Cr, Mn, Fe, Co, Cu, Zn, Pb), while less metals were found to be correlated with the markers TNF α (Al, Cr, Fe, Mn, As) and IL-1 β (Al, Cr, Mn, Fe).

Consequently, the PCA analysis on the metals and health markers did not reveal a clear site discrimination for all monitored sites. The main discriminant components (PC1 and PC2), describing 72.6% of the total variance, were most successful at separating the Shipping, Industry and Train observations, while the Background and Road sites were grouped together (Figure 5.25). PC1 mainly related with the marker HO-1, Industry-interrelated metals (Co, Ni, Cu, As, Ag, Cd, Pb) and Zn (highly associated with both Industry and Shipping) (Table 5.11), and separated Industry, and to a lesser extent Shipping, from Train, Road and Background sites. PC2 related with the pro-inflammatory markers (IL-8, IL-1 β , TNF α), and discriminated Shipping, and in a lower degree Train and Road, from Industry and Background. Additionally, PCA was performed separately on the metal concentrations (i.e., source-specific PM

characteristics) and health markers (potentially related with the metal levels), with the outcomes (not shown) generally confirming the abovementioned site discrimination.

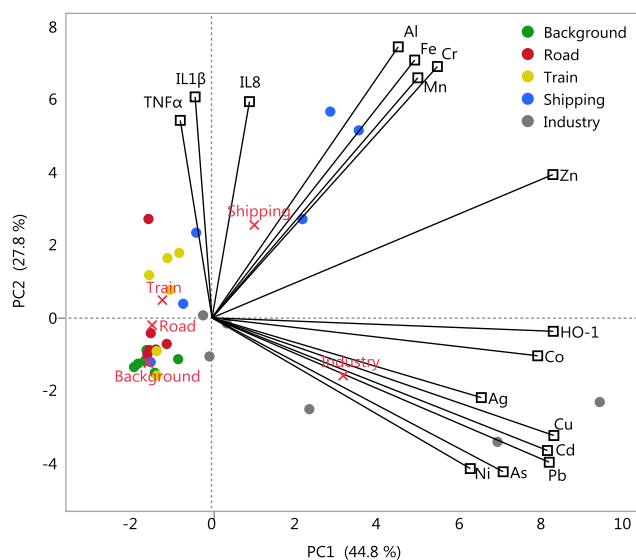


Figure 5.25 - Biplot of PCA (PC1 and PC2) on the metal concentrations (Al, Cr, Mn, Fe, Co, Ni, Cu, Zn, As, Ag, Cd, Pb) and pro-inflammatory and oxidative stress markers (IL-8, IL-1 β , TNF α , HO-1) measured in the Coriolis air samples for the monitored sites (circles) Background (green), Road (red), Train (yellow), Shipping (blue), Industry (grey). PC1 and PC2 account for 72.6% of the total variance.

The air samples collected at the Background and Road sites were the least associated with high metal content (Figure 5.23) and the activation of inflammatory responses (Figure 5.24), due to the low expression of both oxidative stress and pro-inflammatory response markers. Yet, the metal profile at the Road site was rather comparable to that of Train (Table 5.11), and the Road pro-inflammatory responses along PC2-axis were enhanced in comparison with the Background (Figure 5.25). While relatively low metal levels and pro-inflammatory responses could be expected at the Background site, being sheltered from major polluting sources, the outcomes for the Road site are a bit surprising. Road traffic is typically characterized by the release of metal particles (e.g., Fe, Cr, Zn) and vehicle combustion emissions linked with adverse health effects. The first part has been corroborated throughout this thesis, by elemental and magnetic analyses of atmospheric PM filters (§Chapter 5.1) and combined analyses of

leaves located near road traffic emissions (§Chapters 2, 3.1, 3.2). The fact that relatively low pro-inflammatory responses are depicted from the Road collected samples in this study might be explained by the monitoring site conditions per se, rather than the absence of health-relevant PM. At the Road site, a vegetation barrier separated the busy national highway and the back of the private property in which the air samples were taken, at ca. 25 m from the highway (Figure 5.2). This vegetation barrier might have partly diverged the highway traffic emissions, complicating the correct sampling of road traffic pollution at this site. This barrier effect was, however, neither observed for the metal concentrations (still comparable with Train site), nor for the continuous Leckel PM samples (§Chapter 5.1).

From this exploratory study, the air samples obtained at the Industry site, a heavily metal-polluted location, showed a higher oxidative stress potential compared to the other sites. From all monitored sites, the Train and Shipping samples were the most associated with pro-inflammatory response markers, suggesting that these types of source emissions deserve particular attention when assessing the health-risk potential of urban environments.

5.2.4 Conclusions

Within the fingerprinting of PM sources contributing to the multi-source air pollution, the PMF project aimed, among others, to associate magnetic source-specific signatures with health-related PM components such as metals (and UFPs, BC, PAHs; data not shown). Metal particles are hazardous atmospheric contaminants due to their high bioavailability and redox potential, and have been associated with oxidative stress and inflammatory potential. This experiment on the pro-inflammatory and oxidative stress response of air samples collected (with a Coriolis impinger) at the monitored sites revealed useful preliminary information about their health-relevance; still, the collection of more samples is necessary to improve the robustness and statistical power of this study.

With few exceptions, the metal concentrations measured in the collected air samples were comparable with the conventional PM sampling method (Leckel samplers), with highest concentrations being obtained at the Industry site. The expression of oxidative stress marker HO-1, which is involved in the first stage of the cascade of inflammatory responses, was the highest at the Industry site as well. The Train and Shipping sites were the most associated with the pro-inflammatory response markers (IL-8, IL-1 β , and TNF α). As these markers are related with the second stage of inflammatory response (Bernstein et al., 2004), the atmospheric PM conditions at the Train and Shipping sites are suggested to be the most health-concerning within the five tested sites. Preliminary analyses on the atmospheric BC and UFPs levels assessed during the point-time measurements (§5.1.2.2) revealed highest mean values for Shipping, Road and Industry sites.

In order to confirm and gain more insight on the health-relevance of typical urban sources (e.g., road and railway traffic, harbor environments), future research could combine the experimental part of the presented study with testing the pro-inflammatory response of collected PM-loaded filters (from conventional, Leckel samplers), following Bastonini et al. (2011). In the latter, a substantial transcriptional profiling of inflammatory markers was obtained after exposing human monocyte-macrophage U937 cells directly to PM₁₀ filters. Moreover, combining this with magnetic analyses, might deliver some information on the feasibility of using magnetic-based strategies to recognize PM sites or sources of high health-risk potential.

Chapter 5.3

PM fingerprinting towards a magnetic-based
source apportionment tool using leaves

Based on: Castanheiro, A., Hofman, J., Moretti, S., Joosen, S., VMM, Lebeer, S., Blust, R., Lenaerts, S., De Wael, K., Samson, R., 2020. Particulate matter fingerprinting towards a magnetic-based source apportionment tool – the pathway source-air-leaves. (under preparation)

Abstract

Plant leaves can serve as reliable air quality sensors, research has shown. The present chapter reports on the leaf monitoring conducted during the Particulate Matter Fingerprinting (PMF) project, and describes the obtained site-specific elemental and magnetic profiles. Leaf measurements were overall in accordance with the main findings from the atmospheric PM-loaded filters, with leaf SIRM showing a good association with the cumulative PM mass on the filters.

5.3.1 Introduction

The use of plant leaves and other vegetation matrices to sense the surrounding environment has been replicated in a range of climates, ecosystems, urban and non-urban settings, exposure periods, among others (e.g., Capozzi et al., 2016; Dzierżanowski et al., 2011; Grote et al., 2016; Mo et al., 2015; Weber et al., 2014). Plants are relatively cheap, portable and adaptable, and resilient to meteorological conditions, requiring no electricity to sample the atmosphere in which they thrive on. Therefore, each plant or leaf can work as an air quality monitoring station per se. As most methodologies, air leaf monitoring also has some disadvantages, such as the existence of species-specific traits that lead to different accumulation of pollutants (Sæbø et al., 2012; Muhammad et al., 2019; Weerakkody et al., 2017) and their use in controlled scenarios (e.g. vandalism is not uncommon). The capacity of plants for atmospheric monitoring is often evaluated in comparison with atmospheric pollutants (e.g., PM concentrations) registered at the closest air quality station; yet, the simultaneous application of leaf- and conventional-monitoring strategies for atmospheric PM has been hardly tested (Wuytack et al., 2011, 2013), especially in terms of magnetic properties. To the best of our knowledge, parallel or combined leaf-

air magnetic measurements have only been reported in the research of Hofman et al. (2014b), Mitchell and Maher (2009), Mitchell et al. (2010) and Mantovani et al. (2018), but without considering the influence of distinct source-specific conditions.

PM emitted by a certain source (direct source; emission) will, in a first stage, become suspended in the atmosphere (air; suspension), and in a second stage, it can be accumulated on nearby vegetation (leaves; accumulation). The conducted PMF project attempted, among other things, to investigate the pathway source-air-leaves (emission-suspension-accumulation) for the studied source types. For this, dust emitted at several direct sources (e.g., car brake disks) were collected, and all test sites were monitored continuously using plant leaves in addition to atmospheric PM Leckel-sampling. The present study reports solely on the PMF leaf monitoring campaign (§Chapters 5.1 and 5.2 for air monitoring; results on direct sources are not included), aiming to source apportion the monitored sites based on their leaf elemental and magnetic profiles, and to evaluate the leaf monitoring approach against the conventional one.

5.3.2 Materials and methods

An overview of the PMF campaign and monitoring sites can be found in Chapter 5.1, as well as the experimental part (and results) for the conventional monitoring approach using the Leckel PM samplers.

5.3.2.1 Leaf sampling

Fifteen ivy (*Hedera sp.*) plants were obtained from a nursery (Garden Center Claes, BE) on September 12, 2017. After collection of blank (non-exposed; 0w) leaves, groups of three plants were planted together in all-purpose potting soil, inside robust plastic boxes (polypropylene; 43 x 36 x 26 cm, length x width x height). The boxes were perforated at the bottom to allow for water drainage, and properly labelled to prevent vandalism when exposed outdoors. Each box containing three ivy plants was placed at each monitoring site slightly prior to the start of the PM gravimetric sampling (on September 13 - 15). During the weekly visits to the monitoring sites, plants were

carefully watered (avoiding contact with the leaves) if needed, to prevent drought stress. At each site, ivy leaves (exposed since September 13 - 15) were collected at the middle (after three weeks, 3w; on October 4 and 5) and at the end (after seven and a half weeks, 7.5w; on November 6 and 7) of the monitoring campaign. Per leaf sampling event at each site, a total of twelve leaves were collected, four leaves per plant, at ca. 35-60 cm height from the ground and at least 10-15 cm from the potting soil in the box to avoid contamination with soil. The collected leaves were stored in labelled paper bags and transported to the lab. To prevent the use of leaves not present since the beginning of the campaign, newly emergent leaves were removed weekly from the exposed plants.

5.3.2.2 Leaf monitoring: elemental and magnetic PM

Of the twelve leaves per sampling event (0w, 3w, 7.5w) per site (B, R, T, S, I), six leaves (two of each plant) were analyzed for elemental accumulation by ED-XRF and HR-ICP-MS, and three to six leaves were analyzed magnetically and by SEM. All leaves were kept at 4°C awaiting for sample preparation and analysis.

Prior to ED-XRF analysis (non-destructive), similar leaf sizes were obtained by using a circular metallic puncher (48 mm in diameter) on the leaf samples, resulting in rather uniform leaf surface areas (ca. 18 cm²). Determining the elemental composition of leaf-deposited PM by ED-XRF was highly hampered due to the heterogeneous nature of leaf matrices, as discussed in detail in Chapter 4, so these data are not shown. Subsequently, leaves were transferred to acid washed 50 mL glass bottles with 15 mL of ultra-pure water, which were placed on an orbital shaker (GFL 3015, DE) at 180 rpm for 3 min. The selected shaking time had been previously tested on ivy leaves (§4.2.2). The resulting leaf washing water samples were acidified and analyzed by HR-ICP-MS similarly as done for the PM-loaded filters (§5.1.2.3), with detection limits ranging between 0.1 and 0.001 µg L⁻¹. The obtained concentrations (in µg L⁻¹) were normalized to the applied analytical volume and mass values (in µg) are reported.

The leaves investigated for their magnetic properties were first measured for their surface area using a leaf area meter LI-3100C (Licor Biosciences, USA). Subsequently, leaves were dried at 35°C for at least three days in a drying cabinet (Memmert, DE). Similarly to the PM-loaded filters (§5.1.2.3), the leaf samples (three leaves for 0w, and six leaves for 3w and 7.5w) were measured for their magnetic susceptibility (χ_{LF}), $ARM_{200/500}$, ARM_{χ} , SIRM and IRM_{-300} , and the magnetic ratios HIRM, S-ratio, $SIRM/\chi_{LF}$ and $ARM/SIRM$ were calculated. The leaf magnetic results were normalized by the surface area of leaves (and the sample pot volume, 6.7 cm³), resulting in units of m for χ_{LF} and of A for ARM and (S)IRM parameters.

A selection of these magnetically analyzed leaves (three per sampling event per site, one of each exposed ivy plant) were also checked by SEM. Before magnetic analysis, two subsamples were taken from these leaves, one for adaxial and one for abaxial analysis, using a metallic puncher (10 mm in diameter). The leaf subsamples were fixed on aluminum pin stubs using conductive double-sided tape and left at room temperature. The subsamples were coated with carbon (Leica EM ACE600, DE) before being analyzed with a Quanta 250 (FEI, USA) at AXES and EMAT research groups (University of Antwerp, BE); operating parameters have been described in Chapter 4. Secondary electron images (SEI) show the morphology and quantities of deposited particles, whereas backscattered electron images (BSE) illustrate the contrast in composition of high Z elements against the leaf background surface. Illustrative images were taken to visually investigate the accumulation of leaf-surface deposited PM.

5.3.2.3 Artificial passive sampling on stubs

At each monitoring site, an aluminum pin stub with conductive double-sided carbon tape was fixated on top of the Leckel sampler (i.e., at a height of ca. 1.5 m above ground) at the beginning of the monitoring campaign, in order to passively collect atmospheric PM throughout the entire monitoring period. The aluminum stubs were carbon coated and analyzed by SEM as done for the leaf samples. An overall image (magnification 50x) was obtained from the center of each stub, using detectors for

both secondary and backscattered electrons generated with the application of a high-energy electron beam, and yielding SEI and BSE images.

5.3.2.1 Data analysis

Leaf elemental and magnetic enrichment over time were evaluated using linear fits. Kruskal-Wallis and paired-sample Wilcoxon tests were used to check for site-influences in the measured magnetic properties and ratios. Associations between leaf accumulated elements and magnetic parameters were tested using Spearman's correlations, and linear fits were used to check the relationship between leaf SIRM and Fe content across the monitored sites. Finally, leaf SIRM was compared against the cumulative PM filter loads (measured in Chapter 5.1) using linear regression. Statistical analysis were performed in JMP Pro 14.

5.3.3 Results and discussion

5.3.3.1 Leaf elemental accumulation of PM

The main elements governing the leaf washing solutions, measured by HR-ICP-MS, were Na, Mg, K, Ca, Mn, Fe, Pb (Figure 5.27), with largest predominance for Ca and K amongst all monitored sites, while Pb was only relevant at the Industry site. The elements measured in the leaf washing solutions can comprise leaf leachates or constituents, as well as PM once deposited on the leaf surface (Dzierżanowski et al., 2011; Hofman et al., 2014b). Elements Ca and K are associated with foliar exchange and leaching in the form of cations (K^+ and Ca^{2+}), as K^+ is a plant electrolyte and Ca^{2+} is bound to structural plant tissues or enzyme complexes (Draaijers et al., 1994; Kopáček et al., 2009), whereas in PM, Ca and K originate from crustal dust emissions (Tomašević and Aničić, 2010; Vercauteren et al., 2011) (§Chapter 4). The non-exposed leaves were leaf replicates from the plants that were exposed at the sites subsequent to the first leaf collection (0w). For this reason, the elemental starting point of the 0w leaves was rather similar. After three weeks of exposure, most of the main elements (Na, Mg, K, Ca, Mn) decreased in mass (Figure 5.28), likely due to the outdoor exposure to e.g. rain and wind. In addition to rain wash-off losses, this elemental decrease can be due to

the depletion of nutrients in the leaves and the absence of fertilization, when compared to the greenhouse conditions of the nursery garden in which plants had been grown prior to the experiment. At the end of the campaign (after 7.5 weeks) though, some of the elements increased in mass again but mostly not exceeding the initial values before exposure. In fact, the average total mass of elements (27 elements) measured from the leaves was higher for 0 weeks (62 – 84 μg) than for 3 (17 – 76 μg) or 7.5 (33 – 69 μg) weeks, across all sites. The highest final mass values (for 7.5w leaves) were obtained at the Shipping and Industry sites (69 μg both).

The fact that the overall elemental accumulation of PM (Figure 5.26) after more than seven weeks of exposure was not substantial, or not even positive, is not surprising, as similar observations were made for ivy leaves exposed for twelve weeks at a low/moderate road traffic close to the Groenenborger campus of the University of Antwerp (§Chapter 4). In that study, the appearance of new leaves during the monitoring period likely influenced the between-leaves variability and might have led to the close to null total accumulation after three months of exposure. Contrastingly, the hypothesis of new emergent leaves is not possible at the present study, as only leaves exposed from the start of the campaign were used. As a consequence, it might be that seven weeks of exposure are not sufficient to obtain measurable accumulation of atmospheric PM mass on the leaves, but environmental conditions between the measured non-exposed and exposed leaves may be of influence as well. At the greenhouse garden center, plants typically have a great amount of nutrients available without being exposed to e.g. rain and wind, which can explain the relatively high elemental accumulation observed for the 0w leaves. Due to being overall more protected from stress conditions, the wax thickness of those leaves is likely smaller than the thickness of older plant leaves that are exposed outdoors (Hull et al., 1975), and thin wax layers are often associated with high leaching of leaf nutrients (Riederer and Schreiber, 2001). Throughout the monitored period, leaf leaching was highest for the non-exposed leaves, decreased at three weeks of exposure and increased again at the end of the campaign (Figure 5.26).

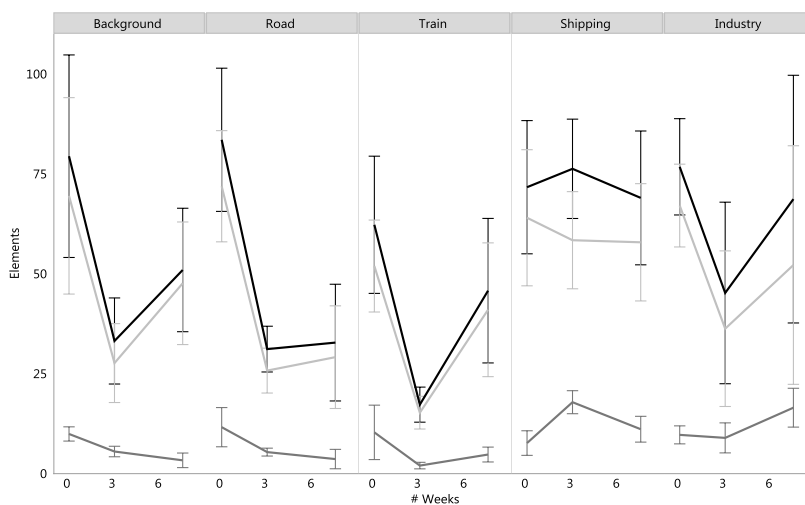


Figure 5.26 – Variation in total mass (in μg) of all elements (black lines), of leaching elements (K, Ca, Mg, Mn; light grey lines) and of their difference (all elements minus leaching elements; dark grey lines) measured from the leaf washing solutions (HR-ICP-MS) per monitoring site throughout the exposure period (at 0, 3 and 7.5 weeks). Lines represent mean values ($n = 6$) and error bars the standard deviation.

The decreasing or stagnating accumulation trends were mostly observed for elements that are related with natural PM sources (Na) and/or with leached leaf components (K, Ca, Mg, Mn) (Tukey, 1970) (Figure 5.28), which are also the elements most contributing to the mass of accumulated PM (Figure 5.27). Therefore, to analyze the accumulation of elements related with anthropogenic contamination, such as Pb and Fe, it should be more relevant to evaluate source-specific effects than to assess the total accumulated mass. At the Background and Road sites, none of the measured elements increased significantly over time. At the Train site, significant increases (linear fit, $p < 0.05$) were observed over time for Fe ($R^2 = 0.33$), Cu ($R^2 = 0.30$), Cd ($R^2 = 0.40$), and Pb ($R^2 = 0.61$). At the Shipping site, increasing accumulations were found for Al ($R^2 = 0.40$) and Si ($R^2 = 0.26$), which are crustal dust related, and for Cr ($R^2 = 0.49$), Fe ($R^2 = 0.58$), Co ($R^2 = 0.33$), and Cd ($R^2 = 0.37$). The high metal diversity observed from the atmospheric PM-loaded filters (§Chapter 5.1) at the Industry site was also visible in the exposed ivy leaves, with accumulation growing significantly for elements Al ($R^2 = 0.40$), Si ($R^2 = 0.86$), Fe ($R^2 = 0.29$), Ni ($R^2 = 0.52$), Cu ($R^2 = 0.64$), As ($R^2 = 0.69$), Ag ($R^2 = 0.67$), Cd ($R^2 = 0.66$), Sb ($R^2 = 0.55$), and Pb ($R^2 = 0.75$).

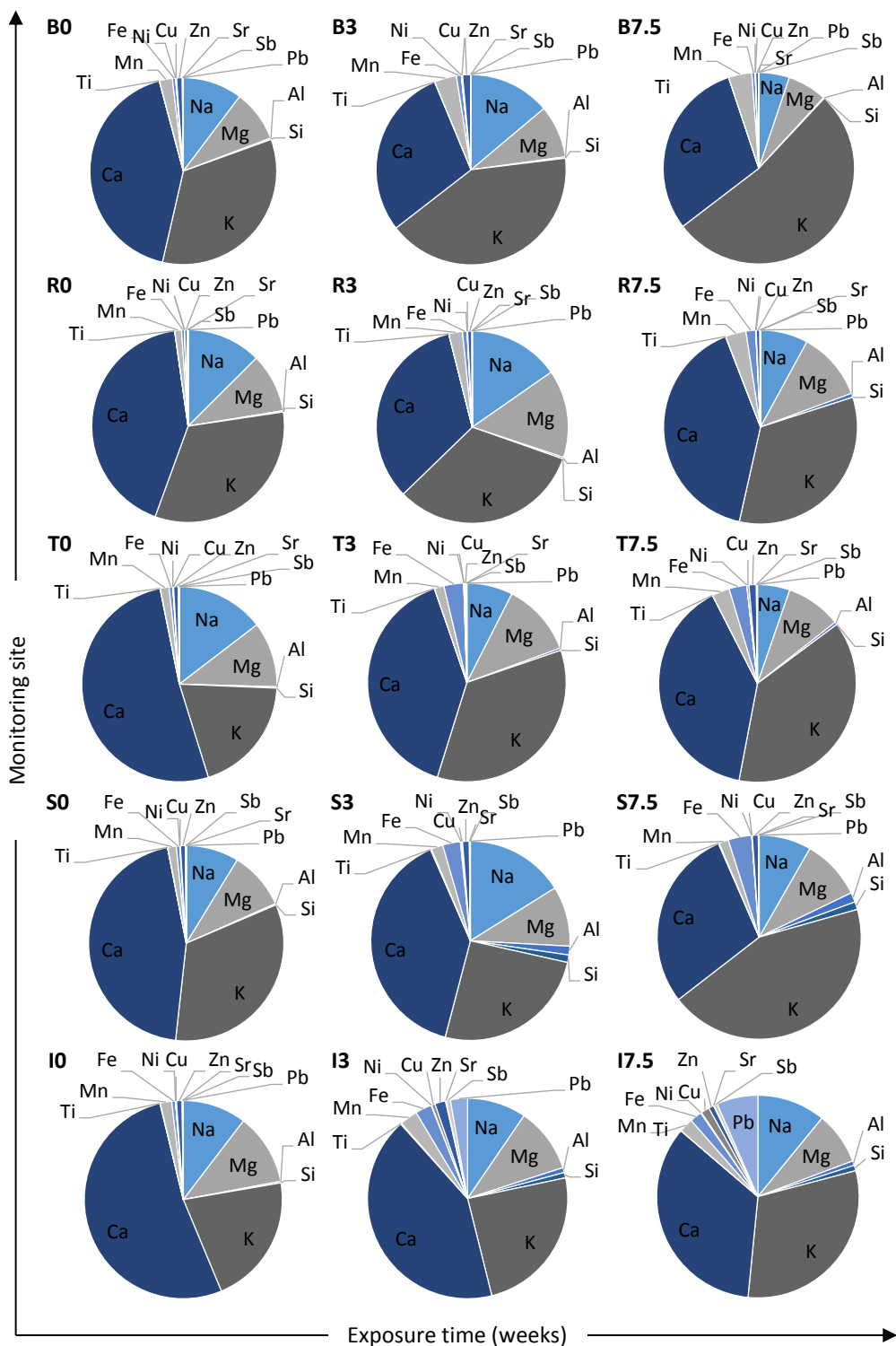


Figure 5.27 – Pie charts of average elemental composition of elements measured by HR-ICP-MS in the leaf washing solutions of exposed ivy at the monitoring sites (B - Background, R - Road, T - Train, S - Shipping, I - Industry), per exposure time (0, 3, 7.5 weeks).

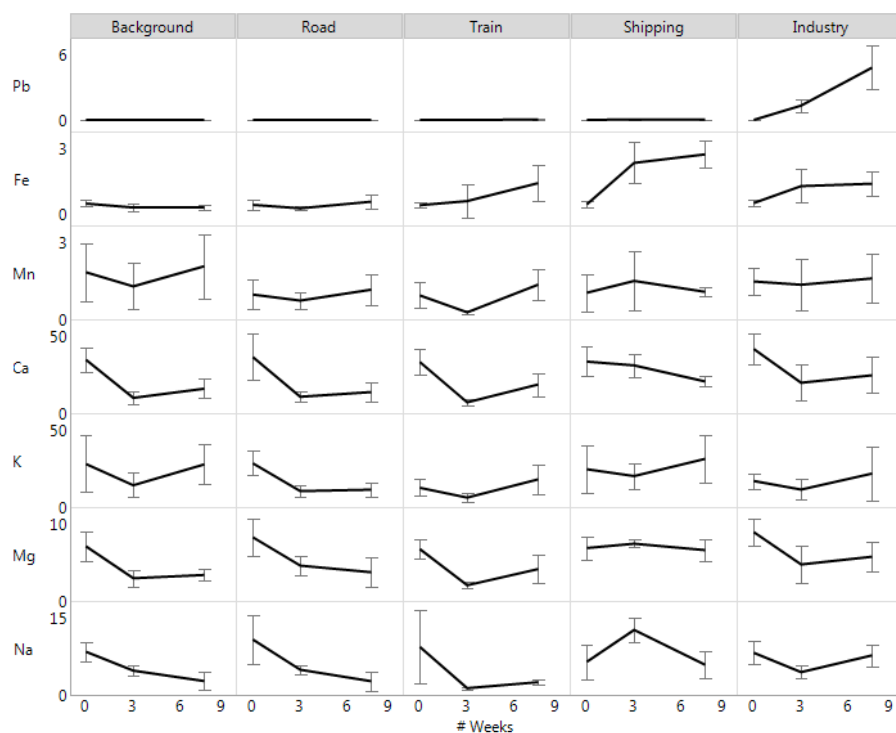


Figure 5.28 – Variation in mass (in μg) of the main elements (Na, Mg, K, Ca, Mn, Fe, Pb) measured from the leaf washing solutions (HR-ICP-MS) per monitoring site throughout the exposure period (at 0, 3 and 7.5 weeks). Lines represent mean values ($n = 6$) and error bars the standard deviation.

5.3.3.2 Leaf magnetic enrichment

The exposed and collected ivy leaves had an average leaf surface area of $19.6 (\pm 5.2)$ cm^2 , and their surface area did not increase substantially during the period of seven and a half weeks. The magnetic susceptibility of all analyzed leaves (normalized for their surface area) was negative, between -3.8 and -1.1×10^{-8} m, indicating that the accumulated PM did not overcome the diamagnetic nature of the leaves (§4.3.3). No significant effect of site (Kruskal-Wallis, $p = 0.34$), neither of exposure time (linear fit, $p = 0.64$), was found for the magnetic susceptibility values (χ_{LF}). But testing the volume susceptibility (k) as measured by the magnetic susceptibility meter (i.e., not normalized for surface area) revealed that the negative values became less negative with exposure time for all monitored sites (linear fits, $p < 0.05$, $R^2 = 0.51 - 0.73$), suggesting an accumulation of magnetic particles.

For ARM and SIRM, values varied between 0.2 and 2.8 μA and between 2.9 and 37.9 μA , respectively, across all monitoring sites. The accumulation of magnetic particles at the end of the monitoring campaign, measured by SIRM, was highest for the Shipping site, followed by the Train, Industry, Road and Background sites, in this descending order (Figure 5.29, Table 5.12). The significant site-influence on the measured leaf ARM and SIRM was confirmed by Kruskal-Wallis tests, on the 3w leaves ($p = 0.012$, $p = 0.007$) and on the 7.5w leaves ($p = 0.004$, $p = 0.03$). Exposure time led to significant increments in both magnetic-concentration indicators and for all sites (linear fits, $p < 0.05$, $R^2 = 0.31 - 0.78$ for ARM, $R^2 = 0.35 - 0.88$ for SIRM).

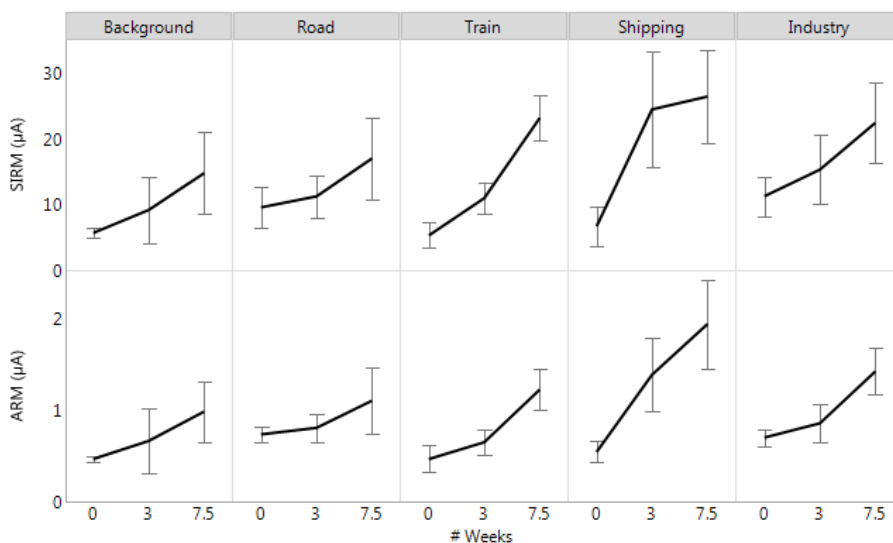


Figure 5.29 - Variation of leaf ARM and SIRM values (μA) per monitoring site throughout the exposure period (at 0, 3 and 7.5 weeks). Lines represent mean values ($n = 3$ at 0 weeks, 6 at 3 and 7.5 weeks) and error bars the standard deviation.

Obtained IRM_{-300} values were comparable with the SIRM values (Table 5.12), with subsequent mean S-ratio close to the unity, between 0.88 – 0.96 for all sites and sampling points. At the maximum exposure time (7.5w), the S-ratio ranged between 0.91 and 0.99 for all monitored sites. As observed for the co-located atmospheric samples (§5.1.3.4), this indicates that the leaf accumulated magnetic particles are dominated by low-coercivity minerals, such as magnetite. The slight increase in the S-ratio with exposure time was also observed for HIRM values (that ranged between 0.05

and 1.34 μA), and appeared to happen at the five monitoring sites (Table 5.12). The calculated $\text{HIRM}_{\%}$ (i.e., $100 \times \text{HIRM}/\text{SIRM}$) which estimates the proportion of high-coercivity minerals (Shu et al., 2000), varied on average from 2.9% to 4.2% across all sites. These values are comparable with the results measured for the PM_{10} -loaded filters, thus suggesting that the exposed ivy leaves can be good magnetic indicators of what happens at the atmospheric level, as registered by conventional air quality monitoring stations.

Because of the little relevance of leaf susceptibility values measured in this study (i.e., all negative), the ratio $\text{SIRM}/\chi_{\text{LF}}$ becomes difficult to interpret. The leaf $\text{SIRM}/\chi_{\text{LF}}$ decreased significantly over time across all sites ($p < 0.05$) and was site-dependent (Kruskal-Wallis, $p = 0.001$), being significantly highest for the Background site (paired-samples Wilcoxon, $p < 0.02$) and lowest for the Shipping (not significant). The negative χ_{LF} values indicate the dominance of diamagnetic minerals, while SIRM results from the fraction of ferrimagnetic remanence-bearing particles. To examine the ratio $\text{SIRM}/\chi_{\text{LF}}$ becomes thus senseless, as two different magnetic mineral classes are being compared. Leaf ARM/SIRM values decreased significantly with the exposure time as well, but only significantly for the Train site ($p = 0.0008$, $R^2 = 0.59$). Higher values in both $\text{SIRM}/\chi_{\text{LF}}$ and ARM/SIRM are often associated with smaller magnetic grain sizes (Hofman et al., 2017), but any conclusions in this regard for the PM accumulated on the leaf samples are premature, due to the large leaf diamagnetic influence (negative χ_{LF}) which overrules the ferro(i)magnetic PM contribution. The use of longer exposure periods in future leaf monitoring campaigns is likely to improve this effect (e.g. Rodríguez-Germade et al., 2014). Leaf SIRM values measured in the present study are within the same order of magnitude as values obtained in other studies (Hofman et al., 2014b; Mantovani et al., 2018). Comparing the values of this study with the ivy leaf SIRM measured at the Groenenborgerlaan site (§Chapter 4) confirms the hypothesis formulated in Chapter 4 that the mixing of new growing leaves within the pre-existing ones may have affected the proper evaluation of leaf-surface accumulation of magnetic particles. At that site, average values of 14 to 15 μA were obtained for leaves exposed during six, nine and twelve weeks, without incremental changes during that

time. These values are very comparable with the values obtained for the Background site in this study after seven and a half weeks of exposure, suggesting on one hand a rather reduced level of pollution at the Groenenborgerlaan site. On the other hand, the hypothesized mixing of new leaves, in addition to PM wash-off due to strong rain events (§4.3.3), appears a valid explanation for the observed SIRM stagnation. The accumulation of magnetic particles in this study over time was rather evident (Table 5.12), even when using a relatively short exposure time (with negligible precipitation; §5.1.2.4).

5.3.3.3 Associations between leaf accumulated elements and magnetic enrichment

Potential associations were checked between the elemental and magnetic enrichment of leaves during this monitoring campaign. Considering mean values only (for 0w, 3w, 7.5w) and all sites, both ARM and SIRM correlated strongly (Spearman, $p < 0.05$) with the content in Al ($\rho = 0.65$, $\rho = 0.68$) and Si ($\rho = 0.69$), as well as with the metals Fe ($\rho = 0.62$, $\rho = 0.75$), Cd ($\rho = 0.83$, $\rho = 0.76$) and Pb ($\rho = 0.59$, $\rho = 0.61$). When considering all analyzed individual leaves (each leaf was either analyzed by HR-ICP-MS or magnetically) instead of the mean values, more associations or none at all were found depending on the monitoring site. No significant correlations were observed between the accumulated elements and ARM or SIRM for the leaves exposed at the Background and Road sites. At the Train site, high leaf ARM and SIRM values indicated high accumulation in Fe, Cu, Pb and Cd ($\rho = 0.56 - 0.68$). At the Shipping site, leaf ARM was correlated with Cr, Fe, Ni and Cd ($\rho = 0.53 - 0.65$), however, this was not equally found for leaf SIRM. For the leaves exposed at the Industry site, significant positive associations were found between measured ARM and SIRM and content in Al, Si, Fe, Cu, Ni, Ag, Cd, Ag, Sb ($\rho = 0.52 - 0.83$). The metal diversity at the Industry site was clearly evidenced by the leaf elemental concentrations, which were also depicted in the measured magnetic properties (Figure 5.29).

Table 5.12 - Mean (in grey) and standard deviation of magnetic properties and ratios measured from the collected exposed ivy leaves (0, 3, 7.5 weeks) across the different monitoring sites (B – Background, R – Road, T – Train, S – Shipping, I – Industry).

	$\chi_{LF} \times 10^{-8}$ (m)		ARM _{200/500} (μ A)		ARM _X $\times 10^{-8}$ (A m ⁻¹)		SIRM (μ A)		IRM ₃₀₀ (μ A)		HIRM (μ A)		S-ratio (-)		SIRM/ χ_{LF} (A m ⁻¹)		ARM/SIRM $\times 10^{-3}$ (-)		
B	0	-2.4	0.6	0.5	0.0	0.1	0.0	5.7	0.8	5.3	0.8	0.21	0.05	0.93	0.02	-250.7	79.5	82.8	14.9
	3	-2.5	1.1	0.7	0.3	0.2	0.1	9.2	5.0	8.4	4.7	0.38	0.17	0.91	0.02	-347.5	101.2	73.4	7.8
	7.5	-2.9	0.7	1.0	0.3	0.2	0.1	14.8	6.2	13.7	5.6	0.57	0.26	0.92	0.01	-501.0	188.7	69.4	9.4
R	0	-2.4	0.6	0.7	0.1	0.2	0.0	9.6	3.1	8.7	2.8	0.42	0.10	0.91	0.01	-432.3	218.2	80.5	19.8
	3	-2.5	0.6	0.8	0.2	0.2	0.0	11.2	3.2	10.4	3.1	0.45	0.12	0.92	0.03	-480.3	223.8	73.2	10.7
	7.5	-2.2	0.7	1.1	0.4	0.3	0.1	17.0	6.2	15.9	5.8	0.58	0.24	0.93	0.01	-797.8	244.4	65.4	5.4
T	0	-2.4	0.4	0.5	0.1	0.1	0.0	5.3	1.9	4.7	1.8	0.30	0.09	0.88	0.02	-219.0	49.0	88.6	12.5
	3	-2.1	0.4	0.6	0.1	0.2	0.0	11.0	2.4	10.5	2.2	0.28	0.15	0.95	0.02	-565.3	230.4	58.9	4.2
	7.5	-2.2	0.4	1.2	0.2	0.3	0.1	23.2	3.5	22.3	3.2	0.44	0.32	0.96	0.02	-1115.5	405.3	52.7	6.1
S	0	-2.7	0.6	0.5	0.1	0.1	0.0	6.7	3.0	6.2	3.1	0.26	0.05	0.91	0.04	-251.3	123.1	85.7	18.0
	3	-2.1	0.8	1.4	0.4	0.3	0.1	24.5	8.7	22.7	8.1	0.91	0.35	0.93	0.01	-1305.5	566.4	58.0	6.4
	7.5	-2.1	0.7	1.9	0.5	0.5	0.1	26.4	7.1	24.7	6.6	0.84	0.26	0.94	0.01	-1358.5	565.4	73.8	7.1
I	0	-2.3	0.4	0.7	0.1	0.2	0.0	11.3	3.0	9.9	2.9	0.68	0.10	0.87	0.03	-514.3	199.5	63.6	10.6
	3	-2.1	0.5	0.9	0.2	0.2	0.1	15.3	5.2	14.2	4.8	0.58	0.22	0.92	0.01	-789.3	484.6	56.9	4.9
	7.5	-2.1	0.6	1.4	0.2	0.4	0.1	22.4	6.0	20.8	5.5	0.82	0.29	0.93	0.01	-1140.2	402.4	64.5	7.7

The relationship between leaf-accumulated Fe and their leaf SIRM was less evident in comparison with the relationships observed for the atmospheric filters (§5.1.3.5). Leaf SIRM was not a linear consequence of the accumulated Fe at the Background, Road and Industry sites ($p > 0.065$), whereas linear associations ($p < 0.04$) were observed from the Fe-SIRM scatterplot for the Train ($R^2 = 0.29$) and Shipping sites ($R^2 = 0.31$) (Figure 5.30). Most environmental magnetic studies do not investigate associations between magnetic properties and the enrichment in elemental Fe, and the ones that do investigate it often refer to a single specific type of PM pollution, such as road traffic (Maher et al., 2008; Yang et al., 2010), or to a general urbanized study area (Urbat et al., 2004; Wang et al., 2017), and not across different PM source types. Therefore, it is difficult to compare our results, in which the occurrence/absence of linear Fe-SIRM relationships appears to depend on the monitored PM source type, with other studies. Despite routinely done in biomonitoring studies (e.g., De Nicola et al., 2015; Sawidis et al., 2011; Tretiach et al., 2011), assessing elemental Fe does not reveal the contribution of Fe oxides or others that have ferro(i)magnetic characteristics (§3.1.3.2, §5.1.3.5).

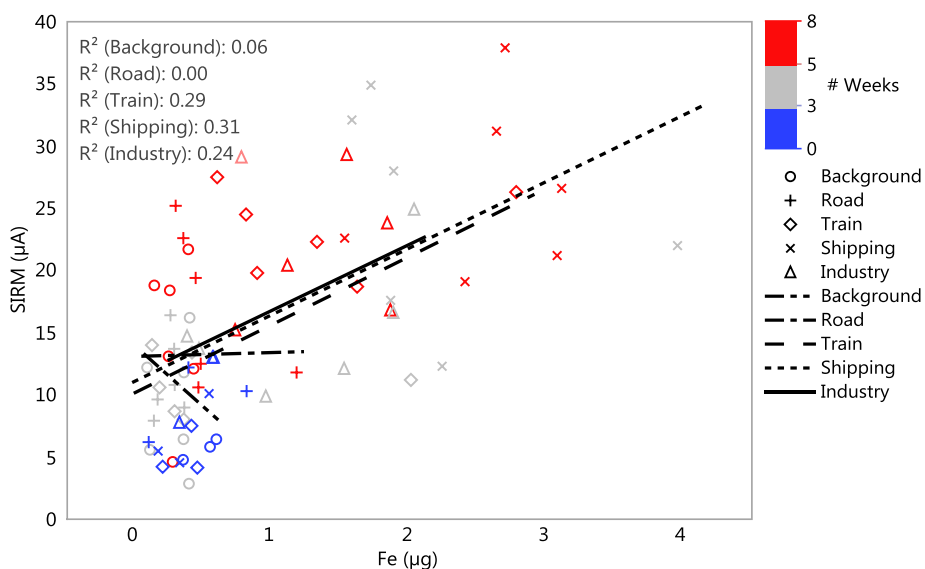


Figure 5.30 – Scatterplot with linear fits (R^2 are given) of SIRM (μA) as a function of elemental Fe (μg) deposited on the ivy leaves exposed at the monitoring sites (Background, Road, Train, Shipping, Industry). Site observations are shown in different symbols (see plot legend), and in colors according to the exposure period (0, 3, 7.5 weeks).

5.3.3.4 Comparison between leaves and filters

The PMF sites were monitored continuously with Leckel PM samplers, yielding daily PM-loaded filters (Chapter 5.1), and by means of active leaf monitoring, for which co-located ivy leaves were collected at the middle and at the end of the exposure period, in addition to pre-exposure leaves. A linear association ($R^2 = 0.74$) was found between the mean leaf SIRM values and the cumulative PM₁₀ filter loads (i.e., summed from the start of the exposure period), considering the different monitoring sites together (Figure 5.31). This seems to corroborate the usefulness of measuring leaf SIRM as a proxy for atmospheric PM concentrations, as it has been reported before (Hofman et al., 2014b; Mantovani et al., 2018; Mitchell and Maher, 2009). Whether or how the observed association might differ across different sites or PM sources could not be clarified in this experiment design.

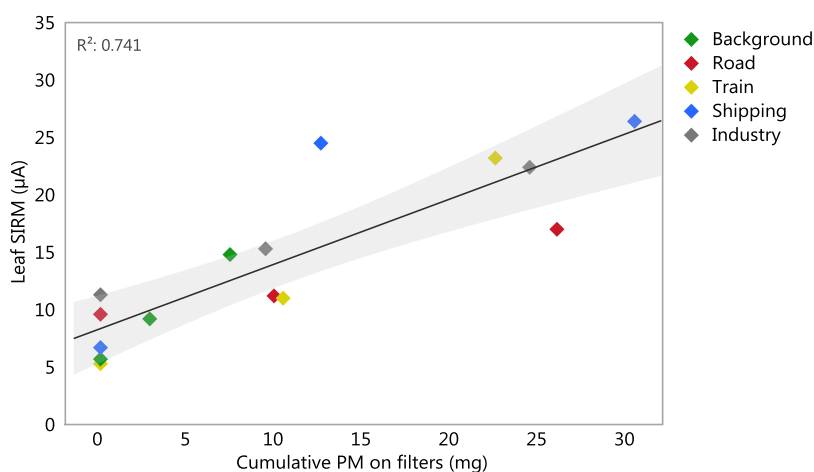


Figure 5.31 – Scatterplot of mean leaf SIRM values against the corresponding cumulative atmospheric PM (mg) collected on the daily PM filters, including all monitoring sites (Background, Road, Train, Shipping, Industry). Black line indicate the linear regression (R^2 is shown) with 95% of confidence (in grey).

Highest magnetic concentrations were measured for the Shipping, Train and Industry leaves. Comparing this outcome with that from the filter samples, the only difference appears to be for the Shipping site. The filters from the Shipping had the lowest SIRM values, whereas the co-located leaves had the highest SIRM. Although the between-

leaves variability for the same exposure conditions was still higher than desired (Table 5.12), which hampers statistical site-comparisons, this might be due to in-wax accumulation of particles at that site. The plants exposed at the Shipping were the least sheltered from the weather conditions (Figure 5.3), without any nearby vegetation or infrastructure that could reduce e.g. the wind speed. Weekly visits to all PMF sites also confirms the Shipping site was the windiest and harshest. Whilst wind can remove surface deposited PM from the leaves (Cai et al., 2017; Terzaghi et al., 2013) wind stress promotes cuticle wax regeneration (Hoad et al., 1992; Neinhuis et al., 2001), which might result in the encapsulation of deposited PM. It should also be noted that, on average, the highest atmospheric PM concentrations were measured at the Shipping site. To understand why this was depicted by the leaf SIRM rather than by the filter SIRM values is a question that remains.

5.3.3.5 Leaf accumulation surfaces

SEM images of the 0w leaves, i.e. prior to the exposure campaign, showed that these leaves were not exempt from deposited particles on their surface. These leaf-accumulated particles may have been derived from the use of pesticides, fertilizers or other operations (e.g., planting, dust resuspension) over time at the plant nursery center, in which plants were also sheltered from wash-off effects due to rain. The particles' elemental content was not only related with natural PM sources, but also elements of high Z number, such as metals, were evident from the BSE obtained images (Figure 5.32). For this reason, the magnetic values measured for these 0w leaves were not zero. This observation, which was less evident in the previous experiment of Chapter 4, demands that plant leaves prior to the start of the monitoring campaign should always be considered in atmospheric monitoring studies. Dedicated leaf particle-analysis using SEM, as described in Chapter 2, was not applied to these samples, so the quantity and composition of surface leaf-deposited particles across the different sites were not estimated.

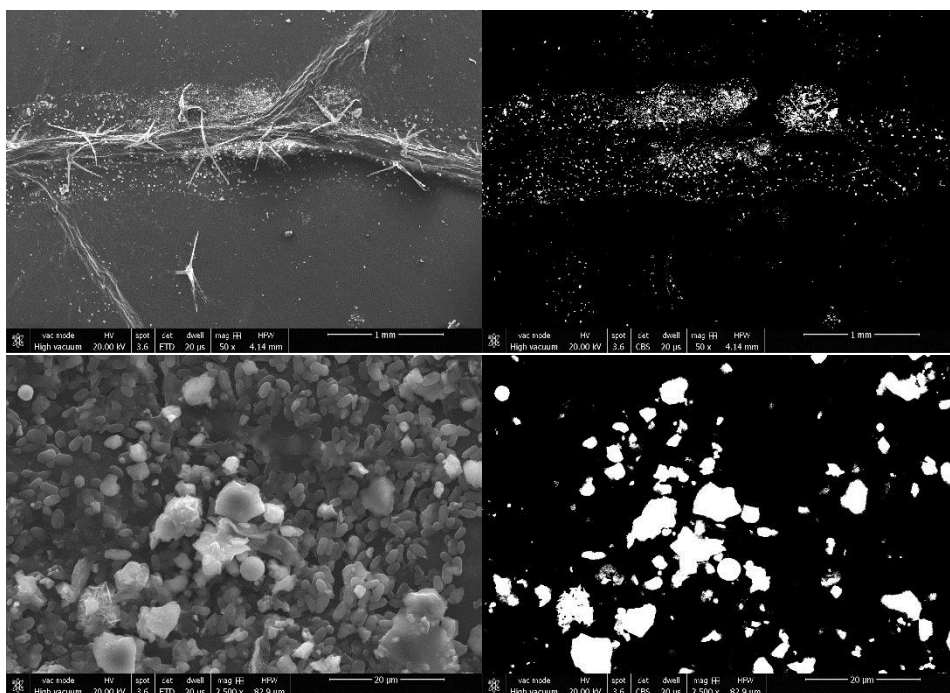


Figure 5.32 – SEM images from ivy leaves prior to the exposure campaign (0w), using the secondary (SEI; left) and the backscattered (BSE; right) electron detectors. Indicated scale is 1 mm and 20 µm for the top and bottom images, respectively.

The artificial SEM stubs exposed at the PMF sites during the entire monitoring period offer the advantage that, compared to plant leaves, they start from a zero accumulation point. SEM images from these surface matrices revealed the lowest particle accumulation at the Background site, whereas the highest accumulation in anthropogenic particles (i.e., in high Z elements; BSE images in Figure 5.33) was registered at the Industry and Shipping sites. While biological-derived PM, namely pollen (Punt et al., 2007), was visible at the stub exposed in the Background site, surrounded mainly by pine trees, more irregular shaped and sized particles were found at the Road site, including combustion-derived particles (Figure 5.34).

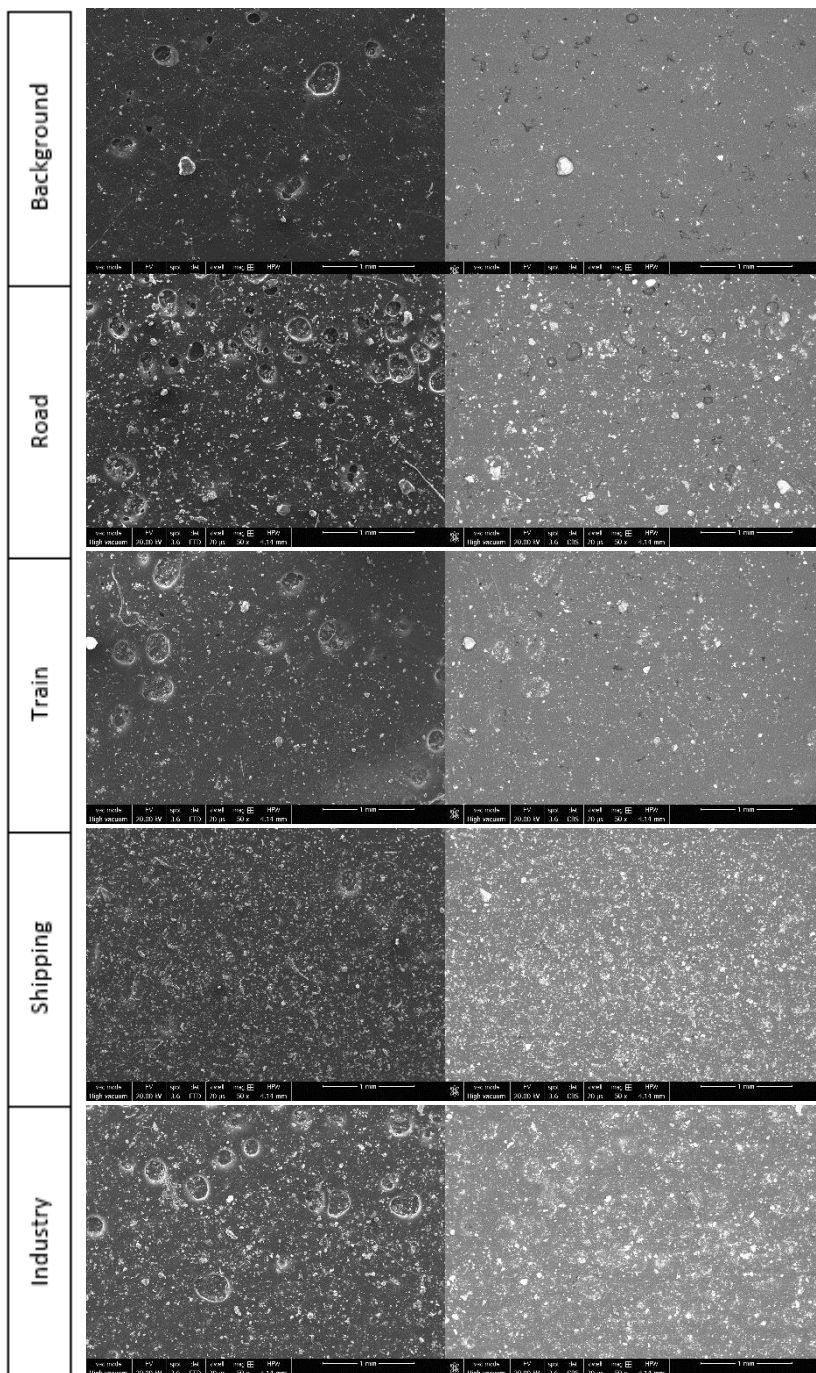


Figure 5.33 – SEM images (magnification of 50x) from artificial stubs exposed at the PMF monitoring sites, using the secondary (SEI; left) and the backscattered (BSE; right) electron detectors.. Indicated scale is 1 µm. Bright particles in BSE reveal high Z elements, such as metals.

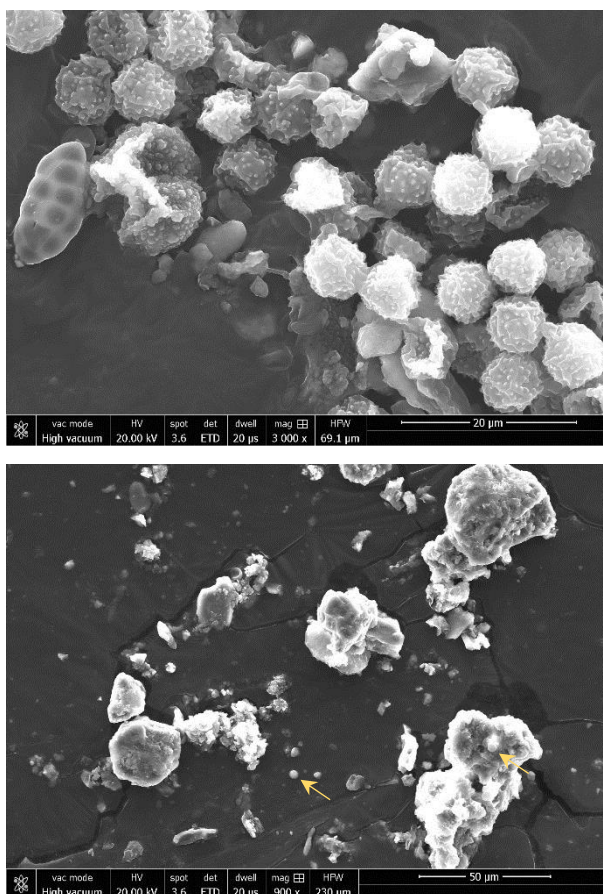


Figure 5.34 – Example of biological PM (pollen) and road traffic PM deposited on the artificial stubs at the Background (top; magnification of 3,000x) and Road (bottom; magnification of 900x) monitoring sites, respectively. Arrows indicate small spherical particles (likely combustion-derived) at the Road stub. Indicated scale is 20 µm and 50 µm for the top and bottom (secondary electron; SEI) images, respectively.

5.3.4 Conclusions

Our results showed that active leaf monitoring of atmospheric pollution at the source-specific PMF sites is useful to obtain time-integrated measures of local atmospheric PM. The measured leaf SIRM showed a good linear association with the cumulative atmospheric PM collected by conventional PM samplers. Although the accumulation of PM on the exposed leaves was not very substantial in terms of total elemental mass, the proportion of metal and magnetic particles increased with exposure time, which indicates the leaf collection/accumulation of anthropogenic PM.

The elemental profiles of exposed leaves were overall consistent with the results previously observed for the atmospheric PM-loaded filters (§Chapter 5.1), and magnetic properties and ratios in this study also indicated the dominance of low-coercivity minerals, as observed in Chapters 4 and 5.1. Combining the application of leaf monitoring with artificial surface matrices passively collecting PM, as the SEM stubs used in this study, appeared useful to grasp on the PM accumulation levels across the different monitoring sites, and is encouraged to be applied in future source fingerprinting studies.

Chapter 6

General conclusions and future perspectives

“Research is formalized curiosity. It is poking and prying with a purpose”

-- Zora N. Hurston

6.1 Research objectives

The overall objective of this PhD research was to gain insights in order to develop a biomagnetic monitoring approach for fingerprinting atmospheric particulate matter in urban settings. To achieve that purpose, the following specific research objectives were engaged:

1. Characterization of major urban source types of PM pollution:
 - a. by means of magnetic, chemical and microscopic techniques, to obtain source-specific magnetic, chemical and morphological PM fingerprints;
 - b. in terms of pro-inflammatory response and oxidative stress potential, to explore the associated health-risk potential.
2. Investigation of potential associations between source-specific magnetic, chemical and morphological PM fingerprints.
3. Evaluation of leaf biomagnetic monitoring as a strategy to infer atmospheric PM levels and characteristics of major PM contributing sources.

Hereafter, these research objectives are discussed in more detail, in light of the conducted research and results obtained throughout this PhD.

6.2 Fingerprinting urban PM sources

The atmospheric world above us comprises an intricate mixture of particulate matter with a wide range in e.g. size and composition, which depend on the emission sources and can vary greatly over time and space (Guevara, 2016; Van den Bossche et al., 2015; Vercauteren et al., 2011). To properly monitor the ambient air quality is particularly challenging in heterogeneous, multi-source urban environments. Local PM variations are rarely detected by air quality monitoring stations, due to their low number and subsequent low spatial resolution (PM concentrations are monitored by 69 stations in Belgium, one station for each 439 km² of land area; www.irceline.be/en). Furthermore,

gravimetric-based monitoring, as typically performed in conventional air quality stations, provides an incomplete representation of PM since e.g. size distribution and chemical composition are not considered. The effective fingerprinting of urban PM sources, if attainable, would enable the identification and quantification of local PM sources, and potentially contribute to the improvement of monitoring strategies and implementation of mitigation policies. Magnetic monitoring is a growing application in the field of environmental monitoring (Hofman et al., 2017), and can supplement commonly used analytical techniques (such as ED-XRF, ICP-MS, SEM/EDX) in the process of characterizing PM on sites exposed to different conditions. Throughout this PhD research, the investigation of site- or source-specific PM fingerprints was carried out using several methodologies, often in combination.

In Chapter 2, particle analysis of PM deposited on ivy leaves across different environments was done using computer controlled SEM/EDX. The physicochemical features measured on ca. 40,000 leaf-deposited particles from low-polluted (forested and rural) and high-polluted sites (under the influence of road and railway traffic, and of a metal industry) revealed both common and site-specific PM₂₋₁₀ characteristics. Elements associated with natural PM sources (e.g., Si, Ca, Al, Na) were the highest composition contributors at the low-polluted sites, whilst health-concerning metals such as Pb, As, Cu and Zn highly enriched the leaf-deposited particles near the metal recycling plant. Leaves subjected to road and railway traffic showed the most alike composition fingerprints, with high and equivalent enrichment in Fe, an element linked with both combustion- and abrasion/friction-emissions processes, in addition to crustal matter (McIntosh et al., 2007; Rai, 2013). Although this study considered only the fraction of PM₂₋₁₀ particles, the size distribution was, across all monitoring sites, biased towards the small-sized particles, which are often connected with adverse health effects (Harrison and Yin, 2000). And the fact that metal enrichments were two to three times higher for the small-sized particles than for the coarse fraction, especially for road and railway particulates, illustrates the health relevancy of small-sized PM. The leaves analyzed by SEM/EDX for their surface deposited PM were additionally measured magnetically, in Chapter 3.1, with leaf SIRM pinpointing railway

and industry exposed-leaves as the ones accumulating the highest concentrations of magnetic particles. Significant associations found between leaf SIRM and a range of trace metals (Fe, Cu, Zn, Cd, Pb, and Mn) on the accumulated leaf particles, corroborates the use of leaf SIRM as an overall indicator of atmospheric metal pollution (Maher et al., 2008; Moreno et al., 2003; Yin et al., 2013; Zhang et al., 2012).

The joined methodology of leaf SIRM and SEM/EDX particle analysis, established in Chapter 3.1, was extended to a large-scale European campaign (in the context of COST Action FP1204 “Greeninurbs”; www.greeninurbs.com) across 20 different cities, described in Chapter 3.2. Leaf samples from a single, common, deciduous tree species (*Platanus x acerifolia*) were collected at the end of the growing season, from trees located close to a heavy-trafficked street and within a urban park, for every participating city. Common regional background PM composition and concentration were observed across the 20 investigated cities, while certain local conditions, such as the influence of e.g. salt aerosol sources (Malmö, Salzburg, Aveiro) or a dry continental climate and arid steppe landscape (Yerevan), were possible to identify from the combined elemental and magnetic results. The validation of this combined methodology by monitoring leaf-deposited atmospheric PM across different countries and climate types, demonstrated the fingerprinting potential of this approach.

Lastly, a PM fingerprinting campaign (Chapter 5), that we called PMF project, was set up to comprehensively characterize urban PM sources of interest in the region of Antwerp, Belgium. This project comprised, among others, simultaneous atmospheric PM sampling (as performed by air quality stations) and leaf monitoring (using ivy leaves) for an uninterrupted period of seven and a half weeks at five different monitoring sites. These sites were selected to represent as much as possible conditions of road, railway and shipping traffic, in addition to the previously studied metal recycling plant and a background site. Daily atmospheric PM₁₀ filters were analyzed gravimetrically, chemically and magnetically, using a combination of analytical methods. Atmospheric PM₁₀ concentrations, that were always below the European reference value (50 µg m⁻³), had mean values decreasing in the order shipping > road

> industry > train. The main governing elements were Na, Fe, Ca, K, and Mg, with the industry site presenting the highest concentrations and the most diversified metal profile, including Pb, As, Ag, Sb, Mn. The composition profiles for road and train sites were similar, in agreement with the observations previously obtained from ivy leaves exposed at sites with road and railway traffic as prevalent polluting sources (Chapters 2 and 3.1). The shipping site could be considered as in between those two source types (road and railway traffic, and industry).

The magnetic site-fingerprinting was less straightforward than the chemical-based characterization, with all magnetically measured samples being dominated by low-coercivity minerals with grain sizes ca. between 0.1 and 5 μm , across all sites. Filter SIRM results, that decreased in the order train > industry > road > shipping, did not reflect the measured PM_{10} concentrations; instead, SIRM was best linked with the content in Fe, especially for road and railway traffic ($R^2 > 0.90$). The leaf monitoring results were overall in accordance with the filter results, both chemically and magnetically, with a particular exception: the highest mean leaf SIRM was measured at the site with the highest PM_{10} concentration, i.e. the shipping, for which, in contrast, the lowest mean filter SIRM was obtained. To understand why the site-order PM_{10} concentrations were depicted by the leaf SIRM rather than by the filter SIRM values is a question that remains.

6.3 Source apportionment techniques

The panoply of urban PM sources intermingled in the atmosphere complicates their individual fingerprinting and subsequent apportionment. Multi-approach monitoring studies of atmospheric PM deliver valuable information in terms of source signatures, and their similarities and dissimilarities, as it was demonstrated throughout this PhD research. A compendium of the methodologies used and their main considerations (advantages, limitations, ...) is presented in Table 6.1. Main outcomes and suggested improvements to the methodologies and techniques employed throughout this research can be found in the corresponding chapters.

In terms of methodology, SEM/EDX analysis appeared a useful approach to gather information on large quantities of leaf-deposited particles. The automated detection and analysis of particles should be matter of further investigation though, as the accuracy of this procedure (e.g. in terms of thresholds used), and subsequent analytical outcomes, was not examined yet. To analyze the same leaf samples repeatedly can elucidate about this methodology reproducibility, as well as repeating it using different sets of threshold values for the detection of particles.

Magnetic leaf SIRM measurements demonstrated great potential to discriminate between source types (Chapter 3.1) or local variations between streets and urban parks across 20 European cities (Chapter 3.2), confirming biomagnetic monitoring as an effective source apportionment tool (Hofman et al., 2017). The exposure of plant leaves to atmospheric conditions leads to the invariable accumulation of magnetic particles, which are ubiquitously present in PM. This magnetic enrichment over time was noticeable too for background sites, distant from urban PM polluting sources, and it was higher for higher levels of anthropogenic pollution (Chapters 4, 5.1, 5.3). Leaf SIRM serves as a reliable source apportionment tool when comparing sites that are primarily exposed to known, single specific sources. In such cases, which is the majority in enviromagnetic studies (e.g., Matzka and Maher, 1999; Moreno et al., 2003; Rai et al., 2013), leaf SIRM is interpreted in relation to the SIRM values measured at the other sites. This should not be considered a flaw of the methodology, as it happens for all analytical methodologies; metal enrichment or gravimetric concentrations (i.e., legislated approach), and also leaf SIRM, are considered large or small depending on the sampling pool in which they stand. The identification of source types from absolute SIRM (or metal concentration, PM concentration, ...) values seems thus unrealistic. Yet, to gain insight on the associations between magnetic properties and physicochemical properties of PM, and other associated pollutants (such as PAHs, NO_x), may aid in developing more comprehensive source apportionment strategies. Throughout this research, SIRM was positively correlated with atmospheric PM mass, Fe content and a range of trace metals (Chapters 2, 3.1, 3.2, 5.1, 5.3).

The compilation of microscopic, elemental and magnetic data in order to build sound source-specific PM signatures is a key challenge, as PM does not stay unaltered and confined to the point emission sources. Multivariate data analysis techniques, such as principal component analysis (PCA), are essential to explore multi-approach datasets in an attempt to investigate potential relationships and patterns, that might be source-specific. PCA was often applied to the datasets gathered during this research, allowing to identify both common and site-specific PM characteristics. In a step forward, predictive and classification models were used to evaluate which PM variables had the most discriminatory potential, and how they performed in source apportioning PM. Random Forest (RF) models to predict the environment or source type (forest, rural, road, train, industry) of leaf-deposited PM based on the particle morphology, size and elemental composition, were satisfactory, with a generalized R^2 of 0.83 and a misclassification rate of 0.28 (Chapter 2). Still, the classification accuracy (CA) varied between 36% and 51%, meaning that in the best case scenario about half of the leaf-deposited particles were correctly attributed to their source type.

From the PMF filters dataset (Chapter 5.1), RF models were built considering solely the atmospheric PM_{10} concentrations (as regularly monitored by air quality stations), the elemental concentrations and the magnetic properties, as well as all possible combinations. To include all information (PM and elemental concentrations, magnetic properties) improved the model predictive power ($R^2 = 0.88$, misclassification rate of 0.03) compared to considering only the PM concentrations, with CA increasing from 25% to 76% up to 92% to 100%. The measured magnetic properties were accountable for 16% of the decision tree splits in the RF model, whilst the elemental concentrations remained the main classification predictors. Gravimetric PM concentrations contributed only 1% to the site classification, suggesting once more that conventional gravimetric-based PM monitoring has little power to discriminate between sampling locations mainly exposed to distinct PM sources. This discrimination can better be achieved by complementing traditional air quality monitoring systems with elemental and magnetic information, from which magnetic analyses are more time- and cost-effective than chemical determination.

Table 6.1 - Summary of considerations (deliverables, advantages, limitations, used medium, cost) on the analytical methods used throughout this PhD research for monitoring and fingerprinting atmospheric PM. From the performed room-temperature magnetic measurements, SIRM was the most used and is presented as a stand-alone methodology, as magnetic analyses is a vast topic. Cost is rated from “€” to “€€€€€”, from lower to higher costs in terms of main instruments.

Method	Deliverables	Advantages	Limitations	Medium	Cost
Air-pumped gravimetric	– Mass and concentration of PM within certain size	– Standardized and regulated method – Daily-averaged values – Possibility to investigate different size fractions (PM ₁₀ , PM _{2.5} , PM ₁) – Non-destructive	– Laborious filter pre-and post-weighing – No indication of composition – Biased towards high-mass PM (e.g. crustal) – Time-consuming maintenance – Electricity-powered sampling	– Filters: common approach used across air quality monitoring stations – Leaves: N. a.	€€
SIRM	– Magnetic concentration indicator	– Very simple sample preparation – Cost and time-effective – Many media possible – Association with metals and PM – Non-destructive – Environment-friendly	– No fixed relationship with PM concentrations, as it looks rather to composition – Less commonly used than chemical/gravimetric methodologies	– Both filters and leaves – Leaves: can be dried or fresh	€€
SEM/EDX	– Visualization – SE/BSE images – Morphology and elemental composition of individual particles	– Simple sample preparation for filter/leaves – Small sample size required – Qualitative/quantitative deliverables depending on the research goals	– Expensive – Limited access – Trained user required – Time-consuming particle analysis – Reproducibility of quantification uncertain	– Filters: quartz fiber filters do not allow PM visualization – Leaves: need to be dried and coated for high-vacuum	€€€€€
ED-XRF†	– Elemental concentrations	– Commonly used by regulatory air quality networks – Non-destructive	– Spectra need to be quantified to obtain concentrations – Require a thin-film approximation	– Filters: large Si spectra in quartz filters prevent estimation of Si, Al – Leaves: thin-film approximation not possible	€€€
HR-ICP-MS†	– Elemental concentrations	– Commonly used methodology	– Destructive – Not environmental-friendly	– Both filters and leaves	€€€€
Mobile sensors	– PM concentrations, particle counts	– Low-cost options – Real-time measurements – Portable measurements	– Reliability uncertain – Reliable sensors are costly – Maintenance and sensitivity	– Filters/leaves: N. a.	€ to €€€€

† Analytical methodologies used mainly through collaborations.

N. a.: not applicable.

From the PM sites/sources investigated throughout this research, discriminating between road and railway traffic was the most difficult task, because they showed very comparable elemental profiles, on both filter- and leaf-collected PM. Specifically the metal signatures of road and traffic were much alike, including in terms of Fe content. Magnetic concentration-indicators, such as SIRM, were key to separate those two sources (train > road), which, bearing in mind their similar Fe content, suggests different magnetic signatures. Ferro(i)magnetic Fe particles are the main contributors to magnetic remanence measurements, whereas SEM/EDX, ED-XRF and HR-ICP-MS only measure elemental Fe. Therefore, it was hypothesized that different Fe chemical structures, in terms of mineralogy or partitioning in metallic Fe vs. iron oxide (Muxworthy et al., 2002, 2003; Revuelta et al., 2014; Sagnotti et al., 2009), could explain the equal Fe content vs. different SIRM responses. Although abrasion at railway tracks and car disk brakes, and releases from diesel and gasoline exhaust pipes, have been associated with distinguishable magnetic features (Kim et al., 2007; Moreno et al., 2014; Sagnotti et al., 2009), the range of magnetic analyses performed during this research were not able to clarify this knowledge gap on the road/railway apportionment. Railway traffic conditions revealed, across the different studies presented in this PhD thesis, higher magnetic enrichment in comparison to road traffic. The fact that the highest pro-inflammatory response potential was also measured for railway samples, along with shipping, encourages future research on railway emissions and exposure.

6.4 Applicability of leaf magnetic monitoring strategies

Atmospheric dust deposition on plant leaves enables the collection of site-specific PM. Still, the underlying dynamics of leaf particle accumulation should be considered for the development of leaf biomagnetic monitoring of atmospheric PM. A leaf-level comprehensive analysis of atmospheric dust accumulation was carried out throughout a period of three months, considering two plant species (ivy, *Hedera sp.*, and strawberry, *Fragaria sp.*) with distinct leaf macro- and micro-morphology. Plant species were exposed at the same moderate road traffic site, and leaves collected

every three weeks were analyzed for their magnetic signature, morphology and elemental content. Dust accumulation was observed both visually (SEM microscopy) and magnetically, while metal enrichment was limited and more variable over time. Ivy accumulated more dust (elements/magnetically/SEM) than strawberry leaves, even though strawberry leaves are characterized by the presence of long trichomes and a rugged micromorphology, which are considered important leaf traits to capture atmospheric dust. In addition to accumulating less, strawberry leaves also seemed to be more susceptible to wash-off effects. The magnetic enrichment (in small-grained, single/pseudo-single domain magnetite-like particles) was not species-specific, reflecting a common contributing source. Variations in terms of pollution contributions, meteorological phenomena, species-specific traits, particle deposition (and encapsulation) vs. micronutrients depletion, were discussed in light of the conducted monitoring campaign. Although not completely elucidative in the performed study, the multifactorial leaf dust accumulation process can better be understood through a combination of techniques (e.g. elements/magnetic/SEM).

Leaves and (quartz) filters were the two major medium collector types used to investigate atmospheric PM across different sites and conditions. The gravimetric-based filter approach is the standardized and legislated method for monitoring PM, thus, allowing for spatial/temporal comparisons. The main limitations of this gravimetric-based filter approach for PM source apportionment is that typically only a low spatial resolution can be achieved due to practical issues and financial limitations, and that PM mass is not source-specific. As PM is greatly influenced by meteorological conditions, gravimetric PM concentrations vary day by day, often consistently across different sites (gravimetric PMF results). Therefore, site or source comparisons based on daily-averaged PM concentrations should be done for similar days and over a period of time, to prevent source-specificities to be overlooked by seasonal/temporal effects.

Monitoring PM by means of plant leaves allows for high spatial resolution campaigns, as plants are relatively cheap, portable and adaptable, resilient to meteorological conditions, and require no electricity to sample the atmosphere in which they grow.

Therefore, each plant or leaf can work as an air quality monitoring station per se, enabling the separation of different environments and urban activities, as illustrated throughout this PhD research. Additionally, many citizen science projects (www.uantwerpen.be/nl/projecten/airbezen/; only in Dutch) based on leaf magnetic monitoring have been successfully carried out by the Environmental and Urban Ecology (EUREC-Air) research group.

To ally leaf monitoring strategies with magnetic measurements (time- and cost-effective, non-destructive and environmental-friendly) is thus encouraged as a reliable approach for the monitoring and source apportionment of atmospheric PM. Yet, several considerations must be taken into account, namely, concerning the time integration of pollutants (active or passive monitoring; evergreen vs. deciduous plants), species-specific traits (e.g., trichome density, cuticular wax) and plant availability in the area of study. In this PhD research, leaves of ivy and strawberry plants and of plane tree leaves have been used as PM sensors. From these, ivy plants are suggested as the overall best choice for future monitoring studies. On one hand, ivy is evergreen, allowing sampling throughout the year. Ivy is also quite resilient to harsh weather conditions, and commonly available in urban and non-urban environments in most of Europe, thus, it is also less prone to vandalism acts. Leaf age and pre-exposure conditions of ivy leaves should be taken into consideration and/or controlled depending on the research question at hand.

6.5 Future perspectives

Attempting to fulfill the initial objectives of this PhD research led to several additional questions along the way, while also a few issues remained unclarified. The distinction between road and railway traffic should be investigated further for their proportion in metallic iron and iron oxides, possibly by including low/high temperature magnetic measurements, Raman and Mössbauer spectroscopy. The high health-relevance of railway emissions revealed by the PMF project also encourages future research on railway pollution and derived health-effects. The collection of direct source-specific

dust samples (e.g., from railway tracks, car and ship exhaust pipes) in the PM pathway source-air-leaves, should be incorporated in future PM fingerprinting studies. Future research steps should comprise the analysis of dust samples, as well as of point time measurements obtained using mobile sensors including BC and UFPs and filter PAHs, collected and considered during the PMF project.

To strengthen the application of leaf magnetic monitoring as a source apportionment tool, large scale, high spatial resolution studies should be carried out. This should deliver more insights on how PM fingerprints behave spatially and in largely mixed, multi-source urban settings, and contribute to the development of this methodology to a point at which major PM sources can be pinpointed from urban samples of unknown background. Although leaves should not exclude the use of filters for monitoring PM, they offer the possibility to monitor sites or conditions (e.g. indoor vs. outdoor, along high-store buildings, or on non-urbanized, electricity-free sites) in which conventional PM sampling is not possible. Furthermore, the parallel investigation of both leaves and air-pumped filters may enable some type of intercalibration between both approaches, which will be eventually required to standardize leaf monitoring techniques for atmospheric PM.

Throughout this PhD research, elemental characterization and magnetic analyses were combined to apportion different environments and source types, and their discrimination was achieved rather successfully. Yet, the individual application of the magnetic properties and ratios used throughout this research would not be able to clearly recognize which PM source(s) are of most relevance at a certain site. To improve the magnetic characterization of source-specific PM, and link it with e.g. elemental concentrations, future research on the topic should incorporate additional magnetic parameters, such as thermomagnetic and hysteresis curves. Following a complete understanding of the magnetic composition, concentration and domain size of major PM sources, efforts would be necessary to identify or find potential magnetic source-specific indicators, if possible based on the magnetic properties most easily measurable. As it is sometimes difficult to study isolated PM sources in real life

conditions, it would be of interest to carry out PM fingerprinting campaigns (similar to the PMF project herein described) on controlled, artificially-generated PM, and study the relationships between specific PM composition, size and concentration, and the range of magnetic properties and ratios available.

Appendices

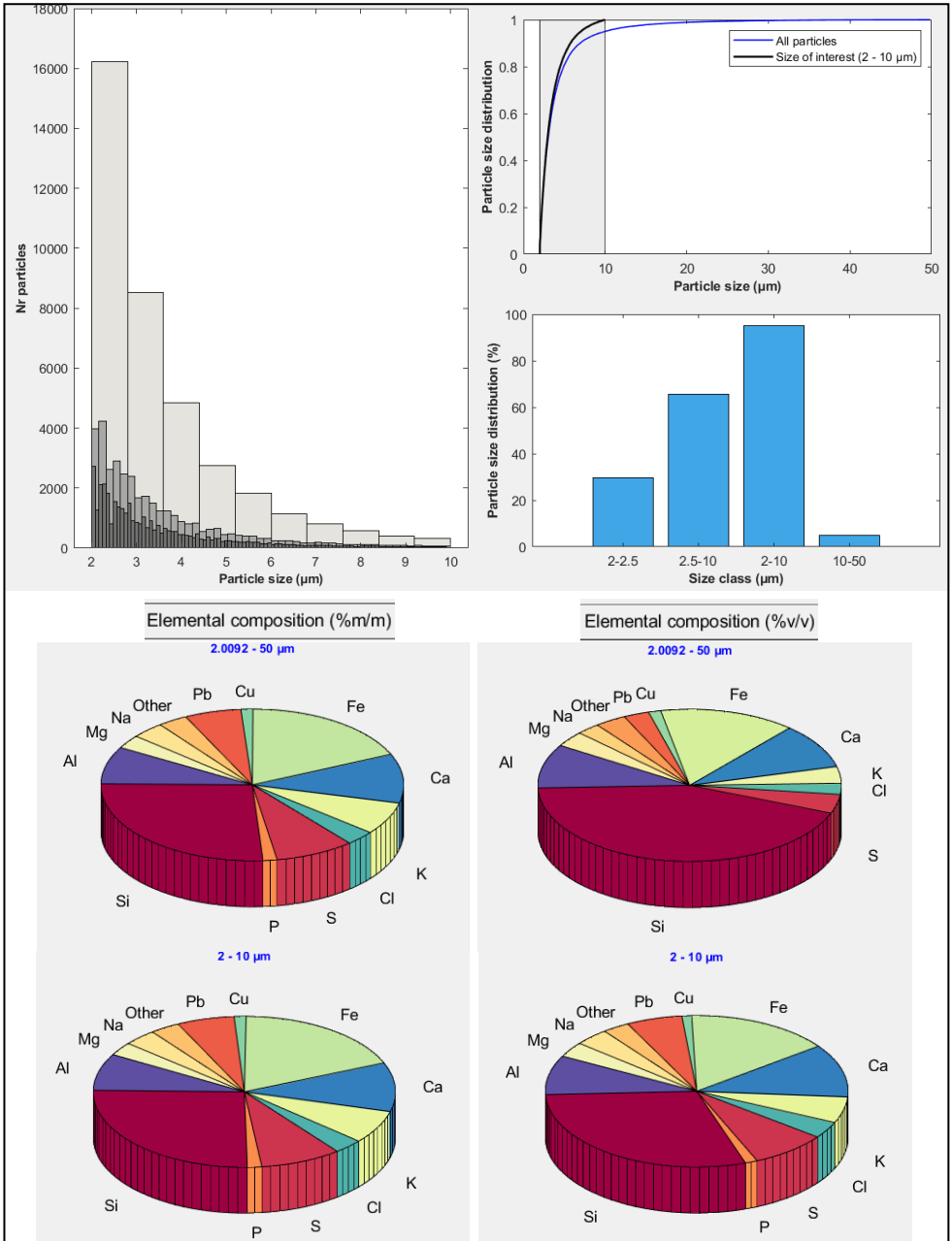


Figure A.1 - Illustration of particle size distribution and average elemental composition (in both weight (% m/m) and volume (% v/v) percentages) for the totality of analyzed leaf-deposited particles (PM₂₋₅₀) and for PM₂₋₁₀, as delivered by the developed MATLAB function scripts.

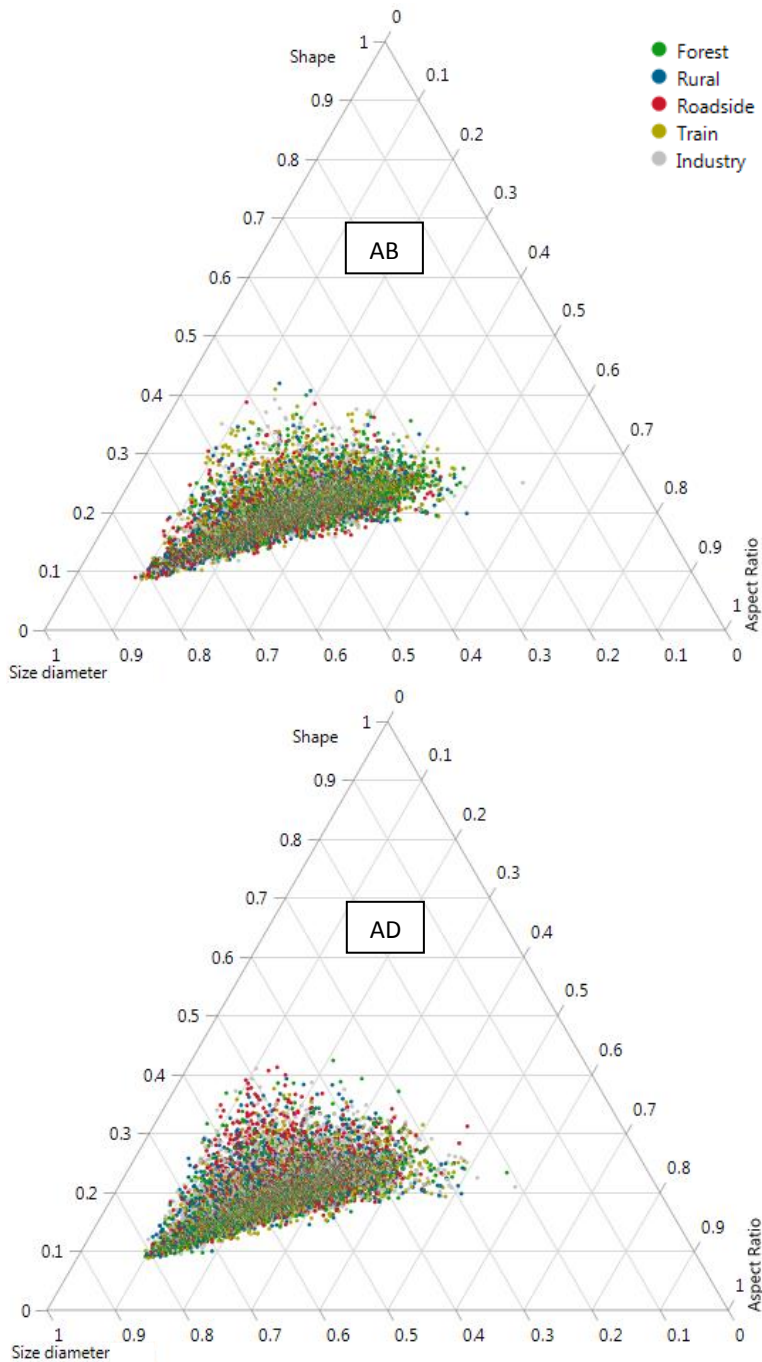


Figure A.2 – Ternary plots of particle size diameter, aspect ratio and shape (or circularity) of leaf-deposited PM_{2-10} on the abaxial (AB; top) and adaxial (AD; bottom) leaf sides, from all studied source types. All morphological information (size diameter, aspect ratio, shape) appears scaled from 0 to 1 to display the distribution and variability of analyzed particles, and each dot corresponds to an individual leaf-deposited particle. Particle size diameter ranged from 2.01 to 9.99 μm , aspect ratio from 1.05 to 14.73 and shape from 0.93 to 8.47.

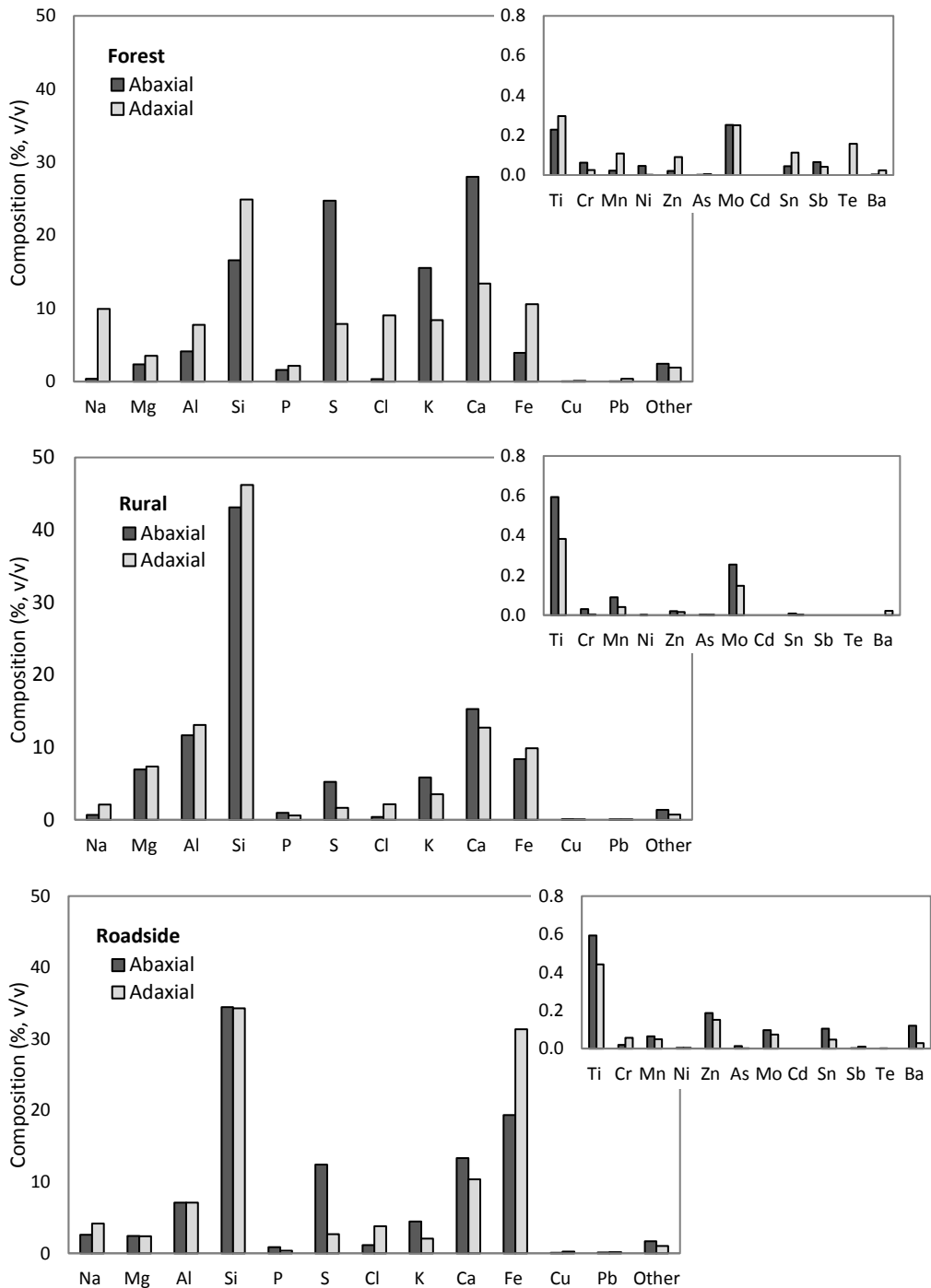


Figure A.3 – Weighted-volume percentages (% v/v) of the major elements and trace elements (inset) quantified on the leaf-deposited particles (PM₂₋₁₀) by SEM/EDX. The class “Other” include all other remaining elements that are not considered major elements, i.e. including the trace elements shown in the inset. The composition profiles consider separately the leaf-deposited particles found on the abaxial (dark grey) and adaxial (light grey) side of ivy leaves.

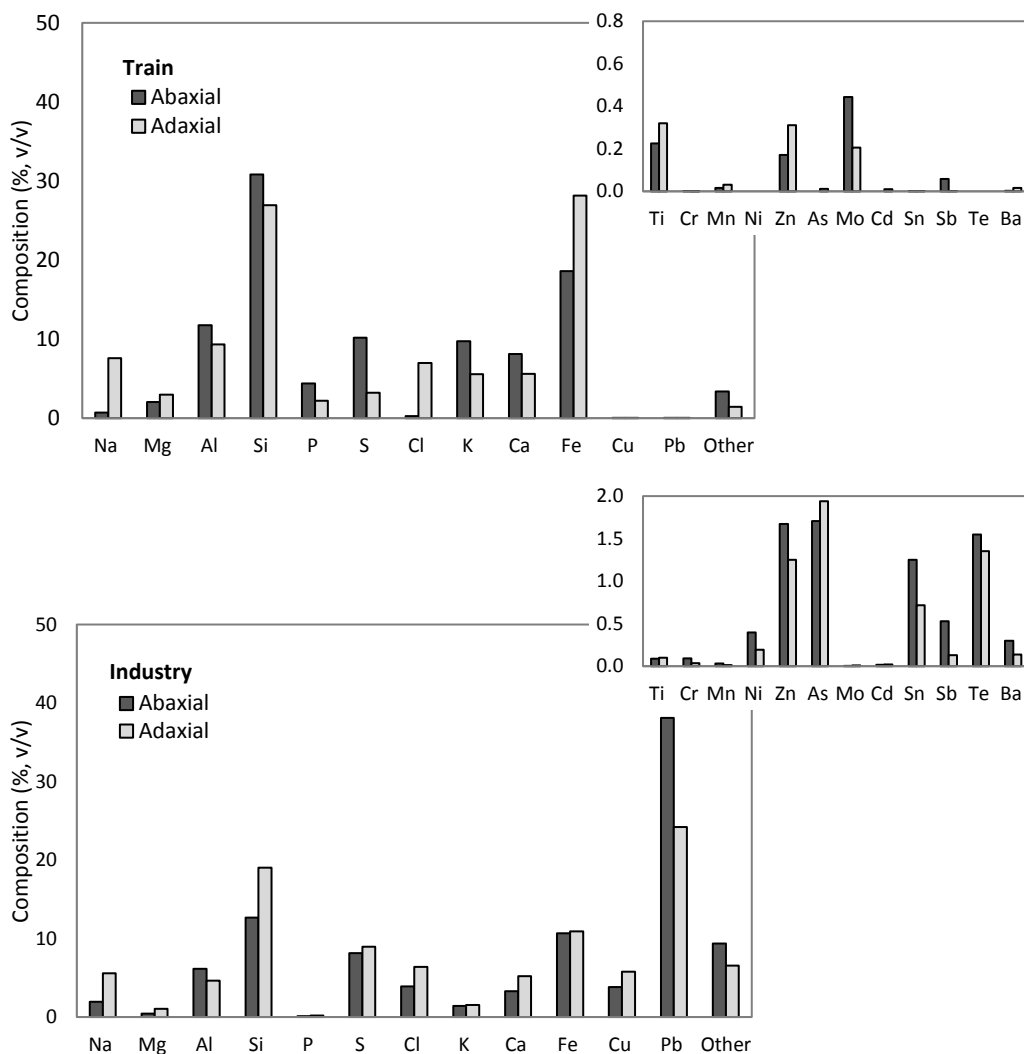


Figure A.3 – (continuation) Weighted volume percentages (% v/v) of the major elements and trace elements (inset) quantified on the leaf-deposited particles (PM_{10}) by SEM/EDX. The composition profiles consider separately the leaf-deposited particles found on the abaxial (dark grey) and adaxial (light grey) side of ivy leaves. The class “Other” include all other remaining elements that are not considered major elements, i.e. including the trace elements shown in the inset.

Table A.1 – Spearman’s correlation coefficients (ρ) on the elemental composition of leaf-deposited particles (% m/m; major elements) per source type. Significant associations are shown in bold ($p < 0.05$), with values < 0.005 indicated with “-”.

		Forest											
Rural	ρ	Na	Mg	Al	Si	P	S	Cl	K	Ca	Fe	Cu	Pb
	Na		0.26	0.17	0.12	0.17	-0.19	0.82	-0.12	-0.15	0.08	-0.01	0.01
	Mg	0.05		0.35	0.21	0.02	-0.21	0.26	-0.05	-0.14	0.27	-	-0.02
	Al	0.18	0.12		0.75	-0.15	-0.54	0.07	-0.17	-0.41	0.56	-	-0.02
	Si	0.03	-0.25	0.36		-0.22	-0.63	0.04	-0.30	-0.50	0.44	-	-0.01
	P	0.04	-0.08	-0.03	-0.19		0.11	0.24	0.26	-0.13	-0.10	-0.02	-
	S	0.04	-0.16	-0.14	-0.32	0.25		-0.15	0.22	0.64	-0.52	-0.06	-0.04
	Cl	0.53	0.09	0.14	-0.07	0.16	0.18		-0.09	-0.12	0.07	-0.03	-
	K	0.01	-0.01	0.44	-	0.22	0.26	0.04		-0.04	-0.28	-0.08	-0.05
	Ca	-	0.34	-0.29	-0.61	0.15	0.40	0.13	-0.03		-0.42	-0.08	-0.03
	Fe	0.01	0.04	0.38	-0.06	0.02	-0.05	0.12	0.12	-0.23		0.11	-
	Cu	-0.04	-0.06	-0.01	-0.11	-0.03	-0.02	-0.04	-0.11	-0.10	0.07		0.13
	Pb	-0.01	-0.02	-	-0.01	-0.01	-0.01	-	0.01	-	-0.01	-0.02	

		Roadside											
Train	ρ	Na	Mg	Al	Si	P	S	Cl	K	Ca	Fe	Cu	Pb
	Na		0.20	0.15	-0.04	0.01	0.15	0.57	0.13	0.21	-0.23	-0.09	-0.03
	Mg	0.13		0.38	0.10	0.01	0.15	0.10	0.35	0.25	-0.16	-0.04	-0.03
	Al	-0.10	0.49		0.50	0.08	-0.05	0.07	0.41	-	-0.08	-0.09	-0.02
	Si	-0.13	0.32	0.72		-0.06	-0.27	-0.08	0.18	-0.26	-0.28	-0.15	-0.02
	P	0.02	-0.24	-0.39	-0.45		0.11	0.07	0.07	0.10	0.01	-0.05	0.01
	S	0.10	-0.21	-0.45	-0.54	0.44		0.04	0.34	0.55	-0.26	-0.04	-0.01
	Cl	0.68	0.09	-0.21	-0.24	0.12	0.10		-0.06	0.13	-0.02	-0.01	-
	K	-0.23	0.03	0.16	-0.04	0.20	0.20	-0.24		0.27	-0.33	-0.17	-0.02
	Ca	0.17	-0.06	-0.26	-0.35	0.16	0.47	0.17	0.06		-0.38	-0.15	-
	Fe	-0.13	-0.01	0.01	-0.07	0.06	-0.25	0.01	-0.27	-0.14		0.20	-0.03
	Cu	-0.02	-0.03	-0.05	-0.04	-0.02	-	0.01	-0.08	-0.03	0.07		0.02
	Pb	-0.01	-0.02	-0.03	-0.03	-0.01	0.03	-	-0.02	-0.02	-0.03	0.13	

Industry	ρ	Na	Mg	Al	Si	P	S	Cl	K	Ca	Fe	Cu
	Na											
	Mg	0.21										
	Al	0.13	0.23									
	Si	0.15	0.21	0.51								
	P	0.01	0.03	0.01	-							
	S	0.16	-	-0.22	-0.20	-0.02						
	Cl	0.29	0.07	-0.05	-0.02	0.06	0.07					
	K	0.21	0.19	0.27	0.28	0.03	0.10	0.08				
	Ca	0.12	0.14	0.09	0.16	0.06	-0.01	-0.07	0.01			
	Fe	0.02	0.15	0.34	0.34	0.03	-0.20	-0.05	0.06	0.08		
	Cu	-0.07	-0.07	-0.06	-0.20	0.01	-0.09	0.31	-0.19	-0.17	-0.06	
	Pb	-0.24	-0.27	-0.33	-0.28	-0.03	0.02	-0.21	-0.10	-0.10	-0.35	-0.23

Table A.2 - Spearman's correlation coefficients (ρ) between the (not mass-normalized) magnetic properties measured on the PM-loaded filters (PM₁₀ filters comprise Road, Train, Shipping and Industry sites; PM_{2.5} filters comprise the Background site). Only statistically significant coefficients are shown ($p < 0.05$; $p < 0.01$ in italic).

Spearman's correlation ρ	χ_{LF} (-)	ARM (A m ⁻¹)	SIRM (A m ⁻¹)	SIRM/ χ_{LF} (A m ⁻¹)	
χ_{LF} (-)		0.81	0.83	-0.87	PM ₁₀
ARM (A m ⁻¹)	0.40		0.97	-0.97	
SIRM (A m ⁻¹)	0.42	0.80		-0.99	
SIRM/ χ_{LF} (A m ⁻¹)	-0.46	-0.79	-1.00		
	PM _{2.5}				

Table A.3 - Descriptive statistics (mean in grey; standard deviation as Std Dev; median, min and max values) of non-normalized magnetic properties and ratios from the daily PM₁₀-loaded filters (PM_{2.5} for the Background) across the different monitoring sites (B – Background, $n = 33$; R – Road, $n = 41$; T – Train, $n = 43$; S – Shipping, $n = 45$; I – Industry, $n = 45$).

	χ_{LF} x10 ⁻⁶ (-)	ARM x10 ⁻⁴ (A m ⁻¹)	SIRM x10 ⁻⁴ (A m ⁻¹)	SIRM/ χ_{LF} x10 ³ (A m ⁻¹)	
B	-6.65	1.54	1.54	-2.37	Mean
	0.15	0.44	0.44	0.98	Std Dev
	-6.66	1.49	1.49	-2.17	Median
	-6.91	0.89	0.89	-5.60	Min
	-6.19	2.70	2.70	-1.15	Max
R	-5.80	3.24	3.24	-8.59	Mean
	0.65	1.27	1.27	5.10	Std Dev
	-5.96	3.05	3.05	-7.53	Median
	-6.70	1.09	1.09	-29.39	Min
	-3.00	6.08	6.08	-1.79	Max
T	-5.96	3.44	3.44	-9.69	Mean
	0.66	1.80	1.80	8.89	Std Dev
	-6.14	2.88	2.88	-6.91	Median
	-6.65	1.38	1.38	-43.41	Min
	-3.17	7.61	7.61	-2.44	Max
S	-6.21	2.80	2.80	-6.18	Mean
	0.45	1.21	1.21	3.43	Std Dev
	-6.23	2.77	2.77	-5.70	Median
	-6.76	1.02	1.02	-16.62	Min
	-4.05	5.75	5.75	-1.52	Max
I	-6.11	3.36	3.36	-7.09	Mean
	0.37	1.58	1.58	3.99	Std Dev
	-6.24	2.77	2.77	-5.61	Median
	-6.69	1.68	1.68	-20.14	Min
	-5.15	8.38	8.38	-2.59	Max

Table A.4 – Spearman’s correlation coefficients (ρ) between considered variables (PM and elemental concentrations and magnetic properties, not mass-normalized) and the three main discriminant components from PCA analysis (PC1, PC2, PC3). Only statistically significant coefficients are shown ($p < 0.05$), with values in bold corresponding to the best association between each variable and the PCs.

Spearman’s correlation ρ	PC1	PC2	PC3
PM	0.74		0.22
Na	-0.42	0.41	0.53
Mg	-0.24	0.39	0.69
Al	0.83		0.22
Si		0.44	0.15
K	0.53		0.33
Ca	0.69	0.22	0.48
Ti	0.82		0.24
V	0.42		0.43
Cr	0.84	-0.16	-0.23
Mn	0.90		
Fe	0.90	-0.39	-0.19
Co	0.61	0.38	
Ni	0.44	0.53	0.27
Cu	0.66		-0.45
Zn	0.69	0.17	-0.21
As	0.46	0.33	-0.28
Rb	0.24		0.22
Sr	0.23	0.42	0.59
Mo	0.75	-0.39	-0.20
Ag	0.16	0.67	
Cd	0.54	0.37	-0.16
Sb	0.52	0.32	-0.27
Pb	0.50	0.44	
χ	0.82	-0.33	-0.19
ARM	0.90	-0.30	
SIRM	0.90	-0.39	-0.16
S-Ratio	0.16		-0.41
SIRM/ χ	-0.90	0.40	0.18
ARM/SIRM	-0.54	0.57	0.26

Table A.5 – Confusion matrices of predicted to actual observations for the training dataset, for the Random Forests based on the atmospheric PM₁₀ concentrations (“PM”), elemental concentrations (“Elem”), magnetic properties (“Magn”) and all possible combinations (i.e., “PM & Elem”, “PM & Magn”, “Elem & Magn”, “PM & Elem & Magn”). The classification accuracy (CA, ratio of correctly classified observations to the total of observations) per monitoring site is also included.

		Predicted				CA
Actual		Road	Train	Shipping	Industry	
PM	Road	5	5	5	5	25%
	Train	1	22	4	2	76%
	Shipping	0	7	23	2	72%
	Industry	0	6	3	15	63%
		Predicted				CA
Actual		Road	Train	Shipping	Industry	
Elem	Road	18	1	1	0	90%
	Train	0	29	0	0	100%
	Shipping	0	0	31	1	97%
	Industry	0	1	0	23	96%
		Predicted				CA
Actual		Road	Train	Shipping	Industry	
Magn	Road	8	6	6	0	40%
	Train	1	22	5	1	76%
	Shipping	0	3	28	1	88%
	Industry	0	4	7	13	54%
		Predicted				CA
Actual		Road	Train	Shipping	Industry	
PM & Elem	Road	18	1	1	0	90%
	Train	0	29	0	0	100%
	Shipping	0	0	32	0	100%
	Industry	0	3	0	21	88%
		Predicted				CA
Actual		Road	Train	Shipping	Industry	
PM & Magn	Road	13	4	3	0	65%
	Train	1	23	4	1	79%
	Shipping	0	3	28	1	88%
	Industry	0	1	3	20	83%
		Predicted				CA
Actual		Road	Train	Shipping	Industry	
Elem & Magn	Road	18	1	1	0	90%
	Train	0	29	0	0	100%
	Shipping	0	0	32	0	100%
	Industry	0	1	0	23	96%
		Predicted				CA
Actual		Road	Train	Shipping	Industry	
PM & Elem & Magn	Road	19	1	0	0	95%
	Train	0	29	0	0	100%
	Shipping	0	0	32	0	100%
	Industry	0	2	0	22	92%

Castanheiro, A., Samson, R., De Wael, K., 2016. Magnetic- and particle-based techniques to investigate metal deposition on urban green. *Science of the Total Environment* 571, 594–602.

Castanheiro, A., Joos, P., Wuyts, K., De Wael, K., Samson, R., 2019. Leaf-deposited semi-volatile organic compounds (SVOCs): An exploratory study using GCxGC-TOFMS on leaf washing solutions. *Chemosphere* 214, 103–110.

Castanheiro, A., *Hofman, J., Nuyts, G., Joosen, S., Spassov, S., Blust, R., Lenaerts, S., De Wael, K., , Samson, R., 2020. Leaf accumulation of atmospheric dust: biomagnetic, morphological and elemental evaluation using SEM, ED-XRF and HR-ICP-MS. *Atmospheric Environment* 221, 117082.

*Hofman, J., **Castanheiro, A.**, Nuyts, G., Joosen, S., Spassov, S., Blust, R., De Wael, K., Lenaerts, S., Samson, R., 2019. Impact of urban street canyon architecture on local atmospheric pollutant levels and magneto-chemical PM₁₀ composition: an experimental study in Antwerp, Belgium. *Science of the Total Environment*, 135534.

*Equal contribution

Baldacchini, C., **Castanheiro, A.**, Maghakyan, N., Sgrigna, G., Verhelst, J., Alonso, R., Amorim, J.H., Bellan, P., Bojović, D.Đ., Breuste, J., Bühler, O., Cântar, I.C., Cariñanos, P., Carriero, G., Churkina, G., Dinca, L., Esposito, R., Gawroński, S.W., Kern, M., Le Thiec, D., Moretti, M., Ningal, T., Rantzoudi, E.C., Sinjur, I., Stojanova, B., Aničić Urošević, M., Velikova, V., Živojinović, I., Sahakyan, L., Calfapietra, C., Samson, R., 2017. How Does the Amount and Composition of PM Deposited on *Platanus acerifolia* Leaves Change Across Different Cities in Europe? *Environmental Science & Technology* 51, 1147–1156.

Hofman, J., Maher, B.A., Muxworthy, A.R., Wuyts, K., **Castanheiro, A.**, Samson, R., 2017. Biomagnetic Monitoring of Atmospheric Pollution: A Review of Magnetic Signatures from Biological Sensors. *Environmental Science & Technology* 51, 6648–6664.

Declercq, Y., Samson, R., **Castanheiro, A.**, Spassov, S., Tack, F.M.G., Van De Vijver, E., De Smedt, P., 2019. Evaluating the potential of topsoil magnetic pollution mapping across different land use classes. *Science of the Total Environment* 685, 345–356.



Ana Castanheiro



Portuguese based in Antwerp



12/11/1990



ana.castanheiro@hotmail.com



anacastanheiro



(+32) 0485 936615

EDUCATION

PhD Bioscience Engineering | University of Antwerp, BE

Scientific research on biomonitoring and fingerprinting of particulate matter pollution for source apportionment techniques 2014-2019

FWO-SB fellowship: 01/2016-12/2019

Dehousse UA: 11/2014-12-2015

Integrated projects:

- COST Action FP1204 "Greeninurbs", 2014-2016. European-level campaign using plane tree leaves as bio-indicators for urban air quality.
- Urban Action Clinic, Ghent, 2015. Citizen science project to raise awareness on urban air quality; collected data for habitat quality mapping.

Integrated Master in Biological Engineering | TÉCNICO Lisbon, PT

BSc + MSc programme

2008-2014

Erasmus training program at University of Antwerp, BE (02-06/2014)

Master thesis: A comparative study between biomagnetic analysis and scanning electron microscopy of particulate matter deposition on urban green

Training during PhD | ADS/StatUA/FLAMES, University of Antwerp, BE

- Statistical principles & multivariate data analysis
 - R workshop & MATLAB fundamentals
 - Methods in research design
 - Personal effectiveness
 - Grow your future career
-

- COST Action FP1204 Training School on “Implementation of green infrastructure approach to link environmental and social aspects in the research on urban forests” | Pieve Tesino, IT. 2015 (1 week)
 - Castle Meeting short course on magnetic hysteresis and susceptibility | Dourbes, BE. 2016 (3 days)
-

- Dutch (Level B1-B2) | Linguapolis, University of Antwerp

Scientific conferences & symposiums

- 2015
 - 7th International Workshop on Biomonitoring of Atmospheric Pollution (BIOMAP7), Lisbon (PT). *Oral presentation*
- 2016
 - National Symposium for Applied Biological Sciences, Antwerp (BE). *Oral presentation* (award on topic Ecosystem monitoring and management)
 - Chemistry Conference for Young Scientists (ChemCYS), Blankenberge (BE). *Oral presentation*
 - Studiedag: Starters in het natuur en bosonderzoek, Brussels (BE). *Oral presentation*
 - 13th GCxGC Symposium, Riva Del Garda (IT). *Poster (presented by Pieter Joos)*
 - 15th Castle Meeting - New Trends on Paleo, Rock and Environmental Magnetism, Dinant (BE). *Oral presentation*
 - 18th International Conference on Heavy Metals in the Environment, Ghent (BE). *Oral presentation*
- 2017
 - National Symposium for Applied Biological Sciences, Leuven (BE). *Poster*
 - Green Infrastructure: Nature Based Solutions for Sustainable and Resilient Cities, Orvieto (IT). *Poster*
- 2018
 - 8th International Workshop on Biomonitoring of Atmospheric Pollution (BIOMAP8), Dubna (RU). *Oral presentation & Poster*
- 2019
 - Faculty Research Day 2019, University of Antwerp (BE). *Oral presentation*

Educational experience

Supervision of BSc thesis students:

- 2014-2015 Sam Baelus, Bets Goetschalckx. Vangen stadsbomen meer fijnstof dan we denken? Promotor: Roeland Samson.
- 2018-2019 Kimber Diels, Iana Goeman, Qian xin Liang. Straatstof in Antwerpen: magnetische en chemische karakterisering. Promotors: Roeland Samson, Karen Wuyts.

Supervision of MSc thesis students:

- 2015-2016 Robbe Van Hoofstat. On the use of citizen science and magnetic biomonitoring to explain spatial variation of urban particulate matter. Promotor: Roeland Samson.
- 2016 Bram Pawlak. Analyse van contaminanten aanwezig op klimopbladeren met behulp van beeldvormende XRF en SEM. Promotors: Karolien De Wael, Koen Janssens; co-supervision with Stijn Legrand.
- 2017 Lodewijk Lefevre. Magnetic monitoring of the impact of atmospheric pollution on vineyards in Serbia. Promotor: Roeland Samson; co-supervision with Karen Wuyts.
- 2017-2018 Sam Vandervoort. Interaction between air pollution and urban green: particulate matter encapsulation in leaves. Promotor: Roeland Samson.
- 2018 Kathleen Leemans. Biomagnetic source apportionment of leaf-deposited particles: AIRbezen Oost-Vlaanderen 2017 as a case study (MSc Individual Project). Promotors: Roeland Samson, Karen Wuyts.
- 2019 Hanne Hendrickx. Biomagnetic monitoring of air pollution in the area near a metal processing industry. Promotors: Roeland Samson, Karen Wuyts.

- Ackerfield, J., Wen, J., 2002. A morphometric analysis of *Hedera L.* (the ivy genus, Araliaceae) and its taxonomic implications. *Adansonia ser.* 3 24, 197–212.
- Alfani, A., Bartoli, G., Rutigliano, F.A., Maisto, G., Virzo De Santo, A., 1996. Trace metal biomonitoring in the soil and the leaves of *Quercus ilex* in the urban area of Naples. *Biological Trace Element Research* 51, 117–131.
- Almeida, S.M., Pio, C., Freitas, M.C., Reis, M.A., Trancoso, M.A., 2006. Approaching PM_{2.5} and PM_{2.5} - 10 source apportionment by mass balance analysis, principal component analysis and particle size distribution. *Science of the Total Environment* 368, 663–674.
- Amato, F., Lucarelli, F., Nava, S., Calzolari, G., Karanasiou, A., Colombi, C., Gianelle, V. L., Alves, C., Custódio, D., Eleftheriadis, K., Diapouli, E., Reche, C., Alastuey, A., Minguillón M. C., Severi, M., Becagli, S., Nunes, T., Cerqueira, M., Pio, C., Manousakas, M., Maggos, T., Vratolis, S., Harrison, R. M., Querol, X., 2016. Case studies of source apportionment and suggested measures at Southern European cities. In: *Airborne particulate matter - sources, atmospheric processes and health. Issues in Environmental Science and Technology No. 42*, pp. 168-259. The Royal Society of Chemistry, Cambridge.
- Amato, F., Nava, S., Lucarelli, F., Querol, X., Alastuey, A., Baldasano, J.M., Pandolfi, M., 2010. A comprehensive assessment of PM emissions from paved roads: Real-world emission factors and intense street cleaning trials. *Science of the Total Environment* 408, 4309–4318.
- Amato, F., Pandolfi, M., Moreno, T., Furger, M., Pey, J., Alastuey, A., Bukowiecki, N., Prevot, A.S.H., Baltensperger, U., Querol, X., 2011. Sources and variability of inhalable road dust particles in three European cities. *Atmospheric Environment* 45, 6777–6787.
- Amato, F., Pandolfi, M., Viana, M., Querol, X., Alastuey, A., Moreno, T., 2009. Spatial and chemical patterns of PM₁₀ in road dust deposited in urban environment. *Atmospheric Environment* 43, 1650–1659.
- Amato, F., Schaap, M., Denier van der Gon, H.A.C., Pandolfi, M., Alastuey, A., Keuken, M., Querol, X., 2013. Short-term variability of mineral dust, metals and carbon emission from road dust resuspension. *Atmospheric Environment* 74, 134–140.
- Amorim, J.H., Rodrigues, V., Tavares, R., Valente, J., Borrego, C., 2013. CFD modelling of the aerodynamic effect of trees on urban air pollution dispersion. *Science of The Total Environment* 461–462, 541–551.
- Anderson, J.O., Thundiyil, J.G., Stolbach, A., 2012. Clearing the air: A review of the effects of particulate matter air pollution on human health. *Journal of Medical Toxicology* 8, 166–175.
- Aranda, P.S., LaJoie, D.M., Jorczyk, C.L., 2012. Bleach gel: A simple agarose gel for analyzing RNA quality. *Electrophoresis* 33, 366.
- Arroyo, J.P., Schweickert, A.J., 2015. The respiratory cycle. In: *Back to basics in physiology*. Elsevier, pp. 61–79.
- Baker, E.A., Hunt, G.M., 1986. Erosion of waxes from leaf surfaces by simulated rain. *New Phytologist* 102, 161–173.
- Bakker, M.I., Vorenhout, M., Sijm, D.T.H.M., Kollöffel, C., 1999. Dry deposition of atmospheric polycyclic aromatic hydrocarbons in three *Plantago* species. *Environmental Toxicology and Chemistry* 18, 2289–2294.
- Baldacchini, C., Castanheiro, A., Maghakyan, N., Sgrigna, G., Verhelst, J., Alonso, R., Amorim, J.H., Bellan, P., Bojović, D.Đ., Breuste, J., Bühler, O., Cântar, I.C., Cariñanos, P., Carrero, G., Churkina, G., Dinca, L., Esposito, R., Gawroński, S.W., Kern, M., Le Thiec, D., Moretti, M., Ningal, T., Rantzoudi, E.C., Sinjur, I., Stojanova, B., Aničić Urošević, M., Velikova, V.,

- Živojinović, I., Sahakyan, L., Calfapietra, C., Samson, R., 2017. How does the amount and composition of PM deposited on *Platanus acerifolia* leaves change across different cities in Europe? *Environmental Science & Technology* 51, 1147–1156.
- Baldacchini, C., Sgrigna, G., Clarke, W., Tallis, M., Calfapietra, C., 2019. An ultra-spatially resolved method to quali-quantitative monitor particulate matter in urban environment. *Environmental Science and Pollution Research* 26, 18719–18729.
- Banerjee, S., Roy, S., Chen, J., Chakravorty, D., 2000. Magnetic properties of oxide-coated iron nanoparticles synthesized by electrodeposition. *Journal of Magnetism and Magnetic Materials* 219, 45–52.
- Barima, Y.S.S., Angaman, D.M.D.M., N'gouran, K.P., Koffi, N.A.N.A., Tra Bi, F.Z.F.Z., Samson, R., 2016. Involvement of leaf characteristics and wettability in retaining air particulate matter from tropical plant species. *Environmental Engineering Research* 21, 121–131.
- Barmpadimos, I., Keller, J., Oderbolz, D., Hueglin, C., Prévôt, A.S.H., 2012. One decade of parallel fine (PM 2.5) and coarse (PM 10-PM 2.5) particulate matter measurements in Europe: Trends and variability. *Atmospheric Chemistry and Physics* 12, 3189–3203.
- Barthlott, W., Neinhuis, C., Cutler, D., Ditsch, F., Meusel, I., Theisen, I., Wilhelm, H., 1998. Classification and terminology of plant epicuticular waxes. *Botanical Journal of the Linnean Society*.
- Bastonini, E., Verdone, L., Morrone, S., Santoni, A., Settimo, G., Marsili, G., La Fortezza, M., Di Mauro, E., Caserta, M., 2011. Transcriptional modulation of a human monocytic cell line exposed to PM10 from an urban area. *Environmental Research* 111, 765–774.
- Beckett, K.P., Freer-Smith, P.H., Taylor, G., 1998. Urban woodlands: Their role in reducing the effects of particulate pollution. *Environmental Pollution* 99, 347–360.
- Beckett, K.P., Freer-Smith, P.H., Taylor, G., 2000. Particulate pollution capture by urban trees: Effect of species and windspeed. *Global Change Biology* 6, 995–1003.
- Bernstein, J.A., Alexis, N., Barnes, C., Bernstein, I.L., Nel, A., Peden, D., Diaz-Sanchez, D., Tarlo, S.M., Williams, P.B., Bernstein, J.A., 2004. Health effects of air pollution. *Journal of Allergy and Clinical Immunology* 114, 1116–1123.
- Bilo, F., Borgese, L., Dalipi, R., Zacco, A., Federici, S., Masperi, M., Leonesio, P., Bontempi, E., Depero, L., 2017. Elemental analysis of tree leaves by total reflection X-ray fluorescence: New approaches for air quality monitoring. *Chemosphere* 178, 504–512.
- Booth, C.A., Walden, J., Neal, a., Smith, J.P., 2005. Use of mineral magnetic concentration data as a particle size proxy: A case study using marine, estuarine and fluvial sediments in the Carmarthen Bay area, South Wales, U.K. *Science of the Total Environment* 347, 241–253.
- Bourliva, A., Christophoridis, C., Papadopoulou, L., Giouri, K., Papadopoulos, A., Mitsika, E., Fytianos, K., 2017. Characterization, heavy metal content and health risk assessment of urban road dusts from the historic center of the city of Thessaloniki, Greece. *Environmental Geochemistry and Health* 39, 611–634.
- Bradshaw, L., 2018. Antwerp is one of 50 most-polluted cities in the world. *Flanders Today*, 29 October 2018. www.flanderstoday.eu/antwerp-one-50-most-polluted-cities-world. Accessed 3 August 2019.
- Breiman, L., 2001. Random Forests. *Machine Learning* 45, 5–32.
- Breyse, P.N., Delfino, R.J., Dominici, F., Elder, A.C.P., Frampton, M.W., Froines, J.R., Geyh, A.S., Godleski, J.J., Gold, D.R., Hopke, P.K., Koutrakis, P., Li, N., Oberdörster, G., Pinkerton, K.E., Samet, J.M., Utell, M.J., Wexler, A.S., 2013. US EPA particulate matter research centers: Summary of research results for 2005-2011. *Air Quality, Atmosphere and Health* 6, 333-355.
- Buekers, J., Deutsch, F., Veldeman, N., Janssen, S., Panis, L.I., 2014. Fine atmospheric particles from agricultural practices in Flanders: From emissions to health effects and limit values. *Outlook on Agriculture* 43, 39–44.

- Cai, M., Xin, Z., Yu, X., 2017. Spatio-temporal variations in PM leaf deposition: A meta-analysis. *Environmental Pollution* 231, 207–218.
- Calfapietra, C., Fares, S., Loreto, F., 2009. Volatile organic compounds from Italian vegetation and their interaction with ozone. *Environmental Pollution* 157, 1478–1486.
- Capozzi, F., Giordano, S., Di Palma, A., Spagnuolo, V., De Nicola, F., Adamo, P., 2016. Biomonitoring of atmospheric pollution by moss bags: Discriminating urban-rural structure in a fragmented landscape. *Chemosphere* 149, 211–218.
- Cassee, F., Héroux, M.-E., Gerlofs-Nijland, M.E., Kelly, F.J., 2013. Particulate matter beyond mass: recent health evidence on the role of fractions, chemical constituents and sources of emission. *Inhalation Toxicology* 25, 802–812.
- Castanheiro, A., Joos, P., Wuyts, K., De Wael, K., Samson, R., 2019. Leaf-deposited semi-volatile organic compounds (SVOCs): An exploratory study using GCxGC-TOFMS on leaf washing solutions. *Chemosphere* 214, 103–110.
- Castanheiro, A., Samson, R., De Wael, K., 2016. Magnetic- and particle-based techniques to investigate metal deposition on urban green. *Science of the Total Environment* 571, 594–602.
- Chen, L., Liu, C., Zhang, L., Zou, R., Zhang, Z., 2017. Variation in tree species ability to capture and retain airborne fine particulate matter (PM_{2.5}). *Scientific Reports* 7, 3206.
- Chillrud, S.N., Epstein, D., Ross, J.M., Sax, S.N., Pederson, D., Spengler, J.D., Kinney, P.L., 2004. Elevated airborne exposures of teenagers to manganese, chromium, and iron from steel dust and New York City's subway system. *Environmental Science & Technology* 38, 732–7.
- Colman Lerner, J.E., Orte, M.A., Giuliani, D., Matamoros, N., Sanchez, E.Y., Porta, A.A., 2016. Volatile and semivolatile organic compounds determination in air. *Comprehensive Analytical Chemistry* 73, 321–342.
- Cook, R.J., 2005. Kappa. In: *Encyclopedia of Biostatistics*. John Wiley & Sons Ltd, Chichester, UK.
- Cuccia, E., Piazzalunga, A., Bernardoni, V., Brambilla, L., Fermo, P., Massabò, D., Molteni, U., Prati, P., Valli, G., Vecchi, R., 2011. Carbonate measurements in PM₁₀ near the marble quarries of Carrara (Italy) by infrared spectroscopy (FT-IR) and source apportionment by positive matrix factorization (PMF). *Atmospheric Environment* 45, 6481–6487.
- Davila, A.F., Rey, D., Mohamed, K., Rubio, B., Guerra, A.P., 2006. Mapping the sources of urban dust in a coastal environment by measuring magnetic parameters of *Platanus hispanica* leaves. *Environmental Science & Technology* 40, 3922–3928.
- De Nicola, F., Baldantoni, D., Sessa, L., Monaci, F., Bargagli, R., Alfani, A., 2015. Distribution of heavy metals and polycyclic aromatic hydrocarbons in holm oak plant-soil system evaluated along urbanization gradients. *Chemosphere* 134, 91–97.
- De Nicola, F., Maisto, G., Prati, M.V. V., Alfani, A., 2008. Leaf accumulation of trace elements and polycyclic aromatic hydrocarbons (PAHs) in *Quercus ilex* L. *Environmental Pollution* 153, 376–383.
- De Nicola, F., Murena, F., Costagliola, M.A., Alfani, A., Baldantoni, D., Prati, M.V., Sessa, L., Spagnuolo, V., Giordano, S., 2013. A multi-approach monitoring of particulate matter, metals and PAHs in an urban street canyon. *Environmental Science and Pollution Research* 20, 4969–4979.
- Declercq, Y., Samson, R., Castanheiro, A., Spassov, S., Tack, F.M.G., Van De Vijver, E., De Smedt, P., 2019. Evaluating the potential of topsoil magnetic pollution mapping across different land use classes. *Science of the Total Environment* 685, 345–356.
- Dedik, A.N., Hoffmann, P., Ensling, J., 1992. Chemical characterization of iron in atmospheric aerosols. *Atmospheric Environment Part A, General Topics* 26, 2545–2548.
- Donald, I., Kerr, M.M., Macdonald, I.R., 1958. Respiratory Phenomena in the Newborn. *Scottish Medical Journal* 3, 151–164.

- Donaldson, K., Stone, V., Borm, P.J.A., Jimenez, L.A., Gilmour, P.S., Schins, R.P.F., Knaapen, A.M., Rahman, I., Faux, S.P., Brown, D.M., MacNee, W., 2003. Oxidative stress and calcium signaling in the adverse effects of environmental particles (PM10). *Free Radical Biology and Medicine* 34, 1369-1382.
- Draaijers, G.P.J., Erisman, J.W., van Leeuwen, N.F.M., Römer, F.G., te Winkel, B.H., Vermeulen, A.T., Wyers, G.P., Hansen, K., 1994. A comparison of methods to estimate canopy exchange at the Speulder Forest. National Institute of Public Health and Environmental Protection, Bilthoven, The Netherlands. Report No. 722108004.
- Dunlop, D.J., 1973. Superparamagnetic and single-domain threshold sizes in magnetite. *Journal of Geophysical Research* 78, 1780–1793.
- Dunlop, D.J., 1981. The rock magnetism of fine particles, *Physics of the Earth and Planetary Interiors* 26, 1-26.
- Dunlop, D.J., 1986. Hysteresis properties of magnetite and their dependence on particle size: A test of pseudo-single-domain remanence models. *Journal of Geophysical Research* 91, 9569-9584.
- Dunlop, D.J., Özdemir, O., 1997. *Rock magnetism: Fundamentals and frontiers*. Cambridge University Press.
- Dzierżanowski, K., Poppek, R., Gawronska, H., Sæbø, A., Gawroński, S.W., 2011. Deposition of particulate matter of different size fractions on leaf surfaces and in waxes of urban forest species. *International Journal of Phytoremediation* 13, 1037–1046.
- EEA, 2013. *Air quality in Europe - 2013 report*. European Environment Agency, Copenhagen, Denmark.
- EEA, 2014. *Air pollution fact sheet 2014, Belgium*. European Environment Agency, Copenhagen.
- EEA, 2019a. *European Union emission inventory report 1990-2017 under the UNECE Convention on Long-range Transboundary Air Pollution (LRTAP)*. EEA Report No 08/2019. European Environment Agency, Luxembourg.
- EEA, 2019b. *Exceedance of air quality standards in urban areas*. www.eea.europa.eu/data-and-maps/indicators/exceedance-of-air-quality-limit-3/assessment-5. Accessed 30 September 2018.
- EPA, 2009. *Integrated science assessment for particulate matter (final report)*. United States Environmental Protection Agency, Washington, DC. EPA/600/R-08/139F, 2009.
- Escobedo, F.J., Kroeger, T., Wagner, J.E., 2011. Urban forests and pollution mitigation: Analyzing ecosystem services and disservices. *Environmental Pollution* 159, 2078-2087.
- Escobedo, F.J., Nowak, D.J., 2009. Spatial heterogeneity and air pollution removal by an urban forest. *Landscape and Urban Planning* 90, 102–110.
- Evans, M.E., and Heller, F., 2003. *Environmental magnetism: Principles and applications of enviromagnetics*. *International Geophysics* 86: 1-299.
- Fischbach, D.B., 1961. Diamagnetic susceptibility of pyrolytic graphite. *Physical Review* 123, 1613–1614.
- Flanders, 2018. www.vlaanderen.be/nl/gemeenten-en-provincies/provincie-antwerpen. Accessed 4 April 2018.
- Flanders, P.J., 1994. Collection, measurement, and analysis of airborne magnetic particulates from pollution in the environment (invited). *Journal of Applied Physics* 75, 5931–5936.
- Freer-Smith, P.H., Beckett, K.P., Taylor, G., 2005. Deposition velocities to *Sorbus aria*, *Acer campestre*, *Populus deltoides* × *trichocarpa* ‘Beaupré’, *Pinus nigra* and × *Cupressocyparis leylandii* for coarse, fine and ultra-fine particles in the urban environment. *Environmental Pollution* 133, 157–167.
- Galvão, E.S., Santos, J.M., Lima, A.T., Reis, N.C., Orlando, M.T.D., Stuetz, R.M., 2018. Trends in analytical techniques applied to particulate matter characterization: A critical review of fundamentals and applications. *Chemosphere* 199, 546–568.

- Garcia-Hurtado, E., Pey, J., Borrás, E., Sánchez, P., Vera, T., Carratalá, A., Alastuey, A., Querol, X., Vallejo, V.R., 2014. Atmospheric PM and volatile organic compounds released from Mediterranean shrubland wildfires. *Atmospheric Environment* 89, 85–92.
- Gargiulo, J.D., Kumar, R.S., Chaparro, M.A.E., Natal, M., Rajkumar, P., 2016. Magnetic properties of air suspended particles in thirty eight cities from south India. *Atmospheric Pollution Research* 7, 626–637.
- Gehrig, R., Hill, M., Lienemann, P., Zwicky, C.N., Bukowiecki, N., Weingartner, E., Baltensperger, U., Buchmann, B., 2007. Contribution of railway traffic to local PM10 concentrations in Switzerland. *Atmospheric Environment* 41, 923–933.
- Goddu, S.R., Appel, E., Jordanova, D., Wehland, F., 2004. Magnetic properties of road dust from Visakhapatnam (India) - relationship to industrial pollution and road traffic. *Physics and Chemistry of the Earth, Parts A/B/C* 29, 985–995.
- Grobéty, B., Giere, R., Dietze, V., Stille, P., 2010. Airborne particles in the urban environment. *Elements* 6, 229–234.
- Gromke, C., Ruck, B., 2009. On the impact of trees on dispersion processes of traffic emissions in street canyons. *Boundary-Layer Meteorology* 131, 19–34.
- Grote, R., Samson, R., Alonso, R., Amorim, J.H., Cariñanos, P., Churkina, G., Fares, S., Thiec, D. Le, Niinemets, Ü., Mikkelsen, T.N., Paoletti, E., Tiwary, A., Calfapietra, C., 2016. Functional traits of urban trees: Air pollution mitigation potential. *Frontiers in Ecology and the Environment* 14, 543–550.
- Guevara, 2016. Emissions of primary particulate matter. In: *Airborne particulate matter - sources, atmospheric processes and health. Issues in Environmental Science and Technology* No. 42, pp. 1-26. The Royal Society of Chemistry, Cambridge.
- Gupta, U.C., Wu, K., Liang, S., 2008. Micronutrients in soils, crops, and livestock. *Earth Science Frontiers* 15, 110–125.
- Hanesch, M., Scholger, R., Rey, D., 2003. Mapping dust distribution around an industrial site by measuring magnetic parameters of tree leaves. *Atmospheric Environment* 37, 5125–5133.
- Hansard, R., Maher, B.A., Kinnersley, R., 2011. Biomagnetic monitoring of industry-derived particulate pollution. *Environmental Pollution* 159, 1673–1681.
- Hansard, R., Maher, B.A., Kinnersley, R.P., 2012. Rapid magnetic biomonitoring and differentiation of atmospheric particulate pollutants at the roadside and around two major industrial sites in the U.K. *Environmental Science & Technology* 46, 4403–4410.
- Harrison, R.M., Yin, J., 2000. Particulate matter in the atmosphere: Which particle properties are important for its effects on health? *Science of The Total Environment* 249, 85–101.
- Hellems, J., Mortier, G., De Paepe, A., Speleman, F., Vandesompele, J., 2007. qBase relative quantification framework and software for management and automated analysis of real-time quantitative PCR data. *Genome Biol.* 8, R19.
- Hoad, S.P., Jeffree, C.E., Grace, J., 1992. Effects of wind and abrasion on cuticular integrity in *Fagus sylvatica* L. and consequences for transfer of pollutants through leaf surfaces. *Agriculture, Ecosystems & Environment* 42, 275–289.
- Hobbie, S.E., Reich, P.B., Oleksyn, J., Ogdahl, M., Zytowskiak, R., Hale, C., Karolewski, P., 2006. Tree species effects on decomposition and forest floor dynamics in a common garden. *Ecology* 87, 2288–97.
- Hoffmann, V., Knab, M., Appel, E., 1999. Magnetic susceptibility mapping of roadside pollution. *Journal of Geochemical Exploration* 66, 313–326.
- Hofman, J., Lefebvre, W., Janssen, S., Nackaerts, R., Nuyts, S., Mattheyses, L., Samson, R., 2014c. Increasing the spatial resolution of air quality assessments in urban areas: A comparison of biomagnetic monitoring and urban scale modelling. *Atmospheric Environment* 92, 130–140.

- Hofman, J., Maher, B.A., Muxworthy, A.R., Wuyts, K., Castanheiro, A., Samson, R., 2017. Biomagnetic monitoring of atmospheric pollution: A review of magnetic signatures from biological sensors. *Environmental Science & Technology* 51, 6648–6664.
- Hofman, J., Staelens, J., Cordell, R., Stroobants, C., Zikova, N., Hama, S.M.L., Wyche, K.P., Kos, G.P.A., Van Der Zee, S., Smallbone, K.L., Weijers, E.P., Monks, P.S., Roekens, E., 2016. Ultrafine particles in four European urban environments: Results from a new continuous long-term monitoring network. *Atmospheric Environment* 136, 68–81.
- Hofman, J., Stokkaer, I., Snauwaert, L., Samson, R., 2013. Spatial distribution assessment of particulate matter in an urban street canyon using biomagnetic leaf monitoring of tree crown deposited particles. *Environmental Pollution* 183, 123–132.
- Hofman, J., Wuyts, K., Van Wittenberghe, S., Brackx, M., Samson, R., 2014a. On the link between biomagnetic monitoring and leaf-deposited dust load of urban trees: Relationships and spatial variability of different particle size fractions. *Environmental Pollution* 189, 63–72.
- Hofman, J., Wuyts, K., Van Wittenberghe, S., Samson, R., 2014b. On the temporal variation of leaf magnetic parameters: Seasonal accumulation of leaf-deposited and leaf-encapsulated particles of a roadside tree crown. *Science of the Total Environment* 493, 766–772.
- Hsu, C.Y., Chiang, H.C., Lin, S.L., Chen, M.J., Lin, T.Y., Chen, Y.C., 2016. Elemental characterization and source apportionment of PM₁₀ and PM_{2.5} in the western coastal area of central Taiwan. *Science of the Total Environment* 541, 1139–1150.
- Hull, H.M., Morton, H.L., Wharrie, J.R., 1975. Environmental influences on cuticle development and resultant foliar penetration. *The Botanical Review* 41, 421–452.
- Hunt, A., Jones, J., Oldfield, F., 1984. Magnetic measurements and heavy metals in atmospheric particulates of anthropogenic origin. *Science of The Total Environment* 33, 129–139.
- Hussein, T., Hämeri, K., Aalto, P.P., Paatero, P., Kulmala, M., 2005. Modal structure and spatial-temporal variations of urban and suburban aerosols in Helsinki - Finland. *Atmospheric Environment* 39, 1655–1668.
- IARC, 2012. Diesel Engine Exhaust Carcinogenic, Press release 213. International Agency for Research on Cancer, Lyon, France.
- Inca, 2006. Inca Energy operator manual, issue 2.1. Oxford Instruments Analytical, UK.
- Jancsek-Turóczi, B., Hoffer, A., Nyíró-Kósa, I., Gelencsér, A., 2013. Sampling and characterization of resuspended and respirable road dust. *Journal of Aerosol Science* 65, 69–76.
- Janhäll, S., 2015. Review on urban vegetation and particle air pollution – Deposition and dispersion. *Atmospheric Environment* 105, 130–137.
- Jayamurugan, R., Kumaravel, B., Palanivelraja, S., Chockalingam, M.P., 2013. Influence of temperature, relative humidity and seasonal variability on ambient air quality in a coastal urban area. *International Journal of Atmospheric Sciences* 2013, 1–7.
- Jeanjean, A.P.R., Buccolieri, R., Eddy, J., Monks, P.S., Leigh, R.J., 2017. Air quality affected by trees in real street canyons: The case of Marylebone neighbourhood in central London. *Urban Forestry & Urban Greening* 22, 41–53.
- Jerrett, M., Arain, A., Kanaroglou, P., Beckerman, B., Potoglou, D., Sahsuvaroglu, T., Morrison, J., Giovis, C., 2005. A review and evaluation of intraurban air pollution exposure models. *Journal of Exposure Science & Environmental Epidemiology* 15, 185–204.
- Jiang, S.Y., Kaul, D.S., Yang, F., Sun, L., Ning, Z., 2015. Source apportionment and water solubility of metals in size segregated particles in urban environments. *Science of The Total Environment* 533, 347–355.

- Jordanova, D., Petrov, P., Hoffmann, V., Gocht, T., Panaiotu, C., Tsacheva, T., Jordanova, N., 2010. Magnetic signature of different vegetation species in polluted environment. *Studia Geophysica et Geodaetica* 54, 417–442.
- Kampa, M., Castanas, E., 2008. Human health effects of air pollution. *Environmental Pollution* 151, 362–367.
- Kardel, F., Wuyts, K., De Wael, K., Samson, R., 2018. Biomonitoring of atmospheric particulate pollution via chemical composition and magnetic properties of roadside tree leaves. *Environmental Science and Pollution Research* 25, 25994–26004.
- Kardel, F., Wuyts, K., Khavanin Zadeh, A.R., Wuytack, T., Babanezhad, M., Samson, R., 2012a. Comparison of leaf saturation isothermal remanent magnetisation (SIRM) with anatomical, morphological and physiological tree leaf characteristics for assessing urban habitat quality. *Environmental Pollution* 183, 96–103.
- Kardel, F., Wuyts, K., Maher, B.A., Hansard, R., Samson, R., 2011. Leaf saturation isothermal remanent magnetization (SIRM) as a proxy for particulate matter monitoring: Inter-species differences and in-season variation. *Atmospheric Environment* 45, 5164–5171.
- Kardel, F., Wuyts, K., Maher, B.A., Samson, R., 2012b. Intra-urban spatial variation of magnetic particles: Monitoring via leaf saturation isothermal remanent magnetisation (SIRM). *Atmospheric Environment* 55, 111–120.
- Keuken, M.P., Moerman, M., Voogt, M., Blom, M., Weijers, E.P., Röckmann, T., Dusek, U., 2013. Source contributions to PM_{2.5} and PM₁₀ at an urban background and a street location. *Atmospheric Environment* 71, 26–35.
- Kgabi, N.A., Mokgwetsi, T., 2009. Dilution and dispersion of inhalable particulate matter. *WIT Transactions on Ecology and the Environment* 127, 229–238.
- Kim, K.-H., Kabir, E., Kabir, S., 2015. A review on the human health impact of airborne particulate matter. *Environment International* 74, 136–143.
- Kim, K.W., Ahn, J.J., Lee, J.H., 2009. Micromorphology of epicuticular wax structures of the garden strawberry leaves by electron microscopy: Syntopism and polymorphism. *Micron* 40, 327–334.
- Kim, W., Doh, S.J., Park, Y.H., Yun, S.T., 2007. Two-year magnetic monitoring in conjunction with geochemical and electron microscopic data of roadside dust in Seoul, Korea. *Atmospheric Environment* 41, 7627–7641.
- King, J., Banerjee, S.K., Marvin, J., Özdemir, Ö., 1982. A comparison of different magnetic methods for determining the relative grain size of magnetite in natural materials: Some results from lake sediments. *Earth and Planetary Science Letters* 59, 404–419.
- Klumpp, A., Ansel, W., Klumpp, G., Belluzzo, N., Calatayud, V., Chaplin, N., Garrec, J.P., Gutsche, H.-J.J., Hayes, M., Hentze, H.-W.W., Kambezidis, H., Laurent, O., Penueas, J., Rasmussen, S., Ribas, A., Ro-Poulsen, H., Rossi, S., Sanz, M.J., Shang, H., Sifakis, N., Vergne, P., Peñuelas, J., Rasmussen, S., Ribas, A., Ro-Poulsen, H., Rossi, S., Sanz, M.J., Shang, H., Sifakis, N., Vergne, P., 2002. EuroBionet: A pan-European biomonitoring network for urban air quality assessment. *Environmental science and pollution research international* 9, 199–203.
- Koch, K., Samson, R., Denys, S., 2019. Aerodynamic characterisation of green wall vegetation based on plant morphology: An experimental and computational fluid dynamics approach. *Biosystems Engineering* 178, 34–51.
- Kocić, K., Spasić, T., Urošević, M.A., Tomašević, M., 2014. Trees as natural barriers against heavy metal pollution and their role in the protection of cultural heritage. *Journal of Cultural Heritage* 15, 227–233.
- Kopáček, J., Turek, J., Hejzlar, J., Šantrůčková, H., 2009. Canopy leaching of nutrients and metals in a mountain spruce forest. *Atmospheric Environment* 43, 5443–5453.

- Kronenberg, J., Bergier, T., 2012. Sustainable development in a transition economy: business case studies from Poland. *Journal of Cleaner Production* 26, 18–27.
- Künzli, N., Kaiser, R., Medina, S., Studnicka, M., Chanel, O., Filliger, P., Herry, M., Horak, F., Puybonnieux-Textier, V., Quénel, P., Schneider, J., Seethaler, R., Vergnaud, J.C., Sommer, H., 2000. Public-health impact of outdoor and traffic-related air pollution: A European assessment. *Lancet* 356, 795–801.
- Laden, F., Neas, L.M., Dockery, D.W., Schwartz, J., 2000. Association of fine particulate matter from different sources with daily mortality in six U.S. cities. *Environmental Health Perspectives* 108, 941–947.
- Lammel, G., Röhrli, A., Schreiber, H., 2002. Atmospheric lead and bromine in Germany: Post-abatement levels, variabilities and trends. *Environmental Science and Pollution Research* 9, 397–404.
- Lecoanet, H., Lèveque, F., Ambrosi, J.P., 2003. Combination of magnetic parameters: an efficient way to discriminate soil-contamination sources (south France). *Environmental Pollution* 122, 229–234.
- Lehndorff, E., Schwark, L., 2010. Biomonitoring of air quality in the Cologne Conurbation using pine needles as a passive sampler – Part III: Major and trace elements. *Atmospheric Environment* 44, 2822–2829.
- Lehndorff, E., Urbat, M., Schwark, L., 2006. Accumulation histories of magnetic particles on pine needles as function of air quality. *Atmospheric Environment* 40, 7082–7096.
- Li, N., Hao, M., Phalen, R.F., Hinds, W.C., Nel, A.E., 2003. Particulate air pollutants and asthma: A paradigm for the role of oxidative stress in PM-induced adverse health effects. *Clinical Immunology* 109, 250–265.
- Lindberg, S.E., Lovett, G.M., 1985. Field measurements of particle dry deposition rates to foliage and inert surfaces in a forest canopy. *Environmental Science & Technology* 19, 238–244.
- Litschke, T., Kuttler, W., 2008. On the reduction of urban particle concentration by vegetation a review. *Meteorologische Zeitschrift* 17, 229–240.
- Liu, L., Guan, D., Peart, M.R., 2012a. The morphological structure of leaves and the dust-retaining capability of afforested plants in urban Guangzhou, South China. *Environmental Science and Pollution Research* 19, 3440–3449.
- Liu, Q., Roberts, A.P., Larrasoana, J.C., Banerjee, S.K., Guyodo, Y., Tauxe, L., Oldfield, F., 2012b. Environmental magnetism: Principles and applications. *Reviews of Geophysics* 50, RG4002.
- Lorenzo, R., Kaegi, R., Gehrig, R., Grobéty, B., 2006. Particle emissions of a railway line determined by detailed single particle analysis. *Atmospheric Environment* 40, 7831–7841.
- Lu, S.G., Bai, S.Q., 2006. Study on the correlation of magnetic properties and heavy metals content in urban soils of Hangzhou City, China. *Journal of Applied Geophysics* 60, 1–12.
- Lu, S.G., Bai, S.Q., Xue, Q.F., 2007. Magnetic properties as indicators of heavy metals pollution in urban topsoils: A case study from the city of Luoyang, China. *Geophysical Journal International* 171, 568–580.
- Lu, S.G., Wang, H.Y., Guo, J.L., 2011. Magnetic enhancement of urban roadside soils as a proxy of degree of pollution by traffic-related activities. *Environmental Earth Sciences* 64, 359–371.
- Lu, S.G., Zheng, Y.W., Bai, S.Q., 2008. A HRTEM/EDX approach to identification of the source of dust particles on urban tree leaves. *Atmospheric Environment* 42, 6431–6441.
- Magiera, T., Jabłońska, M., Strzyszczyk, Z., Rachwał, M., 2011. Morphological and mineralogical forms of technogenic magnetic particles in industrial dusts. *Atmospheric Environment* 45, 4281–4290.
- Maher, B.A., 1986. Characterisation of soils by mineral magnetic measurements. *Physics of the Earth and Planetary Interiors* 42, 76–92.

- Maher, B.A., 2011. The magnetic properties of Quaternary aeolian dusts and sediments, and their palaeoclimatic significance. *Aeolian Research* 3, 87-144.
- Maher, B.A., Ahmed, I.A.M., Davison, B., Karloukovski, V., Clarke, R., 2013. Impact of roadside tree lines on indoor concentrations of traffic-derived particulate matter. *Environmental Science and Technology* 47, 13737–13744.
- Maher, B.A., Ahmed, I.A.M., Karloukovski, V., MacLaren, D.A., Foulds, P.G., Allsop, D., Mann, D.M.A., Torres-Jardón, R., Calderon-Garciduenas, L., 2016. Magnetite pollution nanoparticles in the human brain. *Proceedings of the National Academy of Sciences of the United States of America* 113, 10797–801.
- Maher, B.A., Moore, C., Matzka, J., 2008. Spatial variation in vehicle-derived metal pollution identified by magnetic and elemental analysis of roadside tree leaves. *Atmospheric Environment* 42, 364–373.
- Mantovani, L., Tribaudino, M., Solzi, M., Barraco, V., De Munari, E., Pironi, C., 2018. Magnetic and SEM-EDS analyses of *Tilia cordata* leaves and PM10 filters as a complementary source of information on polluted air: Results from the city of Parma (Northern Italy). *Environmental Pollution* 239, 777–787.
- Marcazzan, G., Vaccaro, S., Valli, G., Vecchi, R., 2001. Characterisation of PM10 and PM2.5 particulate matter in the ambient air of Milan (Italy). *Atmospheric Environment* 35, 4639–4650.
- Marguí, E., Hidalgo, M., Queralt, I., 2005. Multielemental fast analysis of vegetation samples by wavelength dispersive X-ray fluorescence spectrometry: Possibilities and drawbacks. *Spectrochimica Acta - Part B Atomic Spectroscopy* 60, 1363–1372.
- Marguí, E., Queralt, I., Hidalgo, M., 2009. Application of X-ray fluorescence spectrometry to determination and quantitation of metals in vegetal material. *TrAC - Trends in Analytical Chemistry* 28, 362–372.
- Marinello, F., Bariani, P., Savio, E., Horsewell, A., De Chiffre, L., 2008. Critical factors in SEM 3D stereo microscopy. *Measurement Science and Technology* 19, 065705.
- Martinelli, N., Olivieri, O., Girelli, D., 2013. Air particulate matter and cardiovascular disease: A narrative review. *European Journal of Internal Medicine* 24, 295-302.
- Matzka, J., Maher, B.A., 1999. Magnetic biomonitoring of roadside tree leaves: identification of spatial and temporal variations in vehicle-derived particulates. *Atmospheric Environment* 33, 4565–4569.
- McDonald, A.G., Bealey, W.J., Fowler, D., Dragosits, U., Skiba, U., Smith, R.I., Donovan, R.G., Brett, H.E., Hewitt, C.N., Nemitz, E., 2007. Quantifying the effect of urban tree planting on concentrations and depositions of PM10 in two UK conurbations. *Atmospheric Environment* 41, 8455–8467.
- McHugh, M.L., 2012. Interrater reliability: the kappa statistic. *Biochemia medica* 22, 276–82.
- McIntosh, G., Gómez-Paccard, M., Osete, M.L., 2007. The magnetic properties of particles deposited on *Platanus x hispanica* leaves in Madrid, Spain, and their temporal and spatial variations. *Science of the Total Environment* 382, 135–146.
- Mitchell, R., Maher, B.A., 2009. Evaluation and application of biomagnetic monitoring of traffic-derived particulate pollution. *Atmospheric Environment* 43, 2095–2103.
- Mitchell, R., Maher, B.A., Kinnersley, R., 2010. Rates of particulate pollution deposition onto leaf surfaces: Temporal and inter-species magnetic analyses. *Environmental Pollution* 158, 1472–1478.
- Mo, L., Ma, Z., Xu, Y., Sun, F., Lun, X., Liu, X., Chen, J., Yu, X., 2015. Assessing the capacity of plant species to accumulate particulate matter in Beijing, China. *PLoS ONE* 10, e0140664.
- Morani, A., Nowak, D.J., Hirabayashi, S., Calafapietra, C., 2011. How to select the best tree planting locations to enhance air pollution removal in the MillionTreesNYC initiative. *Environmental Pollution* 159, 1040–1047.

- Moreno, E., Sagnotti, L., Dinarès-Turell, J., Winkler, A., Cascella, A., 2003. Biomonitoring of traffic air pollution in Rome using magnetic properties of tree leaves. *Atmospheric Environment* 37, 2967–2977.
- Moreno, T., Martins, V., Querol, X., Jones, T., BéruBé, K., Minguillón, M.C., Amato, F., Capdevila, M., de Miguel, E., Centelles, S., Gibbons, W., 2014. A new look at inhalable metalliferous airborne particles on rail subway platforms. *Science of The Total Environment* 505C, 367–375.
- Moretti, S., 2018. Interplay of bacterial endotoxins and transition metals in the inflammatory capacity of airborne particulate matter. Doctoral thesis, Department of Bioscience Engineering, Faculty of Science, University of Antwerp, Belgium.
- Moretti, S., Smets, W., Hofman, J., Mubiana, K.V., Oerlemans, E., Vandenheuveld, D., Samson, R., Blust, R., Lebeer, S., 2019. Human inflammatory response of endotoxin affected by particulate matter-bound transition metals. *Environmental Pollution* 244, 118–126.
- Moretti, S., Smets, W., Oerlemans, E., Blust, R., Lebeer, S., 2018. The abundance of urban endotoxins as measured with an impinger-based sampling strategy. *Aerobiologia* 1–10.
- Muhammad, S., Wuyts, K., Samson, R., 2019. Atmospheric net particle accumulation on 96 plant species with contrasting morphological and anatomical leaf characteristics in a common garden experiment. *Atmospheric Environment* 202, 328–344.
- Muxworthy, A.R., 2015. Investigation of magnetic particulate matter inside animals' lung tissue: preliminary results. *Studia Geophysica et Geodaetica* 59, 628–634.
- Muxworthy, A.R., Matzka, J., Davila, A., Petersen, N., 2003. Magnetic signature of daily sampled urban atmospheric particles. *Atmospheric Environment* 37, 4163–4169.
- Muxworthy, A.R., Matzka, J., Petersen, N., 2001. Comparison of magnetic parameters of urban atmospheric particulate matter with pollution and meteorological data. *Atmospheric Environment* 35, 4379–4386.
- Muxworthy, A.R., Schmidbauer, E., Petersen, N., 2002. Magnetic properties and Mössbauer spectra of urban atmospheric particulate matter: A case study from Munich, Germany 10, 558–570.
- Muxworthy, A.R., Williams, W., 2009. Critical superparamagnetic/single-domain grain sizes in interacting magnetite particles: Implications for magnetosome crystals. *Journal of the Royal Society Interface* 6, 1207–1212.
- Namgung, H.-G., Kim, J.B., Kim, M.-S., Kim, M., Park, S., Woo, S.-H., Bae, G.-N., Park, D., Kwon, S.-B., 2017. Size distribution analysis of airborne wear particles released by subway brake system. *Wear* 372, 169–176.
- Nečas, D., Klapetek, P., 2012. Gwyddion: an open-source software for SPM data analysis. *Open Physics* 10.
- Neinhuis, C., Koch, K., Barthlott, W., 2001. Movement and regeneration of epicuticular waxes through plant cuticles. *Planta* 213, 427–434.
- Norouzi, S., Khademi, H., Cano, A.F., Acosta, J.A., 2016. Biomagnetic monitoring of heavy metals contamination in deposited atmospheric dust, a case study from Isfahan, Iran. *Journal of Environmental Management* 173, 55–64.
- Nowak, D.J., Crane, D.E., Stevens, J.C., 2006. Air pollution removal by urban trees and shrubs in the United States. *Urban Forestry & Urban Greening* 4, 115–123.
- Ny, M.T., Lee, B.-K., 2010. Size distribution and source identification of airborne particulate matter and metallic elements in a typical industrial city. *Asian Journal of Atmospheric Environment* 4, 9–19.
- Okuda, T., Fujimori, E., Hatoya, K., Takada, H., Kumata, H., Nakajima, F., Hatakeyama, S., Uchida, M., Tanaka, S., He, K., Ma, Y., Haraguchi, H., 2013. Rapid and simple determination of multi-elements in aerosol samples collected on quartz fiber filters by using EDXRF coupled

- with fundamental parameter quantification technique. *Aerosol and Air Quality Research* 13, 1864–1876.
- Olson, E., 2011. Particle shape factors and their use in image analysis-Part 1: Theory. *Journal of GXP Compliance* 15, 85–96.
- Ottelé, M., van Bohemen, H.D., Fraaij, A.L.A., 2010. Quantifying the deposition of particulate matter on climber vegetation on living walls. *Ecological Engineering* 36, 154–162.
- Pabst, W., Gregorova, E., 2007. Characterization of particles and particle systems. *ICT Prague* 27-29.
- Pacyna, J.M., Pacyna, E.G., 2001. An assessment of global and regional emissions of trace metals to the atmosphere from anthropogenic sources worldwide. *Environmental Reviews* 9, 269–298.
- Pandolfi, M., Gonzalez-Castanedo, Y., Alastuey, A., de la Rosa, J.D., Mantilla, E., de la Campa, A.S., Querol, X., Pey, J., Amato, F., Moreno, T., 2011. Source apportionment of PM₁₀ and PM_{2.5} at multiple sites in the strait of Gibraltar by PMF: Impact of shipping emissions. *Environmental Science and Pollution Research* 18, 260–269.
- Pant, P., Harrison, R.M., 2013. Estimation of the contribution of road traffic emissions to particulate matter concentrations from field measurements: A review. *Atmospheric Environment* 77, 78–97.
- Pascal, M., Falq, G., Wagner, V., Chatignoux, E., Corso, M., Blanchard, M., Host, S., Pascal, L., Larrieu, S., 2014. Short-term impacts of particulate matter (PM₁₀, PM_{10-2.5}, PM_{2.5}) on mortality in nine French cities. *Atmospheric Environment* 95, 175–184.
- Pathan, A.K., Bond, J., Gaskin, R.E., 2008. Sample preparation for scanning electron microscopy of plant surfaces--horses for courses. *Micron (Oxford, England: 1993)* 39, 1049–61.
- Peters, J., Baets, B. De, Verhoest, N.E.C., Samson, R., Degroeve, S., Becker, P. De, Huybrechts, W., 2007. Random forests as a tool for ecohydrological distribution modelling. *Ecological Modelling* 207, 304–318.
- Petrovský, E., Zbořil, R., Grygar, T.M., Kotlík, B., Novák, J., Kapička, A., Grison, H., 2013. Magnetic particles in atmospheric particulate matter collected at sites with different level of air pollution. *Studia Geophysica et Geodaetica* 57, 755–770.
- Philibert, A., Loyce, C., Makowski, D., 2013. Prediction of N₂O emission from local information with Random Forest. *Environmental Pollution* 177, 156–163.
- Pinot, P., Silvestri, Z., 2019. Pyrolytic carbon: applications of its diamagnetism in metrology. *International Journal of Metrology and Quality Engineering* 10, 7.
- Poorter, H., Niinemets, Ü., Poorter, L., Wright, I.J., Villar, R., 2009. Causes and consequences of variation in leaf mass per area (LMA): a meta-analysis. *New Phytologist* 182, 565–588.
- Pope, A., Burnett, R.T., Thun, M.J., Calle, E.E., Krewski, D., Ito, K., Thurston, G.D., Thurston, G.D., 2002. Lung cancer, cardiopulmonary mortality, and long-term exposure to fine particulate air pollution. *JAMA* 287, 1132–41.
- Pope, A., Dockery, D.W., 2006. Health effects of fine particulate air pollution: Lines that connect. *Journal of the Air and Waste Management Association* 56, 709–742.
- Popek, R., Gawrońska, H., Wrochna, M., Gawroński, S.W., Sæbø, A., 2013. Particulate matter on foliage of 13 woody species: Deposition on surfaces and phytostabilisation in waxes - a 3-year study. *International Journal of Phytoremediation* 15, 245–256.
- Port of Antwerp, 2018. Update of the annual figures - 2018 is record year for Port of Antwerp, 24 January 2019. www.portofantwerp.com/en/news/2018-record-year-port-antwerp. Accessed 2 August 2019.
- Przybysz, A., Sæbø, A., Hanslin, H.M., Gawroński, S.W., 2014. Accumulation of particulate matter and trace elements on vegetation as affected by pollution level, rainfall and the passage of time. *Science of the Total Environment* 481, 360–369.

- Punt, W., Hoen, P.P., Blackmore, S., Nilsson, S., Le Thomas, A., 2007. Glossary of pollen and spore terminology. *Review of Palaeobotany and Palynology* 143, 1–81.
- Putaud, J.P., Raes, F., Van Dingenen, R., Brüggemann, E., Facchini, M.-C., Decesari, S., Fuzzi, S., Gehrig, R., Hüglin, C., Laj, P., Lorbeer, G., Maenhaut, W., Mihalopoulos, N., Müller, K., Quass, U., Rodriguez, S., Schneider, J., Spindler, G., Brink, H. ten, Tørseth, K., Wiedensohler, A., 2004. A European aerosol phenomenology—2: chemical characteristics of particulate matter at kerbside, urban, rural and background sites in Europe. *Atmospheric Environment* 38, 2579–2595.
- Qadir, R.M., Schnelle-Kreis, J., Abbaszade, G., Arteaga-Salas, J.M., Diemer, J., Zimmermann, R., 2014. Spatial and temporal variability of source contributions to ambient PM₁₀ during winter in Augsburg, Germany using organic and inorganic tracers. *Chemosphere* 103, 263–273.
- Qian, P., Zhou, L., Zheng, X., Dong, Y., Wang, Y., 2014. Magnetic properties of airborne particulate matter in Shanghai during dust storm events and the implications for heavy metal contaminant sources. *Environmental Earth Sciences* 72, 4167–4178.
- Qiao, Q., Huang, B., Zhang, C., Piper, J.D.A., Pan, Y., Sun, Y., 2013. Assessment of heavy metal contamination of dustfall in northern China from integrated chemical and magnetic investigation. *Atmospheric Environment* 74, 182–193.
- Querol, X., Alastuey, A., Rodriguez, S., Plana, F., Ruiz, C.R., Cots, N., Massagué, G., Puig, O., 2001. PM₁₀ and PM_{2.5} source apportionment in the Barcelona Metropolitan area, Catalonia, Spain. *Atmospheric Environment* 35, 6407–6419.
- Querol, X., Alastuey, A., Ruiz, C.R., Artiñano, B., Hansson, H.C., Harrison, R.M., Buringh, E., ten Brink, H., Lutz, M., Bruckmann, P., Straehl, P., Schneider, J., 2004. Speciation and origin of PM₁₀ and PM_{2.5} in selected European cities. *Atmospheric Environment* 38, 6547–6555.
- Rai, P.K., 2013. Environmental magnetic studies of particulates with special reference to biomagnetic monitoring using roadside plant leaves. *Atmospheric Environment* 72, 113–129.
- Reimann, C., De Caritat, P., 2000. Intrinsic flaws of element enrichment factors (EFs) in environmental geochemistry. *Environmental Science and Technology* 34, 5084–5091.
- Reizer, M., Juda-Rezler, K., 2016. Explaining the high PM₁₀ concentrations observed in Polish urban areas. *Air Quality, Atmosphere & Health* 9, 517–531.
- Revuelta, M.A., McIntosh, G., Pey, J., Pérez, N., Querol, X., Alastuey, A., 2014. Partitioning of magnetic particles in PM₁₀, PM_{2.5} and PM₁ aerosols in the urban atmosphere of Barcelona (Spain). *Environmental Pollution* 188, 109–117.
- Riederer, M., Schreiber, L., 2001. Protecting against water loss: Analysis of the barrier properties of plant cuticles. *Journal of experimental botany* 52, 2023–2032.
- Ristić, M., Perić-Grujić, A., Antanasijević, D., Ristić, M., Aničić Urošević, M., Tomašević, M., 2013. Plants as monitors of lead air pollution. In: *Pollutant Diseases, Remediation and Recycling*; Lichtfouse, E., Schwarzbauer, J., Robert, D., Eds.; Springer, Vol. 4, pp 390–431.
- Rodrigues, C.M., Bio, A., Amat, F., Vieira, N., 2011. Artisanal salt production in Aveiro/Portugal - an ecofriendly process. *Saline systems* 7, 3.
- Rodríguez-Germade, I., Mohamed, K., Rey, D., Rubio, B., García, A., 2014. The influence of weather and climate on the reliability of magnetic properties of tree leaves as proxies for air pollution monitoring. *Science of The Total Environment* 468–469, 892–902.
- Sæbø, A., Hanslin, H.M., Gawronska, H., Gawronski, S.W., Baraldi, R., Rapparini, F., 2013. Characterization of urban trees and shrubs for particulate deposition, carbon sequestration and BVOC emissions. *Acta Horticulturae* No. 990, 509–517.
- Sæbø, A., Popek, R., Nawrot, B., Hanslin, H.M., Gawronska, H., Gawroński, S.W., 2012. Plant species differences in particulate matter accumulation on leaf surfaces. *Science of The Total Environment* 427–428, 347–354.

- Sagnotti, L., Macrì, P., Egli, R., Mondino, M., 2006. Magnetic properties of atmospheric particulate matter from automatic air sampler stations in Latium (Italy): Toward a definition of magnetic fingerprints for natural and anthropogenic PM₁₀ sources. *Journal of Geophysical Research: Solid Earth* 111, 1–17.
- Sagnotti, L., Taddeucci, J., Winkler, A., Cavallo, A., 2009. Compositional, morphological, and hysteresis characterization of magnetic airborne particulate matter in Rome, Italy. *Geochemistry, Geophysics, Geosystems* 10.
- Sant’Ovaia, H., Lacerda, M.J., Gomes, C.R., 2012. Particle pollution - An environmental magnetism study using biocollectors located in northern Portugal. *Atmospheric Environment* 61, 340–349.
- Sant’Ovaia, H., Marques, G., Santos, A., Gomes, C., Rocha, A., 2015. Magnetic susceptibility and isothermal remanent magnetization in human tissues: A study case. *BioMetals* 28, 951–958.
- Sawidis, T., Breuste, J., Mitrovic, M., Pavlovic, P., Tsigaridas, K., 2011. Trees as bioindicator of heavy metal pollution in three European cities. *Environmental Pollution* 159, 3560–70.
- Scapellato, M.L., Lotti, M., 2007. Short-term effects of particulate matter: An inflammatory mechanism? *Critical Reviews in Toxicology* 37, 461–487.
- Schins, R.P., Lightbody, J.H., Borm, P.J.A., Shi, T., Donaldson, K., Stone, V., 2004. Inflammatory effects of coarse and fine particulate matter in relation to chemical and biological constituents. *Toxicology and Applied Pharmacology* 195, 1–11.
- Schneider, C.A., Rasband, W.S., Eliceiri, K.W., 2012. NIH Image to ImageJ: 25 years of image analysis. *Nature Methods* 9, 671–675.
- Schröder, W., Nickel, S., Schönrock, S., Meyer, M., Wosniok, W., Harmens, H., Frontasyeva, M. V., Alber, R., Aleksiyenak, J., Barandovski, L., Carballeira, A., Danielsson, H., de Temmermann, L., Godzik, B., Jeran, Z., Karlsson, G.P., Lazo, P., Leblond, S., Lindroos, A.-J., Liiv, S., Magnússon, S.H., Mankovska, B., Martínez-Abaigar, J., Piispanen, J., Poikolainen, J., Popescu, I. V., Qarri, F., Santamaria, J.M., Skudnik, M., Špirić, Z., Stafilov, T., Steinnes, E., Stihl, C., Thöni, L., Uggerud, H.T., Zechmeister, H.G., 2016. Spatially valid data of atmospheric deposition of heavy metals and nitrogen derived by moss surveys for pollution risk assessments of ecosystems. *Environmental Science and Pollution Research International* 23, 10457–10476.
- Schwarze, P.E., Øvreik, J., Låg, M., Refsnes, M., Nafstad, P., Hetland, R.B., Dybing, E., 2006. Particulate matter properties and health effects: Consistency of epidemiological and toxicological studies. *Human and Experimental Toxicology* 25, 559–579.
- Selmi, W., Weber, C., Rivière, E., Blond, N., Mehdi, L., Nowak, D.J., 2016. Air pollution removal by trees in public green spaces in Strasbourg city, France. *Urban Forestry & Urban Greening* 17, 192–201.
- Setälä, H., Viippola, V., Rantalainen, A.L., Pennanen, A., Yli-Pelkonen, V., 2013. Does urban vegetation mitigate air pollution in northern conditions? *Environmental Pollution* 183, 104–112.
- Sgrigna, G., Baldacchini, C., Esposito, R., Calandrelli, R., Tiwary, A., Calfapietra, C., 2016. Characterization of leaf-level particulate matter for an industrial city using electron microscopy and X-ray microanalysis. *Science of The Total Environment* 548–549, 91–99.
- Sgrigna, G., Sæbø, A., Gawroński, S.W., Popek, R., Calfapietra, C., 2015. Particulate Matter deposition on *Quercus ilex* leaves in an industrial city of central Italy. *Environmental Pollution* 197, 187–194.
- Shi, J., Zhang, G., An, H., Yin, W., Xia, X., 2017. Quantifying the particulate matter accumulation on leaf surfaces of urban plants in Beijing, China. *Atmospheric Pollution Research* 8, 836–842.

- Shi, M., Wu, H., Zhang, S., Li, H., Yang, T., Liu, W., Liu, H., 2014. Weekly cycle of magnetic characteristics of the daily PM_{2.5} and PM_{2.5-10} in Beijing, China. *Atmospheric Environment* 98, 357–367.
- Shu, J., Dearing, J.A., Morse, A.P., Yu, L., Li, C., 2000. Magnetic properties of daily sampled total suspended particulates in Shanghai. *Environmental Science and Technology* 34, 2393–2400.
- Smets, W., Wuyts, K., Oerlemans, E., Wuyts, S., Denys, S., Samson, R., Lebeer, S., 2016. Impact of urban land use on the bacterial phyllosphere of ivy (*Hedera sp.*). *Atmospheric Environment* 147, 376–383.
- Smith, L.J., McKay, K.O., van Asperen, P.P., Selvadurai, H., Fitzgerald, D.A., 2010. Normal development of the lung and premature birth. *Paediatric Respiratory Reviews* 11, 135–142.
- Song, Y., Maher, B.A., Li, F., Wang, X., Sun, X., Zhang, H., 2015. Particulate matter deposited on leaf of five evergreen species in Beijing, China: Source identification and size distribution. *Atmospheric Environment* 105, 53–60.
- Speak, A.F., Rothwell, J.J., Lindley, S.J., Smith, C.L., 2012. Urban particulate pollution reduction by four species of green roof vegetation in a UK city. *Atmospheric Environment* 61, 283–293.
- Teja, A.S., Koh, P.-Y., 2009. Synthesis, properties, and applications of magnetic iron oxide nanoparticles. *Progress in Crystal Growth and Characterization of Materials* 55, 22–45.
- Tepanosyan, G., Sahakyan, L., Belyaeva, O., Saghatelyan, A., 2016. Origin identification and potential ecological risk assessment of potentially toxic inorganic elements in the topsoil of the city of Yerevan, Armenia. *Geochemical Exploration* 167, 1–11.
- Terzaghi, E., Wild, E., Zacchello, G., Cerabolini, B.E.L., Jones, K.C., Di Guardo, A., 2013. Forest Filter Effect: Role of leaves in capturing/releasing air particulate matter and its associated PAHs. *Atmospheric Environment* 74, 378–384.
- Terzano, C., Di Stefano, F., Conti, V., Graziani, E., Petrojanni, A., 2010. Air pollution ultrafine particles: Toxicity beyond the lung. *European Review for Medical and Pharmacological Sciences* 14, 809–21.
- Thompson, R., Oldfield, F., 1986. *Environmental Magnetism*. Springer Netherlands, Dordrecht.
- Tian, Y.-Z., Chen, G., Wang, H.-T., Huang-Fu, Y.-Q., Shi, G.-L., Han, B., Feng, Y.-C., 2016. Source regional contributions to PM_{2.5} in a megacity in China using an advanced source regional apportionment method. *Chemosphere* 147, 256–263.
- Tittarelli, A., Borgini, A., Bertoldi, M., De Saeger, E., Ruprecht, A., Stefanoni, R., Tagliabue, G., Contiero, P., Crosignani, P., 2008. Estimation of particle mass concentration in ambient air using a particle counter, *Atmospheric Environment*.
- Tittarelli, A., Borgini, A., Bertoldi, M., Desaegeer, E., Ruprecht, A., Stefanoni, R., Tagliabue, G., Contiero, P., Crosignani, P., 2008. Estimation of particle mass concentration in ambient air using a particle counter. *Atmospheric Environment* 42, 8543–8548.
- Tomašević, M., Aničić, M., 2010. Trace element content in urban tree leaves and SEM-EDAX characterization of deposited particles. *Facta universitatis - series: Physics, Chemistry and Technology* 8, 1–13.
- Tomašević, M., Vukmirović, Z., Rajšić, S., Tasić, M., Stevanović, B., 2005. Characterization of trace metal particles deposited on some deciduous tree leaves in an urban area. *Chemosphere* 61, 753–760.
- Tretiach, M., Pittao, E., Crisafulli, P., Adamo, P., 2011. Influence of exposure sites on trace element enrichment in moss-bags and characterization of particles deposited on the biomonitor surface. *Science of The Total Environment* 409, 822–830.
- Tukey, H.B., 1970. The leaching of substances from plants. *Annual Review of Plant Physiology* 21, 305–324.

- UNECE, 2012. Decision 2012/2, ECE/EB.AIR/111/Add.1. Amendment of the text of and annexes II to IX to the 1999 Protocol to Abate Acidification, Eutrophication and Ground-level Ozone and the addition of new annexes X and XI. [www.unece.org/fileadmin/DAM/env/documents/2013/air/ECE_EB.AIR_111_Add.1__EN_G_DECISION_2.pdf](http://www.unece.org/fileadmin/DAM/env/documents/2013/air/ECE_EB.AIR_111_Add.1_EN_G_DECISION_2.pdf).
- Urbat, M., Lehndorff, E., Schwark, L., 2004. Biomonitoring of air quality in the Cologne Conurbation using pine needles as a passive sampler - Part I: Magnetic properties. *Atmospheric Environment* 38, 3781–3792.
- USDA, 1999. The United States National Arboretum, United States Department of Agriculture. *Platanus x acerifolia* “Columbia” and “Liberty”, www.usna.usda.gov/Newintro/platanus.pdf.
- Valavanidis, A., Fiotakis, K., Vlachogianni, T., 2008. Airborne particulate matter and human health: Toxicological assessment and importance of size and composition of particles for oxidative damage and carcinogenic mechanisms. *Journal of Environmental Science and Health, Part C* 26, 339–362.
- Valavanidis, A., Vlahoyianni, T., Fiotakis, K., 2005. Comparative study of the formation of oxidative damage marker 8-hydroxy-2'-deoxyguanosine (8-OHdG) adduct from the nucleoside 2'-deoxyguanosine by transition metals and suspensions of particulate matter in relation to metal content and redox reactivity. *Free Radical Research* 39, 1071–1081.
- Van den Bossche, J., Peters, J., Verwaeren, J., Botteldooren, D., Theunis, J., De Baets, B., 2015. Mobile monitoring for mapping spatial variation in urban air quality: Development and validation of a methodology based on an extensive dataset. *Atmospheric Environment* 105, 148–161.
- Van Dingenen, R., Raes, F., Putaud, J.P., Baltensperger, U., Charron, A., Facchini, M.C., Decesari, S., Fuzzi, S., Gehrig, R., Hansson, H.C., Harrison, R., Hüglin, C., Jones, A.M., Laj, P., Lorbeer, G., Maenhaut, W., Palmgren, F., Quass, U., Rodriguez, S., Schneider, J., Ten Brink, H., Tunved, P., Tørseth, K., Wehner, B., Weingartner, E., Wiedensohler, A., Wählin, P., 2004. A European aerosol phenomenology - 1: Physical characteristics of particulate matter at kerbside, urban, rural and background sites in Europe. *Atmospheric Environment* 38, 2561–2577.
- Vandesompele, J., De Preter, K., Pattyn, F., Poppe, B., Van Roy, N., De Paepe, A., Speleman, F., 2002. Accurate normalization of real-time quantitative RT-PCR data by geometric averaging of multiple internal control genes. *Genome Biol.* 3, RESEARCH0034.
- Vercauteren, J., Matheeußen, C., Wauters, E., Roekens, E., van Grieken, R., Krata, A., Makarovska, Y., Maenhaut, W., Chi, X., Geypens, B., 2011. Chemkar PM10: An extensive look at the local differences in chemical composition of PM10 in Flanders, Belgium. *Atmospheric Environment* 45, 108–116.
- Verosub, K.L., Roberts, A.P., 1995. Environmental magnetism: Past, present, and future. *Journal of Geophysical Research* 100, 2175.
- Viana, M., Amato, F., Alastuey, A., Querol, X., Moreno, T., Dos Santos, S.G., Herce, M.D., Fernández-Patier, R., 2009. Chemical tracers of particulate emissions from commercial shipping. *Environmental Science and Technology* 43, 7472–7477.
- Viana, M., Kuhlbusch, T.A.J., Querol, X., Alastuey, a., Harrison, R.M., Hopke, P.K., Winiwarter, W., Vallius, M., Szidat, S., Prévôt, a. S.H., Hueglin, C., Bloemen, H., Wählin, P., Vecchi, R., Miranda, a. I., Kasper-Giebl, a., Maenhaut, W., Hitzenberger, R., 2008. Source apportionment of particulate matter in Europe: A review of methods and results. *Journal of Aerosol Science* 39, 827–849.
- Viippola, V., Whitlow, T.H., Zhao, W., Yli-Pelkonen, V., Mikola, J., Pouyat, R., Setälä, H., 2018. The effects of trees on air pollutant levels in peri-urban near-road environments. *Urban Forestry and Urban Greening* 30, 62–71.

- VMM, 2017. Luchtkwaliteit in het Vlaamse Gewest. Jaarverslag Immissiemeetnetten – 2016 (in Dutch). www.vmm.be/publicaties/luchtkwaliteit-in-het-vlaamse-gewest-2016.
- Vranckx, S., Vos, P., Maiheu, B., Janssen, S., 2015. Impact of trees on pollutant dispersion in street canyons: A numerical study of the annual average effects in Antwerp, Belgium. *Science of The Total Environment* 532, 474–483.
- Vu, T. V., Delgado-Saborit, J.M., Harrison, R., 2015. Review: Particle number size distributions from seven major sources and implications for source apportionment studies. *Atmospheric Environment* 122, 114–132.
- Vuković, G., Urošević, M.A., Goryainova, Z., Pergal, M., Škrivanj, S., Samson, R., Popović, A., 2015. Active moss biomonitoring for extensive screening of urban air pollution: Magnetic and chemical analyses. *Science of The Total Environment* 521–522, 200–210.
- Walker, S.C., Allen, S., Bell, G., Roberts, C.J., 2015. Analysis of leaf surfaces using scanning ion conductance microscopy. *Journal of Microscopy* 258, 119–126.
- Wang, B., Xia, D., Yu, Y., Jia, J., Nie, Y., Wang, X., 2015b. Detecting the sensitivity of magnetic response on different pollution sources - A case study from typical mining cities in northwestern China. *Environmental Pollution* 207, 288–298.
- Wang, H., Shi, H., Li, Y., Yu, Y., Zhang, J., 2013. Seasonal variations in leaf capturing of particulate matter, surface wettability and micromorphology in urban tree species. *Frontiers of Environmental Science & Engineering* 7, 579–588.
- Wang, J., Li, S., Li, H., Qian, X., Li, X., Liu, X., Lu, H., Wang, C., Sun, Y., 2017. Trace metals and magnetic particles in PM 2.5: Magnetic identification and its implications. *Scientific Reports* 7, 1–11.
- Wang, L., Gong, H., Liao, W., Wang, Z., 2015a. Accumulation of particles on the surface of leaves during leaf expansion. *Science of The Total Environment* 532, 420–434.
- Watson, J. G., Chow J. C., Chen, L.-W. A., Engling, G., Wang, X. L., 2016. Source apportionment: Principles and methods. In: *Airborne particulate matter - sources, atmospheric processes and health. Issues in Environmental Science and Technology No. 42*, pp. 72-119. The Royal Society of Chemistry, Cambridge.
- Weber, F., Kowarik, I., Säumel, I., 2014. Herbaceous plants as filters: Immobilization of particulates along urban street corridors. *Environmental pollution (Barking, Essex : 1987)* 186, 234–40.
- Weber, S., Hoffmann, P., Ensling, J., Dedic, A.N., Weinbruch, S., Mieke, G., Gütlich, P., Ortner, H.M., 2000. Characterization of iron compounds from urban and rural aerosol sources. *Journal of Aerosol Science* 31, 987–997.
- Weerakkody, U., Dover, J.W., Mitchell, P., Reiling, K., 2017. Particulate matter pollution capture by leaves of seventeen living wall species with special reference to rail-traffic at a metropolitan station. *Urban Forestry and Urban Greening* 27, 173–186.
- Weerakkody, U., Dover, J.W., Mitchell, P., Reiling, K., 2018. Evaluating the impact of individual leaf traits on atmospheric particulate matter accumulation using natural and synthetic leaves. *Urban Forestry & Urban Greening* 30, 98–107.
- Weibel, E.R., 2009. What makes a good lung? *Swiss Medical Weekly* 139, 375–86.
- WHO, 2006. Air quality guidelines for particulate matter, ozone, nitrogen, dioxide and sulfur dioxide. Global update 2005, summary of risk assessment. World Health Organization. WHO/SDE/PHE/OEH/06.02.
- WHO, 2013. Review of evidence on health aspects of air pollution – REVIHAAP Project Technical Report. WHO Regional Office for Europe.
- WHO, 2015. www.who.int/gho/urban_health/situation_trends/urban_population_growth/. Accessed 28 September 2018.
- WHO, 2016. www.who.int/mediacentre/news/releases/2016/air-pollution-estimates/. Accessed 28 September 2018.

- WHO, 2018. www.who.int/news-room/detail/02-05-2018-9-out-of-10-people-worldwide-breathe-polluted-air-but-more-countries-are-taking-action. Accessed 28 September 2018.
- WHO, 2019. [www.who.int/en/news-room/fact-sheets/detail/ambient-\(outdoor\)-air-quality-and-health](http://www.who.int/en/news-room/fact-sheets/detail/ambient-(outdoor)-air-quality-and-health). Accessed 20 August 2019.
- Wilkinson, K.E., Lundkvist, J., Netrval, J., Eriksson, M., Seisenbaeva, G.A., Kessler, V.G., 2013. Space and time resolved monitoring of airborne particulate matter in proximity of a traffic roundabout in Sweden. *Environmental Pollution* 182, 364–370.
- Wilson, J.G., Kingham, S., Pearce, J., Sturman, A.P., 2005. A review of intraurban variations in particulate air pollution: Implications for epidemiological research. *Atmospheric Environment* 39, 6444–6462.
- Wilson, W.E., Chow, J.C., Claiborn, C., Fusheng, W., Engelbrecht, J., Watson, J.G., 2002. Monitoring of particulate matter outdoors. *Chemosphere* 49, 1009–1043.
- Wu, Z., Hu, M., Lin, P., Liu, S., Wehner, B., Wiedensohler, A., 2008. Particle number size distribution in the urban atmosphere of Beijing, China. *Atmospheric Environment* 42, 7967–7980.
- Wuytack, T., Samson, R., Wuyts, K., Adriaenssens, S., Kardel, F., Verheyen, K., 2013. Do leaf characteristics of white willow (*Salix alba* L.), northern red oak (*Quercus rubra* L.), and scots pine (*Pinus sylvestris* L.) respond differently to ambient air pollution and other environmental stressors? *Water, Air & Soil Pollution* 224, 1635.
- Wuytack, T., Wuyts, K., Van Dongen, S., Baeten, L., Kardel, F., Verheyen, K., Samson, R., 2011. The effect of air pollution and other environmental stressors on leaf fluctuating asymmetry and specific leaf area of *Salix alba* L. *Environmental Pollution* 159, 2405–2411.
- Wuyts, K., Hofman, J., Van Wittenberghe, S., Nuyts, G., De Wael, K., Samson, R., 2018. A new opportunity for biomagnetic monitoring of particulate pollution in an urban environment using tree branches. *Atmospheric Environment* 190, 177–187.
- Xia, D., Wang, B., Yu, Y., Jia, J., Nie, Y., Wang, X., Xu, S., 2014. Combination of magnetic parameters and heavy metals to discriminate soil-contamination sources in Yinchuan — A typical oasis city of Northwestern China. *Science of The Total Environment* 485, 83–92.
- Xie, R.K., Seip, H.M., Leinum, J.R., Winje, T., Xiao, J.S., 2005. Chemical characterization of individual particles (PM₁₀) from ambient air in Guiyang City, China. *Science of The Total Environment* 343, 261–272.
- Yamamoto, N., Bibby, K., Qian, J., Hospodsky, D., Rismani-Yazdi, H., Nazaroff, W.W., Peccia, J., 2012. Particle-size distributions and seasonal diversity of allergenic and pathogenic fungi in outdoor air. *The ISME journal* 6, 1801–11.
- Yang, J., McBride, J., Zhou, J., Sun, Z., 2005. The urban forest in Beijing and its role in air pollution reduction. *Urban Forestry & Urban Greening* 3, 65–78.
- Yang, T., Liu, Q., Li, H., Zeng, Q., Chan, L., 2010. Anthropogenic magnetic particles and heavy metals in the road dust: Magnetic identification and its implications. *Atmospheric Environment* 44, 1175–1185.
- Yatkin, S., Gerboles, M., Borowiak, A., 2012. Evaluation of standardless EDXRF analysis for the determination of elements on PM₁₀ loaded filters. *Atmospheric Environment* 54, 568–582.
- Yatkin, S., Gerboles, M., Borowiak, A., Tanet, G., Pedroni, V., Passarella, R., Lagler, F., 2011. Evaluation of EDXRF for the Determination of Elements in PM₁₀ Filters., Eur 24983. Publications Office of the European Union.
- Yin, G., Hu, S., Cao, L.W., Roesler, W., Appel, E., 2013. Magnetic properties of tree leaves and their significance in atmospheric particle pollution in Linfen City, China. *Chinese Geographical Science* 23, 59–72.

- Yli-Pelkonen, V., Setälä, H., Viippola, V., 2017. Urban forests near roads do not reduce gaseous air pollutant concentrations but have an impact on particles levels. *Landscape and Urban Planning* 158, 39–47.
- Zhang, C., Qiao, Q., Appel, E., Huang, B., 2012. Discriminating sources of anthropogenic heavy metals in urban street dusts using magnetic and chemical methods. *Journal of Geochemical Exploration* 119–120, 60–75.
- Zhang, W., Yu, L., Lu, M., Hutchinson, S.M., Feng, H., 2007. Magnetic approach to normalizing heavy metal concentrations for particle size effects in intertidal sediments in the Yangtze Estuary, China. *Environmental Pollution* 147, 238–244.
- Zhao, X.Q., Liu, B.X., Liang, Y., Hu, Z.Q., 1996. Oxidation behavior and magnetic properties of metallic ultrafine particles. *Journal of Magnetism and Magnetic Materials* 164, 401–410.
- Zhou, W., Apkarian, R.P., Wang, Z.L., Joy, D., 2006. Fundamentals of Scanning Electron Microscopy (SEM). In: *Scanning Microscopy for Nanotechnology*. Springer, New York, pp. 1–40.

“It always seems impossible until it's done”

-- Nelson Mandela